UNIVERSITY OF SOUTHAMPTON

FACULTY OF ENGINEERING AND PHYSICAL SCIENCES
SCHOOL OF ENGINEERING

The Mechanical Behaviour of Fibre Reinforced Railway Ballast

by

Edgar Ferro

Thesis for the degree of Doctor of Philosophy

August 2018

University of Southampton

Faculty of Engineering and Physical Sciences

School of Engineering

Thesis for the degree of Doctor of Philosophy

Abstract

The Mechanical Behaviour of Fibre Reinforced Ballasted Track

By Edgar Ferro

Ballasted track is the most traditional form of railway track but is still widely predominant and able to cope with high performance demands, such as those typical of high speed lines. A major disadvantage of ballasted track is its tendency to settle with the passage of trains, mainly due the accumulation of permanent deformation in the ballast under cyclic loading. This leads to track geometry deterioration, as the settlement is unlikely to be uniform, jeopardising the safety of train operations and ride quality. Therefore, costly maintenance operations, e.g. tamping, are periodically required to restore the correct ballast level. Also, rail transport demand is growing in many parts of the world, increasing the need for track maintenance while reducing the maintenance windows. In light of this, the mechanical behaviour of ballast has been widely studied and techniques to improve it have been proposed.

A novel technique with the potential to reduce ballast settlement is fibre reinforcement, which consists of the addition of unbound randomly placed discrete fibres. It is widely accepted that fibre reinforcement provides additional strength to granular materials ranging from sand to gravel. Hence, it can potentially reduce ballast tendency to settle by increasing the particle interlocking. Fibre reinforcement seems suitable to railway ballast, as it is expected to maintain adequate track stiffness and permeability, not produce planes of weakness, and be compatible with standard maintenance operations. Moreover, fibres can be potentially obtained from recycled materials, separated from ballast after use for recycling, and added either during ballast cleaning or renewals. Nevertheless, the effect of fibre reinforcement on the deformability of granular materials, especially under cyclic loading, remains unclear.

This research investigated the mechanical behaviour of fibre reinforced railway ballast through full-size laboratory tests, reproducing a section of single-line track extended to the shoulder and subjected to a sinusoidal load representative of train passage. The tests explored the effect of fibre dimensions and content for two different types of inclusions, i.e. filament-like and tape-like fibres. It was found that the addition of properly selected fibres can reduce track settlement, increase the long-term support of the sleeper ends, and reduce ballast damage. This might be explained by the fibres inhibiting the micro-movements exhibited by the particles in each load cycle, while the effect of the additional confinement was secondary. However, the holistic understanding of the mechanics of fibre-reinforcement would require further experiments designed specifically to capture ballast behaviour at the particle scale.

Contents

List of Tables

List of Figures

Declaration of Authorship

I, Edgar Ferro, declare that the thesis entitled “The Mechanical Behaviour of Fibre Reinforced Railway Ballast” and the work presented in the thesis are both my own, and have been generated by me as the result of my own original research.

I confirm that:

- This work was done wholly or mainly while in candidature for a research degree at this University;
- Where any part of this thesis has previously been submitted for a degree or any other qualification at this University or any other institution, this has been clearly stated;
- Where I have consulted the published work of others, this is always clearly attributed;
- Where I have quoted from the work of others, the source is always given. With the exception of such quotations, this thesis is entirely my own work;
- I have acknowledged all main sources of help;
- Where the thesis is based on work done by myself jointly with others, I have made clear exactly what was done by others and what I have contributed myself;
- Parts of this work have been published as:

  Ferro E., Ajayi O., Le Pen L., Zervos A. & Powrie W. (2016). “Settlement response of fibre reinforced ballast.” 11th World Congress on Railway Research. Milan, Italy.

Signed: ……..

Date:…….

Acknowledgements

This research was financially supported by the Engineering and Physical Sciences Research Council (EPSRC).

I would like to express my sincere gratitude to Dr Antonis Zervos, Dr Louis Le Pen and Professor William Powrie, who gave me the opportunity to work on this research and offered me constant support and invaluable advice.

I also would like to thank Dr Taufan Abadi, who gave me precious help in the laboratory, especially during my first year in Southampton, and most importantly friendship and laughter.

I am very grateful to the laboratory staff, who provided me with the help I needed for my laboratory work. In particular, Dr Andrew Robinson, Dave Lynock, Earl Peters, Roger Newton, Karl Scammel, Harvey Skinner and Andy Morgan.

Last but not least, I would like to thank my parents, Marvi and Aldo, my siblings, Yara and Jayme, and my girlfriend Sara, who have always been very close, despite the distance.

Abbreviations

BOEF	Beam on Elastic Foundation
DPC	Damp Proof Course
C-FS	Cyclic full size
C-T	Cyclic triaxial
CH	Cliffe Hill
clSa	Clayey sand
CWR	Continuously welded rail
FEM	Finite element method
Gr	Gravel
LC	Load cell
LVDT	Linear variable displacement transducer
M-RS	monotonic ring shear
M-T	Monotonic triaxial
MS	Mount Sorrel
PA	Polyamide
PE	Polyethylene
PP	Polypropylene
PSD	Particle size distribution
NR	Network Rail
Sa	Sand
saGr	Sandy gravel
SB	Scaled ballast
SRTF	Southampton Railway Testing Facility
USP	Under Sleeper Pad

Symbols

α	Cant angle
α_i	Pixels to mm conversions factor at time i
A	Geogrid aperture size
$A_{c,av}$	Average cumulative sleeper/ballast contact over the sleeper base
$A_{c,m}$	Cumulative sleeper/ballast contact area under the middle of the sleeper
$A_{c,r}$	Average cumulative sleeper/ballast contact area under the rails
A_{fp}	Area of fibre per particle (or fibre content by area)
$A_{fp,max}$	Maximum value of A_{fp} to avoid extensive fibre overlapping
A_N	Normalised area of a fibre, i.e. $W_f L_f / D_{50}^2$
β	deviator ratio
B	Breadth of rectangular uniformly loaded area (Steinbrenner's solution)
C_u	Coefficient of uniformity

$\Delta d_{a,b}$	Movement of a lateral plate's target (in mm) between time a and b
Δd_i	Movement of a lateral plate's target (in mm) at time i
Δe_{max}	Increase in void ratio at maximum fibre content
Δe_{max}^{loose}	Δe_{max} in loose conditions
Δe_{max}^{dense}	Δe_{max} in dense conditions
Δe_{max}^{rel}	Increase in compactability (difference between Δe_{max}^{loose} and Δe_{max}^{dense})
ΔM	Particle mass loss
ΔM_p	Particle mass loss percentage
ΔS_{av}	Average shear stress increment
d_1	Settlement or settlement accumulated in first cycle (depending on context)
D_{10}, D_{50}, D_{60}	Particle dimensions at 10%, 50% and 60% passing
DAF	Dynamic amplification factor
d_f	Fibre diameter
D_{r0}	Initial relative density
D_w	Train wheel diameter
ε_1	Permanent strain accumulated in first cycle or vertical strain
ε_a, ε_1	Axial or vertical strain
ε_3	Horizontal strain
ε_s, ε_q	Shear strain
ε_v, ε_p	Volumetric strain
E_{eq}	Equivalent Young modulus over a load cycle
E_f	Fibre Young modulus
$E_r I_r$	Rail Young modulus by second moment of area
e, e_0	Void ratio, initial void ratio
e_{min}, e_{max}	Minimum and maximum void ratio
f	Primary train loading frequency
F_b	Force at break for a single filament-like fibre, i.e. polypropylene rope
F_c	Centrifugal force, according to D'Alambert's principle
ϕ_{conn}	Particle connected porosity
Φ_N	Ratio volume of solids to total volume
$F_r(x)$	Rail seat force
f_t, f_n	Tangential and normal components of interparticle contact force
G_0	Shear modulus at small strain
G_s	Specific gravity
γ_N	Plastic shear strain at cycle N
h	Cant or super elevation
h_c	Distance between track and vehicle centre of gravity
η, η'	Fibre aspect ratio and modified aspect ratio
k_d	Factor accounting for the longitudinal distribution of the wheel load
k_p	Dynamic attenuation factor for wheel load, accounting for the rail pads
k_r	Rail support stiffness (for Winkler's method)
k_v	Dynamic amplification factor, equivalent to DAF

k_w	Winkler's support stiffness
Λ	characteristic length to calculate train loading primary frequency f
λ	Distance (pixels) between centres of consecutive squares of a lateral plate's target
λ_k	Characteristic length (for Winkler's method)
L	Length of rectangular uniformly loaded area (Steinbrenner's solution)
l	Distance (mm) between centres of consecutive squares of a lateral plate's target
λ_f	Linear density of filament like-fibres (PP rope)
L_f	Fibre length
L_{fp}	Length of fibre per particle (fibre content by length)
$L_{fp,max}$	Maximum value of L_{fp} to avoid extensive fibre overlapping
μ	Friction coefficient
M_0, M_f	Particle mass before and after a test
N	Number of cycles
N_{fp}	Number of fibres per particle (N_f/N_p)
N_p	Number of particles
p', p^*	Hydrostatic effective stress
$p(x)$	Winkler's elastic base reaction
q, q^*	Deviatoric stress
q/p'	Stress ratio
$(q/p')_p$	Stress ratio at peak
$q(x)$	Distributed load
Q	Normal train reaction at the rails
Q_d, Q_{qs}	Dynamic and quasi-static components of Q
$Q_{qs,i}$, $Q_{qs,o}$	Quasi-static components of Q for inner and outer rail
ρ_{min}, ρ_{max}	Minimum and maximum bulk density
R	Radius of rail track curve
RFC	Relative fibre content
RFC_{tape}^{th}	Theoretical relative fibre content for tape-like fibres
σ_c	Confining stress
σ_1', $\overline{\sigma}_1$	Effective vertical stress
σ_3', $\overline{\sigma}_3$	Effective confining stress
σ_{crit}	Critical confining stress
σ_n	Normal stress (shear tests)
σ_v	Vertical stress
S, S_h	Settlement, ballast lateral spreading
s	Sleeper spacing
u	Distance between rail and sleeper end
U_c	Ratio of $A_{c,m}$ to $A_{c,r}$
V	Train speed
V_f, V_p, V_s	Volume of fibres, particles, solids
V_{fr}	Volumetric fibre content (also X)

$V_{fr,max}$	Maximum value of V_{fr} to avoid extensive fibre overlapping
$V_{fr,max}^{th}$	Theoretical maximum value of V_{fr} for tape-like fibres based on simplified model
W_f	Fibre width
w_f, w_s	Weight of fibres, solids
w_{fr}	Weight fibre ratio (or fibre content by weight)
$w_r(x)$	Rail deflection
X	Volumetric fibre content (also V_{fr})
x	Coordinate along the length of the rail
Y_i	Average position of a lateral plate's target in pixels at time i
z	Vertical coordinate under corner of rectangular uniformly loaded area (Steinbrenner's solution)

1 INTRODUCTION

1.1 Overview

With the first passenger train run in 1821, the UK railways are the oldest in the world. Originally tracks were laid directly on the ground but railway engineers realised that the sleepers required a resilient support that could spread the load over the subgrade and allow for corrections of the track level; hence by 1930 all tracks were laid on stone ballast (Claisse & Calla, 2006).

Today, most of UK's railway infrastructure is owned by Network Rail (NR), which manage 20,000 miles of track (Network Rail, 2018b). Despite rail representing a very traditional mode of transport, it has enjoyed a renaissance in recent years, as passenger journeys on NR's lines doubled over the past 20 years and are expected to increase by another 40% by 2040 (Network Rail, 2018a). This can be partly attributed to road congestion and increasing petrol prices but also to a general increase in travelling; in contrast to roads, rail lines do not provide a point to point connection but are safer, faster and more reliable; in addition, railway transport is more energy efficient and produces less pollution, noise and vibration (Abadi, 2014).

There are two main forms of railway track: ballasted track and slab track. Although the former is more traditional, it represents over 99% of NR's plain lines (Godley, 2015) and is still able to satisfy high performance demands, such as those typical of high speed lines. A major drawback of ballasted track is that it experiences plastic settlement, owing to the ballast's tendency to exhibit permanent deformation under cyclic loading typical of train passage. As track settlement is typically not uniform, track geometry deteriorates and costly periodic maintenance operations, such as tamping, are required to restore the track level. However, tamping damages the ballast, increasing the rate of settlement after each tamp until the track has to be fully renewed.

Over a 30 year period, ballast may be tamped about 10 times before a full renewal (Ajayi, 2014) and is responsible for most track temporary speed restrictions (Godley, 2015). Therefore, there are potential advantages if ballasted track could be modified to increase its durability both in terms of intervals between maintenance interventions and overall life cycle. This can be achieved through interventions of any of the components of the railway track, as they interact to provide track stability and quality. This research focuses on ballast mechanical behaviour and proposes a novel method to improve it.

1.2 Research purpose & knowledge gap

The mechanical behaviour of railway ballast under cyclic loading representative of train passage has been widely investigated and a number of techniques to improve it have been proposed. For example: the use of more broadly graded ballast, continuous reinforcements (e.g. geogrids and geocells), ballast bonding and the addition of crumb rubber. This research explores the potential of a novel technique for the improvement of ballast mechanical behaviour, namely random fibre reinforcement.

Fibre reinforcement consists of the addition of unbound randomly placed discrete fibres to soil or similar materials to improve their mechanical properties. It is widely accepted that fibres can provide additional strength to a wide range of granular materials, from sand to gravel, especially if lightly confined. Therefore, the addition of fibres to ballast, which is lightly confined coarse angular gravel, might increase particle interlocking and reduce its tendency to settle. Moreover, fibres can bring the following advantages: they should maintain adequate track stiffness and permeability, not produce planes of weakness, are expected to be compatible with standard maintenance operations, can be potentially added during ballast cleaning or renewals, are unlikely to segregate during service, can be obtained from recycled materials and separated from ballast after use for recycling.

Nevertheless, fibre ability to increase the shear strength of very coarse granular materials, such as railway ballast, has not been investigated. Moreover, the influence of the fibres on their deformability remains unclear, especially under cyclic loading. Therefore, further research is required to assess the potential of fibre-reinforcement to improve the performance of railway ballast.

In light of this, this research explores the potential of the addition of fibres to reduce the permanent deformation of railway ballast through full-size laboratory tests. These were carried out in the Southampton Railway Testing Facility (SRTF), a laboratory representation of a section of single line track extended to the shoulder and subjected to a sinusoidal load representative of train passage. Compared with element tests, e.g. triaxial tests, the full-size tests can reproduce more realistically the stresses to which ballast is subjected on a real railway track. On the other hand, they are often more difficult to interpret, as sample stresses and strains are not uniform.

This research improves the understanding of the mechanical behaviour of ballasted track, shows the potential benefits of different types of fibre (i.e. tape-like and filament-like fibres) on it and contributes to the current knowledge on the behaviour of fibre reinforced granular materials subjected to cyclic loading.

1.3 Aim and objectives

This research is aimed at assessing the potential of random fibre-reinforcement to reduce ballast tendency to settle, hence reduce track geometry deterioration and maintenance costs. This aim is reached through the following objectives:

- Analyse the current literature to understand the mechanical behaviour of railway ballast, in particular its deterioration under cyclic loading typical of train passage, and the potential benefits of the addition of randomly placed fibres.
- Determine generic parameters to express the characteristics of the reinforcement (e.g. fibre dimensions, content and disruption of the packing of the particles).
- Develop common procedures for the preparation of full-size tests in the Southampton Railway Testing Facility and methods for data acquisition able to capture the main characteristics of ballast mechanical behaviour.

- Assess the effects of the addition of fibres of different dimensions, content and type on ballasted track behaviour.
- Analyse test results to understand the general mechanical behaviour of ballasted track, the effect of fibre addition on it, and provide a likely explanation for the mechanics of fibre-reinforcement.
- Summarise all findings, including those not strictly related to fibre reinforcement, to provide input for further research.

1.4 Report organisation

This report consists of nine chapters that can be subdivided into three main functional parts.

The first part (Chapter 2 to Chapter 4) provides a general understanding of the mechanical behaviour of railway ballast and fibre-reinforced granular materials to identify the potential benefits of adding fibres to ballast and provide the basis for the understanding of the mechanics of fibre-reinforced ballast:

- Chapter 2 provides a basic description of ballasted track main components, train load and its transfer from the wheel to the subgrade through the ballast bed.
- Chapter 3 discusses the deterioration of railway ballast, hence track geometry, under the train passage, based on the current literature. It describes ballast settlement response, identifies the main mechanisms responsible for it, and presents existing techniques of track improvement through interventions to the ballast layer.
- Chapter 4 reviews the existing literature on the behaviour of fibre reinforced granular materials under monotonic and cyclic loading to identify the potential advantages of the addition of fibres to railway ballast and aid the understanding of its mechanics.

The second part (Chapter 5 to Chapter 7) describes the full size tests on fibre reinforced ballast carried out as part of this research and their results:

- Chapter 5 presents the materials and methods used for testing fibre reinforced ballast. It describes: the full-size testing apparatus; the two types of ballast and fibre used; the parameters used to describe the characteristics of the ballast-fibre mixture; the techniques implemented to capture sample response during the tests; and the common procedures for test preparation. Finally, it provides an overview of the testing programme.
- Chapter 6 describes the output of the first series of full-size tests, in which Cliffe Hill ballast and tape-like fibres were used. Test results are expressed in terms of sleeper settlement and resilient deflections, longitudinal pressure in the ballast, and contact area at the sleeper-ballast interface.
- Chapter 7 describes the results of a second series of full-size tests, in which Mount Sorrel ballast was used, which was aimed at assessing the performance of a different type of fibre (i.e. filament-like fibres) against the tape-like fibres. As with the first batch of tests,

results are expressed in terms of sleeper settlement and resilient deflections, ballast longitudinal pressure and sleeper-ballast contact area. Moreover, tests permitted to assess particle degradation and, some of them, ballast lateral spreading.

The third part of this report (Chapter 8 and Chapter 9) analyses test results (second part) in conjunction with the literature review (first part) to provide a general description of the effect of fibre addition on the mechanical behaviour of ballasted track, explain the mechanics of fibre reinforced ballast and provide recommendations for future research:

- Chapter 8 considers all test results to improve the general understanding of ballasted track mechanical behaviour, describe the effect of the addition of fibres on it, and provide a likely explanation of the mechanics of fibre reinforcement. The latter, is inferred from the macro-scale behaviour of the samples in combinations with the current-knowledge on the mechanics of ballast and fibre-reinforcement, described mainly in Chapter 3 and Chapter 4 respectively.
- Chapter 9 summarises the main characteristics of the mechanical behaviour of unreinforced and fibre-reinforced ballasted track, and provides recommendations for further research.

2 BALLASTED RAILWAY TRACK

2.1 Introduction

This study focuses on the behaviour of railway ballast and, in particular, on the potential benefits of random fibre reinforcement. However, ballast is only one of the many components forming the railway track, which as a system must provide stability, durability, safety and ride quality. Thus a comprehensive understanding of ballast behaviour requires a general understanding of the behaviour of track structure.

This chapter provides a basic description of the railway structure. The first part presents the main track components and their functions, while the second one describes train loads and how they are transmitted from the wheels to the subgrade through the railway embankment. Finally, the main track characteristics are summarised.

2.2 Rail track structure

The two main types of rail structure are ballasted and slab track. Although the former is the more traditional, it is largely predominant and with good design and maintenance can still satisfy high performance demands, such as those typical of high speed lines. The typical section of ballasted track is shown in Figure 2-1. Its components can be classified into two categories: superstructure and substructure. The former is the upper part, consisting of rails, fastenings and sleepers. The latter is formed of ballast, subballast and subgrade.

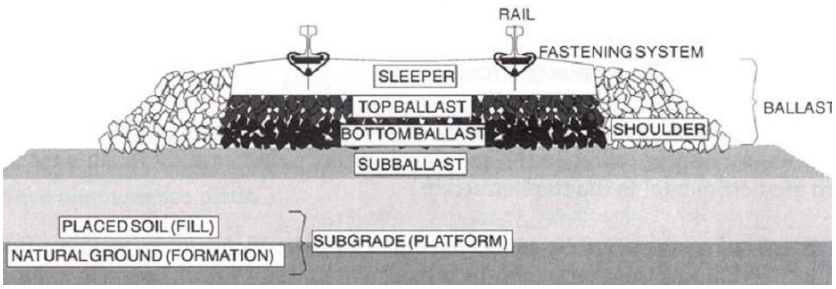

Figure 2-1. Typical section of a ballasted rail track (Selig & Waters, 1994)

2.2.1 Rails

Rails are longitudinal steel elements that guide and support train wheels. Their most important characteristics are their strength, stiffness and smoothness. Rails must be strong and stiff to resist the forces imparted by the wheels and distribute them longitudinally over the adjoining sleepers. They must also have smooth surfaces to guide the wheels, while minimising dynamic effects. Surface defects are associated with load dynamic amplification, which accelerates track deterioration and hence increases maintenance needs. Detailed rail specifications are provided by the standards, e.g. BS EN 13674:2011.

Rails are generally manufactured in fixed lengths and joined using bolts or welds (Figure 2-2). Bolted joints are more traditional and less costly to install and repair. However, they introduce

surface discontinuities, which reduce ride quality and cause stress concentrations. The probability of failure and track deterioration is usually greater in proximity to bolted connections. For this reason, at least on heavily trafficked and high speed lines, they have often been replaced with continuously welded rail (CWR). Although installation and repair costs are higher, CWR can represent a more cost-effective solution, as it reduces maintenance needs. However, it must be observed that CWR does not allow for longitudinal deformation. Thus they need greater lateral confinement to prevent thermal buckling, which can severely damage track geometry (Figure 2-3).

a) b)

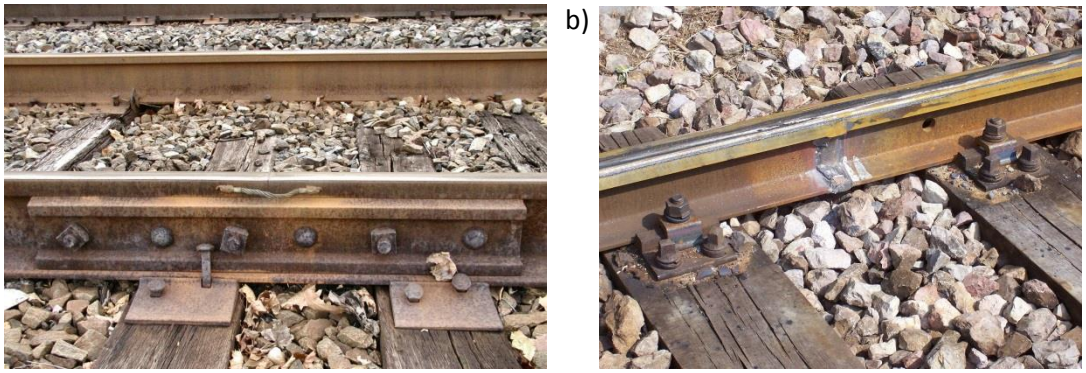

Figure 2-2. a) Bolted joint, b) Continuous welded rails (CWR) (http://en.wikipedia.org/wiki/Track_(rail_transport))

Figure 2-3. CWR track exhibiting thermal buckling (https://tti.tamu.edu/group/crr/current-research/thermal-buckling/)

2.2.2 Rail fastening

Rail fastenings connect the rail to the sleeper. They consist of clips and rail pads (Figure 2-4), permitting only small vertical and rotational movements. Connection deformability improves ride comfort and reduces stress concentration at the rail-sleeper interface, hence the risk of track or vehicle damage. Detailed specifications can be found in the standards, e.g. BS EN 13481:2012.

2.2.3 Sleeper

Sleepers are laid on ballast and connected to the rails through the fastening system. They maintain the correct rail gauge, distribute the rail seat load over the ballast surface at an acceptable stress level and react against crib and shoulder ballast to resist horizontal movements. To exercise these functions sleepers must have adequate strength, stiffness and durability. The

standards classify sleepers based on their material. Typically concrete (BS EN 13230-1:2009; BS EN 13230-2:2009; BS EN 13230-3:2009; BS EN 13230-4:2009; BS EN 13230-5:2009), wood (BS EN 13145:2001+A1:2011) and steel (BS 500:2000). Recently plastic sleepers have also become popular (Draft BS ISO 12856:2012).

Modern sleepers are typically made of pre-stressed concrete and can be mono-block or duo-block. The former comprise a single beam (Figure 2-5a), the latter two separate blocks joined by a steel section (Figure 2-5b). Mono-block sleepers are heavier and hence offer better track stability under dynamic loading. On the other hand, as ballast settlement is greater at the sleeper ends, they are susceptible to centre-binding, i.e. the loss of contact beneath the rail seats (Section 2.3.2.2).

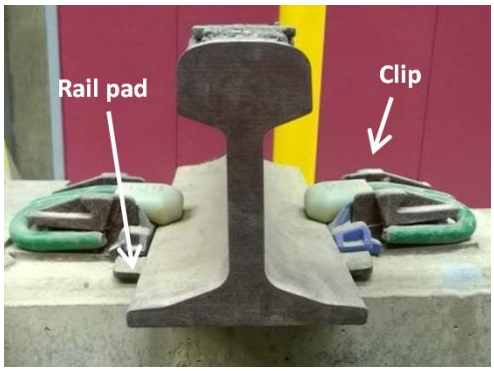

Figure 2-4. Typical sleeper-rail connection

a)

b)

Figure 2-5. (a) Mono-block and (b) duo-block sleeper

2.2.4 Ballast

Ballast is a very coarse aggregate placed beneath, between and beside the sleepers (Figure 2-1). The layer of ballast laid above the sleeper soffit level is called crib ballast while the ballast at either sleeper end is referred to as shoulder.

The main structural functions of the ballast are to provide a stable support for the sleepers, to transmit the loads to subballast and subgrade at an acceptable stress level, to resist horizontal forces, and to provide a certain degree of track confinement, which contributes to track stability

(Section 3.2.2). In addition, ballast provides almost instantaneous drainage, absorbs noise/vibrations and inhibits vegetation growth.

Usually the thickness of the ballast layer is in the range 250 mm to 350 mm, but thicker layers can be used on particularly weak subgrades to further attenuate stresses. Shoulders are usually laid at an angle up to 45 degrees to the horizontal plane, i.e. close to ballast natural angle of repose. However, shallower shoulders provide greater confinement and hence increase the resistance to lateral forces, reduce the probability of thermal buckling and inhibit ballast permanent deformations (Abadi et al., 2016b).

Ballast is usually obtained from freshly crushed high quality aggregate, as prescribed by BS EN 13450:2002, but the type of rock depends on local availability. Its most important characteristics are the particle size distribution (PSD), the particle shape and surface roughness, and the resistance of the parent rock to mechanical and chemical actions.

The PSD affects ballast behaviour under both monotonic and cyclic loading. Norms usually prescribe uniform gradations to guarantee almost instantaneous drainage and avoid particle segregation. For example, according to the British Standards the PSD must fall within one of the six categories shown in Table 2-1 and, in particular, Network Rail requires it to fall within category A, represented in Figure 2-1. However, as will be explained in Section 3.4.2, well-graded ballast has greater shear strength and exhibits smaller permanent deformations under repeated loads, owing to the smaller volume of voids, the higher particle coordination number and the greater sleeper-ballast contact area.

Particle shape and roughness have a great influence on material strength and resistance to plastic deformations. In particular, angular particles provide a higher degree of interlocking (i.e. greater ability of particles to fit together firmly, for example, through their surface projections) which increases ballast strength and reduces plastic deformation (Holtz & Gibbs, 1956; Raymond, 2002; Indraratna et al., 2011); similarly, particle surface roughness contributes to interlocking through the mobilisation of interparticle resistance (Raymond, 1985; Thom & Brown, 1988; Thom & Brown, 1989; Indraratna et al., 2011).

Ballast must be obtained from strong and weathering-resistant rock as mechanical and chemical actions can break down particles diminishing track durability (Section 3.3.3). For example, granite, widely used on UK lines, provides adequate resistance to mechanical and chemical actions. It contains minerals of very different hardness and hence, although it wears faster than uniformly hard rocks, maintains freshly rough particle surfaces (Lees & Kennedy, 1975).

Finally, it must be mentioned that ballast accumulates plastic deformations under repeated loading that, if non-uniformly distributed, alter track geometry. This process is essential to this research and is discussed in more detail in Chapter 3.

Table 2-1. Categories of ballast grading (BS EN 13450:2002.)

Sieve size mm	Railway ballast size 31,5 mm to 50 mm			Railway ballast size 31,5 mm to 63 mm		
	Percentage passing by mass					
	Grading category					
	A	B	C	D	E	F
80	100	100	100	100	100	100
63	100	97 to 100	95 to 100	97 to 99	95 to 99	93 to 99
50	70 to 99	70 to 99	70 to 99	65 to 99	55 to 99	45 to 70
40	30 to 65	30 to 70	25 to 75	30 to 65	25 to 75	15 to 40
31,5	1 to 25	1 to 25	1 to 25	1 to 25	1 to 25	0 to 7
22,4	0 to 3	0 to 3	0 to 3	0 to 3	0 to 3	0 to 7
31,5 to 50	≥ 50	≥ 50	≥ 50	-	-	-
31,5 to 63	-	-	-	≥ 50	≥ 50	85

NOTE 1 The requirement for passing the 22,4 mm sieve applies to railway ballast sampled at the place of production.

NOTE 2 In certain circumstances a 25 mm sieve may be used as an alternative to the 22,4 mm sieve when a tolerance of 0 to 5 would apply (0 to 7 for category F).

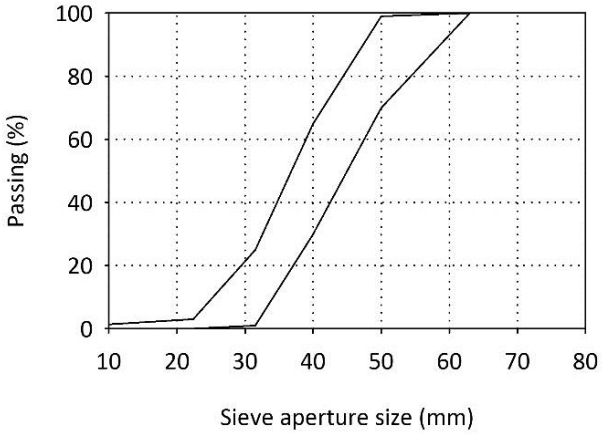

Figure 2-6. Ballast grading category A (plotted on linear axes, as ballast is very uniform)

2.2.5 Subballast

Subballast is a 100 mm to 150 mm thick layer of granular material, e.g. sand or well-graded gravel, separating the ballast from the subgrade. Its main functions are load distribution, drainage and separation/filtering. Subballast must be well-compacted to distribute the load uniformly and evenly over the subgrade. Moreover, its PSD must be properly selected to dissipate the pore water pressures generated under cyclic loading while preventing the upward migration of fines and reducing the attrition with the natural soil, which otherwise can form slurries (Selig & Waters, 1994). The subballast layer should be always present on modern railway tracks, although the use of geosynthetics as separator layers may allow reducing its thickness (Sharpe & Caddick, 2004).

2.2.6 Subgrade

Subgrade is natural soil, placed fill material or a combination of them. Usually it is the weakest part of the substructure and track components must be designed to attenuate the wheel load seen by the subgrade to acceptable levels. Although the subgrade is subjected to relatively small stresses, it can exhibit significant resilient deflections. Especially when critical speed issues are expected (e.g. on high speed lines), natural soil might have to be reinforced to limit the amplitude

of track deflections to levels compatible with train passage (Hu et al., 2016; Mezher et al., 2016). Moreover, as observed in Section 3.4.3, softer subgrades are typically associated with greater plastic deformation of the ballast layer.

2.3 Train load

2.3.1 Wheel force

Track forces are associated with train passage and temperature variations. Train wheels exert vertical, lateral and longitudinal forces on the track. Vertical and lateral forces are associated with vehicle axle weight, centrifugal force and wind pressure. The longitudinal forces are determined by vehicle acceleration. Temperature variations cause significant longitudinal stresses in continuously welded rails that, if track confinement is inadequate, lead to track lateral buckling. For the purpose of this research, only the component of the wheel force perpendicular to the track is considered, as it is the main cause of ballast degradation.

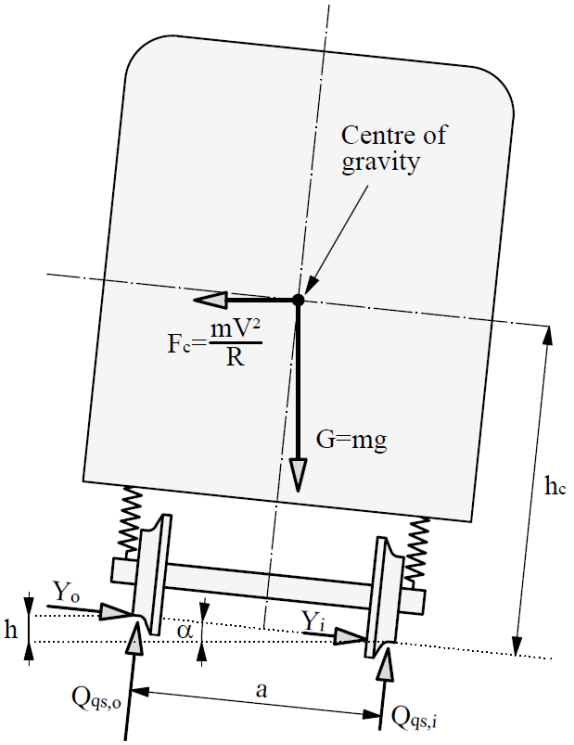

Figure 2-7. Quasi-static train forces, as represented in Priest et al. (2013)

The normal reaction at the rails Q is composed of a quasi-static component Q_{qs} and a dynamic component Q_d:

$$Q = Q_{qs} + Q_d \tag{2-1}$$

The quasi-static forces acting on a train of mass per wheelset m (and weight G) travelling at speed V on a curve of radius R and cant h (cant angle α) and subjected to negligible wind pressure are shown in Figure 2-7, where h_c is the distance between track and centre of gravity, F_c is the centrifugal force that considers the centripetal acceleration according to D'Alambert's principle,

$Q_{qs,o}$ and $Q_{qs,i}$ are the normal reactions at the outer and inner rail, and $Q_{qs,o}$ and $Q_{qs,i}$ are the lateral ones. The quasi-static rail reactions can be calculated via simple equilibrium equations. In particular, the normal reaction at the outer rail, which is the main responsible for ballast deterioration, is:

$$Q_{qs,o} = \frac{mg}{2}\left(\cos\alpha - 2\,\frac{h_c}{a}\,\sin\alpha\right) + \frac{mV^2}{R}\left(\frac{h_c}{a}\cos\alpha + \frac{\sin\alpha}{2}\right) \tag{2-2}$$

The dynamic component Q_d is more difficult to evaluate, being affected by several factors (e.g. vehicle weight and speed, track irregularities, rail and wheel conditions, substructure properties, bogie characteristics etc.). Thus, for simplicity, it is often estimated as the product of the quasi-static component Q_{qs} and an empirical coefficient DAF, namely the dynamic amplification factor:

$$Q = Q_{qs}\,(1 + DAF) \tag{2-3}$$

The dynamic amplification factor is usually calculated using empirical correlations. Typically, it is expressed as a function of V or V/D_w, where D_w is the wheel diameter, while the other factors affecting the dynamic response are implicit in the empirical coefficients (Sadeghi, 2008). For example, as cited in Indraratna et al. (2011), Li & Selig (1998) proposed the following expression, which is recommended by the American Railway Engineering Association (AREA):

$$DAF = (1 + 0.0052\,V/D_w) \tag{2-4}$$

where V is the train speed in km/h and D_w is the wheel diameter in metres. Similarly, prEN-13230-6:2014 suggests calculating the dynamic factor as a function of V, as shown in Figure 2-8. However, the suggested values of DAF are based on field measurements in typical track conditions and are calculated as the mean plus two times the standard deviation. Thus, for particularly well maintained tracks they may be over-conservative, as observed in prEN-13230-6:2014.

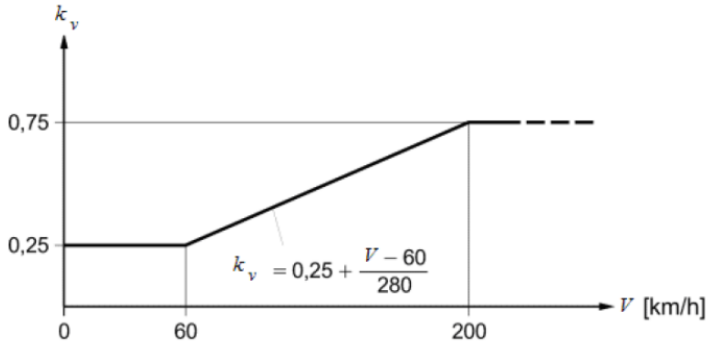

Figure 2-8. Load amplification factor in typical track conditions according to prEN-13230-6:2014; k_v is equivalent to the dynamic amplification factor DAF

2.3.2 Load distribution

The total wheel force is transmitted to the track in three steps:

1. It is imparted to the rails, which distribute it longitudinally between the sleepers, while the dynamic effects are damped by the rail pads.

2. The rail seat forces are spread by the sleepers over a limited number of sleeper-ballast contact points.
3. The contact forces diffuse through the substructure and reach the subgrade.

Each of the points above is discussed in more detail in the following sections. In particular, simple methods to estimate sleeper forces and stresses in the substructure are presented.

2.3.2.1 Longitudinal load distribution

The rails distribute the wheel load longitudinally and the Winkler method, based on the theory of the beam on elastic foundation (BOEF), is typically used to estimate the forces imparted to each sleeper (Esveld, 2001; Indraratna et al., 2011; prEN-13230-6:2014).

The governing equation for a uniform straight rail on elastic foundation is:

$$E_r I_r \frac{\partial^4 w_r}{\partial x^4} + p(x) = q(x) \tag{2-5}$$

where $w_r(x)$ is the rail deflection, $q(x)$ is the distributed load, $p(x)$ is the elastic base reaction, x is the coordinate along the length of the rail, and E_r and I_r are the rail Young modulus and second moment of area respectively. The elastic reaction $p(x)$ is the product of the support stiffness k_w and the vertical deflection $w_r(x)$:

$$p(x) = k_w w_r(x) \tag{2-6}$$

By substituting (2-6) into (2-5), the governing equation becomes:

$$E_r I_r \frac{\partial^4 w_r}{\partial x^4} + k_w\, w_r(x) = q(x) \tag{2-7}$$

The analytical solution of Equation (2-7) for an infinite straight rail subjected to the wheel force Q applied in $x = 0$ is:

$$w_r(x) = \frac{Q\ \lambda_k}{2\ k_w}\ e^{-\lambda_k x}\ (\cos \lambda_k x + \sin \lambda_k x) \tag{2-8}$$

$$p(x) = \frac{Q\ \lambda_k}{2}\ e^{-\lambda_k x}\ (\cos \lambda_k x + \sin \lambda_k x) \tag{2-9}$$

where λ_k is the characteristic length, defined as:

$$\lambda_k = \sqrt[4]{\frac{k_w}{4E_r I_r}} \tag{2-10}$$

As sleepers provide a discrete support, the following assumptions are necessary to calculate the sleeper forces:

$$F_r(x) = s\ p(x) \tag{2-11}$$

$$k_r = s\ k_w \tag{2-12}$$

where $F_r(x)$ is the rail seat force at a distance x from the wheel, k_r is the rail support stiffness and s is the sleeper spacing. By substituting (2-11) and (2-12) into (2-8), (2-9) and (2-10), the solution of the governing equation can be rewritten as follows:

$$w_r(x) = \frac{Q\ \lambda_k\ s}{2\ k_r}\ e^{-\lambda x}\ (\cos\lambda_k x + \sin\lambda_k x) \tag{2-13}$$

$$F_r(x) = \frac{Q\ \lambda_k\ s}{2}\ e^{-\lambda_k x}\ (\cos\lambda_k x + \sin\lambda_k x) \tag{2-14}$$

$$\lambda_k = \sqrt[4]{\frac{k_r/s}{4E_r I_r}} \tag{2-15}$$

The equations above can be used to calculate rail seat deflections and loads (w_r, F_r) knowing the rail section characteristics (E_r, I_r), the rail support stiffness (k_r), the sleeper spacing (s) and the wheel force (Q).

The BOEF theory accounts for the longitudinal distribution of the quasi-static wheel force. However, rail seat loads are affected by other factors, e.g. the dynamic effect and variability of the support stiffness. For example, prEN-13230-6:2014 suggests using the model shown in Figure 2-9, where A_{nom} is the quasi-static component of the axle force, k_v is the dynamic amplification factor, k_p is a dynamic attenuation factor and k_d accounts for the load longitudinal distribution. The dynamic amplification factor k_v can be calculated as explained is Section 2.3.1. The factor k_p accounts for the presence of the rail pads and ranges from 0.78 (high attenuation pads) to 1 (low attenuation pads). The factor k_d can be calculated using the Winkler method or, for standard tracks (i.e. rails heavier than 46 kg/m and a < 65 cm), assumed equal to 0.5, meaning that typically only 50% of the wheel force reaches the sleeper directly underneath it. Finally, the design rail seat load is obtained by amplifying the maximum load by 1.35 to account for the variability of the support conditions.

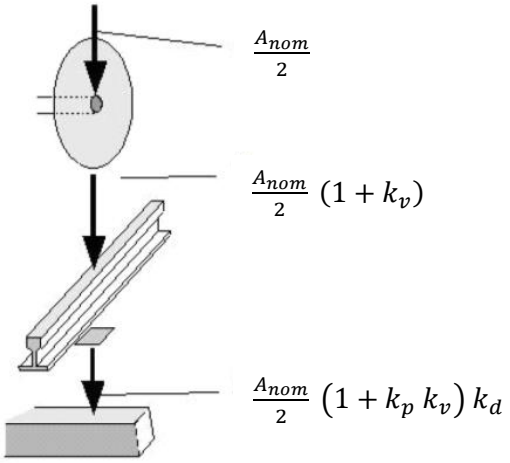

Figure 2-9. Force transmission from wheel to sleepers; A_{nom} is the quasi-static axle load; k_v , k_p and $k_d$account for dynamic effects, rail pads and longitudinal distribution respectively (prEN-13230-6:2014).

2.3.2.2 Load distribution over ballast surface

Ballast provides the sleeper with a discrete support, as ballast particle size (in the range 25 mm to 50 mm) is significant compared with sleeper dimensions (i.e. about 300 mm x 2500 mm). It has been estimated that for a mono-block concrete sleeper on standard graded ballast the total number of contact points, although it varies over time, falls within 100 and 200 (Shenton, 1978; Abadi et al., 2015). However, Abadi et al. (2015) observed that the number of contacts can be increased through interventions to the ballast layer (e.g. the increase in proportion of finer particles), the use of different sleeper types (e.g. wooden or plastic sleepers) or the use of Under Sleeper Pads (USPs).

Although at discrete points, ballast reaction is usually assumed to form a continuous stress distribution. It is widely known that the stress distribution at the sleeper-ballast interface is not uniform and varies over time. Experimental investigations have shown that stresses follow a ω-shaped distribution, such as that represented in Figure 2-10, which becomes more uniform over time, as the sleeper-ballast contact beneath the rail seats reduces (Talbot, 1933; Shenton, 1978; Sadeghi, 2008; Abadi et al., 2015). This is associated with the accumulation of plastic deformations in the substructure, especially beneath the sleeper ends, where the confinement is smaller (Section 3.2). Eventually, it may lead to the formation of a gap between the sleeper ends and the ballast, with the sleeper being supported mainly at its centre. This condition is known as sleeper centre-binding and is associated with particularly large deflections of the sleeper ends and rails, which may jeopardise the safety of train operations. Therefore, periodic maintenance operations, e.g. tamping, are required to stabilise the track by compacting the ballast underneath the rail seats. A successful tamping restores the support between the sleeper ends and the ballast, hence accentuate the ω-shaped distribution of the ballast pressures (Figure 2-11, Sadeghi, 2010).

For design purposes, the pressure distribution is often over-simplified. A typical simplification involves assuming a constant ballast reaction beneath the rail seats over an effective length, as shown in Figure 2-12, where Q is the wheel load, u is the distance between the rail and the sleeper end and $2u$ is the effective length.

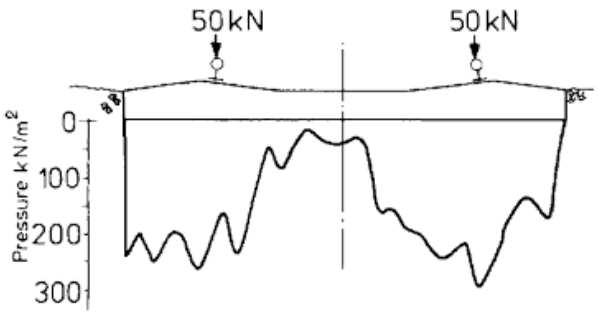

Figure 2-10. Stresses beneath the sleeper from field measurements (Shenton, 1978)

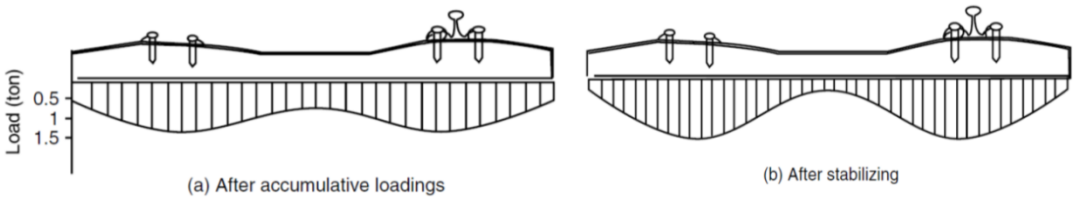

Figure 2-11. Representation of the stresses beneath the sleeper (a) before and (b) after tamping according to field measurements (Sadeghi, 2010)

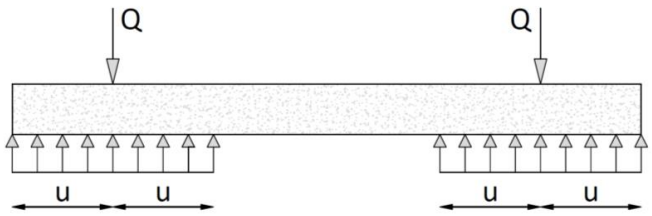

Figure 2-12. Simplified sleeper-ballast stress distribution by Esveld (2001)

2.3.2.3 Substructure pressures

There are several methods to evaluate the stresses in the substructure. A simple approach consists of assuming that the ballast, subballast and subgrade behave as semi-infinite elastic media so that known elastic analytical solutions can be used. For a point load the analytical solution is well-known (Boussinesq, 1985). For different loading conditions (e.g. uniformly loaded line, strip or rectangular area) stresses can be obtained through integration of the point load solution. In particular, the stresses in the substructure can be calculated using the solutions for uniformly loaded rectangular area provided by Steinbrenner (1934) or Newmark (1935). As illustrated in Venkatramaiah (2006), Steinbrenner's solution is expressed in graphical form (Figure 2-13) while Newmark's solution is expressed by the following equation:

$$\sigma_z = \frac{q}{4\,\pi}\left[\frac{2\,m\,n\,\sqrt{m^2+n^2+1}}{m^2+n^2+1+m^2\,n^2}\cdot\frac{m^2+n^2+2}{m^2+n^2+1}+\tan^{-1}\frac{2\,m\,n\,\sqrt{m^2+n^2+1}}{m^2+n^2+1-m^2\,n^2}\right] \qquad (2\text{-}16)$$

where $m = B/z$ and $n = L/z$ while B, L and z are as shown in Figure 2-13. For further simplification, stresses can be assumed to dissipate with depth in the form of a trapezoid whose sides have an inclination of 2:1 (Figure 2-14).

It must be observed that the methods above provide only a first estimate of the stresses within the substructure as they do not account for stiffness variations between layers, the rigidity of the loaded area and material non-linearities. Therefore, more sophisticated numerical analyses are desirable for an accurate evaluation of the stresses in the substructure, e.g. analyses using the finite element method (FEM) or the Discrete Element Method (DEM).

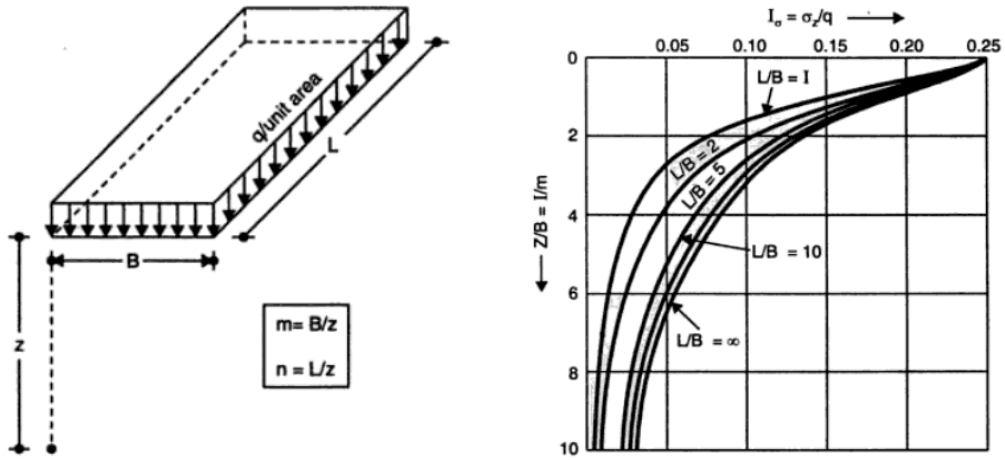

Figure 2-13. Steinbrenner's solution (Steinbrenner, 1934) for a uniformly loaded area, as illustrated in Venkatramaia (2006)

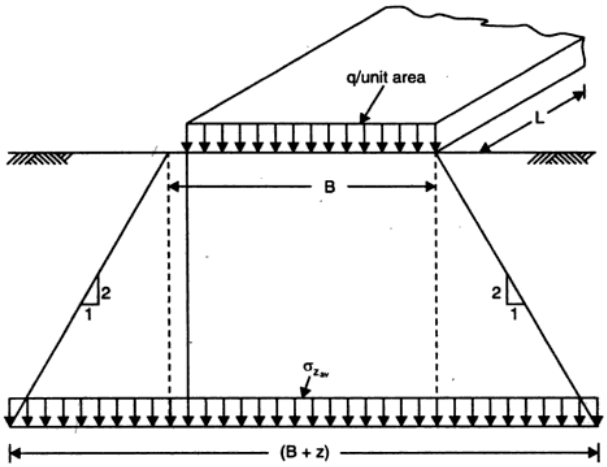

Figure 2-14. Two is to one method (Venkatramaiah, 2006)

2.4 Summary

Ballast is only one of the many components forming the railway to provide stability, durability, ride quality and maintain safe train operations. Track components are classified into two categories: superstructure (rails, fastenings and sleepers) and substructure (ballast, subballast and subgrade). The main characteristics of each component are as follows:

- Rails resist the wheel loads, distribute them longitudinally over the sleepers and provide smooth support for vehicle wheels.
- Fastenings connect rails to sleepers, permitting small vertical and rotational relative movements to improve ride comfort and reduce stress concentrations at the rail-sleeper interface.
- Sleepers spread the rail load over the ballast surface at an acceptable pressure level, maintain rail gauge and react against crib and shoulder ballast to resist longitudinal and lateral movements.

- Ballast is a very coarse aggregate, preferably obtained from crushed high quality rock, that distributes the loads to the subgrade, limits track deformations, resists horizontal movements, confines the track, provides almost instantaneous drainage, absorbs noise/vibrations and inhibits weed growth. Its PSD is uniform to avoid particle segregation and provide adequate drainage; its particles should be angular and rough for high degrees of interlocking. Its parent rock should be selected to offer good resistance to mechanical and chemical actions.

- Subballast is sand or well-graded aggregate that separates ballast from subgrade, spreads the load over the subgrade and provides drainage.

- Subgrade is natural soil, placed fill material or a combination of them; it is usually softer than ballast and can be responsible for significant track resilient deflections; softer subgrades are associated with greater ballast plastic deformations.

Train wheels impart a combination of quasi-static and dynamic forces to the track. Quasi-static forces are calculated using equilibrium equations. Dynamic forces are usually estimated as the product of the quasi-static component and an empirical coefficient, i.e. the dynamic amplification factor. The wheel force is transmitted to the track in three steps:

- It is imparted to the rails, which distribute it longitudinally over the sleepers while the dynamic effects may be damped by the rail pads; sleeper forces can be calculated using the BOEF theory; usually about 50% of the wheel force reaches the sleeper underneath it.

- Sleeper forces are spread over a few hundred contact points but are usually regarded as a continuous stress distribution; stresses follow a ω-shaped pattern which becomes more uniform with track deterioration due to the reduction of contact beneath the rail seats and eventually may reverse, owing to sleeper centre-binding.

- Contact forces diffuse through the substructure to reach the subgrade; stresses can be estimated assuming the substructure to behave as a semi-infinite elastic medium or that the stresses propagates following a 2:1 trapezoid distribution; however, to account for the presence of layers of different stiffnesses and material non-linearities, more complex methods should be adopted, e.g. FEM.

3 BALLAST DETERIORATION

3.1 Introduction

In response to the stresses induced by train passage, track substructure exhibits plastic deformations, leading to track settlement. Uniform settlement does not pose much threat to train traffic. In contrast, differential settlements deteriorate track geometry, as they lead to irregularities in the track geometry which, if excessive, can pose a severe threat to track safety and ride quality. Unfortunately, as substructure deformations are affected by the natural non-homogeneity of geomaterials and the variations of the underlying geology and track build quality, the development of track irregularities is inevitable. Thus, periodic maintenance operations, e.g. tamping, are carried out to restore track geometry and hence, ride quality and safety. Moreover, increasingly onerous loads are being placed on existing ballasted track networks in many parts of the world by more frequent, longer, faster and heavier trains. This reduces the windows of time for maintenance activities while increasing maintenance needs.

Ballast deterioration with train passage, i.e. the accumulation of plastic deformations under repeated loads, is a primary mechanism of track geometry deterioration, as it is the major cause of track settlement (Selig & Waters, 1994). Thus understanding ballast behaviour under cyclic loading is key to developing techniques to extend track life cycle. This chapter describes the process of ballast deterioration and some existing improvement techniques. It is organised in three parts:

- Part one provides an insight into track settlement response, and describes the phases and regimes of ballast permanent deformation under train loading.
- Part two discusses the physical mechanisms responsible for the accumulation of plastic deformation.
- Part three describes five existing techniques for reducing track settlement through interventions on the ballast layer: variation of ballast grading, reinforcement through geogrids, 3D cellular reinforcement, injection of 3D polymeric reinforcement, and addition of crumb rubber.

This chapter provides essential information to understand ballast behaviour, interpret experimental data and assess the advantages (and disadvantages) of fibre reinforcement compared with other improvement methods.

3.2 Ballast permanent deformation

3.2.1 Settlement vs number of cycles curve

As explained in Section 3.1, the main cause of track geometry deterioration is the development of differential settlements in the ballast layer. Differential settlements are associated with the variability of track and soil characteristics and hence cannot easily be reproduced either

experimentally or numerically. However, the average settlement can be used to assess ballast susceptibility to plastic deformation, assuming it to be approximately proportional to the differential settlements. This is justified by field observations carried out by foundation engineers (Skempton & MacDonald, 1956; Ricceri & Soranzo, 1985). For example, Ricceri & Soranzo (1985) reported settlement measurements for a large number of structures built on different types of soil, finding a correlation between the maximum settlement (ρ_{max}) and the angular distortion ($\delta\rho/L$), where $\delta\rho$ is the relative settlement and L the distance between two consecutive points (Figure 3-1). Similarly, in railway engineering, the irregularities in the track geometry are expected to be proportional to the settlement.

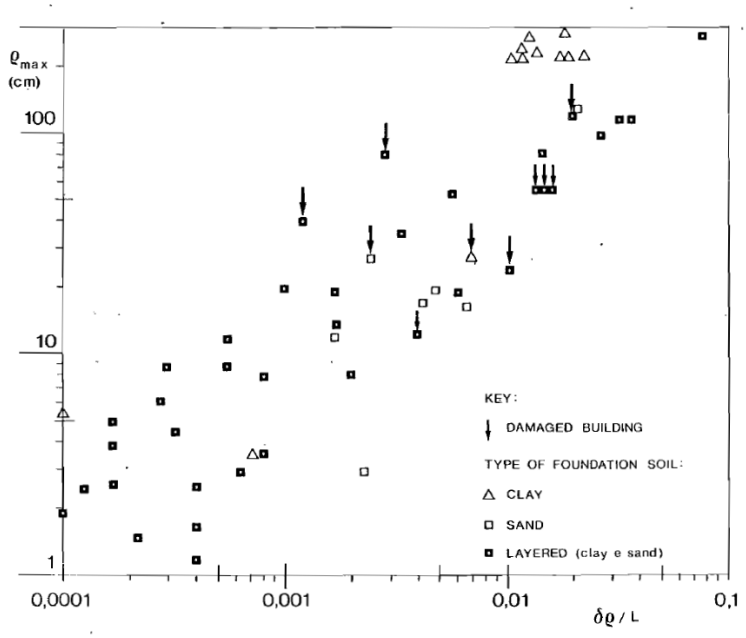

Figure 3-1. Correlation between the maximum settlement (ρ_{max}) and the angular distorsion ($\delta\rho/L$) for structures on different foundation soil (Ricceri & Soranzo, 1985)

Many experimental studies have shown the effect of repeated loading on ballast settlement response (Guérin et al., 1999; Raymond, 2002; Raymond & Ismail, 2003; Sharpe & Caddick, 2004; Brown et al., 2007; Lackenby et al., 2007; Aursudkij et al., 2009; Sun et al., 2014; Indraratna, Thakur, et al., 2010; Indraratna, Nimbalkar, et al., 2010; Leshchinsky & Ling, 2013; Indraratna & Nimbalkar, 2013; Kennedy et al., 2013; Thakur et al., 2013; Aingaran, 2014; Al-Saoudi & Hassan, 2014; Hussaini et al., 2015; Sol-Sánchez et al., 2015; Abadi et al., 2016b; Sol-Sánchez et al., 2016). In general, the relationship between settlement and number of loading cycles is strongly non-linear. In fact, after a rapid initial increase in permanent deformation in the first cycles the settlement rate reduces dramatically. The settlement then increases fairly linearly with the logarithm of the number of cycles, and hence it is often plotted on semi-logarithmic axes. As an example, Figure 3-2 shows typical settlement curves obtained using a large prismoidal triaxial apparatus, plotted on unscaled and semi logarithmic axes. The authors observed that all samples settled rapidly in the first 100,000 cycles, beyond which the settlement rate was small (Indraratna et al., 2011).

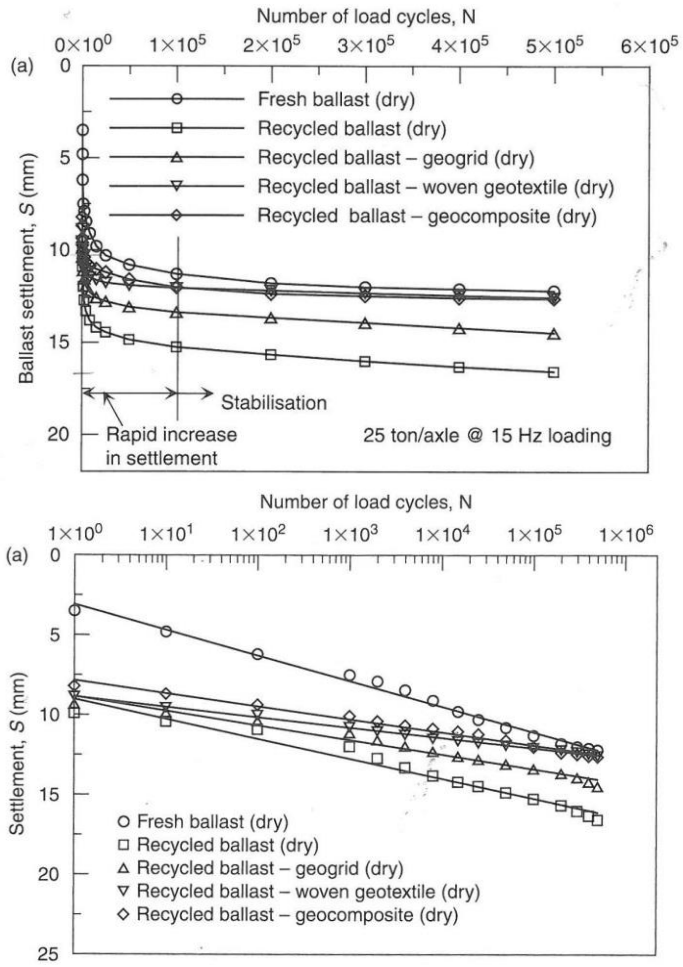

Figure 3-2. Ballast settlement response: a) unscaled axes, b) semi-logarithmic scale (after Indraratna et al., 2011)

A number of empirical models have been proposed to "predict" the settlement, typically as a function of the number of cycles and the load magnitude (Dahlberg, 2001; Abadi et al., 2016a). Abadi et al. (2016a) compared some settlement "predictions" with the results from two full-size tests. The "predictions" were obtained using the models summarised in Table 3-1, where ε is the permanent deformation, S (or d) is the settlement, ε_1 and d_1 are respectively the permanent strain and settlement after the first cycle, and N is the number of cycles. The two full-size tests were carried out at a frequency of 3Hz and are representative of a 20 tonne and a 32 tonne train axle load. As shown in Figure 3-3, the existing models cannot accurately reproduce the experimental results. This is not surprising as most of them account for only a few of the factors affecting ballast settlement, typically the number of cycles and load magnitude. Some models implicitly include other variables within ε_1 (or d_1), as some studies showed the settlement to be a function of the settlement accumulated in the first cycle (Alva-Hurtado and Selig, 1981; Indraratna et al., 2010). However, this can only be true under certain conditions.

It can be concluded that the empirical models found in literature cannot predict track settlement in practical cases because they do not account for the many factors affecting ballast response to cyclic loading. In particular, ballast behaviour depends on: loading conditions (e.g. magnitude, frequency and history), sleeper characteristics (e.g. type and spacing), ballast particle characteristics (e.g. size, shape, angularity, roughness and strength), initial conditions of the

ballast (e.g. density), track geometry (e.g. ballast depth and shoulder dimensions), subgrade/subballast characteristics (e.g. stiffness and frictional properties) and presence of reinforcements (e.g. geogrids and geotextiles).

Table 3-1. Some settlement models (Abadi et al., 2016a)

Model label	Model	Reference	Variables	Empirical constants
ORE	$\varepsilon_N = 0.082\,(100n - 38.2)(\sigma_1 - \sigma_3)^2 \times (1 + 0.2 \log N)$	ORE (1970)	n= porosity, σ_1 & σ_3= principle stresses	
Shenton 1	$\varepsilon_N = \varepsilon_1(1 + 0.2 \log_{10} N)$	Shenton (1978)		
Shenton 2	$S = K_s \frac{A_e}{20}\left(\begin{matrix}(0.69 + 0.028L)\, N^{0.2} + \\ (2.7 \times 10^{-6})N\end{matrix}\right)$	Shenton (1984)	A_e= average axle load, L= tamping lift	K_s
Hettler	$S_N = r\,(F)^{1.6}\,(1 + C \ln (N))$	Hettler (1984)	F= force	C, r
Alva-Hurtado	$\varepsilon_N = (0.85 + 0.38 \log N)\,\varepsilon_1 + (\varepsilon_1)^2 \times (0.05 - 0.09 \log N)$	Alva-Hurtado & Selig (1981)		
Stewart 1	$\varepsilon_N = \varepsilon_1(1 + C \log_{10} N)$	Stewart & Selig (1984)		C
Stewart 2	$d_N = d_1(1 + C_b \log N)$			C_b
Selig 1	$\varepsilon_N = \varepsilon_1(1 + C \log N)$	Selig & Waters (1994)		C
Selig 2	$S_N = 4.318\, N^{0.17}$			
Selig 3	$\varepsilon_N = 0.0035\, N^{0.21}$			
Thom 1	$S = [\log_{10} (N) - 2.4]^2$	Thom & Oakley (2006)		
Thom 2	$S = [\log_{10} (N) - 2.4]^2 \left(\frac{\sigma}{160}\right)\left(\frac{47}{k_s}\right)$		σ= vertical pressure, k_s=subgrade stiffness	
Cedex	$S_N = 0.07\, N^{0.1625}$	Cuellar et al (2011)		
Indraratna	$S_N = S_1(a \log N + 1)$	Indraratna et al (2013)		a

3.2.2 Phases and regimes of ballast settlement

According to laboratory tests, two phases of ballast settlement have been identified: 1) post-compaction densification and 2) long-term settlement (Guérin et al., 1999; Dahlberg, 2001; García-Rojo et al., 2005; Indraratna & Nimbalkar, 2013; Abadi et al., 2016a).

Phase 1 consists of ballast rapid densification in the first load cycles due to particle rearrangements triggered by particle slippages and reorientations. According to Indraratna & Nimbalkar (2013), the rapid densification is also caused by significant particle breakage. However, as explained in Section 3.3.3, particle breakage is usually very limited, at least for strong parent rock materials (like granite), and hence not expected to significantly contribute to the development of plastic deformations. The duration of Phase 1 can vary within a wide range. Indraratna et al. (2011) and Abadi et al. (2016a) observed that its possible duration is 100,000 cycles, corresponding to the second inflection point of the settlement curve plotted on semi logarithmic axes (Figure 3-2 and Figure 3-4). Guérin et al. (1999) noted that it can range from 50,000 cycles to 800,000 cycles depending on the compaction technique used, hence the initial sample density. In the light of this, it is not surprising that Phase 1 is the most affected by experimental variability (Guérin et al., 1999) and that the very first cycles are sometimes disregarded to mitigate the effect of the variability of initial sample conditions (Anderson & Fair, 2008; Abadi, 2014; Aursudkij et al., 2009).

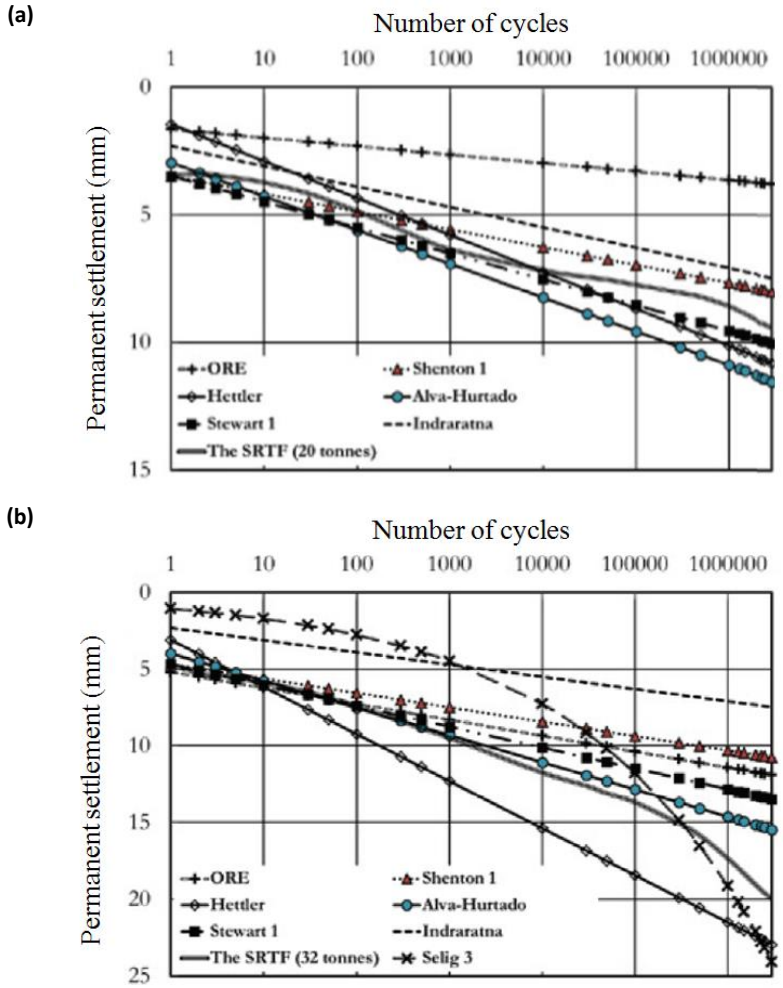

Figure 3-3. Comparison between full size test results (SRTF) and predictions; (a) 20 tonne and (b) 32 tonne train axle (Abadi et al., 2016a)

In the long term, i.e. Phase 2, ballast response is dependent on the severity of the loading, although it is usually characterised by small settlement rate (Section 3.2.4). In general, the behaviour of discrete systems, e.g. soils, subjected to cyclic loading can be described by means of the shakedown concept (Sharp & Booker, 1984; Johnson, 1986; Alonso-Marroquín & Herrmann, 2004; García-Rojo et al., 2005; Sun et al., 2014; Li et al., 2016; Klarbring et al., 2017), which identifies four types of response: elastic, elastic shakedown, plastic shakedown and ratcheting. The types of behaviour are shown schematically in Figure 3-6. If the load amplitude is smaller than the elastic limit, material response is purely elastic and the deformation is recovered after each cycle. When the load magnitude is between the elastic shakedown limit and the plastic shakedown limit, plastic strains are accumulated for a finite number of cycles but eventually the excitation is said to “shakedown” and the response becomes fully resilient (i.e. reversible). In particular, for loads below the elastic shakedown limit the long-term response is purely elastic, otherwise it degenerates into a closed loop, meaning that it becomes resilient but the system can still dissipate energy. Beyond the plastic shakedown limit, plastic strains are accumulated for an indefinite number of cycles due to a slip-stick mechanism usually termed ratcheting, which is described in more detail in Section 3.3.2.

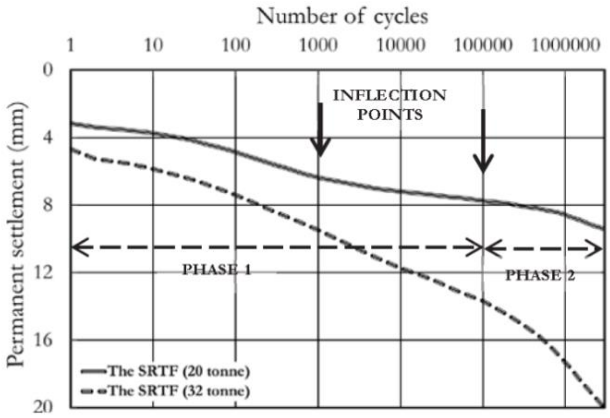

Figure 3-4. Settlement vs number of cycles curves; full size tests on railway ballast (Abadi et al., 2016a)

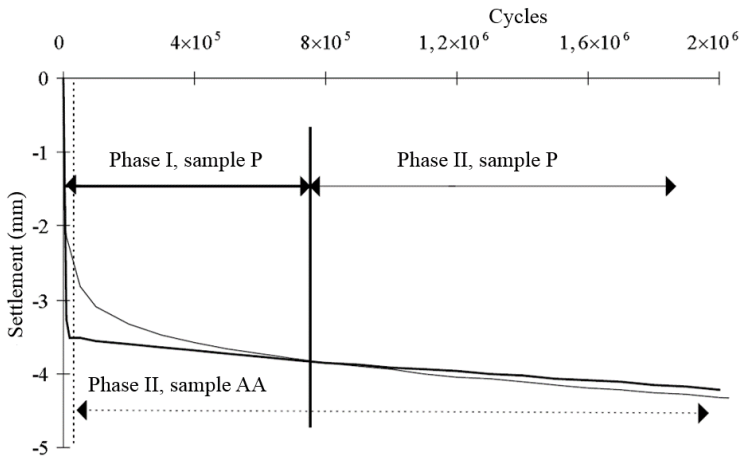

Figure 3-5. Settlement vs number of cycles curves; 1/3 scaled ballast; sample AA, compacted through percussion, has initial bulk density of 1.9 Mg/m^3; sample P, compacted through vibration, has initial bulk density of 1.8 Mg/m^3 (Guérin et al., 1999)

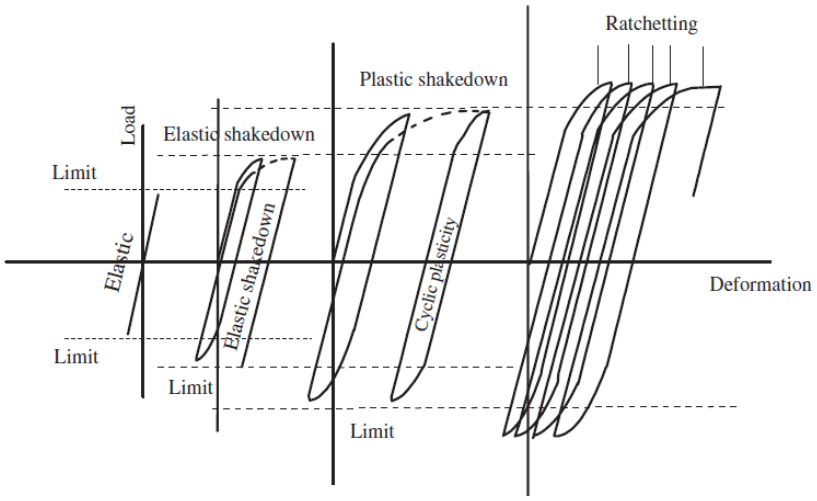

Figure 3-6. Types of shakedown response to cyclic loading (Johnson, 1986; Qian et al., 2016)

The shakedown concept has been used to describe ballast settlement response to cyclic loading (Suiker et al., 2005; Lackenby et al., 2007; Sun et al., 2014; Li et al., 2016). In particular, Sun et al. (2014), based on large triaxial tests carried out by Lackenby et al. (2007), identified three regimes of ballast plastic deformation depending on the applied stress ratio: (I) shakedown, (II) ratcheting and (III) plastic collapse. The values of applied stress ratio associated with each regime are shown in Figure 3-7 for a confining pressure (σ_c) of 60 kPa, representative of track confinement. A purely elastic response was never observed, as ballast behaviour is strongly inelastic and plastic strains are always accumulated. This is in agreement with Alonso-Marroquín & Herrmann (2004) who, based on discrete element analyses, excluded the existence of a purely elastic regime for granular materials subjected to cyclic loading. Shakedown was exhibited when the applied stress ratio was smaller than about 2.3. Ratcheting was distinguished from plastic collapse. The former, in agreement with discrete element analyses (Alonso-Marroquín & Herrmann, 2004; García-Rojo et al., 2005), is characterised by fairly constant long-term settlement rate and was observed for q/p' less than 2.4. For greater applied loads, the settlement rate increased with the cycles leading to the plastic collapse of the structure. Examples of ballast settlement response under increasing load magnitude and frequency are shown in Figure 3-8 and Figure 3-9 respectively. The latter is to some extent representative of the effect of train speed which, as explained in Section 3.2.3, can be related to the loading frequency.

Railway tracks must be designed not only to avoid the plastic collapse but also to minimise the permanent deformation. For this purpose, although ballast response cannot easily be predicted (Section 3.2.1), experiments must be properly designed to provide an indication of track geometry deterioration (Section 3.1). In particular, they must reproduce faithfully ballast stresses under train passage.

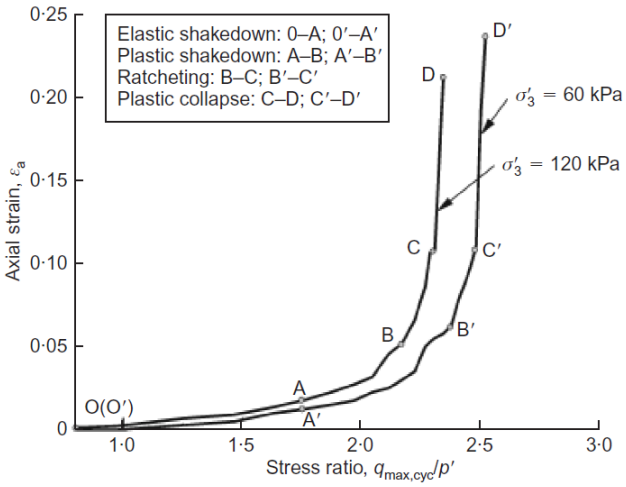

Figure 3-7. Regimes of plastic deformation based on large scale triaxial tests on railway ballast carried out at frequency of 20 Hz (Sun et al., 2014)

3.2.3 Ballast stresses

The accumulation of plastic deformations in the ballast layer under cyclic loading is the primary cause of track geometry deterioration (Section 3.2.2) and, being dependent on the loading characteristics, can be mimicked only if the stresses to which ballast is subjected on track are correctly evaluated.

On modern railway lines the maximum axle load falls between 20 t and 25 t but typically only 50% reaches the sleeper directly underneath it (Section 2.3.2.1). Ballast stresses have been assessed through numerical simulations, laboratory tests and field monitoring (Shenton, 1978; Steward et al., 1985; Selig & Waters, 1994; Powrie et al., 2007; Abadi, 2014). In particular, it has been found that at relatively low frequencies (i.e. less than 10Hz) the maximum vertical stress (σ_v) ranges between 200 kPa and 300 kPa while the confining stress (σ_c) remains between 10 kPa and 60 kPa, meaning that ballast is very lightly confined. However, it must be pointed out that these values are just indicative. In fact, stresses are not uniformly distributed and are time-dependent (Section 2.3.2.2); moreover, they are likely to be higher close to track imperfections, such as abrupt support stiffness variations, wheel/rail defects and bolted rail joints.

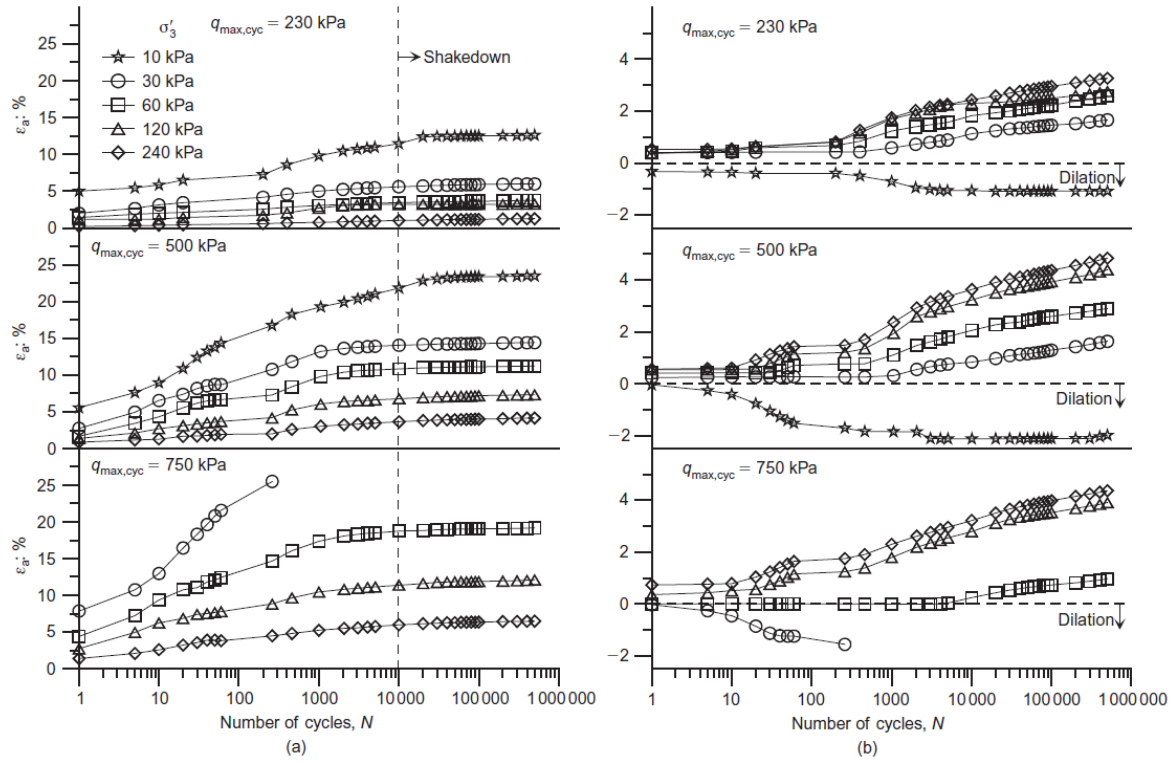

Figure 3-8. Large scale triaxial tests on railway ballast; effect of confining pressure σ'$_3$ and maximum applied deviator stress $q_{max,cyc}$; (a) axial strain vs number of cycles; (b) volumetric strain vs number of cycles (Lackenby et al., 2007)

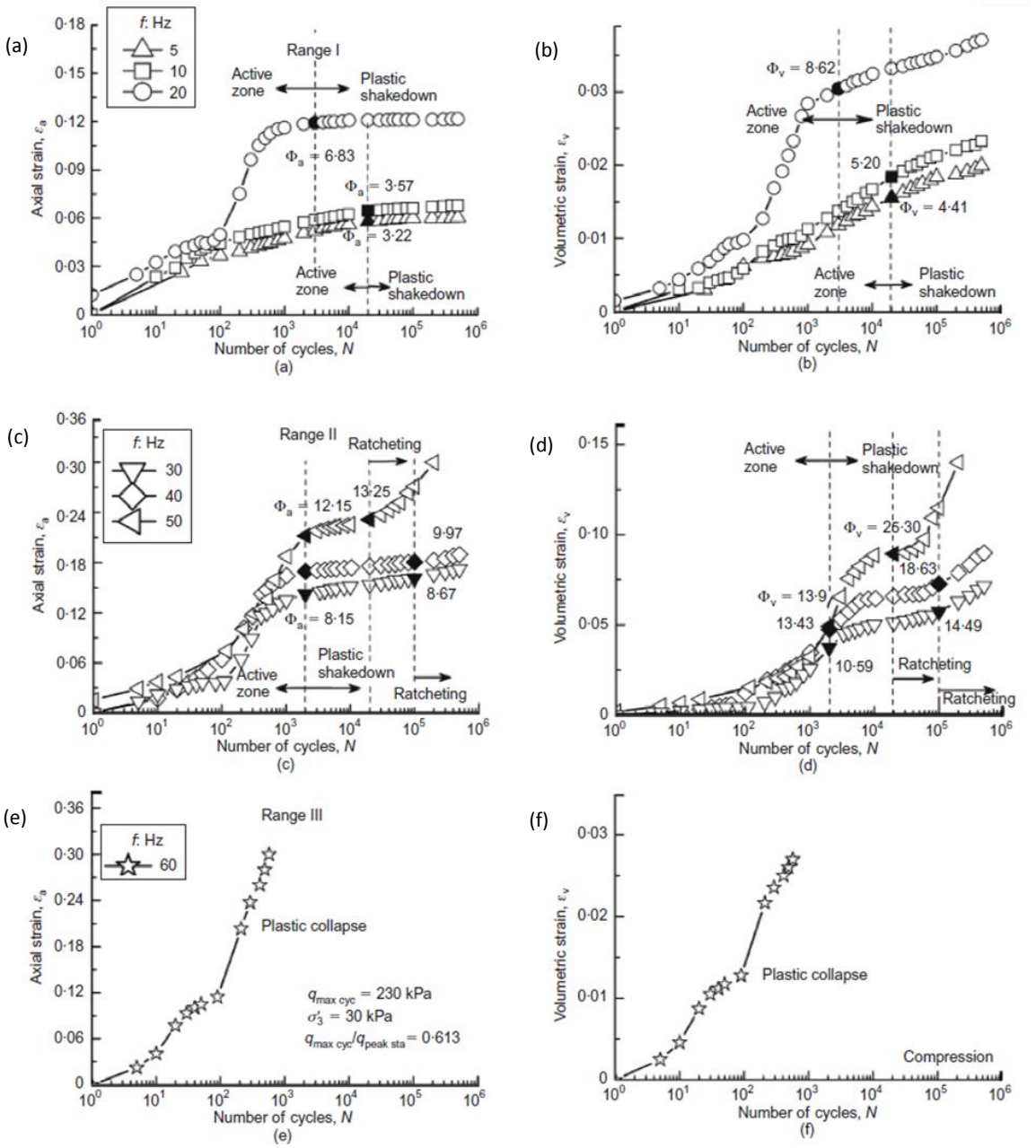

Figure 3-9. Triaxial tests on ballast carried out using a prismoidal apparatus; effect of frequency on permanent strain: (a) and (b) shakedown; (c) and (d) ratcheting; and (e) and (f) plastic collapse (Sun et al., 2014)

It is well known that stresses increase with train speed or, from a different perspective, loading frequency (Section 2.3). Train speed (V) on normal lines is below 200 km/h while high speed trains travel between 200 km/h and 400 km/h. The loading frequency is not unique, as loads are imparted by multiple axles and affected by wheel-rail imperfections (Indraratna et al., 2014; Le Pen et al., 2016). However, to a first approximation, the primary loading frequency f can be estimated as a function of V:

$$f = V/\Lambda \tag{3-1}$$

where the characteristic length (Λ) is typically taken as the axle spacing, which ranges from 1.7 m to 3 m (Aursudkij et al., 2009; Cahill et al., 2014; Indraratna et al., 2014; Hussaini et al., 2015). It

follows that the load frequency is below 20 Hz or 30 Hz on traditional lines ($V \leq 200$ km/h) and between 30 Hz and 60Hz on high speed lines (200 km/h $< V \leq 400$ km/h).

In summary, ballast on track is subjected to maximum vertical stresses of 200 kPa to 300 KPa, confining stresses of 10 kPa to 60 kPa, and, based on very simplified calculations, loading frequencies below 20 Hz or 30 Hz on regular lines and between 30 Hz and 60 Hz on high speed lines.

3.2.4 Regime of ballast settlement under track conditions

Having defined the regimes of plastic deformation (Sections 3.2.2) and the loading characteristics (Section 3.2.3), laboratory tests can be reinterpreted to obtain an indication of ballast settlement response in track conditions.

According to many experiments (Lackenby et al., 2007; Aursudkij et al., 2009; Sun et al., 2014; Sol-Sánchez et al., 2015), for f less than 20 Hz (V less than 200 km/h) ballast long-term behaviour is characterised by marginal accumulation of plastic deformation which reduces with load cycles (Figure 3-8, Figure 3-7, Figure 3-27 and Figure 3-28). Thus the expected regime of plastic deformation is shakedown.

A limited number of experiments investigated ballast response to high frequency loading typical of high speed lines. Based on the experiments carried out by Guérin et al. (1999) and Sun et al. (2014) for f between 20 Hz and 40 Hz (or V between 200 km/h and 300 km/h) ballast might experience ratcheting and accumulate significant plastic deformation without, nonetheless, reaching collapse. Guérin et al. (1999) observed that, under a cyclic loading representative of a train speed of 250 km/h, ballast settlement rate tends to a constant value, as typical of ratcheting. Sun et al. (2014) found that ballast might experience ratcheting under load frequencies of 20 Hz to 30 Hz, beyond which the risk of plastic collapse becomes relevant (Figure 3-9c, Figure 3-9e).

In summary, based on laboratory tests, ballast may experience shakedown on regular lines, i.e. V less than 200 km/h, and ratcheting on high speed lines. For particularly high train speeds, e.g. greater than 300 km/h, plastic deformations might accumulate very rapidly leading to the plastic collapse. However, it is widely known that train speeds can exceed 300 km/h on ballasted track. This is not surprising, as laboratory tests cannot accurately reproduce track behaviour (Section 3.2.1) and an over-simplified relation between frequency and speed has been used (Section 3.2.3).

3.3 The mechanics of ballast deterioration

3.3.1 Mechanisms of ballast settlement

Ballast deterioration is the consequence of complex mechanical processes at the particle scale. Although the understanding of ballast mechanics under repeated loading remains unclear, the main physical mechanisms responsible for its deterioration can be identified. Bathurst & Raymond (1987), as mentioned by Lobo-Guerrero & Vallejo (2006), identified only three main mechanisms:

ballast densification, aggregate degradation and lateral spread. Suiker et al. (2005) observed that permanent deformations can be caused by particle rearrangement and breakage; however, the latter must have only a small influence, as experiments typically show marginal particle degradation. Dahlberg (2001) described ballast mechanics from a closer perspective and hence identified more mechanisms: material densification due to particle rearrangement, ballast penetration into subballast or subgrade, particle breakage and abrasive wear, permanent micro slips between particles, ballast lateral spread and sleeper horizontal movements.

Table 3-2. Main mechanisms of ballast deterioration

Deformation	Mechanism	Characteristics
Volumetric strains (densification)	Particle rearrangement (Section 3.3.2)	• Post-compaction densification • Slip-stick mechanism • Granular segregation
	Particle breakage (Section 3.3.3)	• Mass loss • Reduction of particle interlocking
Lateral strains	Ballast spread (Section 3.3.4)	• Room for further particle rearrangements • Reduction of sleeper-ballast contact beneath the rail seats, leading to sleeper centre-binding
Downward translation	Interpenetration (Section 3.3.53.3.4)	• Subgrade or subballast penetrates ballast leading to permanent settlement

The main physical mechanisms of ballast deterioration have been summarised in Table 3-2. On the macroscale, ballast settlement is associated with material densification (i.e. volume reduction), lateral strains and downward translation. The mechanisms able to cause densification without lateral strains are particle rearrangement and breakage. Lateral strains are associated with ballast lateral spread due to the lack of sufficient track confinement. Downward translation is the consequence of the penetration of ballast particles into subballast or subgrade. However, it must be pointed out that these mechanisms are strongly related; for example, lateral spread makes room for further particle rearrangements which may lead to further densification. Moreover, ballast degradation is also associated with fouling and particle weathering. The main characteristics of the mechanisms are summarised in the right-hand column of Table 3-2 and are discussed in more detail in the following sections.

3.3.2 Particle rearrangement

The term particle rearrangement refers to the particle relative movements, e.g. slips and reorientations, responsible for ballast densification and settlement. As with the settlement, particle rearrangement is expected to occur rapidly in the first cycles, i.e. Phase 1, and slowly in the longer term, i.e. Phase 2 (Section 3.2.2).

The mechanics of particle rearrangement remain unclear, as particle movements cannot be visualised through standard laboratory tests. However, discrete element simulations show that the settlement response of unbound aggregates to cyclic loading can be explained by a slip-stick mechanism that develops without particle breakage and regardless of the load magnitude (Alonso-Marroquín & Herrmann, 2004; García-Rojo et al., 2005). In particular, Alonso-Marroquín & Herrmann (2004) investigated the mechanical response of the 2D particle assembly shown in Figure 3-10a to cyclic loading. The components of each contact force (f_t is the tangential force, f_n is the normal force) were limited by the sliding condition $|f_t| \leq \mu f_n$, where μ is the friction coefficient. The authors found that most of the contacts satisfied the elastic condition $|f_t| < \mu f_n$ but some of them reached the sliding condition $|f_t| = \mu f_n$ (Figure 3-10b). This caused some contacts to slide during loading and stick while unloading (Figure 3-10c), leading to the overall accumulation of plastic deformation (Figure 3-10d), which is accompanied by the reduction of the volume (Figure 3-10e). It must be pointed out that, although the permanent deformation reduced with reducing load magnitude, there is no evidence of a purely elastic response. Moreover, the slip-stick mechanism can be entirely governed by particle surface friction and shape, as it develops without particle breakage.

Another possible cause of particle rearrangement is particle segregation. This involves the downward migration of the smaller particles, which increases the volume of the voids and reduces the coordination number in the upper part, allowing for further particle rearrangements. However, the effect of segregation should be marginal, as usually railway ballast is uniformly graded (Section 2.2.4).

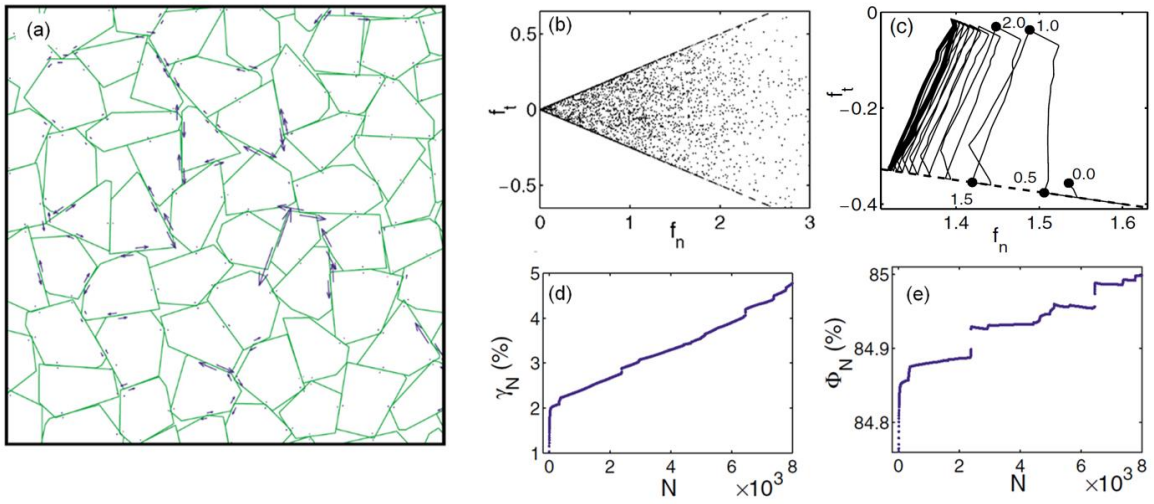

Figure 3-10. Effect of cyclic loading on the deformation of granular materials according to 2D discrete element analyses; (a) particle assembly and field of plastic deformations accumulated at the contacts during one cycle; (b) normalised normal and tangential contact forces (f_n and f_t) plotted within dashed lines representing the sliding condition $|f_t| \leq \mu f_n$; (c) contact force at different times for a sliding contact; (d) plastic shear strain (γ_N) vs number of cycles (N); (d) volume fraction (Φ_N, ratio of the volume of the solids to the total volume of the sample) vs number of cycles (N) (Alonso-Marroquín & Herrmann, 2004)

3.3.3 Particle breakage

Particle breakage is a complex phenomenon, which depends on particle geometry, parent rock characteristics and loading conditions. Breakage contributes to ballast permanent deformation

through the reduction of the particle mass (and volume) and the reduction of particle roughness and angularity. Sample volumetric reduction is an artefact of the increase in the percentage of smaller particles, which migrate downward allowing for further sample densification (Al-Saoudi & Hassan, 2014). The reduction of particle roughness and angularity reduces the degree of particle interlocking, hence the material's ability to resist permanent deformations (Section 2.2.4).

Lees & Kennedy (1975) identified three types of particle breakage: (1) splitting, i.e. particle breakage into approximately equal parts; (2) corner breakage, i.e. breakage of angular projections; and (3) frictional wear, i.e. grinding off of small-scale asperities (Figure 3-11).

Particle breakage can be evaluated through visual inspection but also quantified using simple methods described in the literature (Marsal, 1967; Hardin, 1985; Indraratna, B., Lackenby, J., and Christie, 2005; Abadi, 2014; Sol-Sánchez et al., 2015). Based on large triaxial tests and discrete element analyses, for load frequencies less than 20 Hz to 30 Hz, particle breakage consists mainly of corner breakage and frictional wear while splitting is relevant only at higher frequencies (Hossain et al., 2007; Christie et al., 2009; Thakur et al., 2013; Indraratna, Thakur, et al., 2010). Full-size tests carried out at low frequency not only confirmed that particle splitting and corner breakage are marginal but also showed negligible mass loss (i.e. <0.1%), suggesting small frictional wear (Abadi, 2014). Thus the breakage of ballast particles under train passage should be limited, consisting of a small amount of frictional wear with occasional corner breakage and marginal particle splitting. However, it must be pointed out that on real tracks there are other sources of particle degradation, e.g. tamping (Selig & Waters, 1994; Sol-Sánchez et al., 2016) and chemical attack (Lees & Kennedy, 1975).

Although particle breakage can be quantified, its contribution to track settlement is difficult to assess. As particle degradation is usually marginal, so its contribution to the development of permanent deformations is expected to be limited (Suiker et al., 2005). However, this is not necessarily true, as small variations in particle geometry and roughness might be associated with significant increases in the permanent deformation. According to discrete element analyses reproducing particle splitting and corner breakage, although the former is marginal, breakage is responsible for at least 30% of the settlement (Lobo-Guerrero & Vallejo, 2006; Hossain et al., 2007). However, discrete element models are not fully reliable, as they do not reproduce accurately the shape of real ballast particles, do not account for the frictional wear, are dependent on the assigned particle strength and often allow interparticle penetration. In contrast, laboratory tests, although cannot isolate the effect of particle degradation, do not suggest any strong relations between settlement and breakage. For example, Sol-Sánchez et al. (2015) showed that the addition of crumb rubber to ballast reduced particle degradation but no clear relationship between breakage and settlement could be inferred. Accordingly, Indraratna et al. (2005) showed that increasing the confining stress can increase breakage while reducing the settlement.

(a) (b)

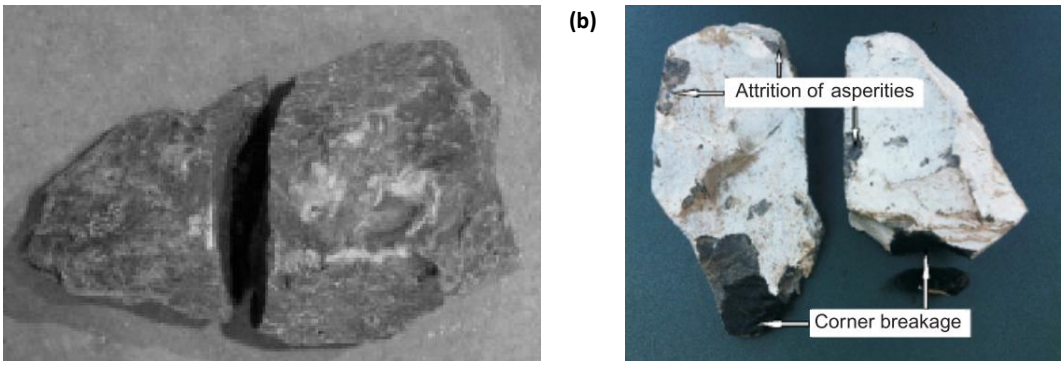

Figure 3-11. Examples of particle breakage: a) Particle splitting (Indraratna, B., Lackenby, J., and Christie, 2005); b) corner breakage and frictional wear (Sun et al., 2014)

3.3.4 Ballast spreading

As ballast is usually lightly confined (Section 3.2.3), track settlement is typically accompanied by lateral spreading. This is clear from the field measurements reported by Indraratna et al. (2010), which show that lateral movements are relevant, being 50% to 75% of the settlement, and follow a trend similar to that followed by the vertical deflections (Figure 3-12).

Despite the lateral deformations, ballast overall volumetric behaviour under cyclic loading representative of track conditions (Section 3.2.3) usually remains compactive, as shown for example in Figure 3-8 and Figure 3-9, causing material stiffness and shear strength to increase (Lackenby et al., 2007; Anderson & Fair, 2008; Indraratna et al., 2010; Indraratna & Nimbalkar, 2013; Aingaran, 2014). Nevertheless, particle lateral migration constitutes a weakness for the track, as it makes room for further particle rearrangements, especially close to the shoulders, leading to sleeper centre-binding (Section 2.3.2.2). Ballast lateral plastic deformation can be reduced by increasing the confining pressure, which also reduces settlement, as shown for example in Figure 3-8. In practice, this can be achieved through interventions that contain the lateral movements, e.g. use of geogrids (Section 3.4). Moreover, as observed in Section 2.3.2.2, lateral spreading reduces the contact beneath the rail seats, leading to increased sleeper resilient deflections, dynamic effects and hence, severe track geometry deterioration.

3.3.5 Interpenetration

As observed by Dahlberg (2001), the penetration of ballast particles into the underlying material (i.e. subballast or subgrade) causes the whole structure to move downward and, especially when differential settlement occurs, contributes to track geometry deterioration. The use of separation layers can reduce this settlement by preventing ballast/subballast/subgrade intermixing. For example, Indraratna et al. (2014) found that the use of a non-woven geotextile installed at the ballast/subballast interface can reduce track settlement by about 13% (Figure 3-13). Sharpe & Caddick (2004) obtained a 45% to 60% reduction by interposing different types of separation layer between the ballast layer and the subgrade.

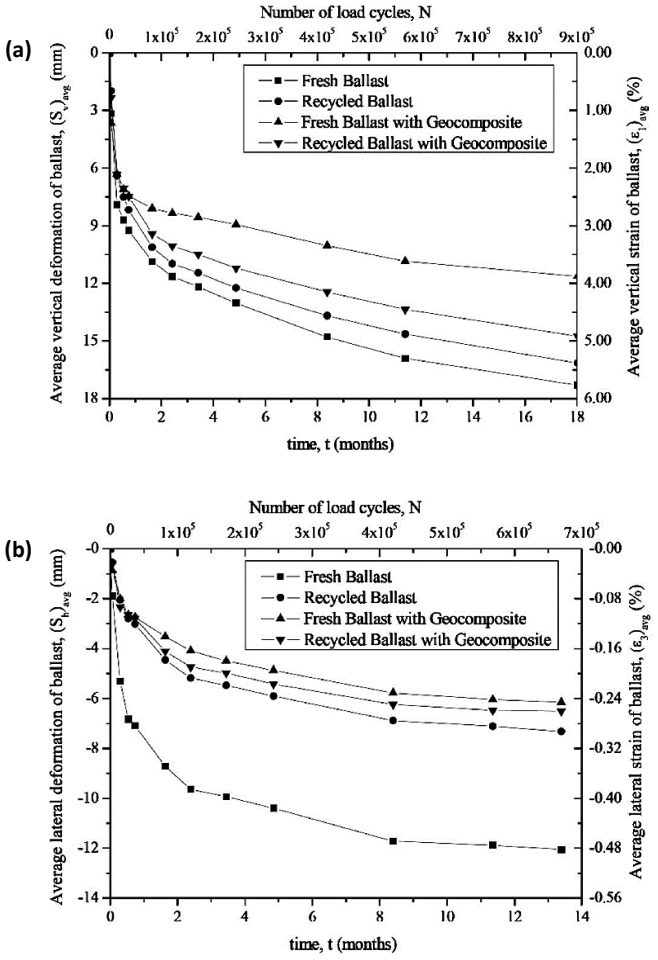

Figure 3-12. Field measurements at Bulli site; effect of Geocomposite (geogrid bonded with non-woven geotextile) on fresh and used ballast; (a) vertical deformations; (b) horizontal deformations (Indraratna et al., 2010)

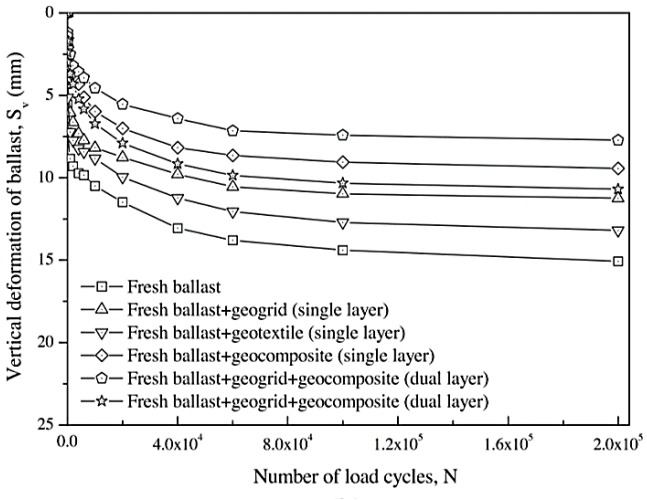

Figure 3-13. Large scale prismoidal triaxial test; effect of geogrids, non-woven geotextiles and geocomposites (i.e. geogrid bonded with non-woven geotextile) on ballast settlement response (Indraratna et al., 2014)

3.4 Reinforcement of railway ballast

3.4.1 Ballast improvement

As observed in Section 3.1, ballast settlement under train passage is a major cause of track geometry deterioration. Therefore, it would be particularly beneficial if ballast life cycle could be extended by inhibiting the accumulation of plastic strains. In this section, five methods to reduce track deterioration through interventions on the ballast layer are described: variation of the grading, use of geogrids, use of 3D cellular reinforcement, ballast bonding and addition of crumb rubber. The analysis of different reinforcement techniques can aid in understanding ballast behaviour and the advantages (and disadvantages) of novel improvement methods, such as fibre reinforcement.

3.4.2 Variation of ballast grading

It is widely known that particle grading has a great influence on granular material behaviour. As shown in Section 2.2.4, ballast is typically uniformly graded to provide free drainage and avoid particle segregation. However, studies have shown that more broadly graded ballast is characterised by greater shear strength and exhibits smaller permanent deformation under repeated loading (Indraratna et al., 2011).

In geotechnical engineering, the uniformity of the PSD can be expressed in terms of coefficient of uniformity:

$$C_u = D_{60}/D_{10} \tag{3-2}$$

where D_{60} and D_{10} are the particle dimensions at 60% and 10% passing respectively. Standard gradations are uniform, i.e. C_u = 1.4 - 1.7. However, cyclic triaxial tests showed that increasing C_u from 1.4 to 2 can reduce permanent deformation by about 30% (Figure 3-14) and particle breakage by over 50% (Indraratna et al., 2011). Similar findings were obtained using the full-size testing rig at the University of Southampton (Abadi et al., 2015; Abadi et al., 2016b): increasing C_u from 1.45 (NR grading) to 1.95 reduced the settlement by 28% (variant 3 in Figure 3-15). The improvements can be explained by the reduction of voids and the increase in coordination number, i.e. the average number of interparticle contacts per particle (Raymond & Diyaljee, 1979; Indraratna et al., 2011; Abadi et al., 2016b).

The use of more broadly graded ballast is compatible with track requirements, as the addition of small quantities of properly selected finer particles does not jeopardise material permeability or cause particle segregation (Abadi, 2014; Abadi et al., 2016b). Moreover, increasing the finer proportion gives bigger sleeper-ballast contact areas (Figure 3-16), and hence is expected to reduce the stresses in the substructure.

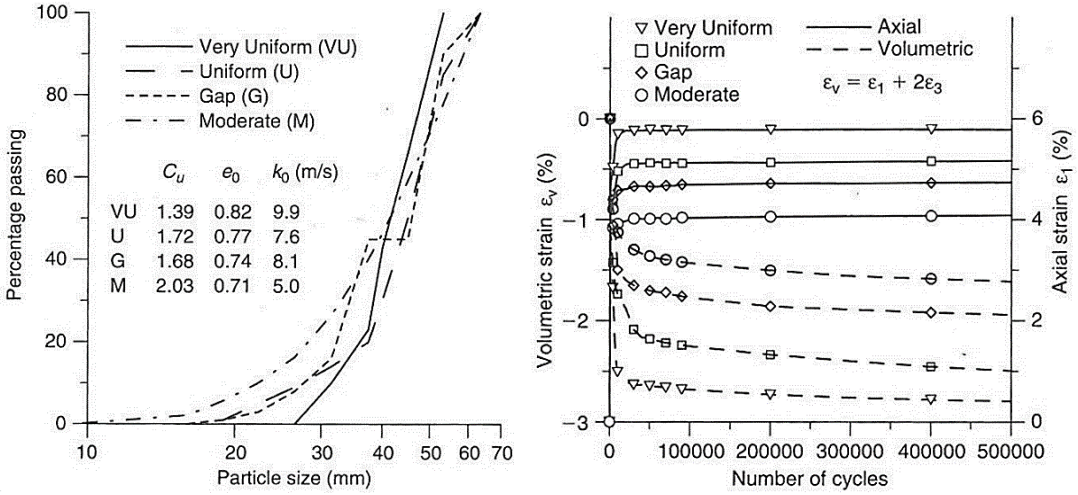

Figure 3-14. Cyclic triaxial tests; effect of C_u on ballast volumetric and axial strains (Indraratna et al., 2011)

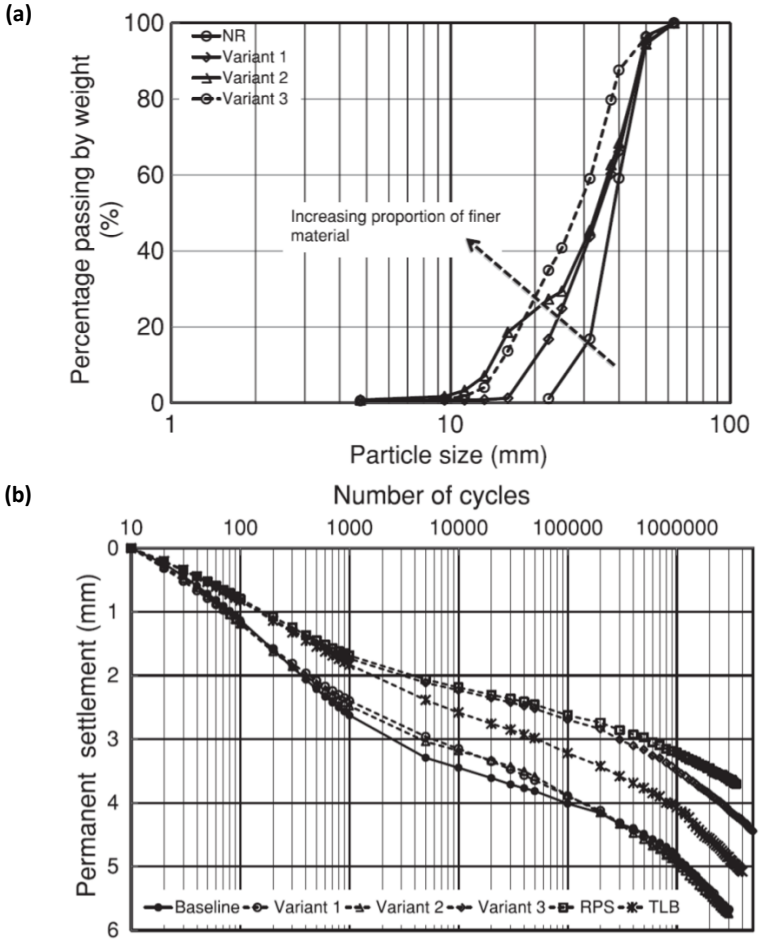

Figure 3-15. Full size tests; (a) modified gradations; (b) settlement response (Abadi et al., 2016b)

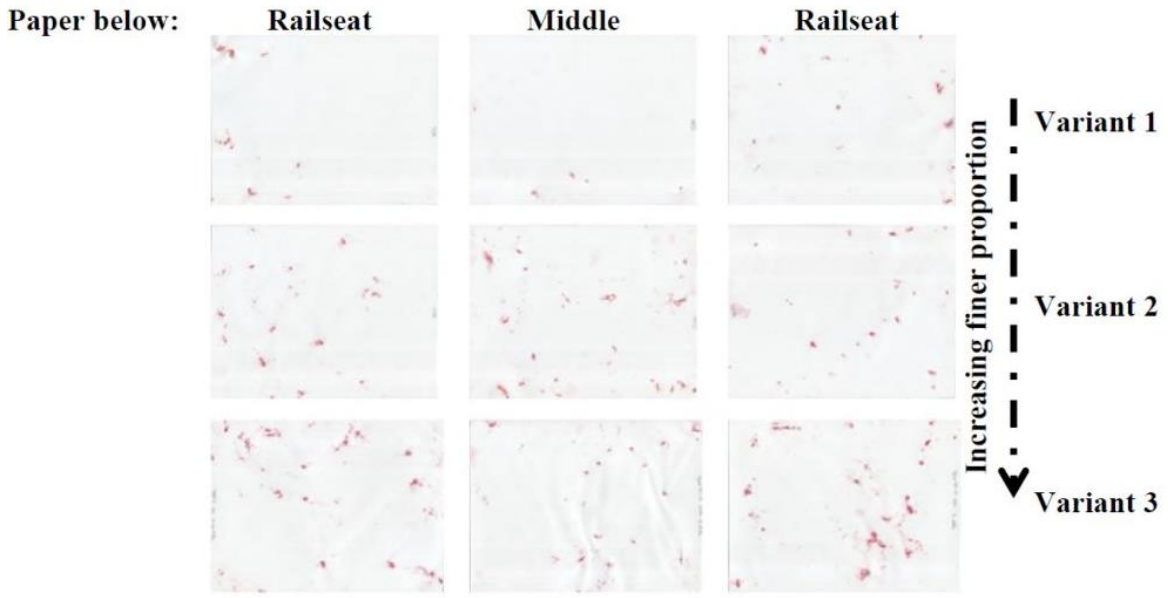

Figure 3-16. Pressure sensitive papers showing sleeper-ballast contact area for different ballast gradations; Variant 1, $C_u = 1.9$; Variant 2, $C_u = 2.5$; Variant 3, $C_u = 1.9$ (after Abadi et al., 2015)

3.4.3 Geogrids

Geogrids are 2D continuous geosynthetic reinforcements typically made of polymeric material (e.g. polypropylene or polyethylene) and provided with regularly distributed rectangular apertures that constrain particle horizontal movement (Figure 3-17a). They are used in one or more horizontal layers to improve soils or similar materials. Compared with soil, geogrids are stiff and strong in tension and increase track confinement by limiting lateral strain. Typical applications include the reinforcement of retaining walls, embankments, steep slopes and, in recent times, ballasted railway tracks (Figure 3-17b).

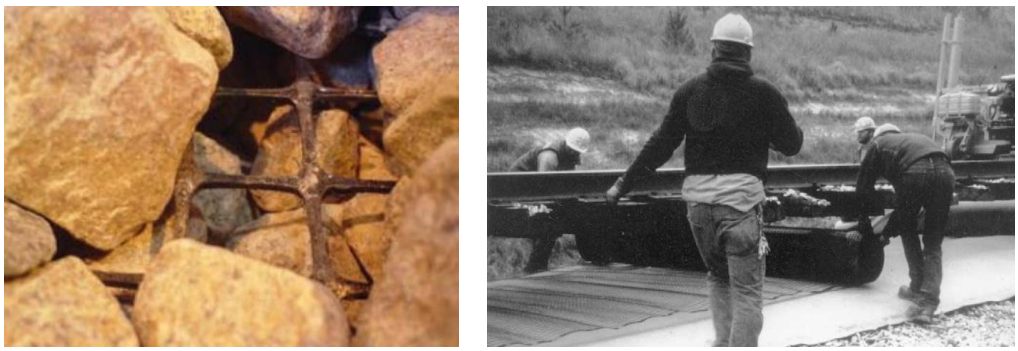

Figure 3-17. (a) geogrid shown during dismantling of a test specimen (after Brown et al., 2007); (b) installation of a geogrid to reinforce railway ballast (after Raymond, 2002)

Experimental studies have shown geogrid ability to improve ballast performance (Bathurst & Raymond, 1987; Gobel et al., 1994; Raymond, 2002; Raymond & Ismail, 2003; Brown et al., 2007; Christie et al., 2009; Indraratna & Nimbalkar, 2013; Hussaini et al., 2015). Geogrids can reduce lateral deformation by 30% to 50%, settlement by 40% to 65% and particle breakage by 40% to 50%, although different testing methods have been used. However, as shown in Figure 3-18, the reinforcement is effective only if the ratio of the aperture size to the average particle size (A/D_{50})

falls between 1.6 and 1.8, and might be ineffective or counterproductive if the ratio is less than 1 (Hussaini et al., 2015; Brown et al., 2007).

For railway application, geogrids are typically placed in a single layer at the ballast-subballast interface. However, experimental studies have shown that they would be more effective if installed at shallower depth and in more layers. Bathurst & Raymond (1987) and Raymond & Ismail (2003) found that the optimum placement depth is 50 mm to 150 mm. Hussaini et al. (2015) enhanced the reinforcing effect by installing a geogrid 65 mm above the ballast-subballast interface, as shown in Figure 3-18. Moreover, it has been found that small further improvements can be obtained through the use of a double layer (Raymond & Ismail, 2003; Indraratna & Nimbalkar, 2013). Nevertheless, on real tracks geogrids cannot be installed in the upper part of the ballast layer, i.e. the optimum placement depth, which is affected by maintenance activities. For example, to allow tamping the minimum placement depth is 100 mm to 150 mm, i.e. the reach of the tines below the sleeper soffit (Bathurst & Raymond, 1987; Raymond & Ismail, 2003).

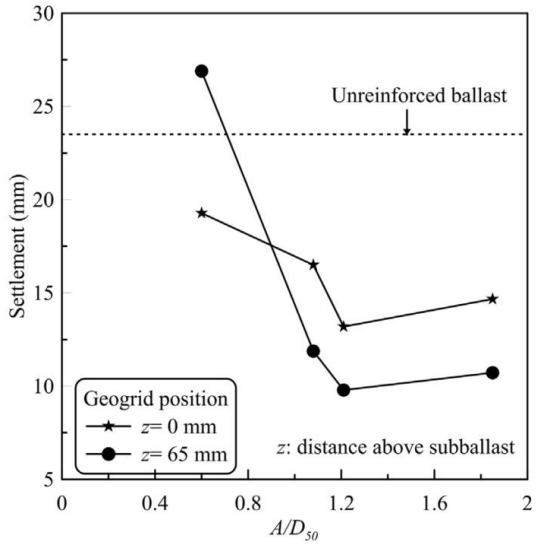

Figure 3-18. Effect of aperture size and placement depth on ballast settlement; z is the distance above ballast-subballast interface; the thickness of the ballast layer below the sleeper soffit was 325 mm (Hussaini et al., 2015)

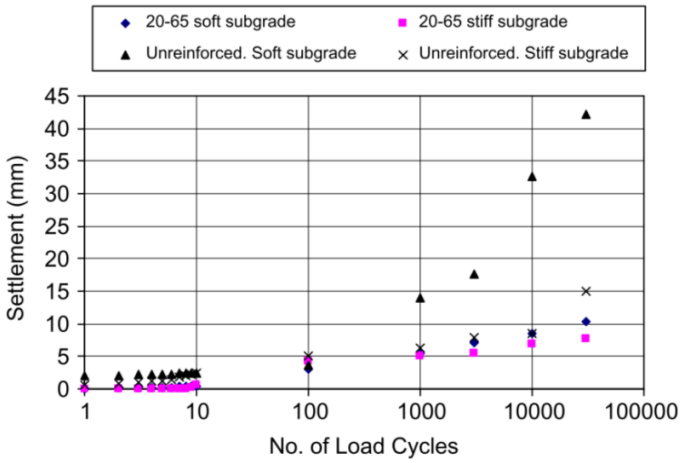

Figure 3-19. Effect of 20-65 geogrid (nominal tensile strength = 20 kN/m, aperture size = 65 mm) on ballast settlement for soft and stiff subgrade, i.e. rubber layer with stiffness of 30 MPa and 90 MPa respectively (Brown et al., 2007)

Finally, the above-mentioned studies noted that the reinforcing effect is more pronounced in those cases in which the settlement is bigger (e.g. softer subgrade, bigger applied load, wet ballast and rounded particles). This is not unexpected, as bigger deformations mobilise greater tensions in the reinforcement and hence increase the lateral confinement. As an example, Figure 3-19 shows that for a very soft subgrade ballast deformations might be exceptionally high but, in these conditions, the effect of the reinforcement is also greater.

3.4.4 Geocells

Geocells were originally developed by the U.S. Army Corps of Engineers and commercialised by Presto Geosystems in the late 1970's to increase vehicular mobility over loose sandy subgrade (Webster & Alford, 1978; Leshchinsky & Hoe Ling, 2013; Presto Geosystems, 2015). They are continuous three-dimensional honeycomb-like structures made of polymeric material, e.g. high density polyethylene, providing infilled soil with cellular confinement (Figure 3-21).

Geocells bring two major advantages: confining and "mattressing" (Dash & Shivadas, 2012; Leshchinsky & H Ling, 2013; Indraratna et al., 2015). The confining effect is obtained through the containment of the lateral movements that, if the reinforcement is properly designed, reduces settlement and particle breakage (Section 3.4.3). The "mattressing" effect involves an increase in infill material rigidity due to the three-dimensional structure of the cell, which leads to a more uniform distribution of the vertical stresses.

Presto Geosystems (2015) reported that geocells have been successfully used for over 30 years in the railway industry to stabilise subballast and subgrade. An example installation is shown in Figure 3-20, where geocells are being filled in with subballast material. Indraratna et al. (2015) showed that the insertion of a layer of geocells into the top part of the subballast can reduce its settlement under cyclic loading by about 20% and increase its resilient modulus by about 15%. Moreover, Dash & Shivadas (2012) showed that geocells placed in the top part of the subballast layer have the potential to contain ballast lateral spread by increasing ballast-subballast friction.

Geocells are not usually placed within the ballast layer partly because they might interfere with track maintenance operations (Indraratna et al., 2015), but also because their ability to reinforce ballast has not yet been proven. Leshchinsky & Ling (2013) installed a layer of geocells at mid-height of a foundation on gravel, representative, to a first approximation, of a railway track (Figure 3-22): geocells halved both lateral and vertical permanent deformations. However, contrasting results were obtained by Kennedy (2011) using a full-scale testing rig consisting of a rigid tank filled with ballast and subballast and loaded through three sleepers (Figure 3-21): geocells gave a 37% increase in track settlement. The author hypothesised that ballast performance might have been worsened by the difficulty of compacting the material within the cells and the lack of particle interlocking across the cell walls. It can also be argued that perhaps the relative cell/particle size was not correctly designed, making the reinforcement counterproductive (the relative aperture/particle size has great influence on geogrid reinforcing effect - Section 3.4.3). Moreover, the rigid walls of the testing rig could have strongly limited ballast lateral deformation, hence the mobilisation of tensions in the reinforcement.

In conclusion, although geocells can improve the subgrade and subballast performance, further studies are needed to prove their ability to reinforce ballast.

Figure 3-20. Geocell installation to stabilise subballast (Presto Geosystems, 2015)

Figure 3-21. (a) Typical geocell system; (b) geocell/ballast layer during preparation of a lab test (Kennedy, 2011)

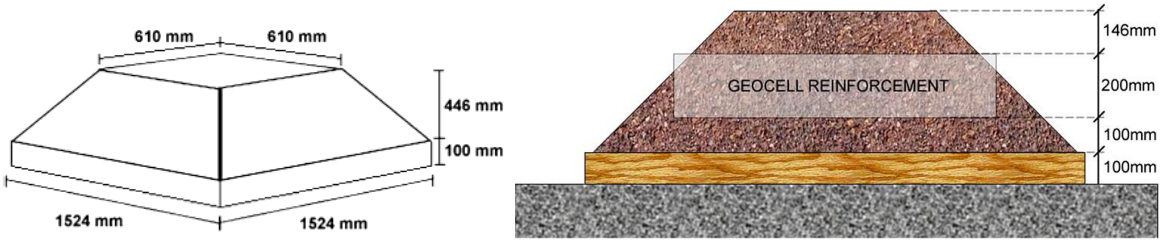

Figure 3-22. Geometry of the gravel foundation tested under vertical cyclic loading by Kennedy (2011)

3.4.5 Ballast bonding

Ballast bonding (or gluing) improves ballast mechanical properties through the addition of polyurethane, which bonds the particles at their contact points while maintaining acceptable drainage (Lakusic et al., 2010; Lee et al., 2017). Polyurethane is formed by injecting a two-component mixture in the ballast bed that hardens over time. Depending on the characteristics of the mixture, different technologies have been developed, e.g. XiTrack (Woodward et al., 2007),

Elastotrack (Dersch et al., 2010) and ERSBallast (Lee et al., 2017). As an example of the potential of ballast bonding to improve the railway track, this section focuses on XiTrack.

XiTrack is obtained by mixing and pouring on the track after compaction two components, an isocyanate and a polyol, and the catalyst that harden over time forming a 3D polymeric cage which reinforces ballast in its preferred state (Woodward et al., 2011b). The polyurethane-ballast mixture, termed GeoComposite, is shown in Figure 3-24. Polymer stiffness and penetration depth can be varied from 100 MPa to 2 GPa and from 100 mm to 500 mm respectively by controlling component's rheology. Other characteristics (e.g. hardness, viscosity, tensile strength and elongation at break) can be also modified depending on need.

Studies have shown that 3D polyurethane reinforcement increases track stiffness, reduces settlement and improves track lateral resistance while maintaining adequate permeability (Woodward et al., 2011a; Woodward et al., 2011b; Kennedy et al., 2013; Woodward et al., 2014). Laboratory tests were conducted to investigate GeoComposite settlement and stiffness response to train passage. The testing rig consisted of a large steel box containing the sample and the load was applied through three half sleepers (Figure 3-23). Experiments showed that the reinforcement can almost entirely eliminate the settlement (Kennedy et al., 2013) and increase the stiffness by 40% to 50% (Woodward et al., 2014). Numerical analyses and a field trial were carried out to assess the GeoComposite's ability to improve the shoulders. It was found that lateral reinforcement (Figure 3-25) can maintain the track lateral alignment by increasing lateral resistance (Woodward et al., 2011a). Moreover, Woodward et al. (2011b) reported that polyurethane reinforcement offers a more uniform stress distribution over the subgrade and is compatible with track drainage requirements, as it reduces the volume of the voids by only ~25%.

Since 2000, XiTrack has been applied to many UK's sites (Kennedy et al., 2013) and, since 2010, also across Europe and Asia (Woodward et al., 2011b) to solve track-related issues at critical sections. For example, this technique has been used to solve gauge clearance issues (Woodward et al., 2011b), retain lateral geometry (Woodward et al., 2011a; Kennedy et al., 2013) and improve track performance in poor conditions (Woodward et al., 2007; Woodward et al., 2014).

Figure 3-23. Full size testing of 3D polyurethane reinforcement (Kennedy et al., 2013)

Figure 3-24. 3D polyurethane reinforcement of ballast (Woodward et al., 2011b)

Figure 3-25. Application of polyurethane reinforcement to shoulder ballast (Woodward et al., 2011a)

3.4.6 Addition of crumb rubber

Sol-Sánchez et al. (2015) studied the behaviour of a mixture of crumb rubber and ballast to reduce aggregate degradation and consumption. Crumb rubber was obtained from used tyres, a widely available waste material. To reduce construction costs and material consumption, no binders were used.

The material was tested under repeated loading representative of train passage. Each test involved filling a rigid box with a ballast-crumb rubber mixture and the load was applied through a wooden block with an aluminium base. Samples were subjected to a sinusoidal vertical cyclic force with a frequency of 4 Hz and a maximum equivalent pressure of 200 kPa and 300 kPa. The crumb rubber content was varied between 5% and 30% by volume, where the latter was established so that almost all voids were filled. Some samples and the test set-up are shown in Figure 3-26.

For the purpose of reducing track geometry deterioration, the greatest advantage of crumb rubber addition resides in the reduction of permanent deformation and particle breakage. Under a maximum pressure of 200 kPa the addition of a small quantity of rubber reduced the settlement. However, higher contents were found counterproductive (Figure 3-27). For a clearer visualisation, the final normalised settlement (i.e. the ratio of the settlement to the settlement for standard

ballast) was plotted against the volumetric content of rubber (Figure 3-29): the addition of 5% rubber content reduced the settlement by 25% while contents greater than 10% increased the permanent deformations. However, under a maximum vertical pressure of 300 kPa significant improvements were obtained using 10% rubber content (Figure 3-28).

Other than reducing the settlement, the presence of soft rubber grains within the voids reduced particle degradation and track stiffness. While the former is an obvious advantage, the latter might be incompatible with train passage. However, according to the authors, the increase in resilient deflections is acceptable if small quantities of rubber are used, i.e. less than 10%. Crumb rubber is expected to reduce ballast permeability and might segregate under repeated loading. However, these potential issues have not been addressed.

Figure 3-26. Ballast-crumb rubber samples and test set-up (Sol-Sánchez et al., 2015)

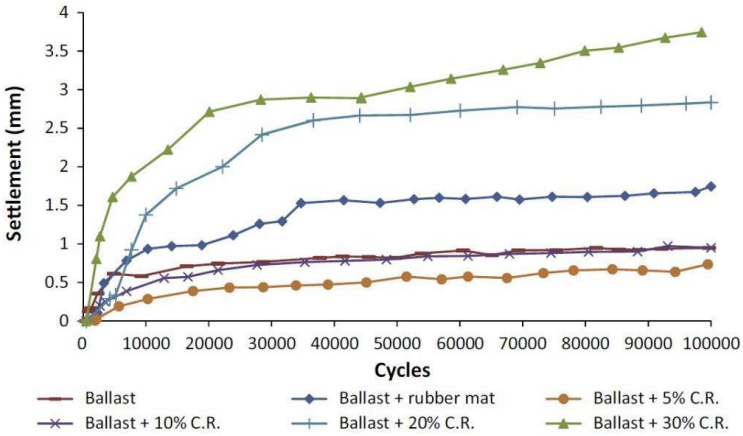

Figure 3-27. Behaviour of ballast-crumb rubber mixture under cyclic loading for a maximum applied stress of 200 kPa (Sol-Sánchez et al., 2015)

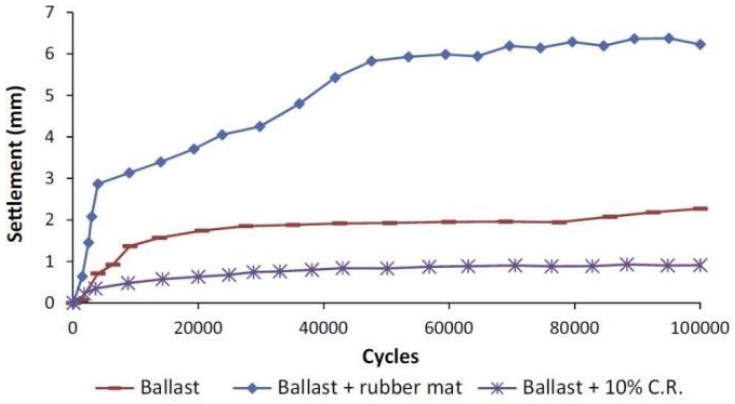

Figure 3-28. Behaviour of ballast-crumb rubber mixture under cyclic loading for a maximum applied stress of 300 kPa (Sol-Sánchez et al., 2015)

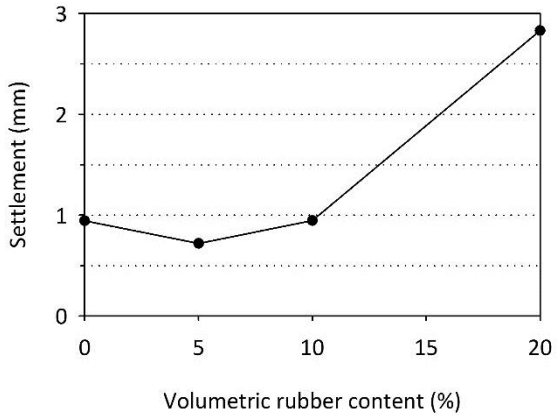

Figure 3-29. Effect of crumb rubber addition on the normalised settlement under maximum stress of 200 kPa (data from Sol-Sánchez et al., 2015)

3.5 Summary

The differential settlement of the ballast layer is a primary mechanism of track geometry deterioration. Thus the understanding of ballast mechanics under repeated loading is of paramount importance for the improvement of the railway track.

A key parameter to assess track geometry deterioration is ballast average settlement. Differential settlements are difficult to reproduce through laboratory tests and can be assumed to be proportional to the average permanent deformation. The main characteristics of ballast settlement response can be summarised as follows:

- Settlement increases approximately linearly with the logarithm of the number of cycles.
- Empirical relationships cannot predict ballast settlement as they do not account for all of the factors affecting its response: load (e.g. magnitude, frequency and history), sleeper characteristics (e.g. type and spacing), particle characteristics (e.g. size, shape, angularity, roughness and strength), initial conditions (e.g. density and bedding), track geometry (e.g. ballast depth and shoulder dimensions), sub-ground material characteristics (e.g. stiffness and frictional properties) and presence of reinforcements (e.g. geogrids and geotextiles).

- Two phases of ballast settlement can be identified:
    - Phase (1) consists of rapid ballast densification due to particle rearrangement; its duration can vary from 50 thousand cycles to 800 thousand cycles and is heavily affected by sample initial conditions, hence preparation technique.
    - Phase (2) is characterised by a smaller accumulation of plastic strain; depending on load severity three regimes plastic deformation have been identified:
        - Shakedown: in the long-term ballast response is essentially resilient, i.e. reversible.
        - Ratcheting: plastic strains are accumulated in each cycle indefinitely at fairly constant rate.
        - Plastic collapse: plastic strains accumulate rapidly until failure.
- On track, ballast is subjected to vertical stresses of 200 kPa to 300 kPa and confining stresses of 10 kPa to 60 kPa; based on a very simplified frequency-speed relation, the loading frequency is 20 Hz to 30 Hz for train speeds of 200 km/h to 250 km/h and 30 Hz to 60 Hz for train speed of 250 km/h to 350 km/h.
- Based on laboratory tests and the very simplified frequency-speed relation, the regime is shakedown for speeds below 200 km/h and ratcheting for speeds of 200 km/h to 300 km/h; based on a series of large triaxial tests, the risk of plastic collapse is relevant above speeds of 300 km/h; however, ballast behaviour on track is different, e.g. train on high speed lines are known to be able to operate safely at > 300 km/h.

The main physical mechanisms responsible for the accumulation of plastic strains have been described. Four main mechanisms (i.e. particle rearrangement, particle breakage, ballast spreading and ballast-subballast-subgrade interpenetration) and three macroscopic effects (i.e. volume reduction, lateral deformation and downward translation) have been identified (Table 3-2). The main characteristics of each mechanism are the following:

- Particle rearrangement
    - Particle rearrangement refers to the relative slips and reorientations responsible for ballast densification and settlement.
    - It is rapid in Phase 1 and slow in Phase 2.
    - Based on discrete element simulations, the accumulation of plastic deformations is explained by a slip-stick mechanism that can develop without breakage and at any stress level.
    - Particle segregation, i.e. downward migration of the finer particles, allows for further densification; however, as ballast is uniformly graded, the segregation should be insignificant unless extensive particle breakage occurs.
- Particle breakage

- There are three types of particle breakage: (a) splitting; (b) corner breakage and (c) frictional wear.
- Breakage can reduce particle volume (by producing fines) and degree of interlocking (by reducing roughness and angularity), facilitating particle rearrangement.
- Under loading representative of train passage, particle breakage may consist of small frictional wear, occasional corner breakage and marginal particle splitting.
- According to discrete element analyses, corner breakage might be responsible for over 30% of the settlement; however, laboratory experiments do not show any clear relations between settlement and breakage.

- Ballast spreading
  - Ballast is lightly confined and spreads laterally under repeated loading.
  - Two main effects of the lateral spread have been identified: (a) an increase in the space available for particle rearrangement; (b) a reduction of sleeper-ballast contact beneath the sleeper ends, which might lead to sleeper centre-binding issues.
- Ballast-subballast-subgrade interpenetration
  - This is the penetration of ballast particles into the underlying material, causing downward translation of the track.

The mechanisms of track deterioration can be inhibited through interventions to the ballast layer. In particular, five improvement methods have been described:

- Variation of ballast grading

  Slight increases of the finer proportion of particles can reduce the settlement while maintaining adequate permeability; this can be explained by the reduction of the volume of the voids, the increase in coordination number and the increase in sleeper-ballast contact area.

- Use of geogrids

  Geogrids constrain lateral movements, reducing settlement and particle degradation; unfortunately, they cannot be placed at optimum depth as they would interfere with maintenance operations; they are often combined with geotextiles, which function as separation layers.

- Use of geocells

  Geocells are continuous 3D honeycomb-like structures made of polymeric material that constrain lateral movements (confining effect) while increasing material rigidity, leading to a more uniform load distribution (“mattressing” effect); however, it is not clear whether they can effectively improve ballast or only subballast and subgrade.

- Ballast bonding

  It consists of the addition of polyurethane, which bonds the particles at their contact points while maintaining acceptable drainage; it makes the settlement negligible and increases the stiffness of the track bed or, if injected only into the shoulders, significantly increases the lateral resistance; it can be effectively used to solve track issues at critical sections.

- Addition of crumb-rubber

  Small quantities of crumb-rubber can reduce ballast settlement and breakage but, on the other hand, reduce stiffness and permeability.

In summary, although ballasted track can still satisfy high performance demands, ballast improvement would reduce track geometry deterioration, especially on high speed lines. This can be achieved through interventions that inhibit the mechanisms responsible for the development of plastic deformation: particle rearrangement, particle breakage, lateral spread and ballast/subballast/subgrade intermixing. Currently, the most feasible interventions are the use of more broadly graded ballast, geogrids and geotextiles. Ballast bonding can be very effective on critical sections. Other techniques, such as the use of geocells or the addition of crumb rubber, have the potential to reduce track permanent deformations but their effectiveness should be further investigated.

4 RANDOM FIBRE REINFORCEMENT

4.1 Introduction

Fibre reinforcement involves the addition of unbound, randomly placed discrete fibres to a granular material to improve its mechanical properties. In particular, it can increase the shear strength through the mobilisation of tension in the fibres. It is well known that fibre reinforcement can effectively reinforce sand. However, recent studies have shown that fibres can also increase the shear strength of coarser granular materials, e.g. gravel, and most importantly reduce their deformation under cyclic loading. Moreover, fibre addition brings other advantages: it maintains adequate material stiffness; it does not introduce planes of weakness; it does not reduce permeability, unless very high contents are used; it is expected to be compatible with standard maintenance operations, e.g. tamping; fibres can be potentially added during ballast cleaning or renewals; they are unlikely to segregate during service, as each of them is held by several particles; they can be made of plastic, a widely available, durable and recyclable material; and they can be separated from ballast after use, so that both components can be recycled, using, for example, techniques of waste sorting able to distinguish materials of different densities.

This chapter reviews the behaviour of fibre reinforced granular materials, highlighting the potential advantages of fibre reinforcement and aiding the understanding of the mechanical behaviour of fibre reinforced ballast. First, the effect of fibre addition on the mechanical response is described with reference to the results of a significant number of experimental studies. Then, the mechanics of fibre reinforcement is discussed, along with the main factors affecting its stress/strain/strength behaviour. Finally, the main characteristics and potential benefits of fibre addition are summarised.

4.2 Mechanical response

4.2.1 Experimental studies

Fibres have been used for decades as an effective technique for soil reinforcement. As reported by Gray & Ohashi (1983), initially they were inextensible, e.g. steel strips, but from the ‘80s the use of flexible materials, e.g. natural or polymeric fibres, has become more popular, as they increase soil ductility as well as providing additional strength.

Herein, the mechanical response of fibre reinforced granular materials is described through the results of recent experimental studies in which flexible polymeric fibres were used. The characteristics of these tests are reported in Table 4-1:

- Type of test: M-T = monotonic triaxial, M-RS = monotonic ring shear, C-T = cyclic triaxial, C-FS = cyclic full size;
- Confining or normal pressure, σ_c or σ_n;
- Type of soil: Sa = sand, clSa = clayey sand, saGr = sandy gravel, Gr = gravel (BS EN ISO 14688-2:2004+A1:2013);
- Average particle size (D_{50}) and coefficient of uniformity (C_u);

- Fibre material: PA = polyamide, PP = polypropylene, PE = polyethylene;
- Volumetric fibre ratio V_{fr}, i.e. the ratio of the volume of fibre (V_f) to the volume of the particles (V_p);
- Fibre dimensions: L_f = fibre length, d_f = diameter of a filament fibre, t_f = thickness of a platy fibre, W_f = width of a platy fibre;
- Sample initial relative density, D_{r0}.

It must be pointed out that different definitions of fibre content have been used in the literature. This makes the comparison between the results presented by different authors not straightforward. Therefore, in this chapter, the fibre content is always expressed in terms of volumetric fibre ratio V_{fr} (Section 5.4.2). Nevertheless, some of the figures reported in this chapter also show the fibre content as expressed in the original papers, with the equivalent values of volumetric fibre ratio only reported in the caption.

Table 4-1. Selection of recent experimental studies on fibre reinforced granular soils

Author	Test		Soil			Fibres					D_{r0} (%)
	Type	σ_c or σ_n (kPa)	Id	D_{50} (mm)	C_u	Mat.	V_{fr} (%)	L_f (mm)	d_f or t_f (mm)	W_f (mm)	
Michalowski & Čermák (2003)	M-T	30-600	Sa	0.2 0.9	1.6 1.5	PA	0-3.2 0-2.5	25.4	0.3	-	70
Heineck et al. (2005)	M-T M-RS	20-500 100	Sa	0.15	1.9	PP	0, 1.5	24.0	0.023	-	70
Santos et al. (2010)	M-T	100-5400	Sa	0.16	2.1	PP	0, 1.5	24.0	0.023	-	50-90
Diambra et al. (2013)	M-T	30-200	Sa	0.32	1.7	PP	0-2.6	35 20 40	0.1 0.03 0.12	- - 1.45	0
Shao et al. (2014)	M-RS	50-250	Sa	0.31	3.5	PP	0-2.5	12	0.1	-	34
Sadeghi & Beigi (2014)	C-T	30, 100	clSa	1.11	349	PP	0-2.95	12	0.023	-	NA
Lirer et al. (2012)	M-T	50	saGr	3	12.5	PP	0, 0.6	50	0.1	-	10-70
Ajayi (2014)	M-T	20	Sa	1.4	1.4	PP	0-4.5	23-47	0.1	2	70
Ajayi et al. (2017b)	M-T	30	Gr	8 13	1.5 1.5	PE	0-6.5 0-3.2	10-100 50-150	0.1	10-50 10-20	100
Abadi (2014)	C-FS	-	Gr	38	1.5	PE	0.6	300	0.1	100	NA

Most studies focused on the effect of fibre addition on sand shear strength (Michalowski & Čermák, 2003; Heineck et al., 2005; Santos et al., 2010; Diambra et al., 2013; Shao et al., 2014; Ajayi, 2014). However, the most recent ones focused on the effect of fibres on gravel shear strength (Lirer et al., 2012; Ajayi, 2014; Ajayi et al., 2017b), and on sand or gravel response to cyclic loading (Sadeghi & Beigi, 2014; Abadi, 2014).

In the following sections, the above-mentioned studies are analysed and compared to illustrate the effect of fibre reinforcement on mobilised shear strength, volumetric response and

deformability of granular materials. It must be pointed out that, although the fibres mobilise tensions affecting the effective stresses, this has been rarely considered in the literature. Therefore, in this chapter, the term "effective" is referred to the stresses applied at the boundaries and is not representative of the stresses effectively seen by the grains, unless otherwise stated, as discussed in more detail in Section 4.3.1.

4.2.2 Mobilised shear strength

Triaxial tests have shown that fibres result in a substantial increase in the mobilised shear strength of a sand (Michalowski & Čermák, 2003; Heineck et al., 2005; Santos et al., 2010; Diambra et al., 2013; Ajayi, 2014). In particular, they can increase the peak stress ratio $(q/p')_p$ by a factor of 1.3 to 1.8 while preventing post-peak strength loss (Figure 4-1 to Figure 4-5). The reinforcing effect is strongly dependent on a number of factors, which are analysed in more detail in Section 4.3.2. For example, sand strength increases with the fibre content (Figure 4-2, Figure 4-3, Figure 4-4), length (Figure 4-3b, Figure 4-4) and aspect ratio η, i.e. the ratio of the length (L_f) to the diameter (d_f) of the fibres (Figure 4-3b, Figure 4-3e). The data reported by Michalowski & Čermák (2003) show also a strong relationship between the increase in peak stress ratio $(q/p')_p$ and a modified aspect ratio $\eta' = L_f/d_f^{0.7}$ (Figure 4-3f). The strength improvements are more pronounced under low confining stress (Figure 4-1 to Figure 4-3), which is reflected in the non-linearity of the failure envelopes of reinforced granular materials, as explained in Section 4.3.2.6.

Results from ring shear tests are consistent with those just mentioned: fibres significantly increase sand shear strength and eliminate post-peak strength loss; the reinforcing effect increases with the amount of reinforcement; and the extent of improvement is greater under low confinement (Figure 4-6, Figure 4-8).

More recent studies have shown that fibres can also effectively reinforce coarser materials, i.e. gravel, although the improvements are less noticeable. The triaxial tests by Lirer et al. (2012) showed that, although fibre addition did not increase the peak shear strength of sandy gravel, it prevented post-peak strength loss (Figure 4-9). However, Ajayi et al. (2017b) showed that properly selected fibres can also increase the peak shear strength of coarse granular materials. They found that the addition of fibres increased the peak stress ratio of 1/5 and 1/3 scaled railway ballast by about 5% and 20% respectively. Moreover, as with sand, the effectiveness of the reinforcement increased with fibre content and length, while the width had smaller effect (Figure 4-10).

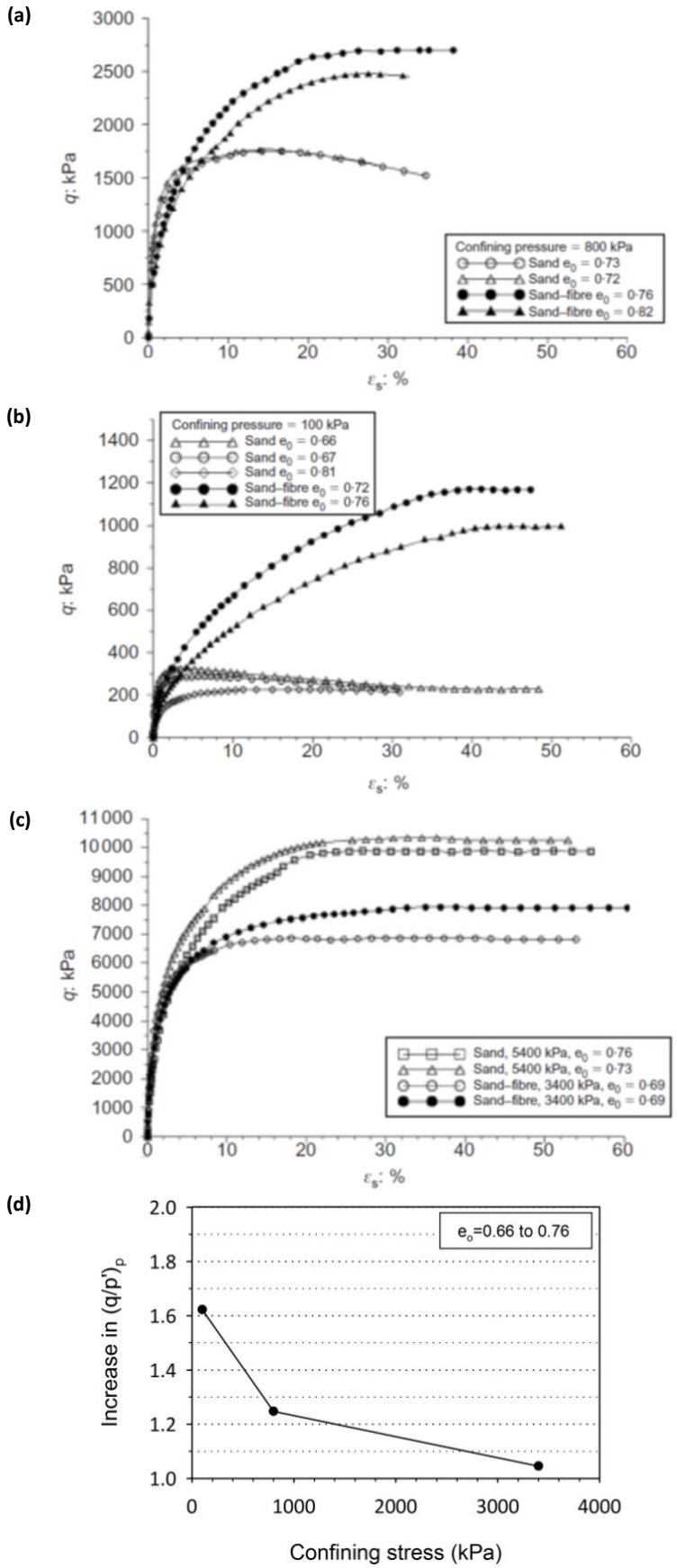

Figure 4-1. Triaxial tests on sand (D_{50} = 0.16, C_u = 2.1) unreinforced and reinforced with 0.5% by mass ($V_{fr} = 1.5\%$) polypropylene fibres (L_f = 24 mm, d_f = 0.023 mm); a), b) and c) deviatoric stress q vs shear strain ε_s (Santos et al., 2010); d) increase in peak stress ratio $(q/p')_p$ vs confining stress (data from Santos et al., 2010)

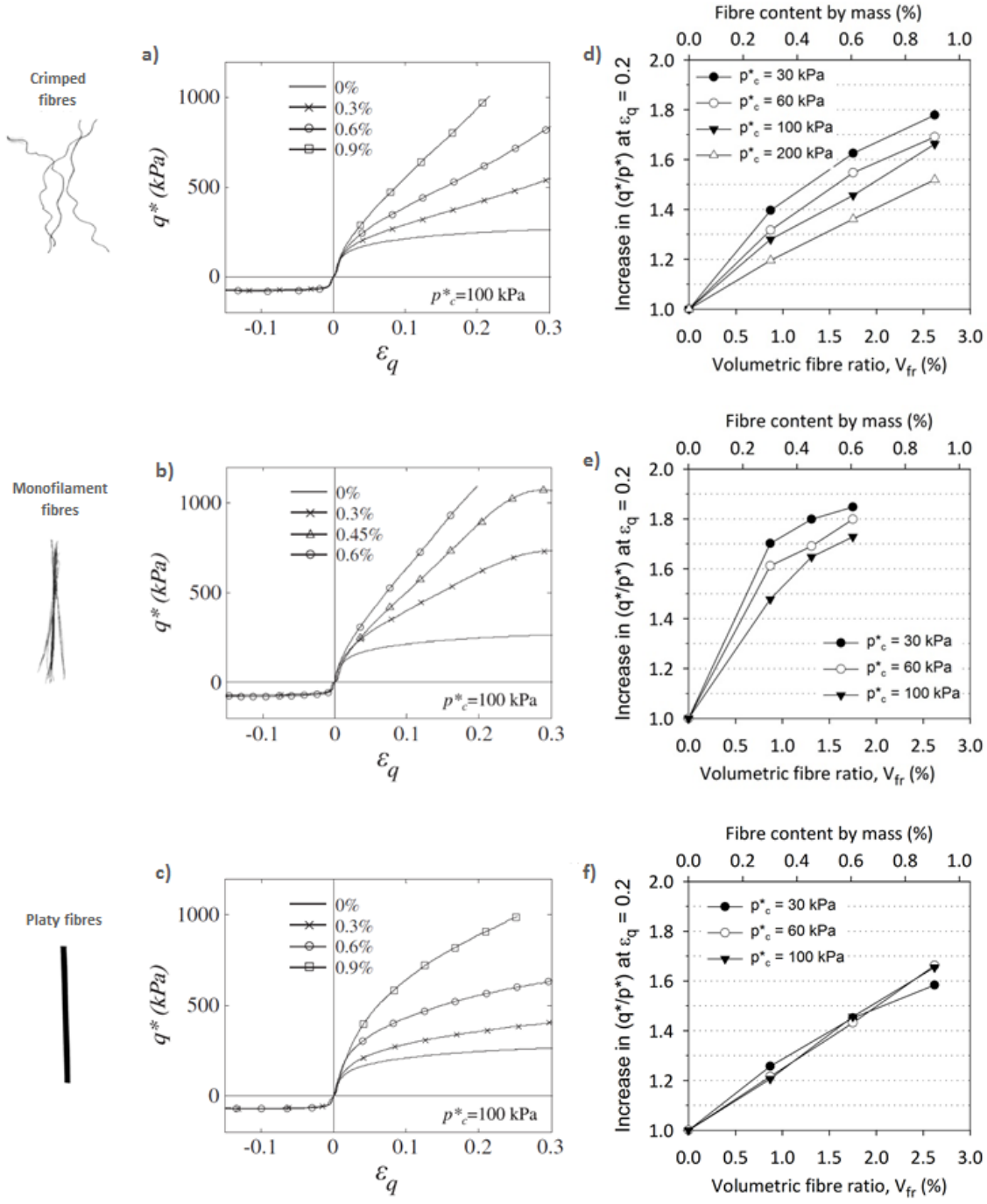

Figure 4-2. Triaxial tests on loose sand (D_r = 0, D_{50} = 0.32 mm, C_u = 1.7) reinforced with different types of polypropylene fibres; effect of fibre content (up to 0.9% by mass, i.e. V_{fr} up to 2.6%) and confining pressure (p_c^*); a), b) and c) deviatoric stress q^* vs deviatoric strain ε_q (Diambra et al., 2013); d), e) and f) increase in deviatoric ratio (q^*/p^*) at 20% deviatoric strain with the fibre content for different values of confining pressure (data from Diambra et al., 2013)

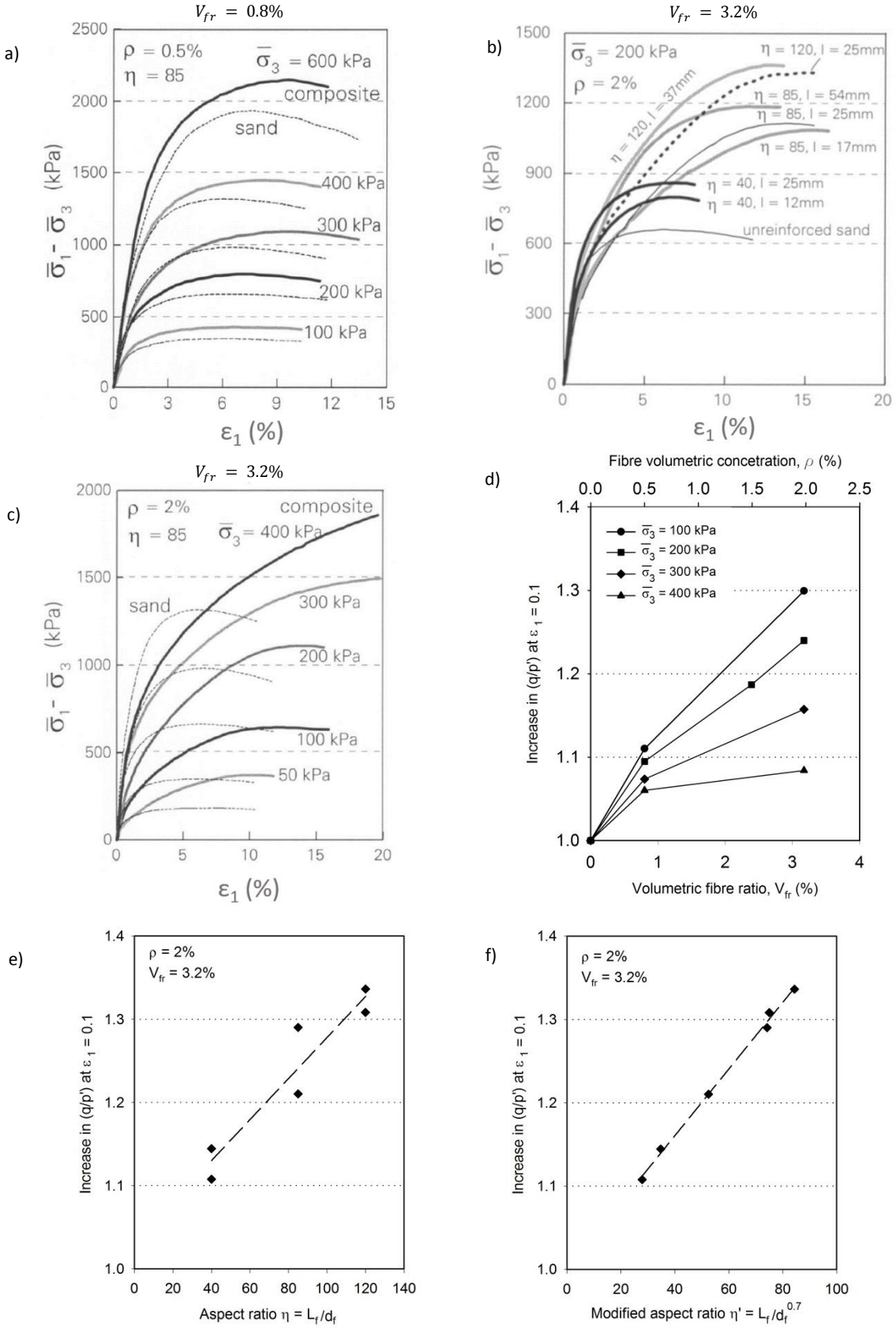

Figure 4-3. Triaxial tests on fine sand (D_{50} = 0.2 mm, C_u = 1.6) reinforced with polyamide fibres (d_f = 0.1 mm); effect of volumetric fibre ratio (V_{fr}), aspect ratio ($\eta = L_f/d_f$) and confining stress ($\bar{\sigma}_3$); fibre content originally expressed in terms of ρ, i.e. the ratio of the volume of fibre to the volume of the sample; a), b) and c) deviatoric stress q vs axial strain ε_1 (Michalowski & Čermák, 2003); d), e) and f) increase in deviatoric ratio (q/p') at ε_1 = 10% (data from Michalowski & Čermák, 2003)

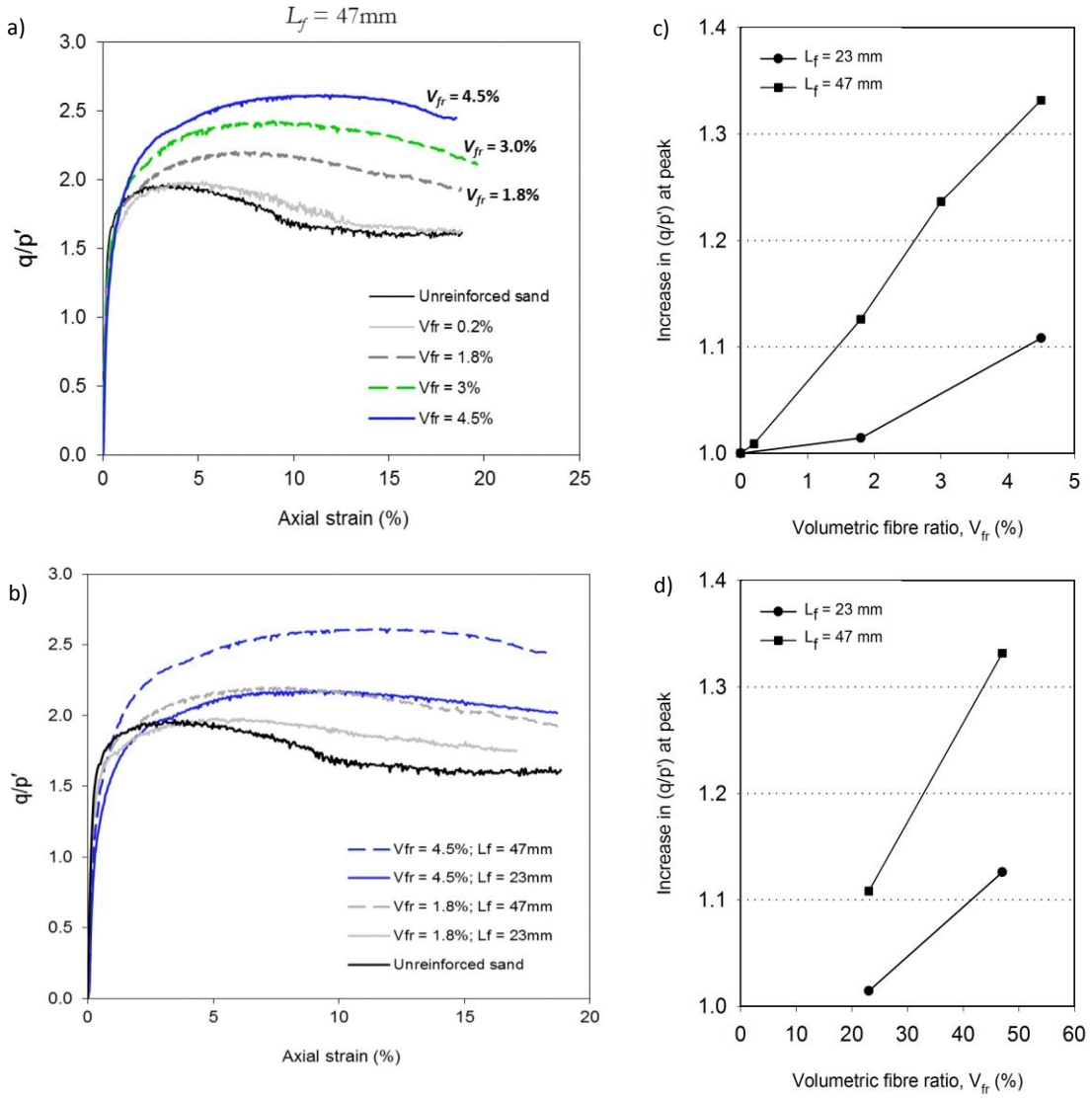

Figure 4-4. Triaxial tests on sand (D_{50} = 1.4, C_u = 1.4) unreinforced and reinforced with platy polypropylene fibres (t_f = 0.1 mm, W_f = 2 mm); effect of volumetric fibre content (V_{fr}) and fibre length (L_f); a) and b) deviatoric ratio (q/p') vs axial strain (Ajayi, 2014); c) and d) increase in deviatoric ratio (q/p') at peak (data from Ajayi, 2014)

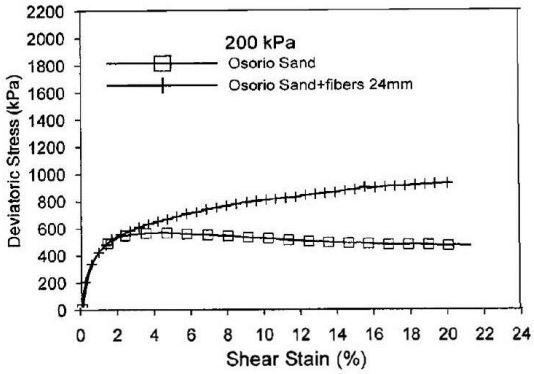

Figure 4-5. Triaxial tests on sand (D_{50} = 0.15 mm, C_u = 1.9) unreinforced and reinforced with polypropylene fibres (L_f = 24 mm, d_f = 0.023 mm); fibre content by mass of 0.5% (V_{fr} = 1.5%) and confining stress of 200 kPa (Heineck et al., 2005)

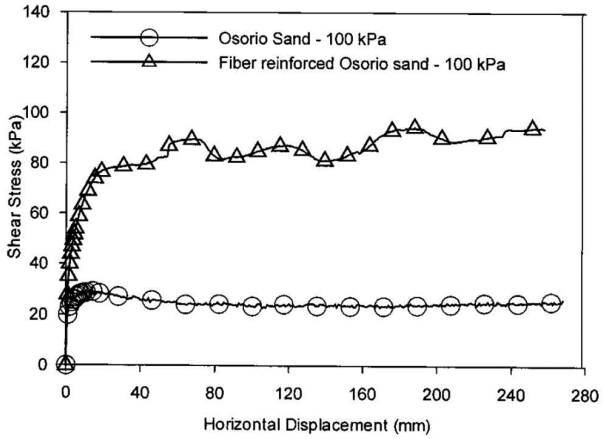

Figure 4-6. Ring shear tests on sand (D_{50} = 0.15 mm, C_u = 1.9) unreinforced and reinforced with polypropylene fibres (L_f = 24 mm, d_f = 0.023 mm); fibre content by mass of 0.5% (V_{fr} = 1.5%) and normal stress of 100 kPa (Heineck et al., 2005)

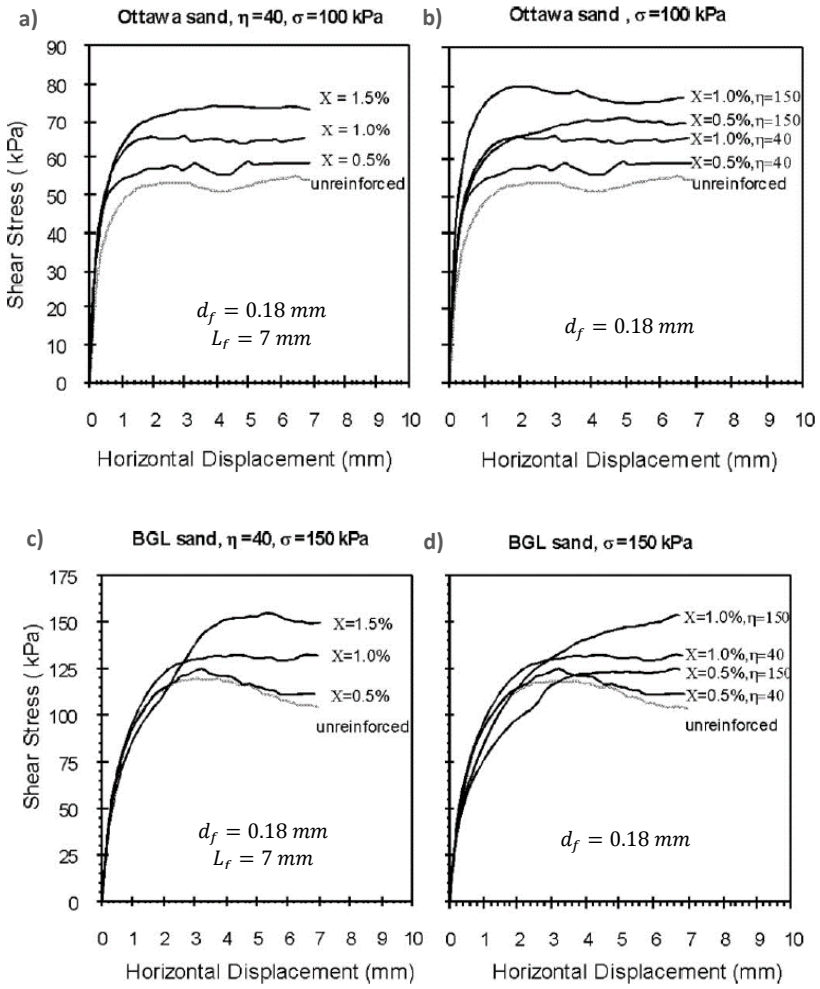

Figure 4-7. Ring shear tests on Ottawa sand (D_{50} = 0.39 mm, C_u = 1.95) and BGL sand (D_{50} = 1.45 mm, C_u = 1.83) reinforced with nylon fibres; (a) and (c) effect of the volumetric fibre content (X), defined as the ratio of the volume of fibre to the volume of the sample ($V_{fr} \cong 2.5\%$ for $X = 1.5\%$); (b) and (d) effect of the aspect ratio $\eta = L_f/t_f$ (Sadek et al., 2010)

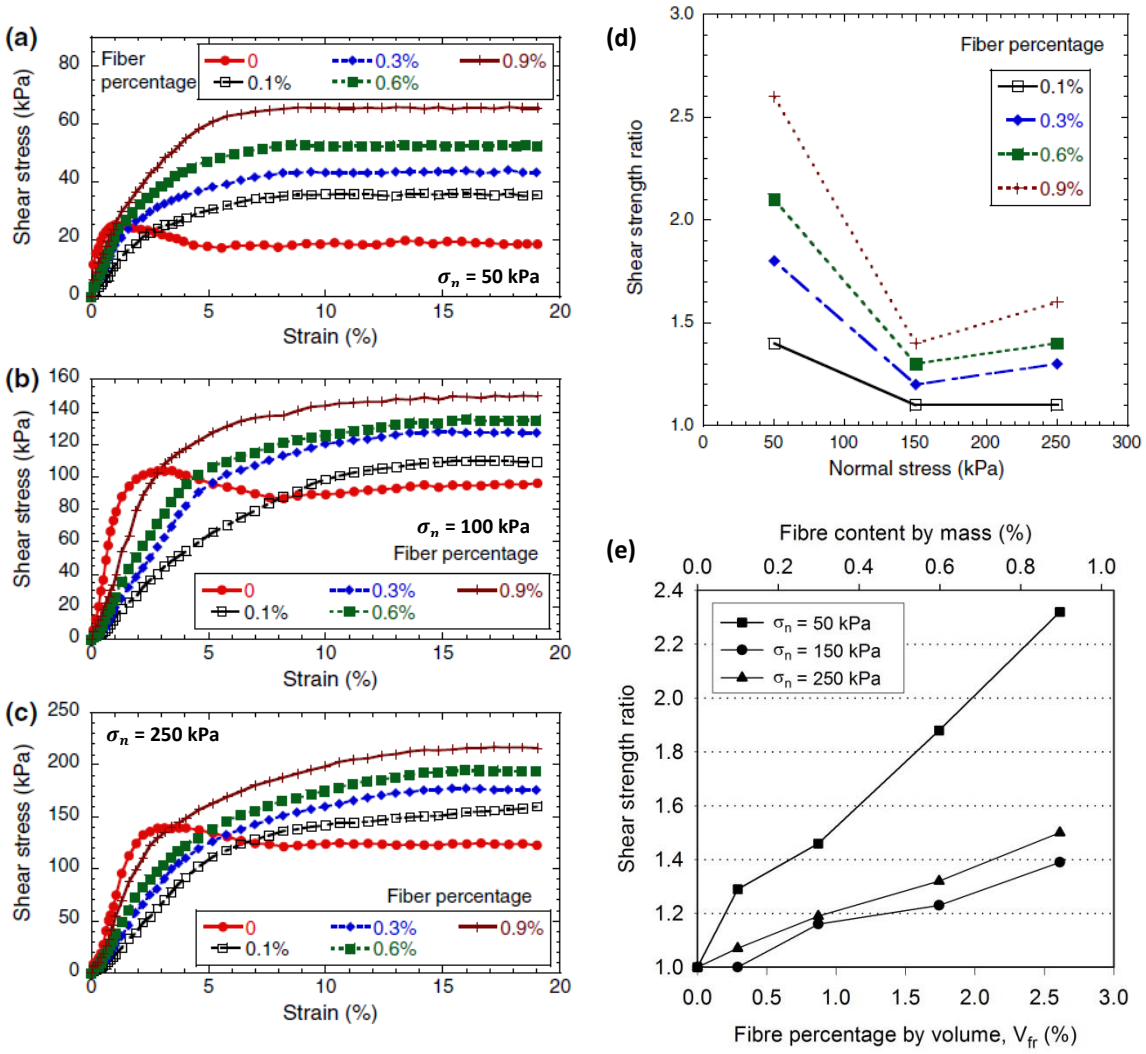

Figure 4-8. Ring shear tests on unreinforced and reinforced sand; fibre content by mass up to 0.9%, i.e. V_{fr} up to 2.6%; effect of fibre content and normal stress; (a), (b) and (c) shear stress vs strain (Shao et al., 2014); (d) and (e) increase in shear strength (data from Shao et al., 2014)

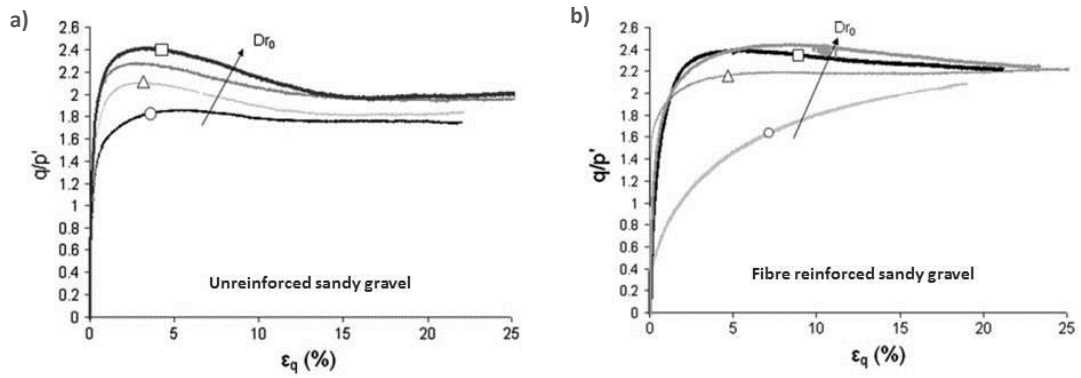

Figure 4-9. Triaxial tests on sandy gravel (D_{50} = 3 mm, C_u = 12.5) unreinforced and reinforced with polypropylene fibres (L_f = 50 mm, d_f = 0.1 mm); fibre content by mass of 0.2% (V_{fr} = 0.6%); initial relative density D_{r0} of 10% to 70%; deviatoric ratio q/p' vs deviatoric strain ε_q (Lirer et al., 2012)

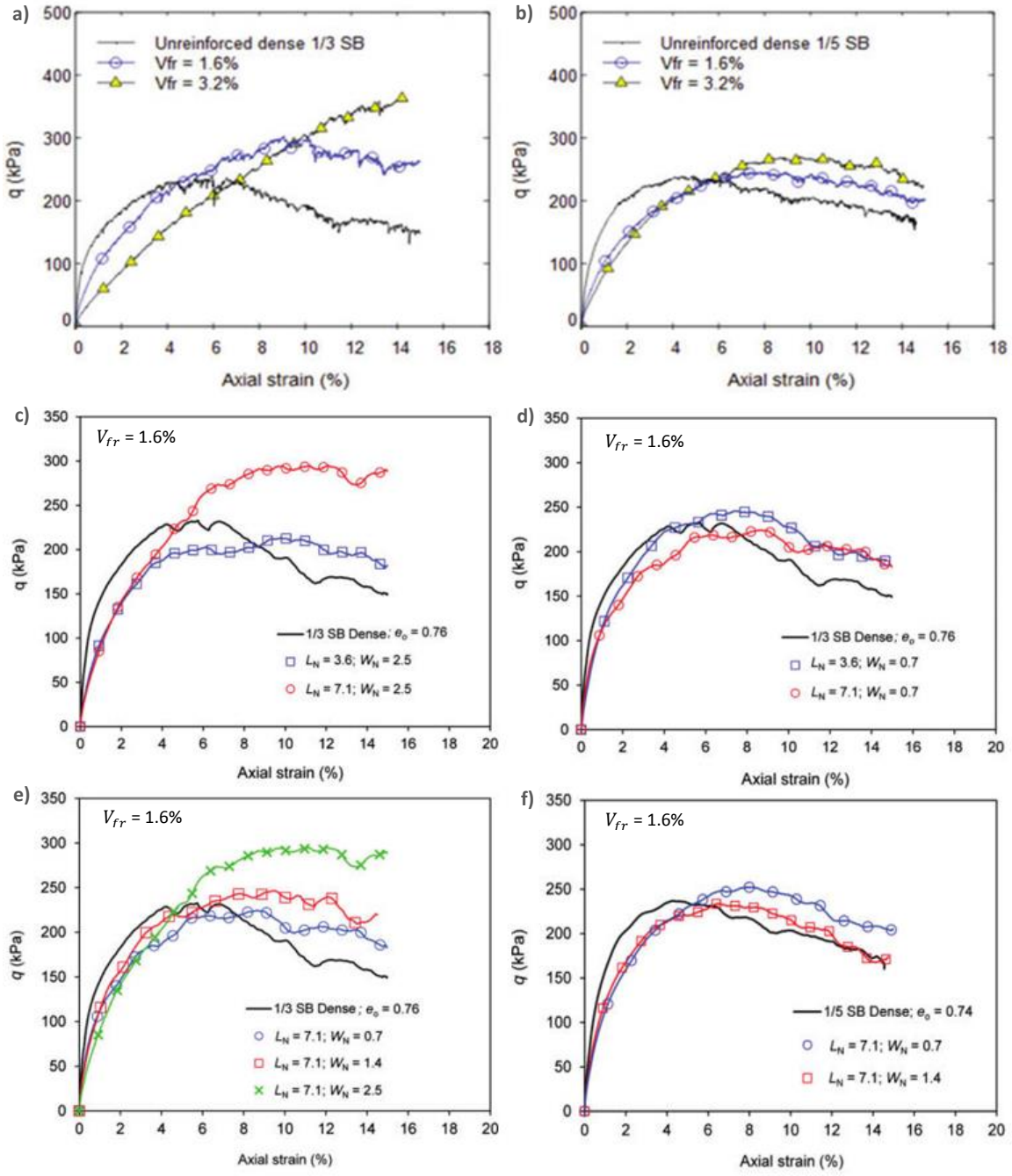

Figure 4-10. Triaxial tests on 1/3 and 1/5 scaled railway ballast (D_{50} = 13 mm and 8 mm, respectively) reinforced with platy polyethylene fibres; deviatoric stress (q) vs axial strain; a) and b) effect of volumetric fibre ratio (V_{fr}) on 1/3 and 1/5 ballast; (c) and d) effect of fibre length ($L_N = L_f/D_{50}$) on 1/3 ballast; e) and f) effect of fibre width ($W_N = W_f/D_{50}$) on 1/3 and 1/5 ballast (Ajayi et al., 2017b)

4.2.3 Volumetric behaviour

Typical volumetric strain vs deviatoric stress curves obtained from triaxial tests using unreinforced and reinforced granular materials, i.e. sands and gravels, are shown below (Figure 4-11 to Figure 4-17). Usually, unreinforced samples are characterised by small initial compression followed by dilation, and fibre addition increases the amount of initial compression while reducing the subsequent dilation, as shown in Figure 4-13 to Figure 4-17 (Michalowski & Čermák,

2003; Heineck et al., 2005; Lirer et al., 2012; Ajayi, 2014; Ajayi et al., 2017b). However, there are exceptions. For example, Diambra et al. (2013) and Santos et al. (2010) found fibres to inhibit the compacting behaviour of lightly compacted or highly confined samples (Figure 4-11 and Figure 4-13b).

Like the mobilised shear strength, the volumetric behaviour of fibre reinforced granular materials is affected by the fibre content. Higher fibre contents are typically associated with greater inhibition of dilation; in contrast, the volumetric response does not seem particularly affected by fibre dimensions, e.g. length and width (Figure 4-15, Figure 4-17).

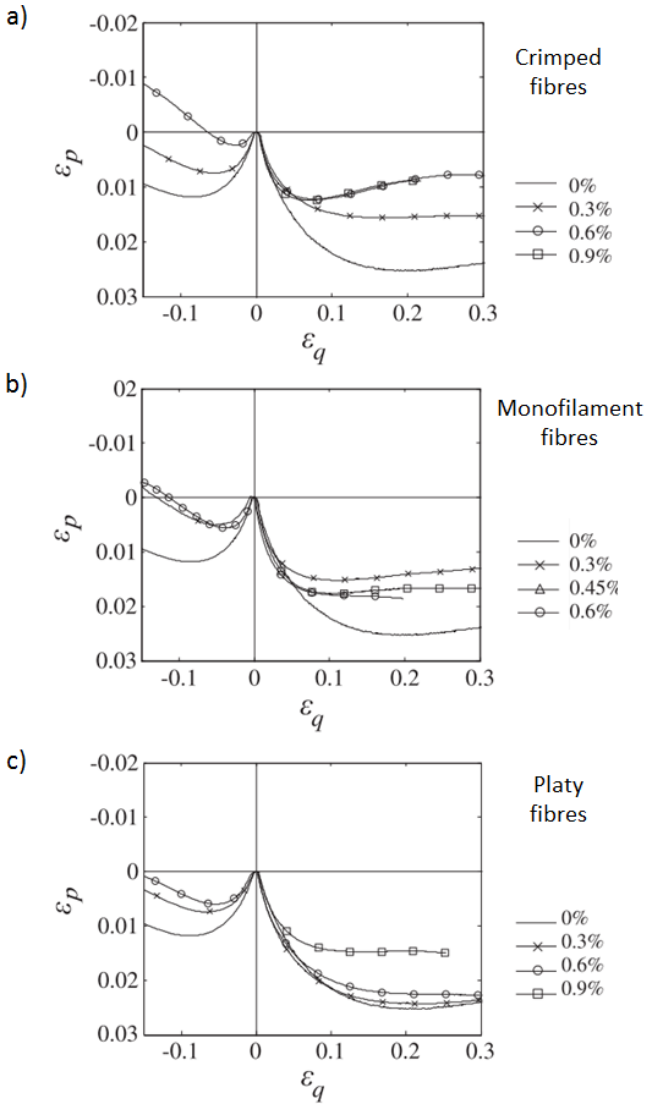

Figure 4-11. Triaxial tests on loose samples ($D_r \cong 0$, D_{50} = 0.32 mm, C_u = 1.7) of sand reinforced with different types of polypropylene fibres; fibre content by mass up to 0.9% (V_{fr} up to 2.6%); confining stress of 100 kPa; volumetric strain ε_p vs deviatoric strain ε_q (Diambra et al., 2013)

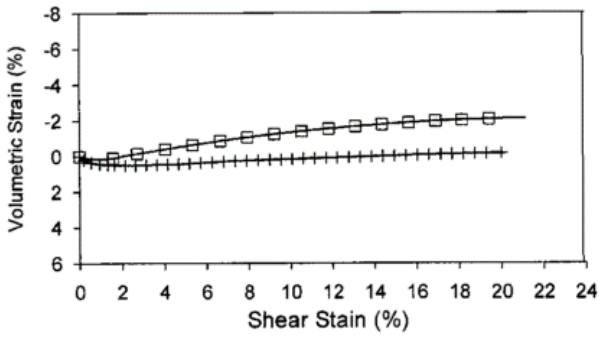

Figure 4-12. Triaxial tests on Osorio sand (D_{50} = 0.15 mm, C_u = 1.9) unreinforced and reinforced with polypropylene fibres (L_f = 24 mm, d_f = 0.023 mm); fibre content by mass of 0.5% ($V_{fr} = 1.5\%$); confining pressure of 200 kPa; volumetric strain vs shear strain (Heineck et al., 2005)

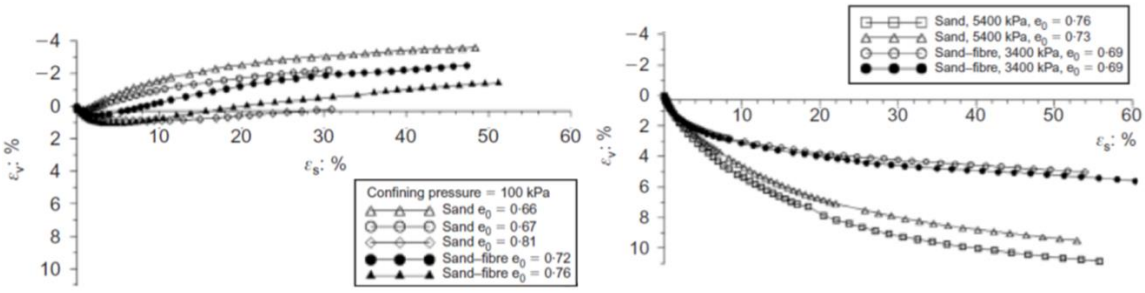

Figure 4-13. Triaxial tests on sand (D_{50} = 0.16 mm, C_u = 2.1) unreinforced and reinforced with 0.5% by mass ($V_{fr} = 1.5\%$) polypropylene fibres (L_f = 24 mm, d_f = 0.023 mm); volumetric strain ε_v vs shear strain ε_s; (a) low confinement; (b) high confinement (Santos et al., 2010)

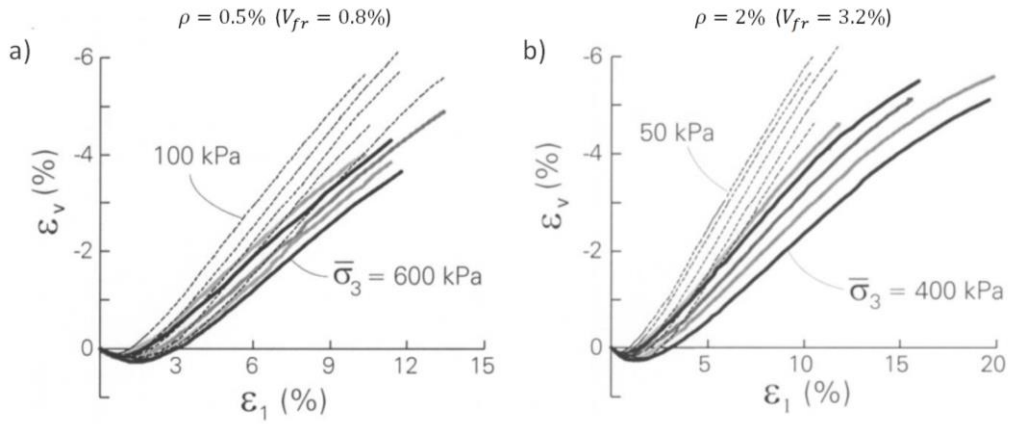

Figure 4-14. Triaxial tests on fine sand (D_{50} = 0.2 mm, C_u = 1.6) unreinforced and reinforced with polyamide fibres (L_f = 25.4 mm, d_f = 0.3 mm, $\eta = L_f/d_f$ = 85); volumetric strain ε_v vs axial strain ε_1; fibre content originally expressed in terms of ρ, i.e. the ratio of the volume of fibre to the volume of the sample; (a) fibre content of ρ = 0.5% (V_{fr} = 0.8%) and confining stress of 100 kPa to 600 kPa; (b) fibre content of ρ = 2% (V_{fr} = 3.2%) and confining stress of 50 kPa to 400 kPa; (Michalowski & Čermák, 2003)

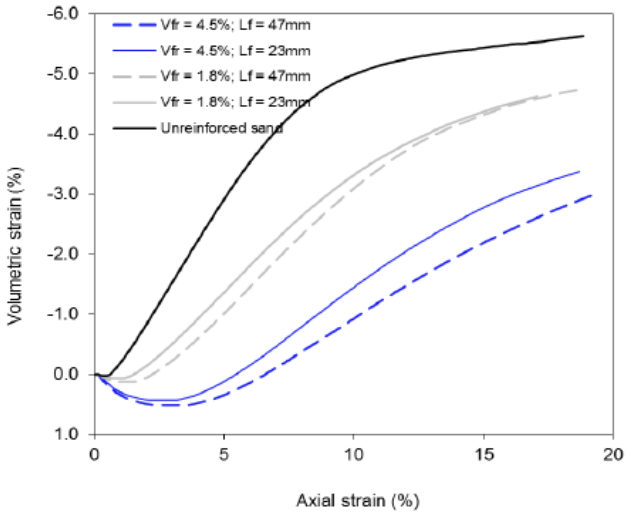

Figure 4-15. Triaxial tests on sand (D_{50} = 1.4, C_u = 1.4) unreinforced and reinforced with platy polypropylene fibres (t_f = 0.1 mm, W_f = 2 mm); effect of fibre content (V_{fr} = 1.8% and 4.5%) and fibre length (L_f = 23 mm and 47 mm); volumetric strain vs axial strain (Ajayi et al., 2014)

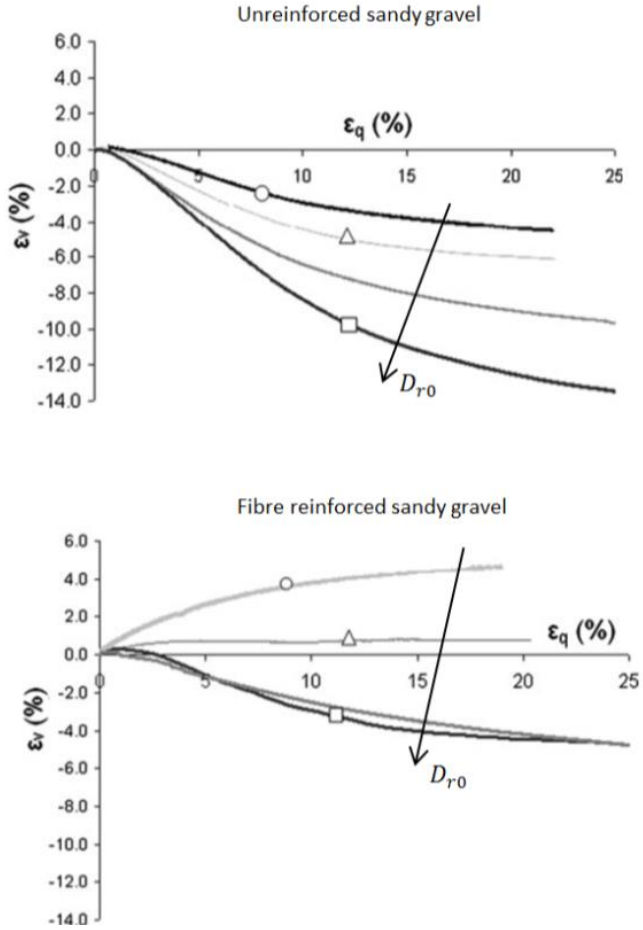

Figure 4-16. Triaxial tests on sandy gravel (D_{50} = 3 mm, C_u = 12.5) unreinforced and reinforced with polypropylene fibres (L_f = 50 mm, d_f = 0.1 mm); fibre content by mass of 0.2% (V_{fr} = 0.6%); initial relative density D_{ro} of 10% to 70%; volumetric strain ε_v vs deviatoric strain ε_q (Lirer et al., 2012)

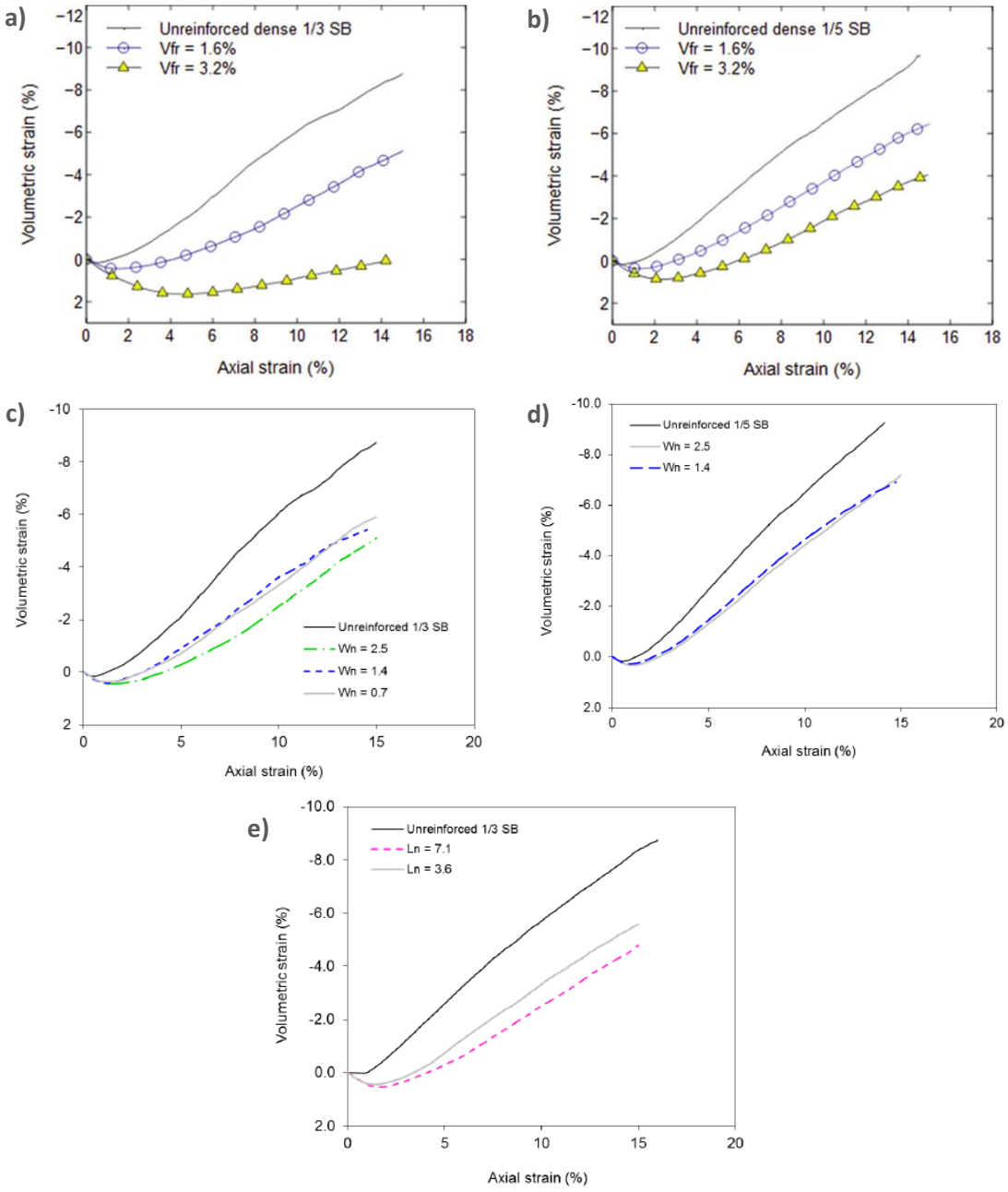

Figure 4-17. Triaxial tests on 1/3 and 1/5 scaled ballast (D_{50} = 13 mm and 8 mm respectively) unreinforced and reinforced with platy polyethylene fibres; volumetric strain vs axial strain; a) and b) effect of fibre content V_{fr} (Ajayi et al., 2017b); c) and d) effect of fibre width, $W_N = W_f/D_{50}$; e) effect of fibre length, $L_N = L_f/D_{50}$ (Ajayi, 2014)

4.2.4 Deformability

The deformability behaviour of fibre reinforced granular materials is complex and not fully understood, as researchers have mainly focused on their strength. In this section, the existing literature is analysed to illustrate the effect of fibre addition on the elastic and plastic strain response.

The behaviour of granular materials under monotonic and cyclic loading is strongly non-linear and inelastic. Thus their deformability cannot be expressed by a single parameter. For this reason, herein, it is described in terms of: (1) stiffness at very small strains; (2) secant stiffness over a load

cycle; (3) initial secant stiffness during first-time loading; and (4) permanent strain under cyclic loading. The elastic behaviour is described by (1) and (2); the plastic behaviour, i.e. the material propensity to suffer irreversible deformation, by (3) and (4).

The elastic strain response of fibre reinforced granular materials is not clear. Cyclic triaxial tests on sand and gravel by Sadeghi & Beigi (2014) and Lirer et al. (2012) showed that fibres can increase the average secant stiffness during the load cycles, especially under low confining and small deviatoric stress (Figure 4-18, Figure 4-19). Heineck et al. (2005) showed that the presence of fibres has almost no effect on sand stiffness at very small strain, which was measured using bender elements (Figure 4-20). Contrasting results were obtained by Abadi (2014) and Ajayi (2014), who found railway ballast resilient deflections to increase with fibre addition (Figure 4-22b).

Under monotonic loading material susceptibility to permanent deformation can be represented by the initial gradient of the stress-strain curves. Usually it reduces with the addition of fibres (Figure 4-1, Figure 4-3, Figure 4-4, Figure 4-9, Figure 4-10) or remains unaffected (Figure 4-2, Figure 4-5). Thus for applied shear stresses lower than the host material peak strength, fibres seem to increase material propensity to develop plastic deformations. This might be explained by the fibres disrupting the packing of the particles and hence, increasing the volume of the voids and, in turn, allowing for greater particle rearrangement. The increase in void ratio with fibre addition has been observed by many (Casagrande, 2005; Santos et al., 2010; Lirer et al., 2012; Ajayi et al., 2014). As cited in Santos et al. (2010), Casagrande (2005) observed that the void ratio values of reinforced sand are higher than those of pure sand. Santos et al. (2010) observed that sand minimum and maximum void ratios increased by 0.5 with the addition of a 1.44% volume of fibres. Lirer et al. (2012) found that the addition of a small quantity of fibres ($V_{fr} = 0.6\%$) increased e_{min} and e_{max} of sandy gravel from 0.19 to 0.23 and from 0.60 to 0.85 respectively. Ajayi et al. (2014) showed that the increase in sand and gravel void ratio is approximately linear with the fibre content and, in agreement with Lirer et al. (2012), more evident for looser samples (Figure 4-21).

Despite the above, a laboratory test carried out by Abadi (2014) using the full-size testing rig described in Section 5.20 showed that fibres can reduce the settlement of railway ballast under cyclic loading (Figure 4-22). This might be related to the type of reinforcement used, i.e. a small amount of thin plastic strips. However, the results from this test should be carefully compared with those obtained from triaxial tests. The latter are characterised by uniform stress that varies periodically with the loading cycles. The testing rig used by Abadi (2014) reproduced more closely the stresses on a real railway track, which varies over time, as the sleeper centre-binds (Section 2.3.2.2) and the ballast spreads laterally (Section 3.3.4). Moreover, the permanent deformation of railway ballast under cyclic loading is strongly dependent on the stiffness of the subgrade (Section 3.4.3). This effect is also not considered by triaxial tests. However, the full-size tests by Abadi (2014) neglect the settlement developed in the first 10 load cycles to eliminate the effect of the bedding errors. These, as will be clearer in Section 8.2.2, may account for more than 35% of the total settlement at 3 million cycles. Thus, although some monotonic triaxial tests suggested that fibres increase soil propensity to develop permanent deformation at low stress/strain level, properly selected fibres might reduce ballast settlement under repeated loading, at least after a relatively small initial settlement corresponding to the first 10 load cycles.

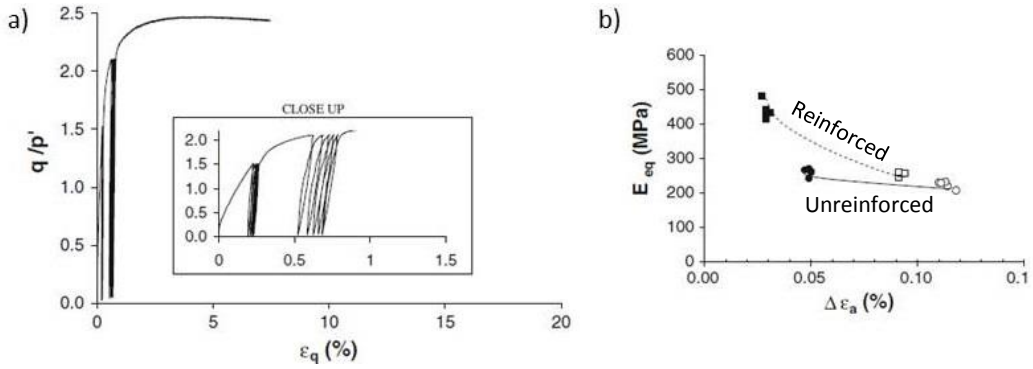

Figure 4-18. Cyclic triaxial test on sandy gravel (D_{50} = 3 mm, C_u = 12.5) reinforced with polypropylene fibres (L_f = 50 mm, d_f = 0.1 mm); equivalent Young modulus E_{eq} at different levels of axial deformation $\Delta\varepsilon_a$; fibre content by mass of 0.2%, i.e. V_{fr} = 0.6% (Lirer et al., 2012)

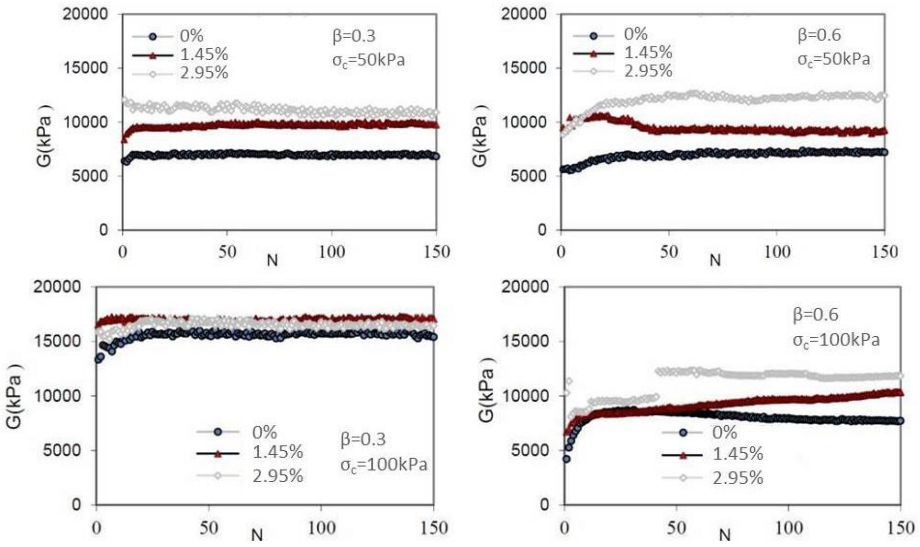

Figure 4-19. Cyclic triaxial tests on clayey sand (D_{50} = 1.11 mm, C_u = 349) unreinforced and reinforced with polypropylene fibres (L_f = 12 mm, d_f = 0.023 mm) ; volumetric fibre contents of 0% to 2.95%; deviator ratio $\beta = \sigma_1/2\sigma_3$ of 0.3 and 0.6, where σ_1 and σ_3 are the major and minor principal stresses, respectively; confining stress (σ_c) of 50 kPa and 100 kPa; shear modulus over a load cycle (G) vs number of cycles (N) (Sadeghi & Beigi, 2014)

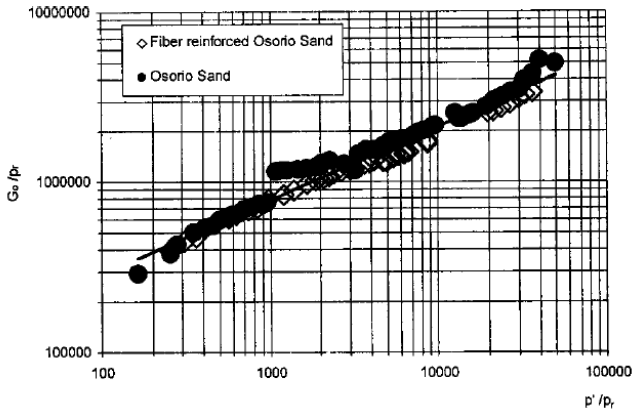

Figure 4-20. Triaxial tests on sand (D_{50} = 0.15 mm, C_u = 1.9) unreinforced and reinforced with polypropylene fibres (L_f = 24 mm, d_f = 0.023 mm); fibre content by mass of 0.5% (V_{fr} = 1.5%); shear modulus at small strain G_0 vs isotropic pressure p'; the reference pressure p_r was taken as 1 kPa; G_0 measured using bender elements during consolidation (Heineck et al., 2005)

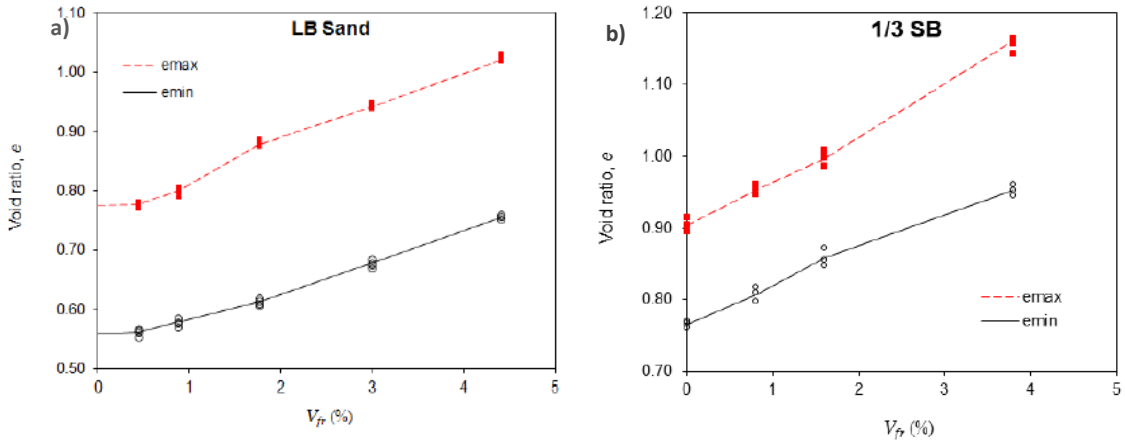

Figure 4-21. Effect of volumetric fibre content (V_{fr}) on the void ratio of: a) sand ($D_{50} = 1.4\ mm$, C_u = 1.4) reinforced with platy polypropylene fibres ($L_f = 23\ mm$, $W_f = 2\ mm$, $t_f = 0.1\ mm$); b) 1/3 scaled railway ballast ($D_{50} = 12\ mm$, C_u = 1.5) reinforced with platy polyethylene fibres ($L_f = 100\ mm$, $W_f = 20\ mm$, $t_f = 0.5\ mm$) (Ajayi, 2014)

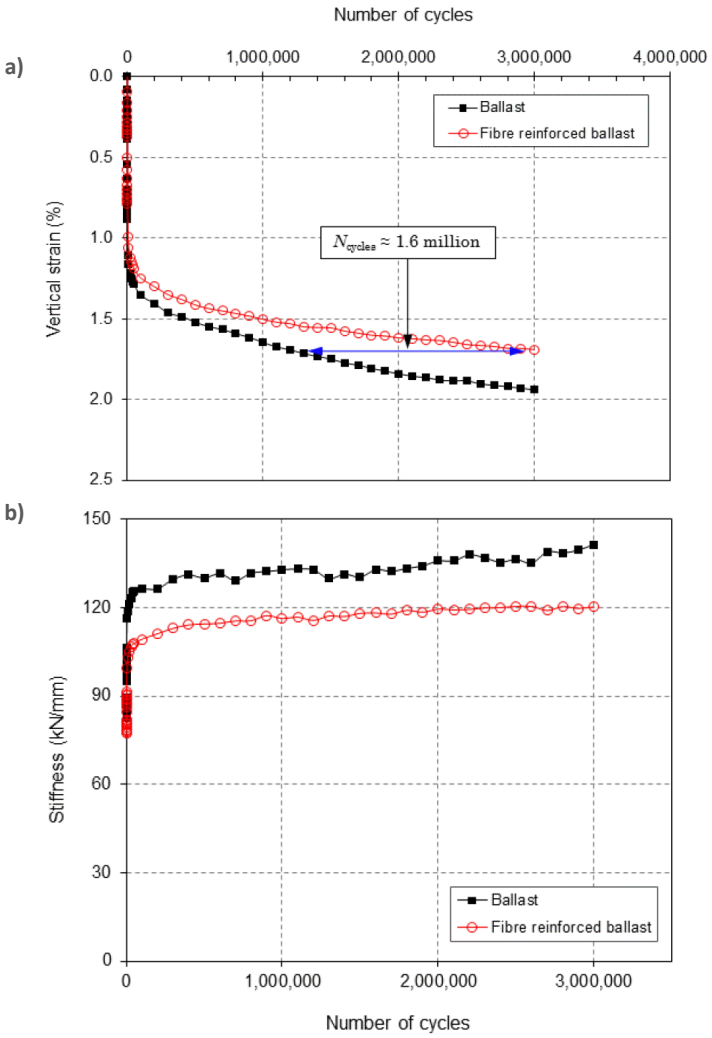

Figure 4-22. Full size cyclic tests on unreinforced and fibre-reinforced railway ballast; volumetric fibre ratio V_{fr} of 0.6%; a) permanent vertical strain and b) sleeper support stiffness vs number of cycles; permanent strain is zeroed after 10 load cycles to mitigate bedding errors (Ajayi, 2014)

4.3 Mechanics of fibre-reinforced granular materials

4.3.1 Fibre-particle interaction

Usually, laboratory experiments focus on the macro-scale behaviour of fibre-reinforced granular materials, e.g. mobilised shear strength and deformability. Therefore, they cannot provide a clear understanding of the mechanics of fibre reinforcement, which would instead require the analysis of fibre-grain interaction at the microscale.

There is general consensus that fibres provide additional confining stress by mobilising tension. Ajayi et al. (2017a) observed that the effect of fibre-reinforcement can be seen from two different perspectives. The most fundamental approach consists in considering that the granular matrix obeys its constitutive law, while the fibres mobilise tensions, affecting the effective stresses seen by the grains. As observed by Ajayi et al. (2017a), this can be taken into account by regarding the contribution of the fibres as an additional confining stress (Figure 4-23). This allowed them to bring the stress/strain response of a fibre reinforced gravel in line with that of its unreinforced granular matrix. The second approach neglects the effect of the tensions in the fibres on the stress/strain/strength response. Thus it expresses the effect of the fibres in terms of additional shear strength, and associates a reinforced material and its unreinforced counterpart with different strength envelopes (Maherer & Gray, 1990; Santos et al., 2010; Lirer et al., 2011).

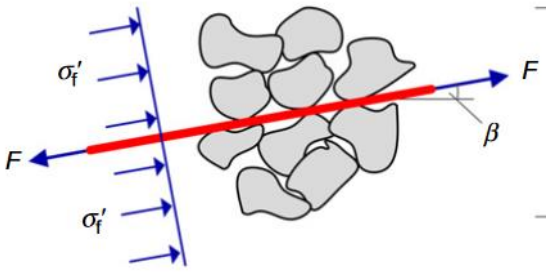

Figure 4-23. Representation of the additional apparent confinement (σ_f') associated with the tension (F) mobilised by the fibres interacting with the grains (Ajayi et al., 2017a)

Maherer & Gray (1990) observed that fibre reinforced sands have curved-linear or bilinear failure envelopes, the former exhibited by uniform rounded sands and the latter by well-graded angular sands (Figure 4-24). Similarly, Santos et al. (2010) found that the critical state envelope in the deviatoric plane for a fibre reinforced sand is bilinear: under low confining stress the failure lines of fibre-sand composite and pure sand diverged while under high confinement they tended to converge (Figure 4-25).

The non-linearity of the failure envelopes of reinforced materials suggests that fibre-particle interaction is affected by the level of confinement. Maherer & Gray (1990) and Santos et al. (2010) interpreted the variation of the gradient of the failure envelopes as the result of the change from a slip to a stretching mechanism: if lightly confined, i.e. the confining stress (σ_c) is smaller than the critical stress (σ_{cr}), fibres slip during deformation; otherwise they stretch or yield (Figure 4-26). Thus smaller values of σ_{cr} are representative of a more effective fibre-particle interaction: if the

particles are more strongly engaged by the fibres, the latter can be stretched under a lower confining stress and provide a greater additional strength. Maherer & Gray (1990) found that σ_{cr} can be reduced (and the strength increased) by increasing fibre aspect ratio, more broadly-graded host materials (Figure 4-27) and reducing grain sphericity (Figure 4-28).

The mechanics of fibre-reinforcement is governed by a large number of factors. Based on the existing literature, the main governing factors are fibre characteristics (e.g. content, dimensions, orientations and mechanical properties), sample conditions (e.g. initial density), load conditions (e.g. confining stress) and particle characteristics (e.g. size, roughness and angularity) (Gray & Ohashi, 1983; Maherer & Gray, 1990; Santoni et al., 2001; Michalowski & Čermák, 2003; Diambra et al., 2007; Sadek et al., 2010; Santos et al., 2010; Lirer et al., 2011; Diambra et al., 2013; Ajayi, 2014; Sadeghi & Beigi, 2014; Shao et al., 2014; Ajayi et al., 2017b). These are discussed in more detail in Section 4.3.2.

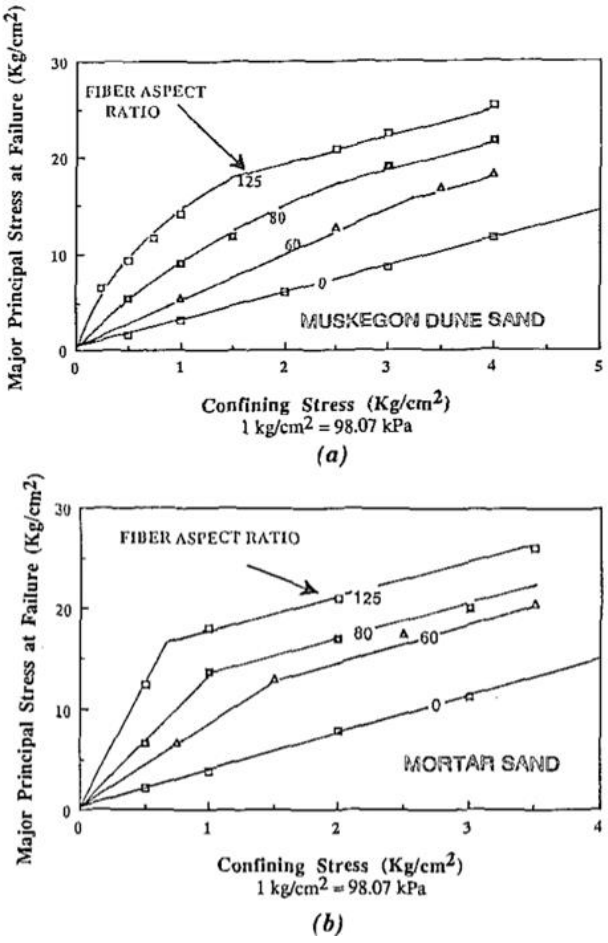

Figure 4-24. Principal stress envelopes from triaxial tests on sand reinforced with glass fibres (fibre content by weight of 3%, d_f = 0.3 mm); (a) Muskegon Dune Sand (D_{50} = 0.41 mm, C_u = 1.5); (b) Mortar Sand (D_{50} = 0.6 mm, C_u = 4.13) (Maherer & Gray, 1990)

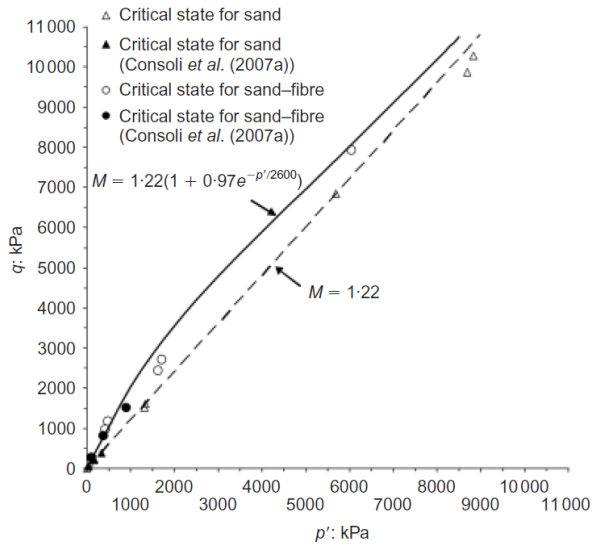

Figure 4-25. Critical state strength envelopes for sand (D_{50} = 0.16 mm, C_u = 2.1, C_c = 1.0) and sand reinforced with polypropylene fibres (L_f = 24 mm, d_f = 0.023 mm) (Santos et al., 2010)

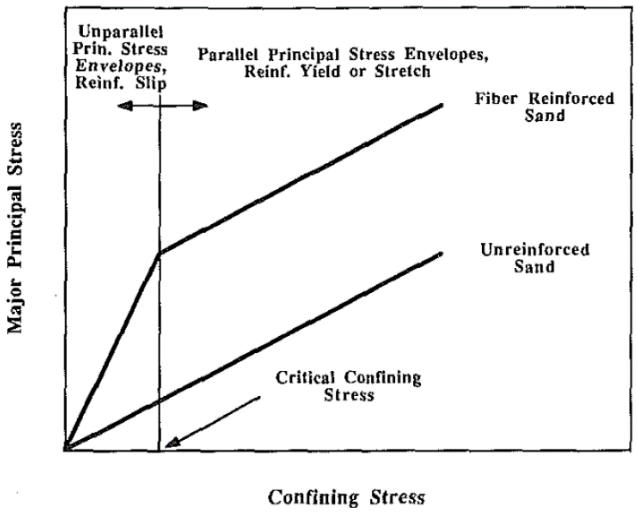

Figure 4-26. Schematic representation of the effect of fibre addition on sand failure envelope (Maherer & Gray, 1990)

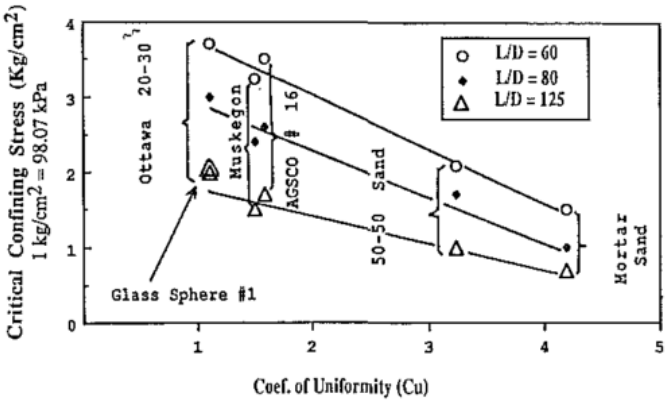

Figure 4-27. Direct shear tests on different sands reinforced with 3% by mass glass fibres($V_{fr} \simeq 3\%$) of different aspect ratios ($\eta = L_f/d_f = 60, 80, 125$); effect of grading (coefficient of uniformity C_u) on the critical confining stress σ_{crit} (Maherer & Gray, 1990)

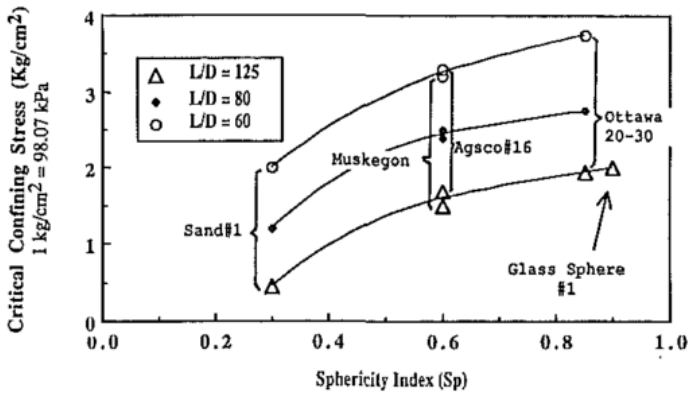

Figure 4-28. Direct shear tests on different sands reinforced with 3% by mass glass fibres ($V_{fr} \simeq 3\%$) of different aspect ratios ($\eta = L_f/d_f = 60, 80, 125$); effect of particle shape (Sphericity Index S_p) on the critical confining stress σ_{crit} (Maherer & Gray, 1990)

4.3.2 Governing factors

4.3.2.1 Fibre content

It is widely accepted that the shear strength and ductility of granular materials increases with the amount of reinforcement. As observed in Section 4.2.2, the strength of granular materials increases fairly linearly with the fibre content (Gray & Ohashi, 1983; Maherer & Gray, 1990; Santoni et al., 2001; Michalowski & Čermák, 2003; Diambra et al., 2013; Shao et al., 2014; Ajayi, 2014; Ajayi et al., 2017b). However, a threshold value seems to exist, above which no further improvements are observed (Maherer & Gray, 1990; Santoni et al., 2001).

As shown in Section 4.2.2, fibre addition usually reduces soil dilation at failure. The propensity to dilate reduces with the fibre content and seems just slightly affected by fibre dimensions, as shown in Figure 4-15 and Figure 4-17 (Ajayi, 2014; Ajayi et al., 2017b).

The effect of fibres on the deformability is unclear, as different studies showed contrasting results (Section 4.2.4). The effect of fibre content on soil resilient response was investigated by Sadeghi & Beigi (2014) through a series of cyclic triaxial tests on sand. They found that the average stiffness over a load cycle increases with the fibre content (Figure 4-19). Michalowski & Čermák (2003) and Ajayi et al. (2017b) noted that the initial secant stiffness under first-time loading reduces with the amount of reinforcement, meaning that under a relatively low stress fibres might increase material permanent deformation (Figure 4-3, Figure 4-10). This could be related to fibre tendency to disruption the natural packing of the particle and hence, reduce material density (Figure 4-21).

Maherer & Gray (1990) noted that, although the additional shear strength increases with increasing fibre content, the critical stress remains unaffected (Section 4.3.1). This can be explained by the proportion of grains engaged by the fibres increasing with the amount of reinforcement, while the mode of fibre/particle interaction (i.e. slipping, stretching or yielding), which according to Maherer & Gray (1990) is related to the critical stress, remains unaffected.

4.3.2.2 Fibre dimensions

The mechanical response of fibre reinforced granular materials is strongly affected by the geometry of the fibres. Fibres are typically filamentous or platy. Filamentous fibres are geometrically described by their length (L_f) and diameter (d_f) while platy (or tape-like) fibres are characterised by their length (L_f), thickness (t_f) and width (W_f). Another important geometrical parameter is the aspect ratio, i.e. the ratio of the fibre length to the fibre diameter ($\eta = L_f/d_f$).

As observed in Section 4.2.2, the strength of fibre reinforced granular materials increases significantly with fibre aspect ratio and length (Maherer & Gray, 1990; Michalowski & Čermák, 2003; Sadek et al., 2010; Ajayi, 2014; Ajayi et al., 2017b). Michalowski & Čermák (2003) found that sand strength increases linearly with the aspect ratio, meaning that sand performance can be improved by either increasing the length of the fibres or reducing the diameter (Figure 4-3). This can be explained by longer fibres mobilising greater fibre-grain frictional resistance and slender ones increasing the number of fibres at a fixed volumetric content (Maherer & Gray, 1990; Michalowski & Čermák, 2003; Sadek et al., 2010; Ajayi et al., 2017b). Moreover, as observed in Section 4.3.1, the increase in fibre aspect ratio is reflected in the reduction of the critical stress, suggesting that slender fibres offer a more effective fibre/particle interaction (Figure 4-27, Figure 4-24). The additional shear strength can also be increased by using longer fibres at constant aspect ratio (Michalowski & Čermák, 2003; Sadek et al., 2010). However, according to Michalowski & Čermák (2003), this might be associated with a scale effect dependent on the relative fibre-grain size. In particular, as also observed by Ajayi et al. (2017), they noted that the reinforcing effect is significant if the fibre length is at least one order of magnitude greater than the average particle size and negligible when similar to the size of the voids.

The volumetric response of reinforced materials does not seem significantly affected by fibre dimensions (Section 4.3.2.1) while the effect of fibre geometry on the deformability has not yet been investigated. However, as observed in Section 5.4.3, fibre dimensions have great influence on the density and hence, might also affect material stiffness and propensity to develop plastic deformations.

4.3.2.3 Fibre orientation

The relative orientation between fibres and principal stresses has great influence on the reinforcing effect. Gray & Ohashi (1983) carried out a series of direct shear tests using different fibre orientations. They found that the optimum fibre orientation is about 60° to the shear surface, i.e. the direction of maximum tensile strain (Figure 4-29a). Accordingly, triaxial compression tests conducted by Michalowski & Čermák (2002) showed that horizontal fibres, hence oriented in the direction of maximum tensile strain, are more effective than vertical ones (Figure 4-29a). As a result of typical compaction procedures, fibres preferred orientation is usually horizontal (Michalowski & Čermák, 2002; Diambra et al., 2007). Thus, as forces on soil are typically vertical, fibres orientation is ideal. Moreover, it is worth pointing out that, regardless of their orientation, fibres do not weaken the soil (Figure 4-29). Therefore, they can be used when smaller horizontal forces are expected, e.g. on railway embankments (Section 2.3).

4.3.2.4 Fibre mechanical properties

The behaviour of reinforced granular materials can be affected by fibre mechanical characteristics, such as strength and stiffness.

Stronger fibres can withstand greater tensions and potentially provide a greater reinforcing effect. However, laboratory tests showed no sign of extensive fibre breakage, unless the confining stress was particularly high (Gray & Ohashi, 1983; Michalowski & Čermák, 2003; Heineck et al., 2005; Lirer et al., 2012; Diambra et al., 2013). Thus, especially for shallow applications, the effect of fibre strength should be marginal.

Stiffer fibres can mobilise greater tensile stresses at a given strain level and, as a result, should provide greater additional confinement. A number of studies provided indications of the effect of fibre stiffness, e.g. fibre Young's modulus (E_f), on the mobilised shear strength (Gray & Ohashi, 1983; Maherer & Gray, 1990; Michalowski & Čermák, 2003). Gray & Ohashi (1983) observed that copper wire fibres ($E_f = 58.9$ GPa) offer only a marginal strength increase compared with Palmyra fibres ($E_f = 16.5$ GPa) (Figure 4-30). Maherer & Gray (1990) observed that Palmyra fibres ($E_f = 16.5$ GPa) and Reed fibres ($E_f = 1.52$ GPa), although characterised by very different values of stiffness, provided similar extents of improvement; only particularly soft fibres, such as Buna-N Rubber ($E_f = 0.01$ GPa), was found to perform poorly (Figure 4-31). Later, triaxial tests by Michalowski & Čermák (2003) showed that the reinforcing effect provided by steel fibres ($E_f \cong 200$ GPa) was only slightly greater than that offered by polyamide fibres ($E_f \cong 2$ GPa) of the same geometry and content (Figure 4-32). Thus, as long as fibres are not extremely deformable, their stiffness does not seem particularly relevant to the reinforcing effect. This might be explained by mostly frictional sand-fibre interaction, i.e. fibres slip through the grains and the mobilised tension is proportional to the fibre/grain friction angle rather than fibre stiffness.

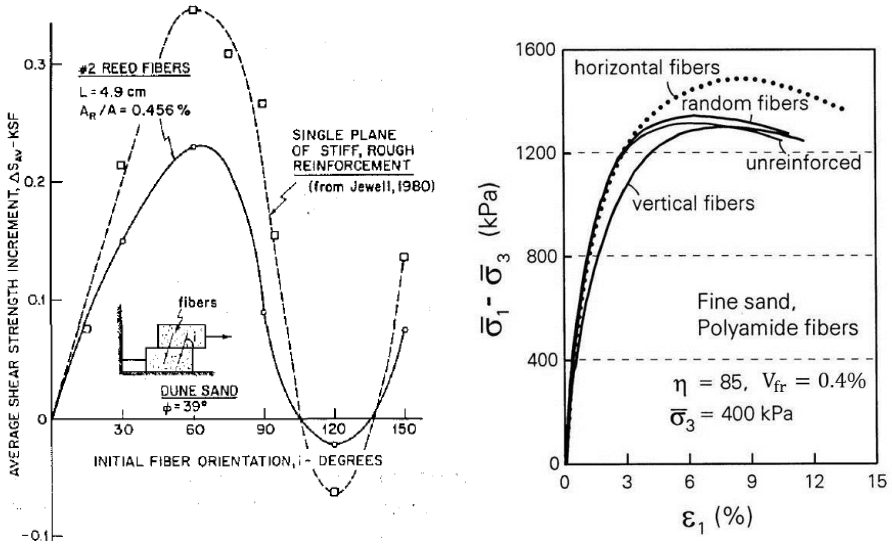

Figure 4-29. Effect of fibre orientation on sand mobilised shear strength: (a) direct shear tests, increase in shear strength vs fibre orientation (Gray & Ohashi, 1983); (b) triaxial tests, deviator stress vs axial strain (Michalowski & Čermák, 2002)

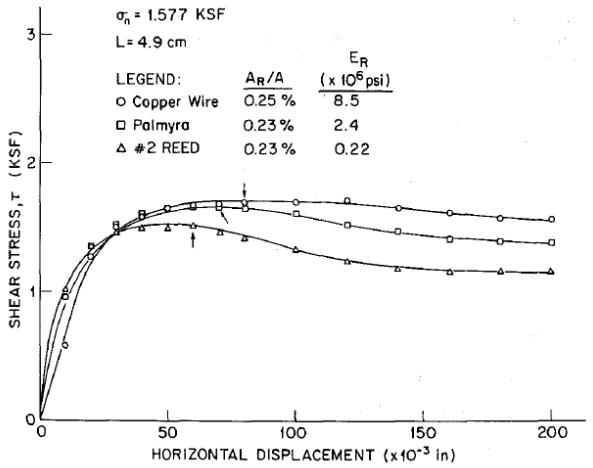

Figure 4-30. Direct shear tests on sand reinforced with fibres of different Young's modulus (E_f): copper wire (E_f = 58.9 GPa), palmyra fibres (E_f = 16.5 GPa), reeds (E_f = 1.52 GPa) (Gray & Ohashi, 1983)

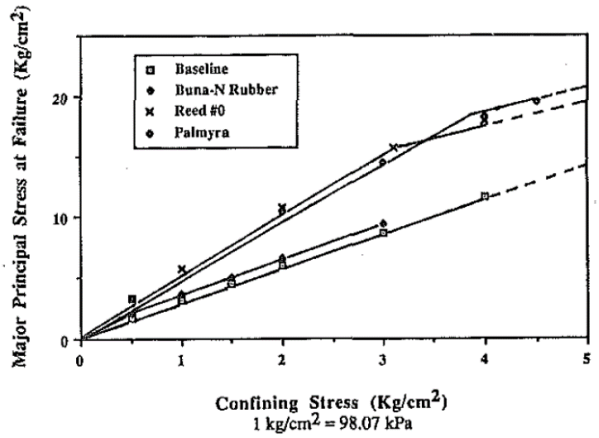

Figure 4-31. Strength envelopes from triaxial tests on unreinforced and reinforced sand ($D_{50} = 0.41\ mm$, $C_u = 1.5$); aspect ratio of 20 and surface friction angle of 30°; Buna-N Rubber: $E_f = 0.01\ GPa$, $d_f = 1.1\ mm$; Reed #0: $E_f = 1.52\ GPa$, $d_f = 1.0\ mm$; Palmyra: $E_f = 16.5\ GPa$, $d_f = 0.58\ mm$ (Maherer & Gray, 1990)

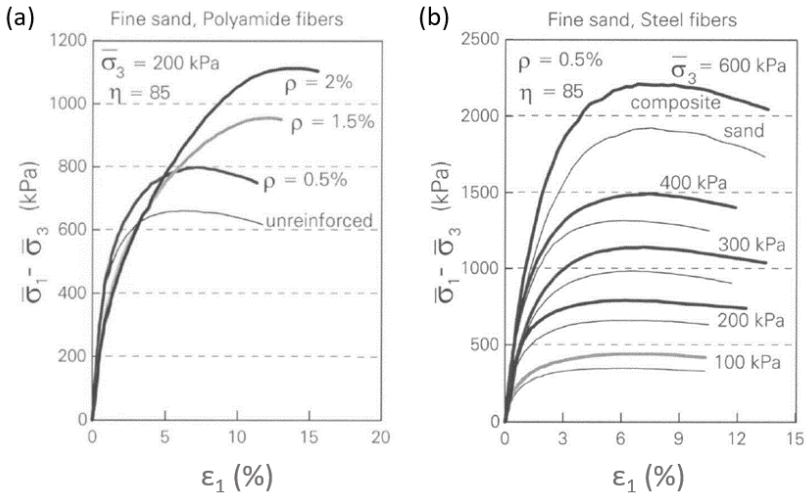

Figure 4-32. Triaxial tests on fine sand ($D_{50} = 0.2\ mm$, $C_u = 1.6$) reinforced with (a) polyamide fibres and (b) steel fibres of same geometry ($L_f = 25.4\ mm$, $d_f = 0.3\ mm$) and volumetric content ($V_{fr} = 0.8\%$) (Michalowski & Čermák, 2003)

4.3.2.5 Granular matrix characteristics and fibre type

Although the interaction between fibres and particles is complex and not fully understood, laboratory studies showed that reinforcement effectiveness is dependent on both soil and fibre properties. Maherer & Gray (1990) found that well-graded sands and small grain sphericity are associated with improved fibre-particle interlocking mechanism, as they reduce the critical stress and increase the shear strength (Figure 4-27). Santoni et al. (2001) compared the performance of different types of polypropylene fibres of similar geometry through a series of unconfined compression tests. They found that, although all types were very effective, fibrillated and tape-like fibres performed better than mono-filament fibres. However, they also noted that fibrillated fibres are more effective than tape-like fibres when added to concrete sand (D_{50} = 0.39 mm) but were outperformed if the host material was Yuma sand (D_{50} = 0.16 mm) (Figure 4-33). This highlights the complexity of fibre-particle interaction, which depends not only on fibre and particle characteristics but also on their combination.

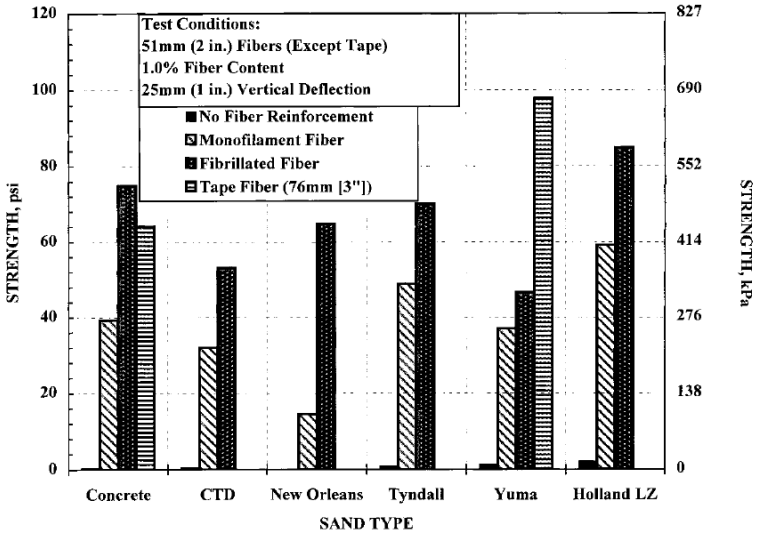

Figure 4-33. Unconfined compression tests on different sand types reinforced with different fibre types; fibre content of 1% by mass, fibre length of 51 mm (monofilament and fibrillated) and 76 mm (tape); sand types: concrete (D_{50} = 0.39 mm, C_u= 2.0); CTD (D_{50} = 0.53 mm, C_u= 4.4); New Orleans (D_{50} = 0.69 mm, C_u= 2.1); Tyndall (D_{50} = 0.21 mm, C_u= 1.4); Yuma (D_{50} = 0.12 mm, C_u= 1.6); Holland sand (D_{50} = 0.12 mm, C_u= 1.6) (Santoni et al., 2001)

4.3.2.6 Confining pressure

As observed in Section 4.2.2, the strength of both unreinforced and reinforced granular materials increases with confining stress but the relative improvements are greater under small confinement (Figure 4-3, Figure 4-5, Figure 4-8, Figure 4-19). This is reflected in the non-linearity of the failure envelopes of fibre-reinforced soils, as explained in Section 4.3.1. Thus fibre reinforcement is particularly attractive for shallow applications (e.g. shallow foundations, roads and embankments).

4.3.2.7 Initial density

The behaviour of fibre reinforced granular materials is affected by sample initial conditions, e.g. the initial density (Gray & Ohashi, 1983; Consoli et al., 2009; Lirer et al., 2012). Gray & Ohashi

(1983) conducted direct shear tests on sand samples of different initial densities. They found that fibres can effectively reinforce sand regardless of its initial density but looser samples required larger strain to mobilise additional shear strength (Figure 4-35). Similarly, triaxial tests on sandy gravel carried out by Lirer et al. (2012) showed that fibres can increase the mobilised shear strength of loose granular materials at large strains but reduce their initial secant stiffness (Figure 4-9). Consoli et al. (2009) studied the effect of the initial density through a series of plate loading tests (the test set-up is shown in Figure 4-34a). They noted that the settlement response of the reinforced samples started diverging from that of the unreinforced ones after a certain initial displacement, which was inversely proportional to the initial relative density (Figure 4-34, b and c). Thus, although fibres can provide additional strength regardless of the initial density, dense particle packings seem able to mobilise it at much smaller strains, avoiding the reduction of the initial stiffness often observed in fibre reinforced granular materials (Section 4.2.4).

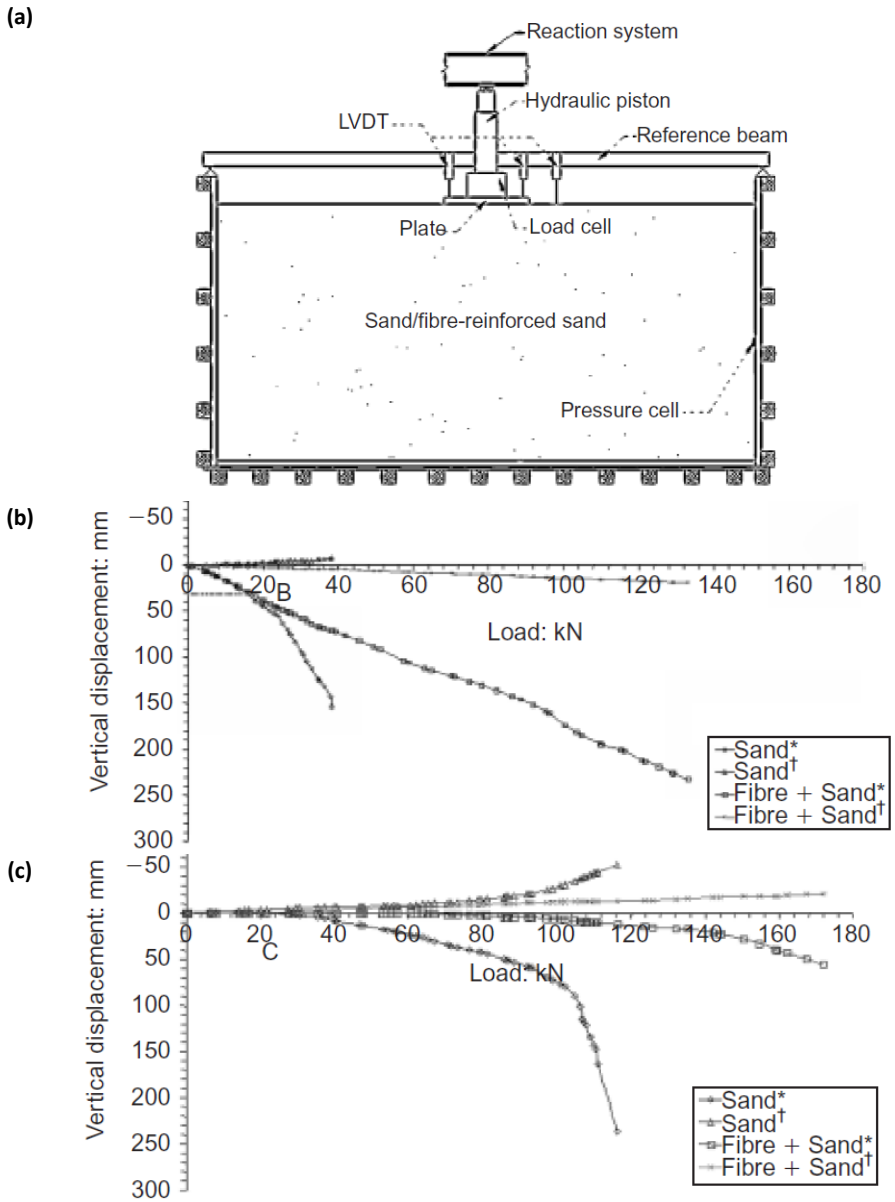

*Figure 4-34. Plate loading tests on sand (D_{50} = 0.16, C_u = 1.9) reinforced with 0.5% by mass polypropylene fibres (V_{fr} = 1.5%) with length of 24 mm and diameter of 0.023 mm; a) test set-up; b) and c) load settlement response for initial densities of 30% and 90% respectively; *readings in plate; †readings out of plate (Consoli et al., 2009)*

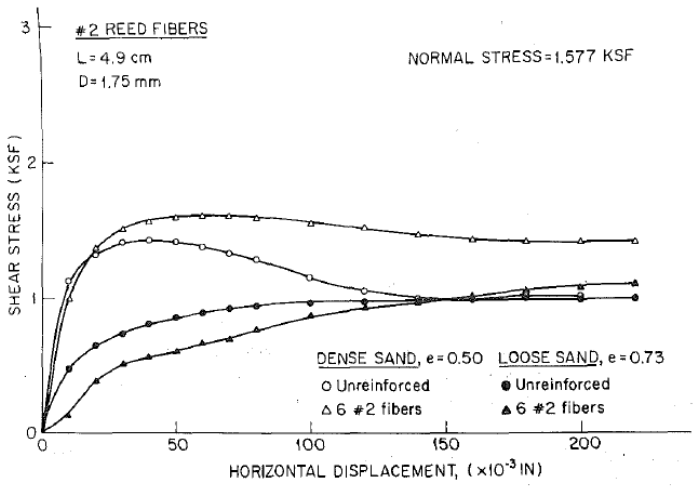

Figure 4-35. Direct shear tests on fibre reinforced sand; effect of sample initial density (Gray & Ohashi, 1983)

4.4 Summary

The behaviour of fibre-reinforced granular materials has been discussed through the analysis of a number of experimental studies. Most of them focused on the additional mobilised strength provided by fibres to materials ranging from sand to gravel subjected to monotonic loading. Only a limited number of them examined the response of these materials to cyclic loading.

Although the mechanics of fibre reinforcement is not fully understood, there is general consensus that fibres provide "additional strength" through the mobilisation of tension. This effect can be regarded in two different ways: as an additional effective confining stress, which increases material's ability to mobilise shear strength without affecting its constitutive law; or as additional shear strength, which leads to different strength envelopes for the reinforced and unreinforced materials. The former approach is the most instructive, as it emphasises the effect of the fibres on the stresses effectively seen by the grains, and may be preferable for fundamental studies. However, it is the least common and practical, as it would require a reliable evaluation of the tensions in the fibres.

The main characteristics of the mechanical response of fibre reinforced granular materials are summarised in Table 4-2. The ability of fibres to increase sand shear strength is well known but recent studies have shown that fibres can also strengthen coarser granular materials, although to a smaller extent. The effect of fibre addition on the deformability, which is of greater interest for this research, is less clear. The elastic stiffness of granular materials is not obviously affected by fibre reinforcement. Fibres tend to increase permanent strain under first-time loading. However, a full-size test using railway ballast showed their potential ability to reduce permanent deformation under cyclic loading. This would be particularly beneficial to the railway industry, as small quantities of fibres could be added to ballast to reduce track settlement, hence deterioration, while maintaining adequate stiffness and permeability.

Usually two different modes of fibre-particle interaction are identified: when lightly confined, fibres slip during deformation and tension is mobilised through fibre-particle interfacial friction; under significant confining stress, they stretch or yield. The confining stress marking the transition

from slip to stretching mechanism may correspond to the change of the gradient of the failure envelope and is termed critical stress (σ_{crit}) (Figure 4-24). Smaller values of σ_{crit} may be representative of more effective fibre-particle interaction (smaller confinement is required to hold firmly the fibres and stretch them).

The effectiveness of fibre-particle interaction and extent of improvement depend on fibre characteristics (e.g. content, dimensions, orientations and mechanical properties), particle characteristics (e.g. size, roughness and angularity), initial conditions (e.g. bulk density) and load conditions (e.g. confining stress). Based on the existing literature, the main factors affecting the behaviour of fibre reinforced granular materials have been analysed and are summarised in Table 4-3. For the purpose of this research, fibre dimensions and content are the most important parameters: the dimensions must be selected to provide significant reinforcing effect, e.g. fibres should be slender and their length at least one order of magnitude greater than the average particle size; the optimum content must be carefully evaluated to strengthen the material without increasing its propensity to settle. In contrast, fibre type and fibre material do not seem to have great influence on the overall performance. Moreover, it is worth pointing out that fibre reinforcement seems particularly suitable to the reinforcement of the railway track: it is particularly efficient under low confinement; fibres preferred orientation (i.e. horizontal) is optimal, being perpendicular to the main load component; and they do not introduce planes of weakness, which would threaten track stability under horizontal loads.

In the light of the above, random fibre reinforcement has the potential to improve ballast performance: it improves its strength, can inhibit its propensity to settle under cyclic loading while maintaining acceptable track stiffness. Moreover, this technique has the following advantages: fibre addition does not create planes of weakness; it maintains high permeability (unless very large contents are used); it is expected to be compatible with standard maintenance operations, e.g. tamping; fibres can be potentially added either during ballast cleaning or renewals; they are unlikely to segregate during service, as each of them is held by several ballast particles; they can be obtained from plastic, a widely available, durable and recyclable material; and they can be separated from ballast after use, so that both components can be recycled.

Table 4-2. Effects of random fibre reinforcement on granular materials

Mobilised peak shear strength	Deviatoric ratio (q/p) increases by up to: 1.9 times for sands ($D_{50} = 0.15$ to 0.3 mm); 1.15 times for gravel ($D_{50} = 13$ mm), but few data are available.
Post-peak shear strength loss	Eliminated (or strongly inhibited) for any granular material ($D_{50} = 0.15$ to 13 mm).
Volumetric behaviour	Dilation is typically inhibited for all types of granular material ($D_{50} = 0.15$ to 13 mm) but exceptions were observed, e.g. materials exhibiting compacting behaviour.
Stiffness	Effect of fibres is unclear: stiffness at very small strain of sand ($D_{50} = 0.15, 1.1$ mm) remained unaffected; stiffness over a load cycle of sand and sandy gravel ($D_{50} = 1.1, 3.0$ mm) increased, especially under low confining stress; but stiffness over a load cycle of very coarse gravel ($D_{50} = 38$ mm) reduced.
Permanent deformation	Permanent deformation of granular materials ($D_{50} = 0.15$ to 13 mm) after first time loading increases or remains unaffected; fibres reduced the permanent deformation of very coarse gravel ($D_{50} = 38$ mm) under cyclic loading but further evidence is desirable.
Particle packing	Void ratio increases linearly with the fibre content, which might increase material susceptibility to accumulate plastic deformations.

Table 4-3. Factors governing the behaviour of fibre reinforced granular materials

Fibre content	- The peak/post peak strength increases with fibre content; dilation reduces, although there are exceptions. This can be explained by the increased proportion of grains engaged by the fibres. - Elastic deformations might reduce with the fibre content while the initial permanent deformations usually increase. This might be due to the increase in the volume of voids.
Fibre dimensions (aspect ratio, length)	- The strength increases fairly linearly with fibre aspect ratio while the critical stress reduces (i.e. better fibre-particle interaction). Longer fibres mobilise greater fibre-grain frictional resistance. Reducing the diameter at fixed content increases the number of fibres interacting with the grains. - The strength increases with fibre length at constant aspect ratio. This might be associated with a scale effect: the reinforcing effect is negligible when fibre length is similar to the size of the voids and significant if one order of magnitude greater. - The volumetric response of reinforced materials does not seem significantly affected by fibre dimensions, but limited studies have been carried out.
Fibre orientation	- As fibres provide additional tensile strength, the optimum fibre orientation is the direction of maximum tensile strain. However, regardless of their orientation, fibres do not introduce planes of weakness.
Fibre mechanical properties (strength, stiffness)	- Fibre strength usually does not affect the behaviour of granular materials, as fibres break only under particularly high confining stress. - Fibre stiffness, unless particularly small, does not seem relevant to the reinforcing effect, suggesting sand-fibre interaction to be predominantly frictional.
Grain characteristics & fibre type	- Well-graded and angular materials allow for greater reinforcing effect. - Fibrillated and tape-like fibres are more effective than mono-filament fibres. - The choice of the optimum fibre type is also dependent on host material properties.
Confinement	- Owing to the non-linearity of the failure envelopes, the relative strength increase is larger under smaller confinement level: fibre reinforcement is ideal for shallow applications.
Initial density	- Denser samples mobilise the additional strength at smaller strain level.

5 MATERIALS, INSTRUMENTATION AND METHODS

5.1 Introduction

The previous chapter described the behaviour of fibre reinforced granular soil, highlighting the potential for fibre reinforcement to increase ballast strength and reduce its propensity to accumulate plastic deformation during repeated loading. In the light of this, full-size tests were carried out in the Southampton Railway Testing Facility to study the behaviour of fibre reinforced ballast under cyclic loading representative of train passage.

This chapter describes materials, instrumentation and methods used in the full-size tests. It provides a description of the testing rig. It presents the characteristics of the ballast, fibres and ballast-fibre mixture, highlighting the effect of fibre addition on the packing of the particles. It describes the techniques implemented to monitor the tests, which were selected/designed to capture the main features of ballast behaviour. Finally, it provides a description of the procedures for test preparation and an overview of the testing programme.

5.2 The Southampton Railway Testing Facility

Tests were conducted in the Southampton Railway Testing Facility (SRTF), a laboratory reproduction of a section of ballasted track in plain strain conditions. Designed by Le Pen (2008), the testing rig was initially adopted to study the behaviour of the sleeper/ballast interface under the lateral forces originating from high speed trains. Later, it was modified by Abadi (2014) to explore the effect of different sleeper/ballast configurations on track response to vertical cyclic loading representative of train passage. This latter set-up was used to study the mechanical behaviour of fibre reinforced ballast.

The testing rig mimics the behaviour of a full-size slice of a single line track extended to the shoulders and including one sleeper, as shown in Figure 5-1b. Its structure, shown in Figure 5-1a, was designed to reproduce plane strain conditions. The vertical sides, 5 m long and 0.65 m high, were constructed from heavy steel sections bolted together and connected by six steel ties to prevent out-of-plane movements. The sides were covered by a double-layer plastic sheet to reduce interfacial friction. The 65 cm gap between the walls represents a typical sleeper spacing.

Each specimen consisted of a G44 mono-block concrete sleeper placed on top of a 30 cm layer of ballast underlain by a 12 mm neoprene rubber mat, consisting of two 3 mm layers underlain by a 6 mm layer. The shoulder slope was 45° in each test, i.e. similar to ballast natural angle of repose. A schematic representation of a sample is shown in Figure 5-2.

The rubber mat mimicked the subgrade and provided realistic sleeper resilient deflections, i.e. 0.5 mm to 1.5 mm (Le Pen et al., 2014; Le Pen et al., 2017). This is particularly important, as a stiffer subgrade leads to smaller ballast settlement, as observed in Section 2.2.6. The rubber layer was designed by Abadi (2014) through specific laboratory tests that reproduced the interaction between the rubber and the ballast particles at realistic levels of pressure. In particular, Abadi (2014) found that the deflection associated with the deformation of the rubber mat is mostly determined by the penetration of the ballast particles into the rubber due to high localised

stresses. However, this produced small permanent indentations only on the surface of the top 3-mm rubber layer, while the other layers were substantially intact after each test. Therefore, the great majority of the overall settlement, usually between 6 mm and 12 mm (Section 8.2.2), must have been associated with the permanent deformation of the ballast. In contrast, the rubber mat, which is much softer than the ballast, was responsible for most of the sleeper resilient deflections.

The load was applied by a hydraulic actuator hanging vertically from a steel reaction frame. The vertical force was applied to two short sections of rail installed on the sleeper through a steel beam placed on top of them, as shown in Figure 5-1c.

The response of each sample to cyclic loading was monitored using different techniques: linear variable displacement transducers (LVDTs) were used to measure the sleeper vertical movements; the longitudinal pressure in the ballast was recorded by means of 16 load cells (LCs) integrated in the side walls; pressure sensitive paper was used to assess the area of contact at the interface between the sleeper and the ballast; marked particles were placed in the ballast bed to quantify their degradation; lateral plates were used to monitor the ballast lateral spreading. These techniques are described in detail in Section 5.5.

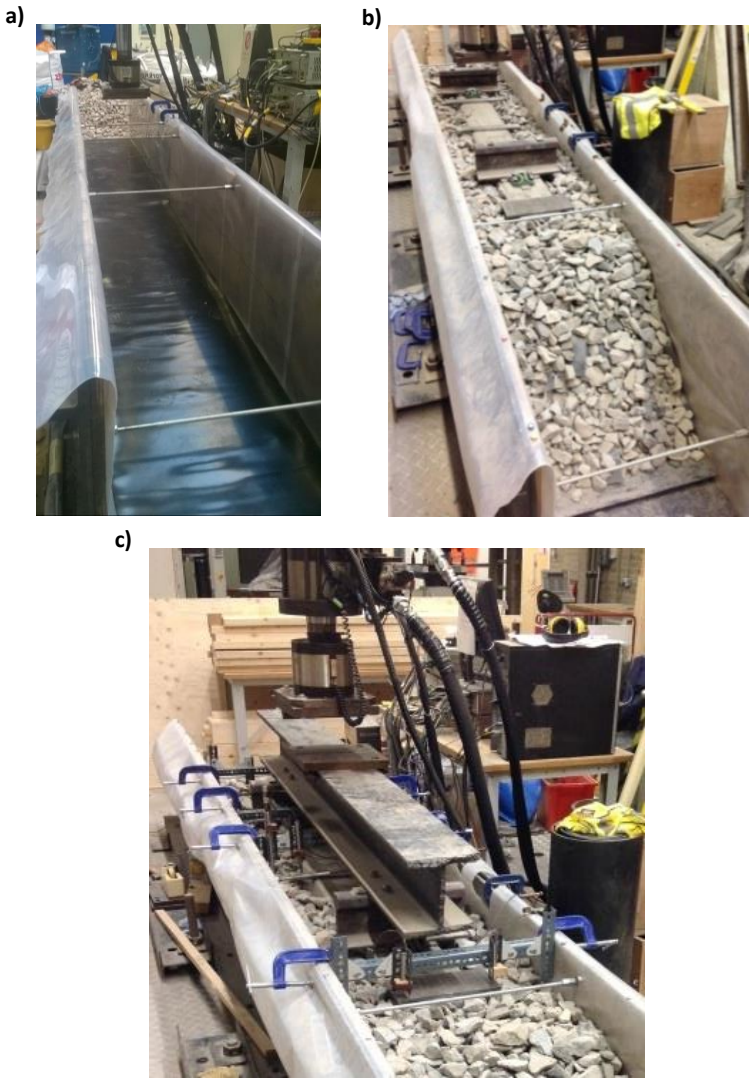

Figure 5-1. Testing rig a) before placing the ballast, b) before placing loading beam and LVDTs and c) ready for testing

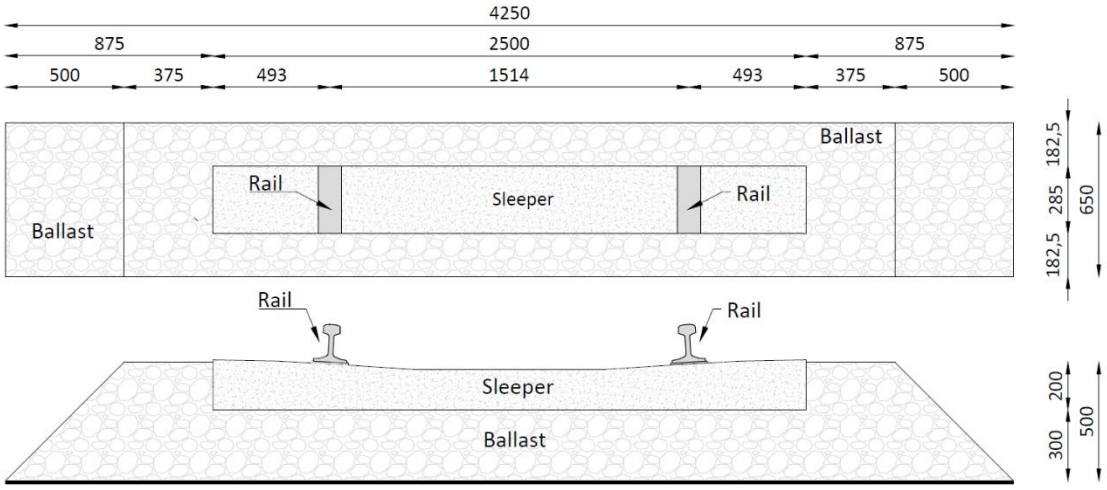

Figure 5-2. Sample geometry (dimensions in mm)

5.3 Materials

5.3.1 Ballast

Two different types of ballast were used: CH ballast and MS ballast. The former, which was used in the first tests, was sourced from Cliffe Hill quarry (Leicestershire, UK). The latter, was excavated from Mount Sorrel quarry (Leicestershire, UK), as CH ballast was no longer available. Both materials were obtained from freshly crushed granite rock but showed different properties and, most importantly, different performance under cyclic loading. Therefore, the tests using CH ballast and those using MS ballast were described separately, as they provided independent self-consistent sets of data.

Typical particles of CH and MS ballast are shown in Figure 5-3, their main properties are summarised in Table 5-1 and their size distribution is represented in Figure 5-4. It must be noted that CH ballast was slightly finer than Network Rail standard specification (cat. A BS EN 13450:2002). However, it is believed to be representative of the range of materials placed on UK railway tracks.

Key properties of CH ballast are the specific gravity (G_s) of 2.80, the water absorption (WA) of 0.34%, the average particle size (D_{50}) of 34 mm, the coefficient of uniformity ($C_u = D_{60}/D_{10}$) of 1.7 and the maximum and minimum void ratios (e_{max} and e_{min}) of 0.99 and 0.71 respectively. The main characteristics of MS ballast are: G_s = 2.66, WA = 0.35%, D_{50} = 41 mm, C_u = 1.4, e_{max} = 0.94 and e_{min} = 0.68. The ballast grading was assessed using a mechanical sieve shaker in accordance with BS EN 933-1:2012. The specific gravity and water absorption were calculated following the procedures described in BS EN 1097-6:2000 but using a Eureka can instead of the wire basket method to measure the volume of the ballast particles. The methods used to measure the maximum and minimum bulk densities, hence void ratios, of the ballast are described in Section 5.4.3.

Both CH and MS ballast were uniformly graded and characterised by similar values of void ratio. These characteristics, and visual inspection, suggest that the particles of CH and MS ballast had similar shape.

The main differences between CH and MS ballast are the average size and specific gravity of the particles, with the former having smaller and denser particles. Moreover, CH particles felt smoother to touch. This, however, should be corroborated by measurements of the roughness of particle surface.

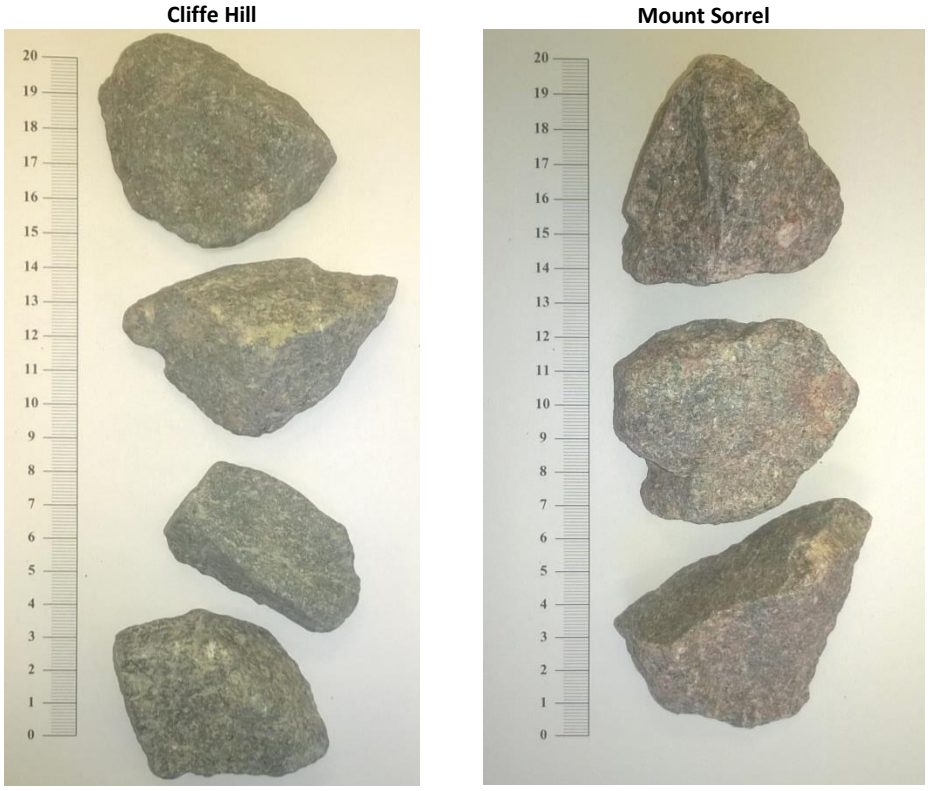

Figure 5-3. Typical Cliffe Hill and Mount Sorrel ballast particles

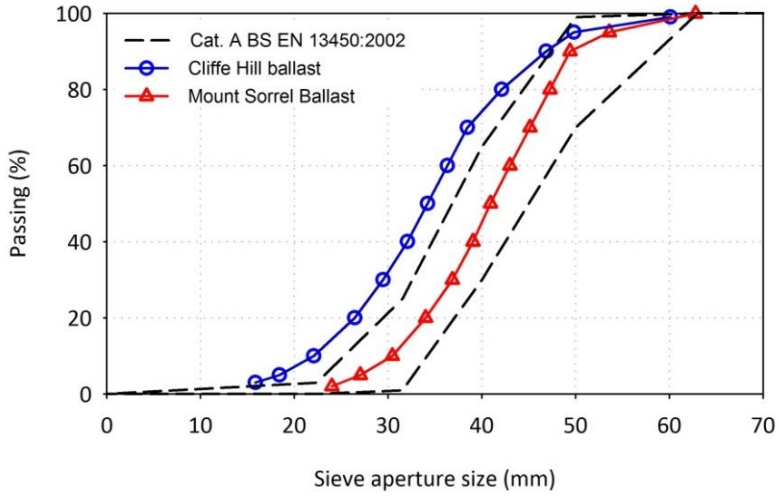

Figure 5-4. Ballast particle size distributions vs NR specifications (Cat. A BS EN 1345:2002)

Table 5-1. Key ballast properties

	CH ballast	MS ballast
Parent rock	Granite	Granite
Colour	Grey	Grey/pink
G_s	2.80	2.66
WA (%)	0.34	0.35
D_{50} (mm)	34	41
$C_u = D_{60}/D_{10}$	1.7	1.4
$C_c = D_{30}^2/(D_{30}D_{60})$	1.1	1.0
ρ_{max} (kg/m^3), e_{min}	1434, 0.99	1387, 0.94
ρ_{min} (kg/m^3), e_{max}	1662, 0.71	1601, 0.68

5.3.2 Fibres

Two types of synthetic fibres were tested: thin tape-like fibres and filament-like fibres. The former were used in the tests using CH ballast and in one using MS ballast. The latter were only used with MS ballast. The tape-like fibres used with CH ballast were obtained from 0.5 mm thick damp proof course (DPC) made of reprocessed polyethylene with area density of 435 kg/m^2 (Figure 5-5a). The tape-like fibres used with MS ballast were also obtained from 0.5 mm thick polyethylene DPC but, due to a delivery error, were from a different manufacturer. They had area density of 400 kg/m^2 and slightly different surface texture (Figure 5-6). The filament-like fibres were obtained from polypropylene three-strand rope of different nominal diameter (Figure 5-5b), whose linear density is reported in Table 5-2.

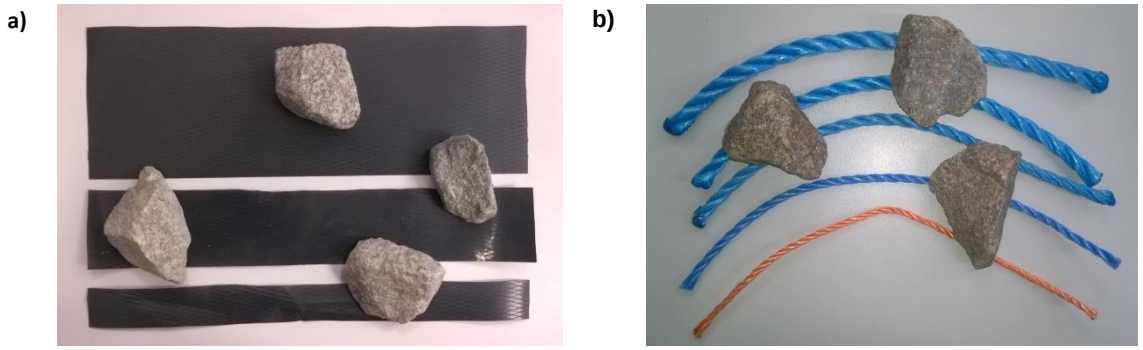

Figure 5-5. Fibres and typical ballast particles; fibre length of 300 mm; a) tape-like fibres and CH ballast particles, width of 25, 50 and 100 mm; b) filament-like fibres and MS ballast particles; nominal diameter of 4, 6, 8, 10 and 12 mm

Figure 5-6. Tape-like fibres used with CH (top-right) and MS ballast (bottom-left)

Table 5-2. Properties of the polypropylene rope

d_f (mm)	4	6	8	10	12
F_b (kN)	2.2	5.4	9.4	14	19.9
λ_f (g/m)	6.2	12.7	21.5	33.9	52.5

d_f : reference diameter, i.e. outer diameter;
F_b : force at break, as reported by supplier (http://uk.rs-online.com/web/)
λ_f : linear density (measured)

5.4 Characteristics of FRB

5.4.1 Fibre dimensions

The dimensions of the tape-like fibres are the thickness (t_f), the width (W_f) and the length (L_f). Those of the filament-like fibres are the length and the diameter (d_f). The behaviour of fibre reinforced granular materials is affected by the size of the fibres relative to the particles (Section 4.3.2.2). Therefore, as suggested by Ajayi et al. (2017), the fibre dimensions were normalised to the average particle size:

$$t_N = \frac{t_f}{D_{50}} \qquad L_N = \frac{L_f}{D_{50}} \qquad W_N = \frac{W_f}{D_{50}} \qquad d_N = \frac{d_f}{D_{50}} \tag{5-1}$$

According to Ajayi (2014), the addition of tape-like fibres produce a significant increase in scaled ballast shear strength if $L_N \geq 7.5$ and $W_N \geq 2.5$.

5.4.2 Fibre content

5.4.2.1 Fibre content by volume and weight

The fibre content is typically expressed in terms of volume or weight, as clear from Chapter 4. The former is often calculated in terms of volumetric fibre ratio (V_{fr}), which is the ratio of the volume of the fibres (V_f) to the volume of the solids (V_s):

$$V_{fr} = \frac{V_f}{V_s} \tag{5-2}$$

The volume of the solids can be calculated as the volume of the particles only ($V_s = V_p$) or the volume of particles and fibres together ($V_s = V_p + V_f$). However, this distinction has little practical importance if the volume of fibre is negligible compared with that of the particles, e.g. less than 5%. Similarly, the fibre content by weight (w_{fr}) is defined as the ratio of the weight of the fibres (w_f) to the weight of the solids (w_s). The volumetric fibre ratio might be more instructive, as it is representative of the proportion of volume occupied by the reinforcement while the fibre content by weight depends on the relative fibre/particle density.

Although widely used, a limitation of the fibre content by volume is its inability to account for the effect of the relative fibre/particle size on the quantity of fibre that can be added to a granular material. This is clear from Table 5-3, which shows that the maximum volumetric content of a

certain tape-like fibre that could be added to gravel reduces with the size of the particles. This is explained by the number of particles, hence the amount of interparticle spaces that can be filled with fibres, reducing with the particle size. Similarly, at constant particle size the volumetric fibre content increases with the thickness of the inclusions, although the number of particles engaged by them does not necessarily vary.

5.4.2.2 Fibre content by area or length

As an alternative, the fibre content can be expressed in terms of area (A_{fp}) and length (L_{fp}). The former can be used for bi-dimensional fibres, e.g. tape-like fibres, the latter for one-dimensional ones, e.g. filament-like fibres. Both A_{fp} and L_{fp} allow to express the amount of reinforcement independently of the fibre thickness or diameter. They are defined as follows:

$$A_{fp} = \frac{N_f \, A_f}{N_p} \tag{5-3}$$

$$L_{fp} = \frac{N_f \, L_f}{N_p} \tag{5-4}$$

where N_f is the number of fibres, N_p is the number of particles, $A_f = W_f \cdot L_f$ is the area of each fibre and L_f is the fibre length. A_{fp} and L_{fp} are representative of the fibre area and length available for engagement per particle. However, they do not consider that the amount of reinforcement that can be added to a granular material is affected by the size of the particles, as explained in Section 5.4.2.1.

It is worth noting that if tape-like fibres of constant thickness are used, like in this research, fibre content by area and volume are equivalent, as the ratio of the volume to the area remains constant. In contrast, for filament-like fibres the volumetric fibre content increases with the square of the diameter of the inclusions, although the total length of reinforcement, and hence the number of particles that can be potentially engaged, remains constant.

5.4.2.3 Relative fibre content

The relative fibre content (RFC) is introduced to consider that the quantity of reinforcement that can be potentially added to a granular material depends on the relative fibre/particle properties, as observed in Section 5.4.2.1. It is generically defined as the ratio of the fibre content (FC) to the maximum fibre content that can be added to a certain material (FC_{max}):

$$RFC = \frac{FC}{FC_{max}} \tag{5-5}$$

$RFC = 0$ if no particles are engaged by the reinforcement and $RFC = 1$ if the number of particles engaged is the maximum, although not necessarily all particles are engaged. Therefore, the relative fibre content provides an intuitive measurement of the amount of reinforcement, independent of the relative fibre/particle properties. However, it requires an estimate of the maximum fibre content which is, to some extent, arbitrary.

In this research, the maximum fibre content was estimated empirically based on the results of a large number of bulk density tests on ballast reinforced with tape-like fibres of different length (L_N = 2.2, 4.4, 8.8) and width (W_N = 0.7, 1.5, 2.2, 2.9), and filament-like fibres of different diameters (d_N = 0.10, 0.15, 0.20, 0.24, 0.29) and constant length (L_N = 7.3). These tests, which are described in Section 5.4.3, were originally aimed at assessing the effect of fibre addition on the packing of the ballast particles. However, they could be also used to estimate the maximum number of fibres that could be added to ballast. For each fibre, several bulk density tests were carried out using increasing values of fibre content until fibre overlapping was considered significant. The maximum fibre content FC_{max} was calculated as the average of the maximum values of fibre content used for each type of fibre plus the standard deviation. For the tape-like fibres the estimated maximum fibre content was $V_{fr,max}$ = 1.23% (or $A_{fp,max}$ = 6.3 cm^2). For the filament-like fibres it was $L_{fp,max}$ = 5.1 cm. Therefore, the relative fibre content RFC is calculated as follow:

$$RFC = \frac{V_{fr}}{V_{fr,max}} = \frac{V_{fr}}{1.23\%} \quad \text{For tape-like fibres}$$
$$RFC = \frac{L_{fp}}{L_{fp,max}} = \frac{L_{fp}}{5.1\ cm} \quad \text{For filament-like fibres} \tag{5-6}$$

It must be pointed out that the values of maximum fibre content estimated based on the bulk density tests ($V_{fr,max}$ for the tape-like fibres and $L_{fp,max}$ for the filament-like fibres) are based on the visual inspection of the samples and, therefore, are dependent on the operator judgement. Therefore, they are intended to be used only for this study, to allow a comparison between the content of tape-like and filament-like fibres, which were both used in the tests on Mount Sorrel ballast. An alternate approach consists in calculating the maximum fibre content theoretically by means of a model that accounts for the relative fibre/particle dimensions. In this research, the empirical approach was preferred for its simplicity and, as soon as the operator does not change, reliability. However, a theoretical approach would be more instructive, as it can highlight the effect of the relative fibre/particle size.

As an example of the theoretical approach, expressions for the relative fibre content and the maximum volumetric content of tape-like fibres are derived using the simple model of Figure 5-7. This is based on the following assumption: spherical particles; perfectly uniform particle size distribution; particle arranged in a simple lattice, characterised by a void ratio of 0.91 and representative of loose conditions (Section 5.3.1); horizontal fibres (Section 4.3.2.3); maximum fibre content if adjacent layers of particles are separated by layers of fibre. Under these assumptions, the maximum theoretical volumetric fibre ratio for tape-like fibres is:

$$V_{fr,max}^{th} = \frac{D_{50}^2\ t_f}{\frac{\pi}{6}\ D_{50}^3} = \frac{6}{\pi}\ t_N \tag{5-7}$$

With D_{50}, t_f and t_N defined in Section 5.4.1. Hence, the theoretical relative fibre content for tape-like fibres is as follows:

$$RFC_{tape}^{th} = \frac{V_{fr}^{th}}{V_{fr,max}^{th}} = \frac{\left(N_f\ A_f\ t_f\right)/\left(N_p\ \frac{\pi}{6}\ D_{50}^3\right)}{\left(D_{50}^2\ t_f\right)/\left(\frac{\pi}{6}\ D_{50}^3\right)} = N_{fp}\ A_N \quad (5\text{-}8)$$

where $N_{fp} = N_f/N_p$ is the number of fibres per particle and $A_N = A_f/D_{50}^2$ is normalised area of reinforcement. As shown in Table 5-3, this model seems consistent with the maximum values of fibre content used for uniformly graded gravel of particle size ranging from 8 mm to 34 mm. While the maximum volumetric fibre content reduced with the size of the particles, the theoretical fibre content remained approximately constant, i.e. ~ 0.5, but is far less than 1. This means that equation (5-8) might be able to express the quantity of reinforcement over a range of particle sizes but underestimates the relative fibre content, as the model of Figure 5-7, and hence equation (5-7), overrates the maximum quantity of reinforcement that can be added to a granular material. As shown in Figure 5-8, a more realistic expression for the maximum volumetric fibre can be obtained by simply fitting experimental data:

$$V_{fr,max} = 1.03\ t_N \quad (5\text{-}9)$$

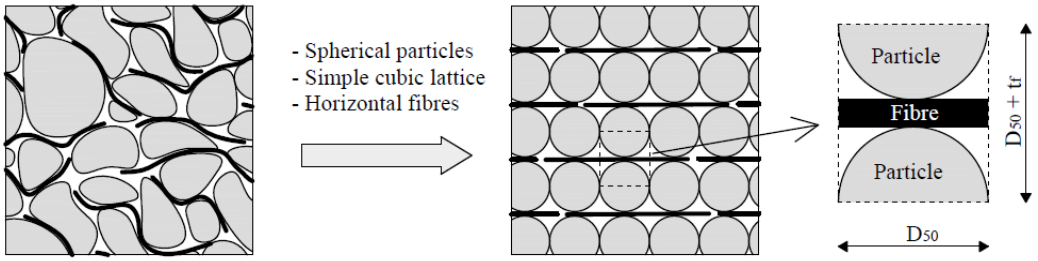

Figure 5-7. Simplified particle assembly assumed to evaluate the maximum fibre content for platy fibres

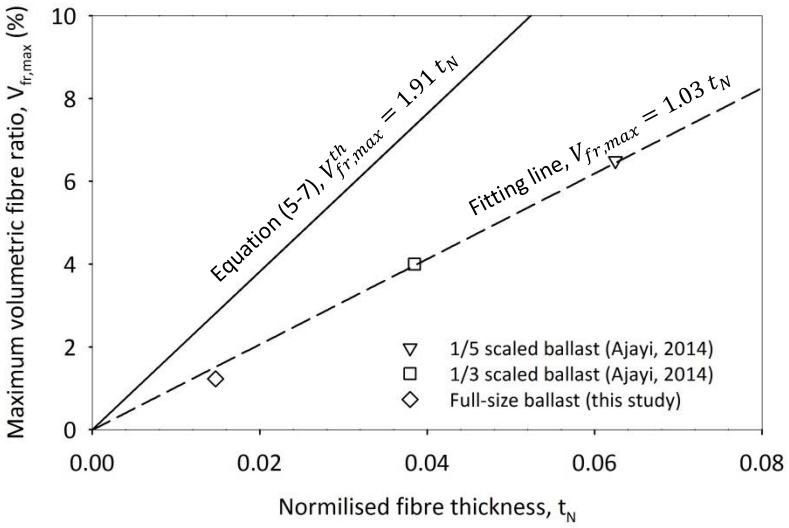

Figure 5-8. Increase in maximum volume of tape-like fibres that can be added to a granular material with the normalised fibre thickness; data points represent the maximum contents of tape-like fibres (obtained from 0.5 mm thick polyethylene damp proof course) used in this study and by Ajayi (2014)*; values are reported in Table 5-3*

Table 5-3. Effect of the particle size on the maximum content of tape-like fibre (obtained from 0.5 mm thick polyethylene damp proof course) that was added to a coarse granular material in this study and in Ajayi (2014)

Ballast type	D_{50} (mm)	t_N	$V_{fr,max}$ (%)	RFC_{tape}^{th}
1/5 scaled ballast (Ajayi, 2014)	8	0.06	6.5	0.54
1/3 scaled ballast (Ajayi, 2017)	13	0.04	4	0.54
Full size ballast (this study)	34	0.01	1.23	0.44

5.4.3 Particle packing

The addition of fibres to a granular material inhibits the packing of its particles, increasing its void ratio and, possibly, its propensity to exhibit volumetric deformation (Section 4.2.4).

Considering this, a large number of density tests were carried out to assess the effect of the addition of tape-like and filament-like fibres of different dimensions on ballast void ratio. CH and MS ballast were used with tape-like and filament-like fibres respectively. In each test, a cubic box with internal edges of 300 mm was filled manually with the ballast/fibres mixture and its content weighed. The box was slightly overfilled and covered with a lid so that the actual height of the sample could be measured. Loose conditions, i.e. maximum void ratio, were obtained by gently placing the ballast into the box; the dense state, i.e. minimum void ratio, by placing the ballast in three layers and vibrating each of them using the base of an electric sieve shaker (Figure 5-9).

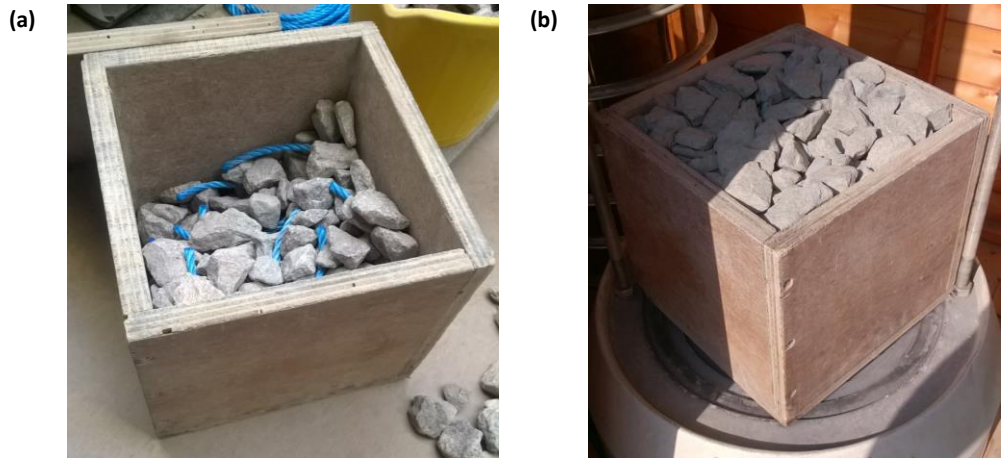

Figure 5-9.Bulk density tests; preparation of a loose sample (a) and a dense one (b)

For unreinforced soil the void ratio is defined as the ratio of the volume of voids (V_v) to the volume of solids (V_s), where the latter corresponds to the volume of the grains, or particles (V_p). In fibre reinforced soils an additional phase is present, i.e. the volume of the fibres (V_f), which might be considered as part of the solids ($V_s = V_p + V_f$) or simply neglected ($V_s = V_p$). As suggested by Ajayi et al. (2014) the former approach might give a reduction of the void ratio due to the increase in volume of the solids, as it includes the volume of fibres. Therefore, it was preferred to calculate the void ratio without considering V_f:

$$e = \frac{V_v}{V_p} \tag{5-10}$$

For the tape-like fibres the influence of fibre content, width and length on ballast void ratio were investigated. For the filament-like fibres only the fibre content and diameter were considered. Hereafter, the fibre dimensions are normalised to the average particle size, equation (5-1), and the amount of reinforcement is expressed in terms of relative fibre content, equation (5-6).

Both types of fibre gave a linear increase in void ratio with the fibre content, as shown in Figure 5-11 and Figure 5-15. This is consistent with the findings by Ajayi et al. (2014), shown in Figure 4-21. The increase in void ratio was less pronounced in dense conditions. Hence, the fitting lines associated with the minimum and maximum void ratio tended to diverge with the fibre content. This is in agreement with Lirer et al. (2012) and Ajayi et al. (2014), as observed in Section 4.2.4, and implies that ballast permanent volumetric deformation during compaction is exacerbated by the addition of fibres.

The disruption of the packing of the particles is represented by the gradient of the lines fitting the experimental data in the void ratio vs fibre content plane. This was termed Δe_{max} , as it also corresponds to the increase in void ratio associated with RFC = 1, i.e. the maximum fibre content. Similarly, the increased propensity to compact of the fibre reinforced material is expressed as the difference between the void ratio increase in loose conditions (Δe_{max}^{loose}) and in dense conditions (Δe_{max}^{dense}). This quantity was termed Δe_{max}^{rel}. The values of Δe_{max}^{loose}, $\Delta e_{max}^{dense}$and Δe_{max}^{rel} for tape-like and filament-like fibres of different dimensions are summarised in Table 5-4 and Table 5-5 respectively.

The effect of the dimensions of the tape-like fibres on the packing of the particles in loose conditions is shown in Figure 5-12. The void ratio increased significantly with the fibre width while the effect of the length was relatively small. For narrow fibres ($W_N \leq 1.5$) the disruption was negligible ($\Delta e_{max}^{loose} \leq 0.02$). Wide ones ($W_N \geq 2.2$) increased significantly the void ratio ($\Delta e_{max}^{loose} \geq 0.13$). The effect of the length was marginal, with Δe_{max}^{loose} = 0.10 for wide and short fibres (W_N = 2.9, L_N = 4.4). The increased disruption of the packing of the particles with the addition of wide fibres might be explained by the two-dimensional behaviour of the wide tape-like fibres: like a plate supported on four sides, they offered a greater resistance to the movement of the particles compared with narrow one-dimensional fibres. This seems confirmed by the presence of a threshold value of fibre width between W_N = 1.5 and W_N = 2.2, below which the disruption of the packing of the particles is negligible and beyond which it suddenly becomes significant.

The effect of the dimensions of the tape-like fibre was different in dense conditions (Figure 5-13). The disruption of the particle packing was less pronounced, with Δe_{max}^{dense} always smaller than 0.10, and the effects of fibre width and length were comparable. The void ratio increase was negligible for $W_N \leq 0.7$ or $L_N \leq 4.4$, with $\Delta e_{max} \leq 0.02$. The relatively small influence of the reinforcement on the minimum void ratio can be explained by the fibres being forced into the voids by the particles, owing to the compacting effort.

Ballast propensity to compact was strongly affected by the width of the tape-like fibres, while the effect of the length was marginal (Figure 5-14). The increase in compactability was marginal for $W_N \leq 1.5$, it increased rapidly for W_N = 1.5 to 2.2, and was approximately constant for $W_N \geq 2.2$.

The effect of the filament-like fibres on the void ratio was similar to that of tape-like fibres (Figure 5-16). The void ratio increased with the size of the fibres, especially in loose conditions.

For dense samples, the disruption was marginal for the thinnest fibres ($\Delta e_{max}^{dense} = 0.02$ for $d_N = 0.1$) and increased gradually with the fibre diameter. Very thick fibres ($d_N = 0.24$) increased in the void ratio by $\Delta e_{max}^{dense} = 0.09$, almost identical to that observed for the wide tape-like fibres, although the latter are very thin. In loose conditions, the effect of the fibres on the void ratio was small for $d_N \leq 0.2$, i.e. $\Delta e_{max}^{loose} = 0.05$-$0.08$, beyond which it increased rapidly, with $\Delta e_{max}^{loose} = 0.19$ for $d_N = 0.29$. Similarly, ballast susceptibility to compaction was marginal for $d_N \leq 0.2$, i.e. $\Delta e_{max}^{rel} \cong 0.03$, beyond which it increased rapidly, with $\Delta e_{max}^{rel} = 0.10$ for $d_N = 0.29$. Therefore, like with the tape-like fibres, there is threshold value of fibre diameter ($d_N \cong 0.2$) below which the fibres have marginal effect on ballast void ratio and propensity to compact.

It can be concluded that fibre addition increases ballast void ratio, especially in loose conditions, and its propensity to compact. However, such effect is strongly affected by the dimensions of the fibres. For the tape-like and filament-like fibres the disruption of the packing particles was marginal for $W_N \leq 0.7$ and $d_N \leq 0.10$, the compactability for $W_N \leq 1.5$ and $d_N \leq 0.2$. Although the effect of the length was secondary, the use of shorter fibres reduced the disturbance to the particles arrangement. However, it is also expected to inhibit the fibre ability to develop tension and hence the effect of the reinforcement (Section 4.3.1). Therefore, fibres should be long but narrow and thin so that they can effectively reinforce the granular matrix without disturbing the natural arrangement of the particles.

Table 5-4. Void ratio increase for CH ballast reinforced with tape-like fibres of different length and width

L_N	W_N	Δe_{max}^{loose}	Δe_{max}^{dense}	Δe_{max}^{rel}
8.8	2.9	0.15	0.10	0.05
8.8	2.2	0.13	0.08	0.05
8.8	1.5	0.07	0.08	-0.01
8.8	0.7	0.01	0.02	-0.01
4.4	0.7	0.01	-0.01	0.02
4.4	1.5	0.03	0.02	0.01
4.4	2.2	0.11	0.02	0.09
2.2	2.2	0.10	0.02	0.08
4.4	2.9	0.10	0.02	0.08
2.2	0.7	0.02	0.00	0.02
2.2	1.5	0.02	0.02	0.00
2.9	2.2	0.10	0.02	0.08

Table 5-5. Void ratio increase for MS ballast reinforced with filament-like fibres of different diameter

L_N	d_N	Δe_{max}^{loose}	Δe_{max}^{dense}	$\Delta\Delta e_{max}$
7.3	0.10	0.05	0.02	0.03
7.3	0.15	0.08	0.06	0.02
7.3	0.20	0.08	0.05	0.03
7.3	0.24	0.13	0.06	0.07
7.3	0.29	0.19	0.09	0.10

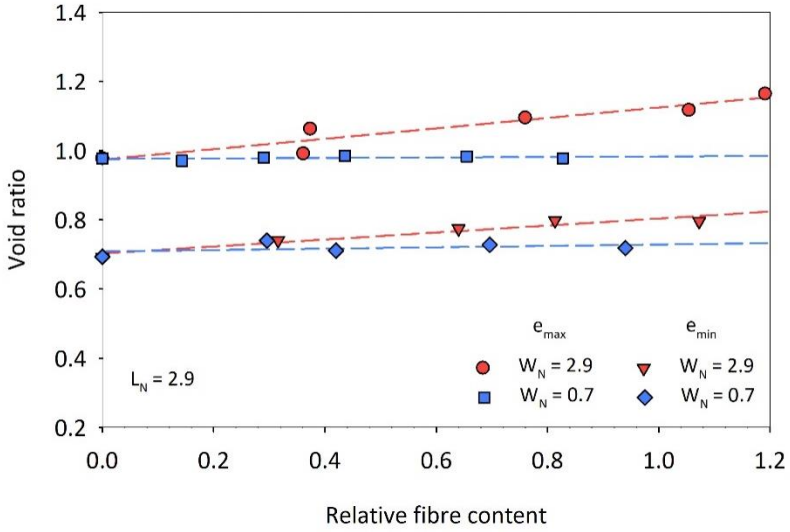

Figure 5-10. Effect of the addition of wide and narrow tape-like fibres on the void ratio of CH ballast

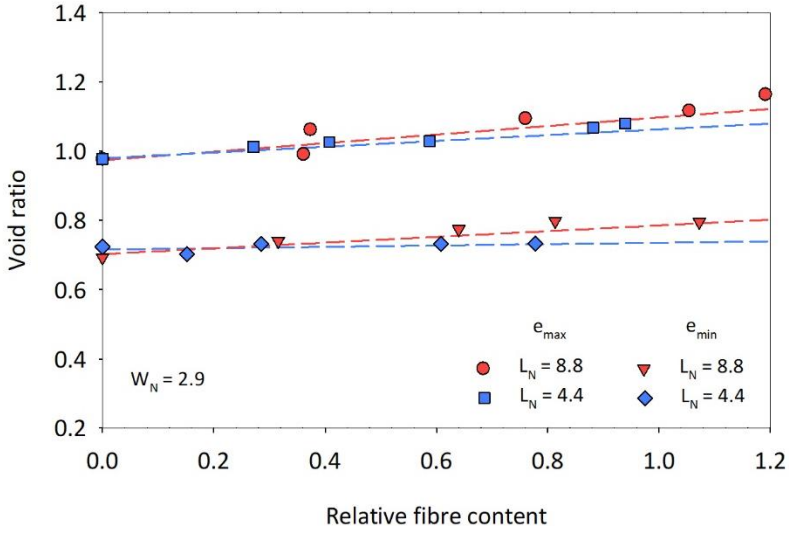

Figure 5-11. Effect of the addition of long and short tape-like fibres on the void ratio of CH ballast

(a)

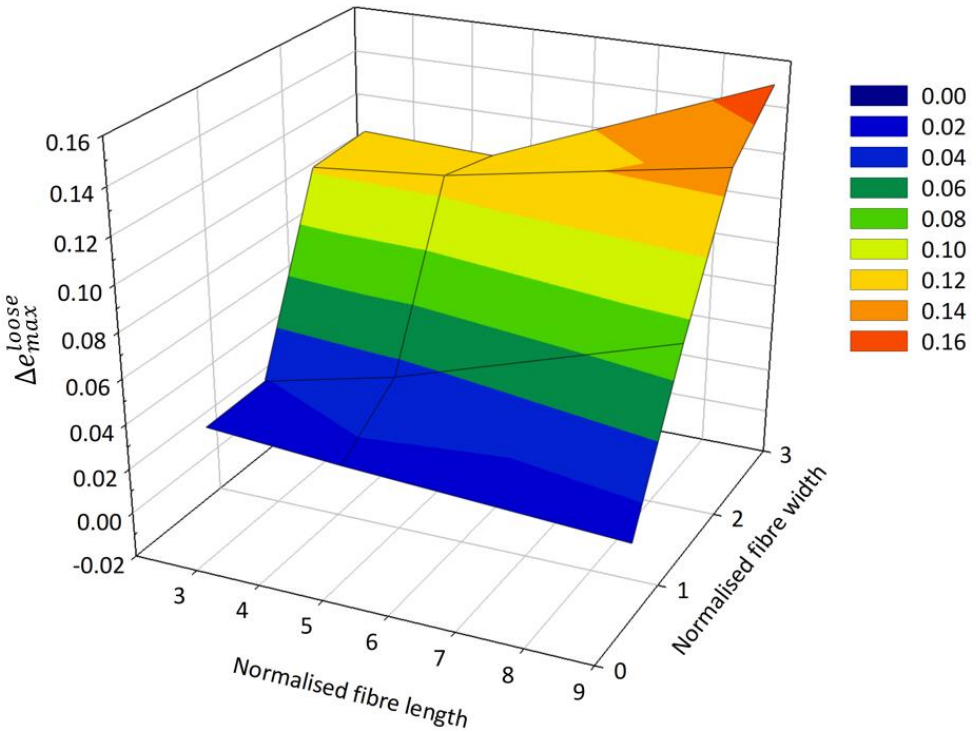

(b)

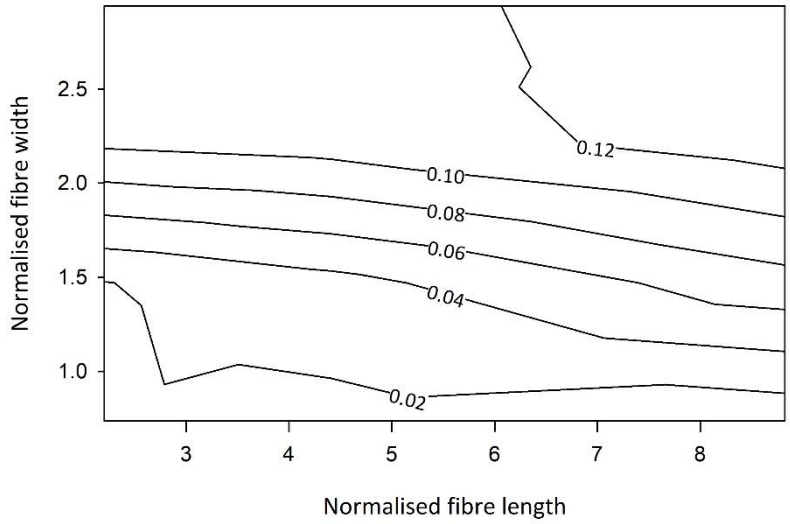

Figure 5-12. Effect of tape-like fibres dimensions on ballast maximum void ratio; (a) 3d mesh; (b) contour map.

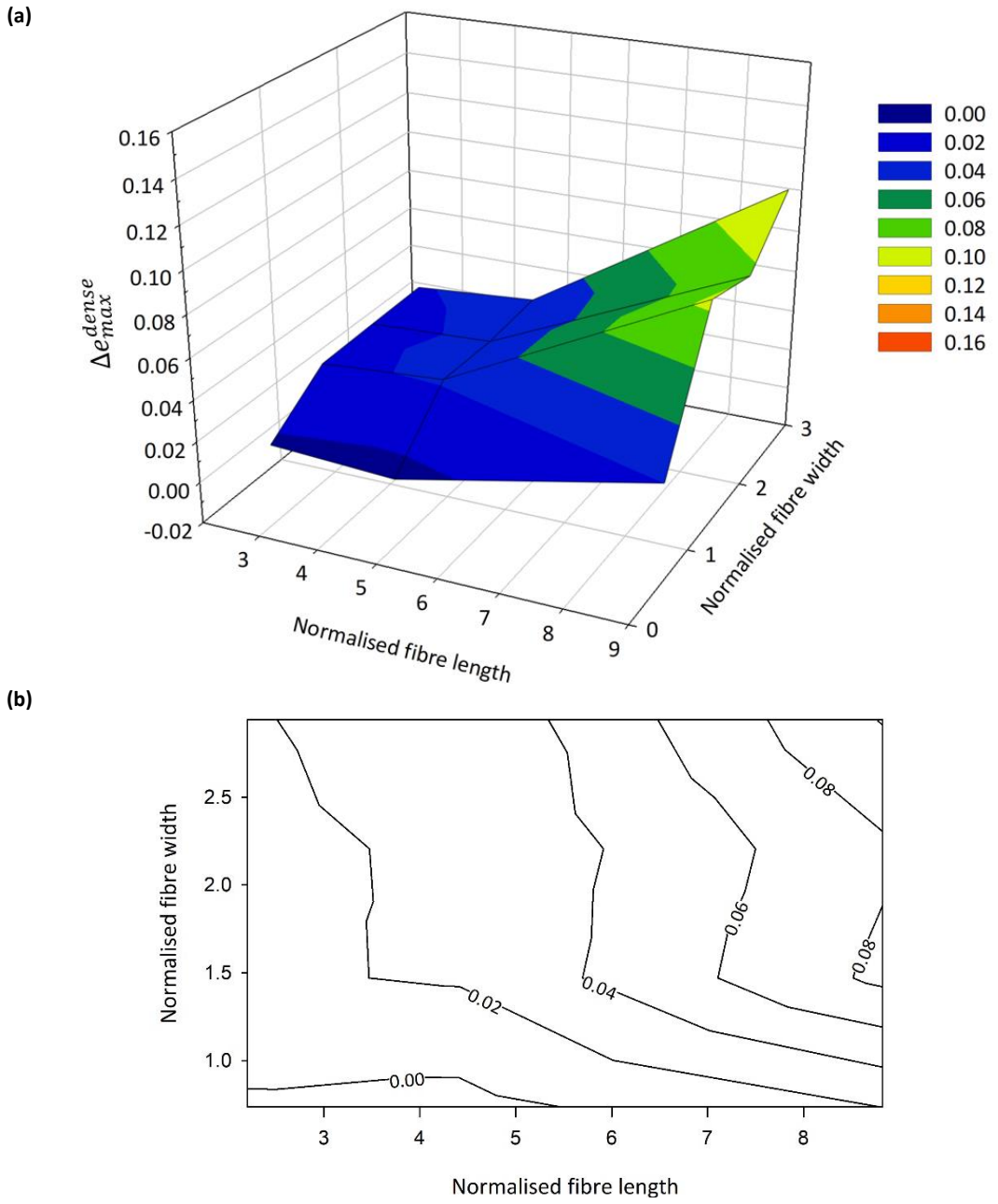

Figure 5-13. Effect of tape-like fibres dimensions on ballast minimum void ratio; (a) 3d mesh; (b) contour map

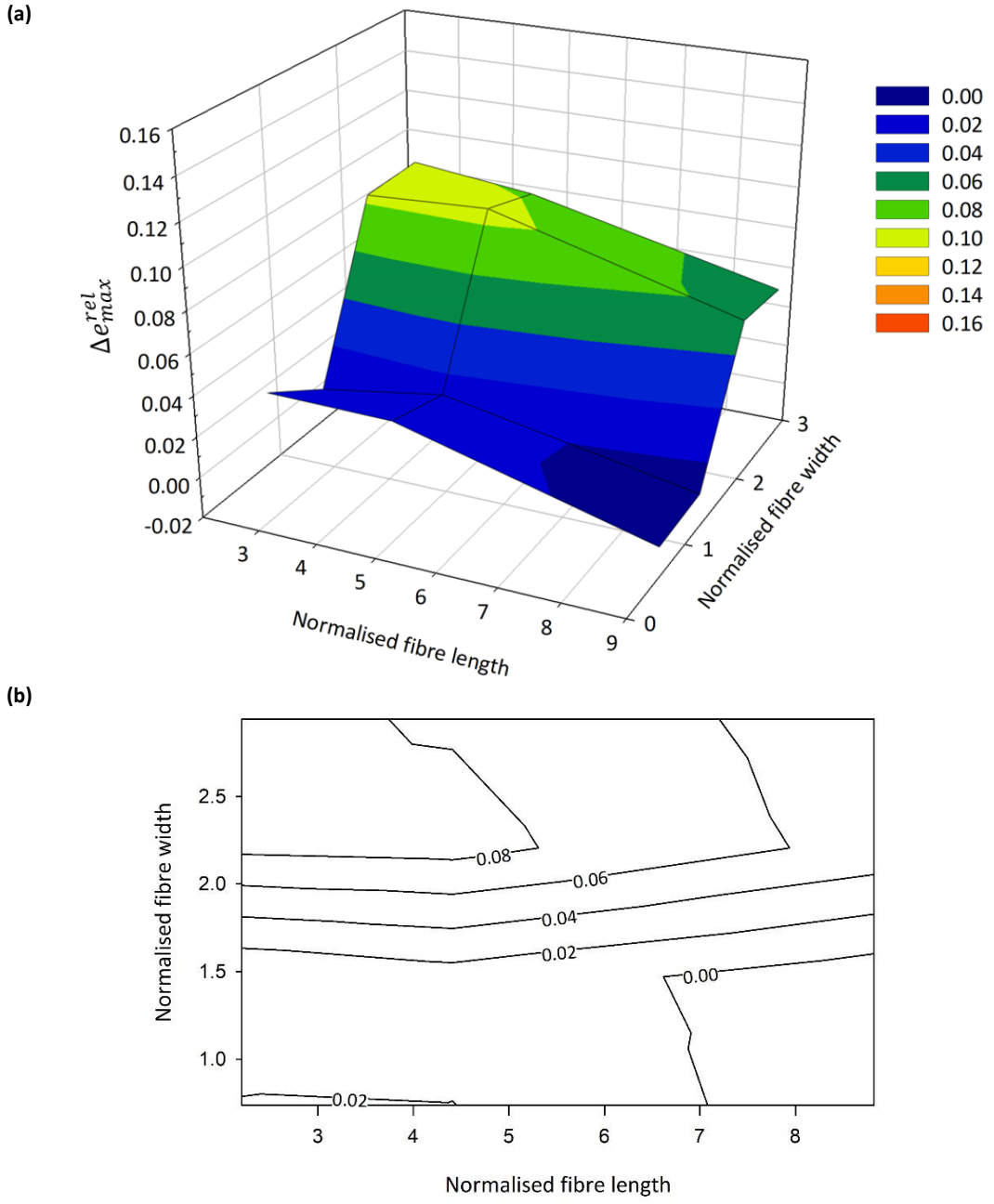

Figure 5-14. Effect of tape-like fibres dimensions on ballast propensity to compact; (a) 3d-mesh; (b) contour map

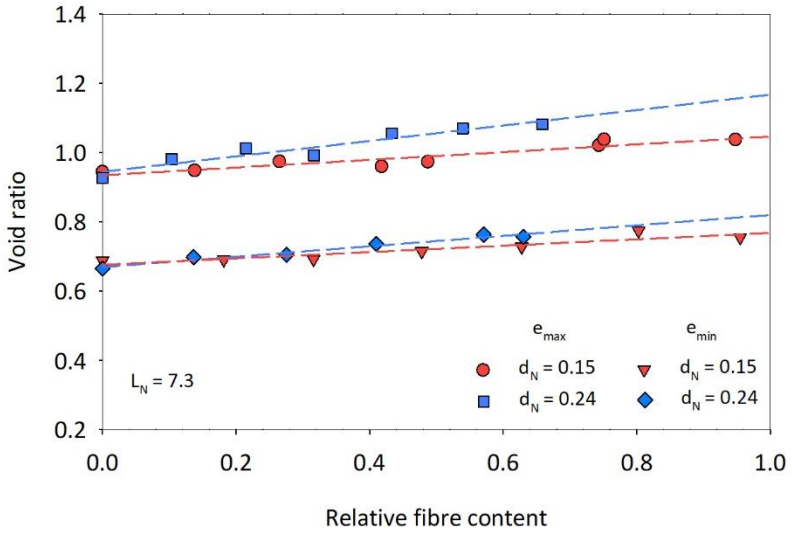

Figure 5-15. Effect of the diameter of the filament-like fibres on the void ratio of MS ballast

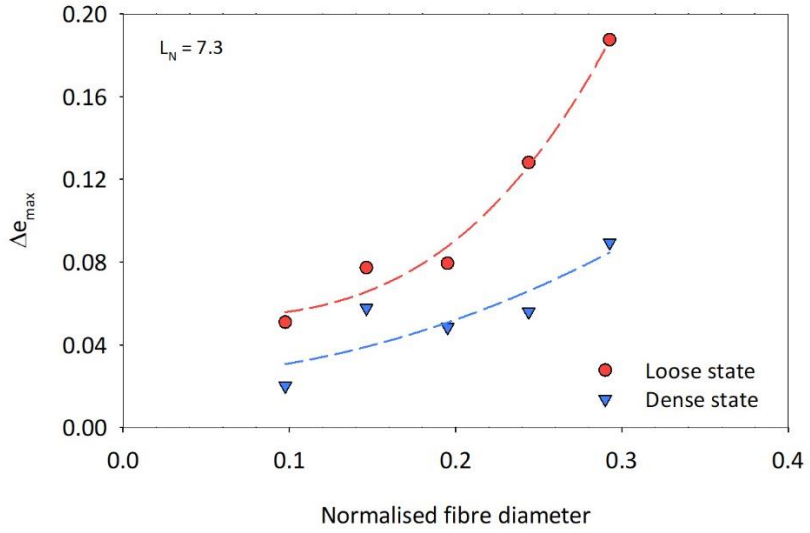

Figure 5-16. Effect of filament-like fibres diameter on MS ballast void ratio

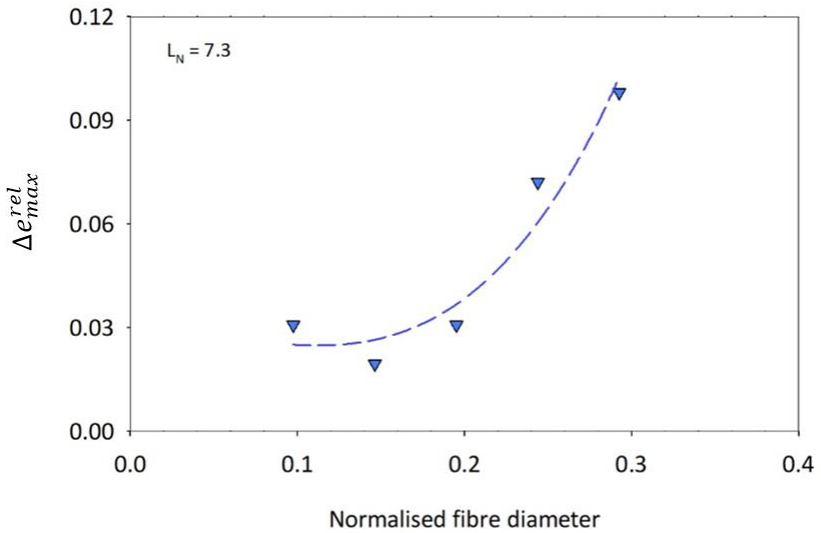

Figure 5-17. Effect of filament-like fibres diameter on MS ballast propensity to compact

5.5 Data acquisition

5.5.1 Sleeper displacements

The sleeper vertical deflections were monitored by means of 8 LVDTs (Linear Variable Displacement Transducers) held by steel brackets clamped to the rigid sides of the rig (Figure 5-18). They were positioned at the sleeper ends, beside the rail seats and at the middle of the sleeper, as shown in Figure 5-19. The sleeper movements are expressed in terms of settlement and resilient deflections. The former represents the permanent vertical movement of the sleeper and was calculated, for each cycle, as the average sleeper deflection at minimum load. The settlement was re-zeroed after the first or the first 10 cycles to mitigate the effect of the variability of sample initial conditions and improve test repeatability (Section 5.6). The resilient movements represent the recovered component of the sleeper deflection and were calculated as the difference between the maximum and the minimum deflection exhibited in each cycle. The average sleeper deflection, either permanent or resilient, was calculated using the weighed area method considering all LVDTs. Data were sampled at a frequency of 1 Hz in the first pseudo-static load cycle and 100 Hz in the successive dynamic cycles (Section 5.6).

Figure 5-18. LVDTs held by steel bracket clamped to the rigid sides of the rig

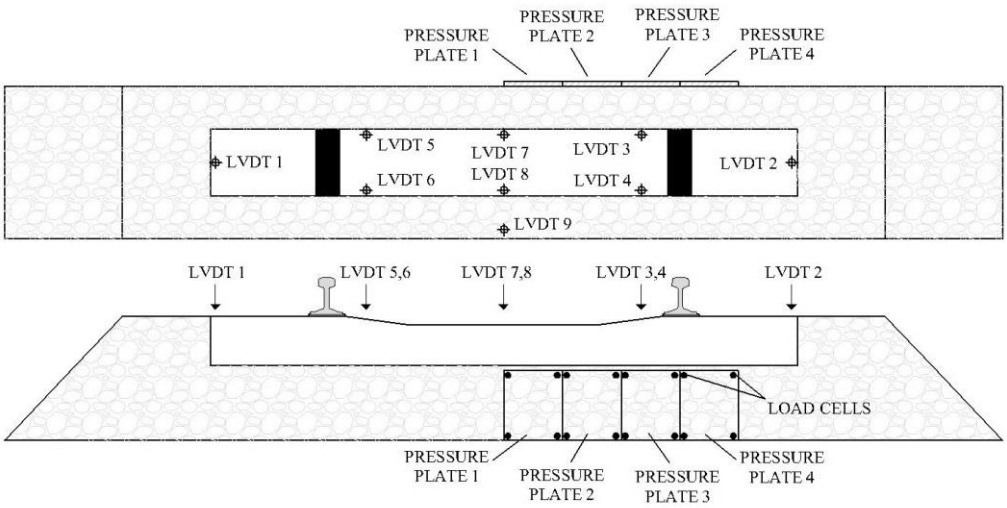

Figure 5-19. LVDTs and pressure plates locations

5.5.2 Ballast longitudinal pressure

The longitudinal pressure in the ballast layer was measured by means of 16 load cells (LCs) installed behind 4 steel plates of 250 mm by 300 mm each, herein termed “pressure plates” (Figure 5-20a). The pressure plates were installed only on one side of the apparatus, as shown in Figure 5-19 and Figure 5-20b. For each plate, the pressure was calculated as the total force taken by the four LCs divided by the area of the plate. Plates 1 and 2 are representative of the longitudinal pressure in the ballast under the middle of the sleeper, plates 3 and 4 of that below the rail seats. LCs data were acquired at a frequency of 1 Hz in the first pseudo-static cycle and 100 Hz in the successive dynamic cycles (Section 5.6).

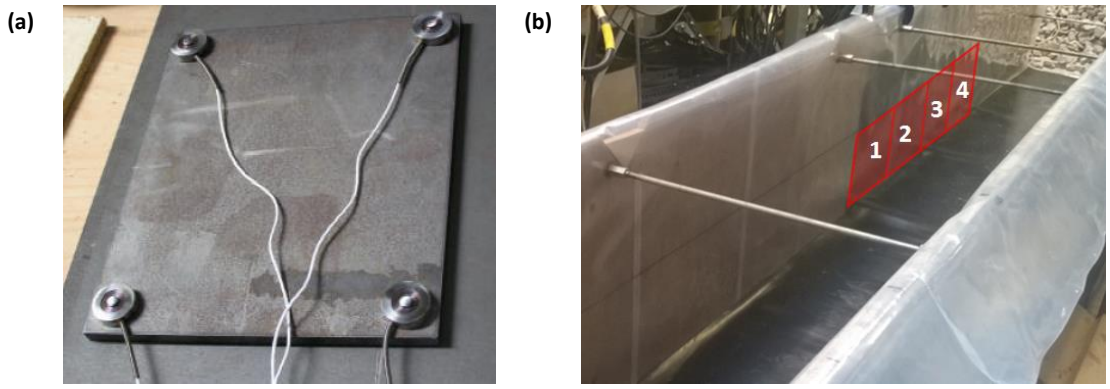

Figure 5-20. (a) Rear of a pressure plate (Le Pen, 2008); (b) location of the pressure plates within the rig

5.5.3 Ballast spreading

Track settlement is always accompanied by lateral spreading, as ballast is typically lightly confined (Section 3.3.4). The spreading can be reduced by interventions that increase track confinement, such as the use of geogrids (Section 3.4.3) or, possibly, fibre reinforcement (Section 4.3.1). Therefore, it should be monitored to obtain a deeper understanding of ballast mechanical behaviour and the effect of track interventions, e.g. random fibre reinforcement, on it.

While track vertical movements can be easily assessed by measuring the sleeper vertical deflections, the lateral spreading is more difficult to monitor. Indraratna et al. (2010) measured it by means of displacement transducers protected inside a 2.5 m long steel housing placed horizontally in the ballast bed below the sleeper. However, to minimise the disturbance to the ballast bed a different technique was developed for this particular study.

A horizontal version of a settlement plate, termed lateral plate, was specifically designed to be installed in the shoulders and fitted with a target so that the lateral movements could be assessed by means of a camera, via digital image analysis. A schematic representation of a lateral plate is shown in Figure 5-21. It consists of a rod rigidly connected to an end plate, which moves with the ballast particles surrounding it. The rod is protected by a tubular section, which serves as a sleeve. A short and larger tube was welded to the end plate to prevent the particles from filling the gap between the plate and the sleeve. A target, marked with nine black squares of known dimensions, is glued to the tip of the rod. The movement of the particles surrounding the end plate causes the rod to slide into the sleeve and the displacement of the target is captured by a camera installed on a rigid steel frame firmly clamped to the sides of the rig. To improve the accuracy the shoulder

was covered with a blackout curtain and constant illumination was provided by a lamp. Some photos of the system used are shown in Figure 5-22, its schematic representation in Figure 5-23.

The cameras could take no more than a picture every 3 seconds and had to be manually synchronised, by means of a timer, so that they would start shooting at the exact start of the test. In the first pseudo-static load cycle, pictures were acquired every 3 seconds. During cyclic loading they were taken every 3 seconds in the first ~1,000 cycles, every hour from 1,000 to ~250,000 cycles and every ~250,000 cycles afterwards.

A Matlab script was used to detect the average position of the target in pixels (Y), calculate the pixel to mm conversion factor (α) and hence the movement of the target (Δd). For a generic picture, taken at the time i, the digital position of the target (Y_i) was calculated as follows:

$$Y_i = \frac{1}{9}\sum_{j=1}^{9} y_{j,i} \tag{5-11}$$

where $y_{j,i}$ is the centroid of each of the 9 squares forming the target at the time i. The pixel to mm conversion factor was calculated for each picture using the following expression:

$$\alpha_i = \frac{1}{6}\sum_{j=1}^{6} \frac{l}{\lambda_{j,i}} \tag{5-12}$$

where l and $\lambda_{j,i}$ are the relative distances, in mm and pixels respectively, between the squares forming the targets (Figure 5-24). Hence, the relative movement of the target between two consecutive pictures was calculated by multiplying the movement, in pixels, by the average conversion factor:

$$\Delta d_i = (y_i - y_{i-1}) \cdot \frac{(\alpha_{i-1} + \alpha_i)}{2} \tag{5-13}$$

Finally, the total movement occurred between time a and b was calculated via integration:

$$\Delta d_{a,b} = \sum_{i=a+1}^{b} \Delta d_i \tag{5-14}$$

It must be pointed out that the lateral plates were only designed after the completion of the tests on CH ballast and hence, were only used in the second series of tests, those using MS ballast. Moreover, they had a small effect on ballast sample response to cyclic loading and, therefore, were only used in a limited number of tests, as explained in more detail in Section 7.7.

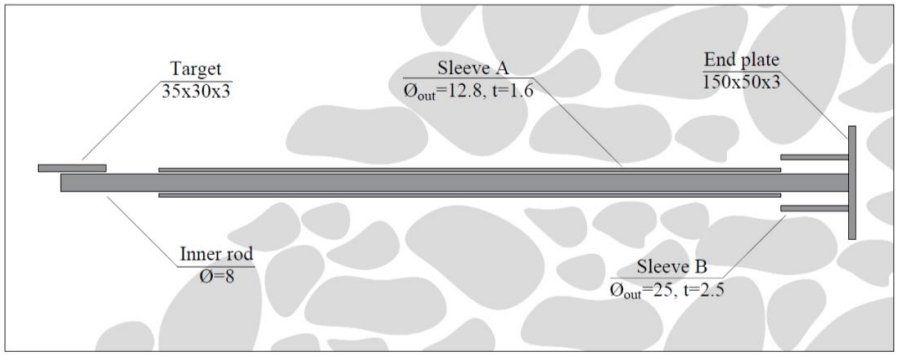

Figure 5-21. Longitudinal section of a lateral plate, specifically designed for this study to measure ballast lateral movements (dimensions in mm)

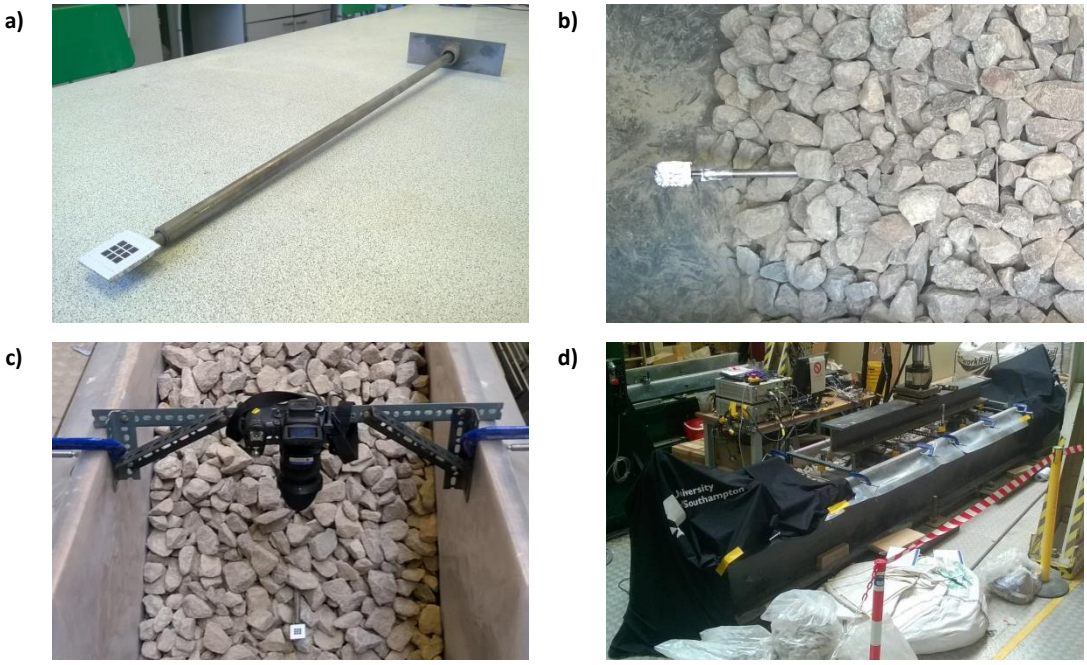

Figure 5-22. Photos of the system developed to monitor the lateral spread: a) lateral plate; b) lateral plate during installation; c) camera and mounting frame; d) set-up ready for testing

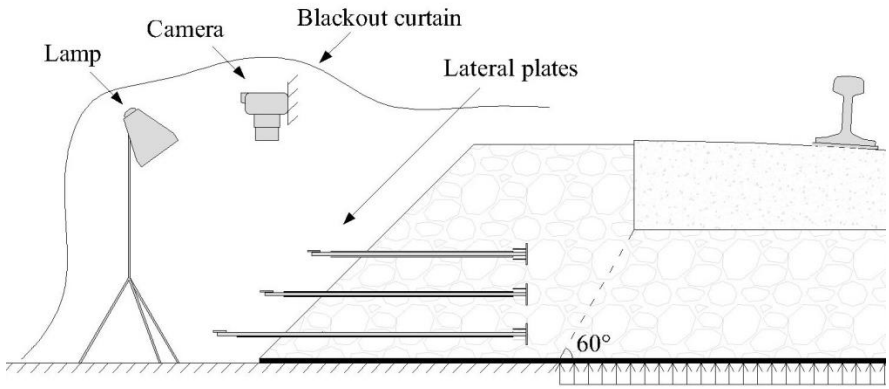

Figure 5-23. Schematic representation of the system developed to assess ballast lateral spreading

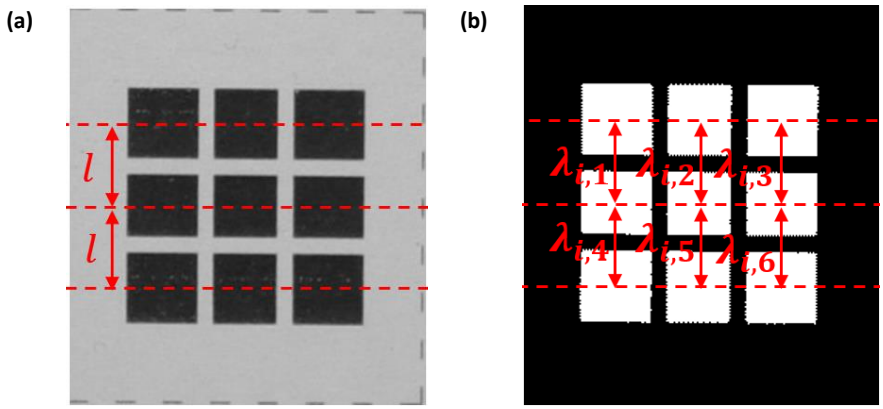

Figure 5-24. Target used to assess the movement of the lateral plates; (a) photo; (b) binary image

5.5.4 Sleeper/ballast contact area

The contact at the interface between the sleeper and the ballast was investigated by means of Fujifilm pressure sensitive paper (AJP Automotive LTD, 2018). It consists of a colour-forming and a colour-developing layer. When pressure is applied, microcapsules on the colour-forming layer are broken and red patches, whose colour density depends on the pressure level, appear on the colour developing layer. There are two types of Fujifilm pressure paper system: the two-sheet type and the mono-sheet type (figure 5-25). The former is suitable for pressures from 0.05 MPa to 50 MPa, the latter for pressures of 10 MPa to 300 MPa. Thus pressure sensitive paper provides, for a certain range of pressures, both the area of contact and level of pressure. The latter requires a calibration process, which should consider the effect of time on the colour intensity (Abadi, 2014).

Pressure paper was used by Abadi et al. (2015) to study the effect of ballast and sleeper interventions to the sleeper/ballast contact area. Similarly, it was used in this research to assess the influence of the addition of fibres on the contact between the sleeper and the ballast. Pressure papers of 200 mm x 270 mm were attached to the sleeper base, in the middle and below both rail seats (Figure 5-26). At each location, both a medium-pressure and a low-pressure two-sheet paper were used. The former was sensitive to pressures of 10 MPa to 50 MPa, the latter to those between 2.5 MPa and 10 MPa.

The papers can theoretically record the maximum pressure applied and the cumulative area imprinted throughout each test. However, the localised pressure exerted by the ballast particles is particularly high and tend to damage the paper, as also observed by Abadi (2014). Therefore, this technique was only used to assess the cumulative area of contact at the sleeper/ballast interface.

Each pressure film was scanned at high resolution right after each test. Then the images of the films were analysed using the commercial software Photoshop. A filter was set up to select the red patches, while the spots damaged by particularly high localised stresses were added manually to the selection. The colour filter was saved and used for all images. The percentage contact area was calculated as the ratio of the area marked by the particles to the total area of the paper.

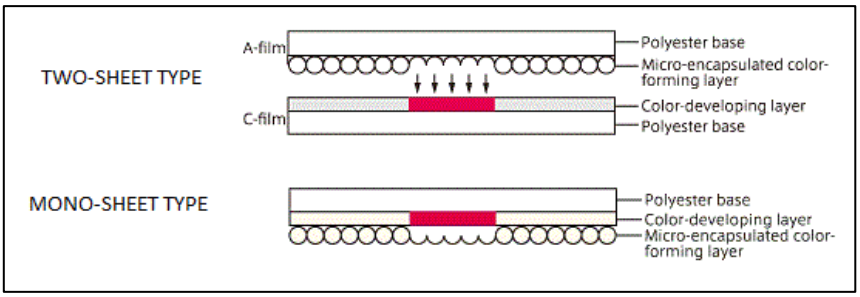

Figure 5-25. Pressure *paper types (*http://www.fujifilmusa.com/products/measurement-films/prescale/film/*)*

Figure 5-26. Pressure paper attached to the sleeper base

5.5.5 Particle degradation

Particle degradation was assessed by measuring the mass reduction and number of broken particles for a statistically significant number of particles placed under the sleeper in the top half of the ballast bed. The former is representative of particle frictional wear and chipping, the latter of particle splitting and corner breakage (Section 3.3.3).

The degradation of the ballast particles was assessed for the tests using MS ballast. Three batches of selected particles, of about 16 kg each, were placed in the top part of the ballast bed, below the middle of the sleeper and the rail seats (Figure 5-27). These particles were prepared as follows: they were sieved and grouped based on their size (i.e. < 31.5 mm, 31.5 mm, 40 mm, 50 mm); those greater than 31.5 mm were coloured with a water based spray paint, marked with their size, washed and allowed to dry at 20°C in a temperature controlled room; the original grading was reconstituted by mixing all fractions together. The particles were placed in the top part of the ballast bed, covered by a thin layer of ballast, i.e. about 8 kg, to avoid direct contact with the sleeper soffit. The selected particles were representative of the top half part of the ballast bed subjected to the loading, as they covered almost 40% of the sleeper area and reached a depth of almost 15 cm (Figure 5-27). They were not placed in direct contact with the sleeper to minimise their abrasion during compaction (Section 5.6) and the breakage of particles due to bedding imperfections, e.g. presence of higher spots. The selected particles just placed in the ballast bed are shown in Figure 5-28.

Typical test results are shown in Table 5-6. The mass loss is expressed as the ratio of the mass reduction (ΔM) to the initial mass (M_0) and was calculated for each particle size. For each test the mass loss was calculated as a weighted average considering all particle sizes. The mass loss of each batch of particles was intended as representative of abrasive wear and particle chipping. Therefore, the batches containing a broken particle were not considered to calculate the mass loss. For this reason, it was convenient to split the particles of the same size into two batches at least (termed a and b in Table 5-6). If a broken particle was present in one of the batches, the other one could be used to calculate the average mass loss, so that all particle sizes were still represented. For example, for test MS.03, although one broken particle was present in one of the two batches representative of the 37.5 mm particles (3a), the other one (3b) could be used to calculate the average mass loss, as shown at the bottom of Table 5-6.

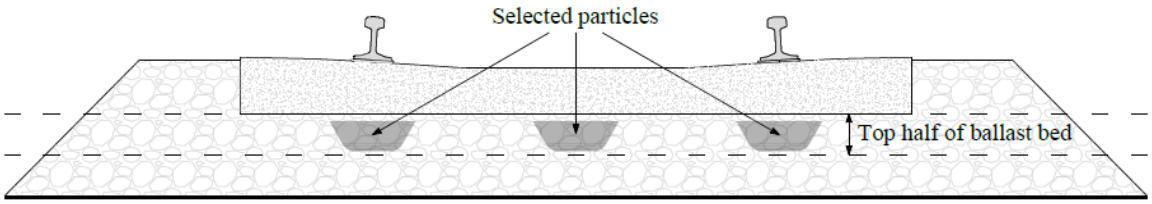

Figure 5-27. Locations of the marked particles used to assess ballast damage

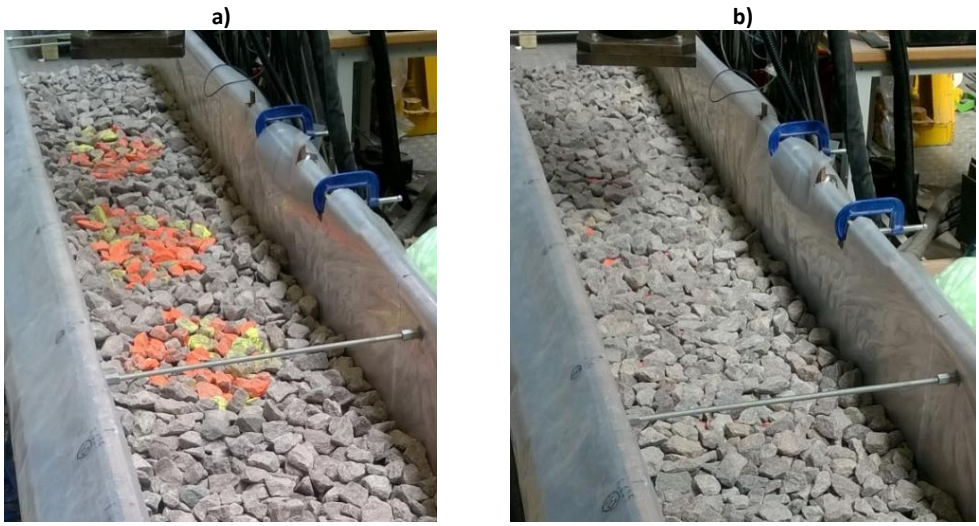

Figure 5-28.Selected ballast particles; a) right after being placed on the ballast bed; b) after being covered with a layer of particles to avoid direct contact with the sleeper.

Table 5-6. Degradation of the ballast particles below the middle of the sleeper in test MS.03; batch 3a was not considered to calculate the average mass loss, as it contains a broken particle.

Batch number	Particle size (mm)	No. of particles	No. of broken particles	Initial mass, M_i (g)	Final mass, M_f (g)	Mass loss, $\Delta M/M_i$ (%)
1a	50	2	0	592.86	592.54	0.054
1b	50	3	0	590.16	589.94	0.037
2a	40	26	0	3626.32	3623.10	0.089
2b	40	26	0	3845.58	3840.76	0.125
3a	37.5	11	1	1170.64	1166.90	0.319
3b	37.5	11	0	1056.92	1055.96	0.091
4a	31.5	12	0	995.5	994.24	0.127
4b	31.5	12	0	894.58	893.86	0.080
			Sum =	**12773**	**Average =**	**0.097***

*Average = (593·0.054+590·0.037+3626·0.089+3856·0.125+2·1057·0.091+996·0.127+895·0.080)/12773 = 0.097%

5.6 Test preparation

Common preparation procedures were used to aid test repeatability. Each test was prepared over three days: in day 1 and 2, the rig is filled to the level intended for the sleeper base (Figure 5-29a); in day 3, the ballast bed is carefully compacted and levelled using an electric compaction plate (Figure 5-29b), sleeper and crib ballast are placed (Figure 5-29c) and the loading beam is positioned on the rails (Figure 5-29d). Further details of test preparation can be found in Table 5-7.

All tests were started about 24 hours after the loading beam had been placed so that, if any creep deformation developed in the ballast and rubber ahead of the tests, its magnitude would have been almost the same in each test. A first load cycle was applied quasi-statically, with a loading rate of 5 kN/s, to check the connections and develop the initial plastic deformations (Figure 5-30a). Then a sinusoidal load was applied at frequency of 3 Hz to 3 million cycles (Figure 5-30b). The load was ranged between 5 kN and 98.1 kN and is representative of a 20 t train axle, as only about 50% of the wheel force is transmitted to the sleeper directly underneath it (Section 2.3.2.1). In each test, the top 3 mm rubber mat forming the resilient layer placed at the bottom of the rig was replaced. Moreover, fresh ballast and new fibres were used. The plastic sheets covering the sides of the rig were only replaced when worn.

Although common procedures were strictly followed for test preparation, the difficulty in levelling the ballast layer, owing to its very coarse nature, led to inevitable bedding imperfections. As observed in Section 3.2.2, their effect on ballast permanent deformation can be strongly mitigated by disregarding the first few loading cycles. This is clear from Figure 5-31, which shows the settlement response for three repeated tests. If all cycles are considered, repeated tests showed errors of 0.4 mm to 2 mm (Figure 5-31a). However, if the first or the first 10 cycles are neglected, the errors become smaller than 0.2 mm and 0.03 mm respectively (Figure 5-31b and c).

Table 5-7. Test preparation procedure

Task	Description	Day 1	Day 2	Day 3	Day 4
1. Replacing worn parts	The top rubber layer mimicking the subgrade and, if worn, the plastic sheet covering the sides of the rig are replaced.	X			
2. Placing ballast bed	Buckets are filled manually with the desired proportion of fresh ballast and new fibres, weighed and placed carefully into the rig to avoid fibre segregation. When the level of the sleeper soffit is reached, lateral plates and selected particles are installed.	X	X		
3. Compaction and levelling	The ballast layer is levelled and compacted by a total of 22 passes of a 26 kg, 400 mm by 320 mm plate vibrator with a 5 kN compactive force.			X	
4. Placing sleeper, loading beam and crib ballast	The loading beam is placed on the bits of rails and the crib ballast is manually poured into the rig using buckets. In each test about 450 kg of crib ballast was used.			X	
5. Installing LVDTs and cameras	Vertical LVDTs (Section 5.5.1) and cameras (Section 5.5.3) are installed on the sleeper and on the ends of the rig respectively.				X
6. Test start	Each test is started about 24 hours after completion of task 4 to allow for similar amount of creep deformation to occur before testing.				X

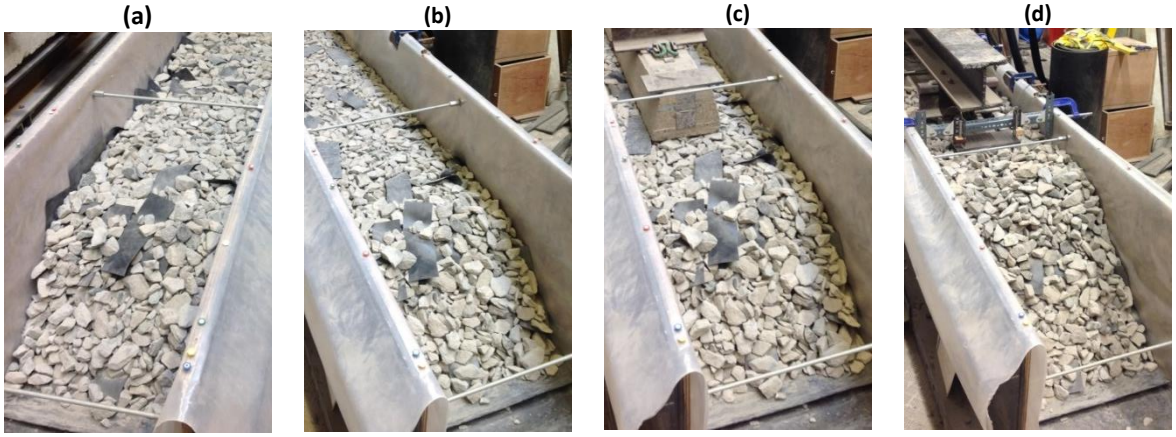

Figure 5-29. Sample of fibre reinforced ballast (a) after the ballast bed was laid, (b) after compaction and levelling; c) after the sleeper was placed, and (d) after placing loading beam and LVDTs

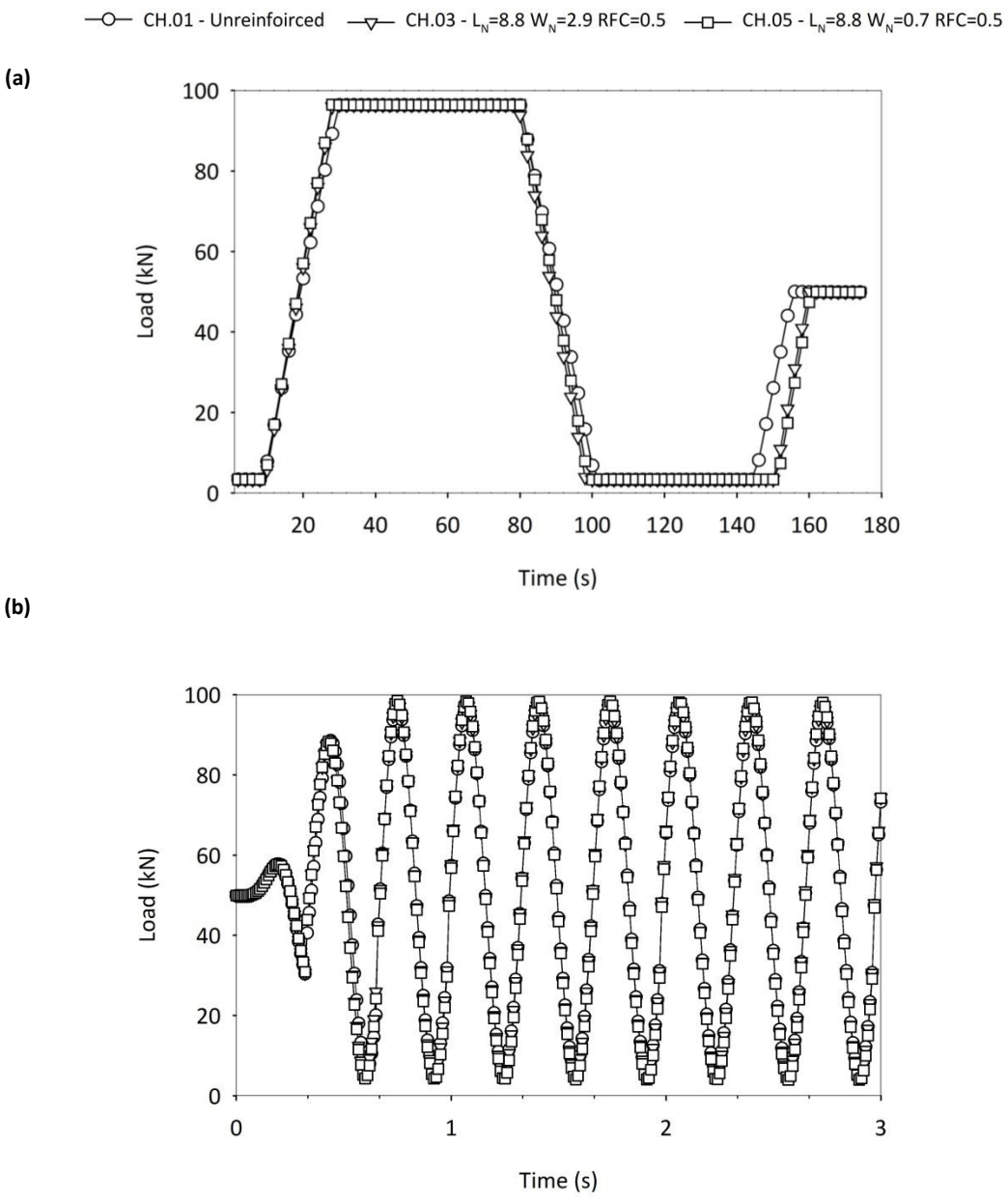

Figure 5-30. Load applied (a) in the first pseudo-static cycle and (b) in the first dynamic cycles for three different tests

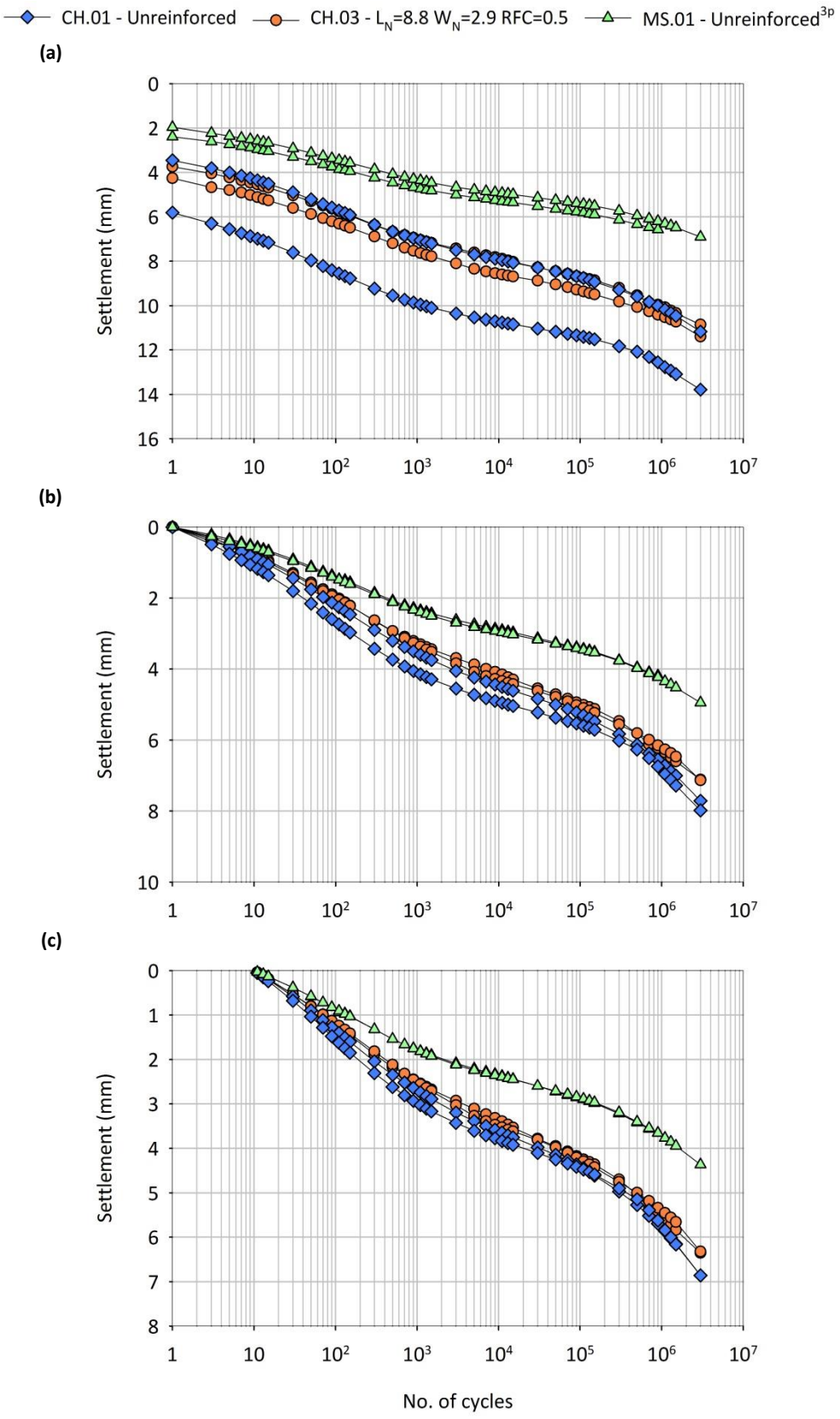

Figure 5-31. Settlement curves for three repeated tests: (a) all cycles, (b) after 1st cycle; (c) after 10th cycle

5.7 Testing programme

The testing programme was aimed at understanding the mechanical behaviour of ballasted track reinforced with synthetic fibres of different characteristics, i.e. dimensions, content and type. The programme was split into two parts: tests using Cliffe Hill (CH) ballast and Mount Sorrel (MS) ballast. In each test a G44 concrete sleeper was used. The sleeper was not damaged by the testing but was replaced with a newer one for precaution after the first part of the programme.

The first series of tests explored the effect of the addition of tape-like fibres, which had been previously tested to a smaller scale under monotonic loading (Section 4.2.1). A further batch of tests explored the potential of an alternative type of inclusion, i.e. filament-like fibres. The tests of the first and second series are not directly comparable, as CH and MS ballast showed very different performance. Therefore, they are described in separate chapters (i.e. Chapter 6 and Chapter 7), while the discussion of all test results is contained in Chapter 8.

The fibre characteristics were varied to understand their effect on ballast behaviour. The tape-like fibres were varied in length (L_f = 75 - 300 mm, L_N = 2.2 - 8.8), width (W_f = 25 - 100 mm, W_N = 0.7 - 2.9) and content (V_{fr} = 0.6 - 1.2%, RFC = 0 - 1). The filament-like fibres were varied in diameter (d_f = 6 - 10 mm, d_N = 0.14 - 0.25) and content (L_{fp} = 0 to 5.1 cm, RFC = 0 to 0.9) while the length was kept constant (L_f = 300 mm, L_N = 7.3). The characteristics of all 25 tests are described in detail in Section 6.2 for CH ballast, and 7.2 7for MS ballast.

5.8 Summary

Full-size tests were carried out to assess the potential of fibre reinforcement to improve the performance of ballasted track. These were carried out in the Southampton Railway Testing Facility, which represents a single sleeper bay of single line track extended to the shoulders in plain strain conditions. In each test, after a first pseudo-static load cycle, a sinusoidal load was applied for 3 million cycles at 3 Hz. The minimum and maximum compressive force was 5 kN and 98.1 kN respectively. The loading is representative of a 20 tonne train axle, assuming a 50% longitudinal load transfer to the adjacent sleepers. Common procedures for test preparation were followed to minimise the variability of sample initial conditions. Moreover, the settlement was re-zeroed after the first load cycle to mitigate the bedding errors and achieve accuracy of less than 0.2 mm.

Two series of tests were carried out. The first one, in which Cliffe Hill ballast was used, explored the potential of thin tape-like fibre to improve track performance. The second one, in which Mount Sorrel ballast was used, investigated the effect of filament-like fibres. Tests explored the effect of fibre dimensions and content, and provided a comparison between the two types of reinforcement tested. Both Cliffe Hill and Mount Sorrel ballast were obtained from freshly crushed granite. The former, however, was characterised by smaller and denser particles, whose surface felt slightly smoother to touch. The tape-like fibres were obtained from polyethylene damp proof course, the filament-like fibres from polypropylene rope.

The fibre dimensions were normalised to the average particles size to account for the relative fibre/particles size. The fibre content was expressed in terms of relative fibre content, i.e. the ratio of the fibre content to the maximum fibre content that can be added to avoid excessive fibre

overlapping. The latter depends on both the characteristics of the particles and reinforcement, and was estimated for the tape-like and filament-like fibres based on the visual inspection of the samples used for the bulk density tests. However, it can be potentially derived also theoretically, using a suitable model that considers the characteristics of both the particles and the reinforcement. A simplified example of this latter approach was provided to highlight the importance of the relative fibre/particle size on the maximum amount of reinforcement allowed by a certain granular matrix.

Bulk density tests were carried out to understand the effect of the fibres on the void ratio, hence the packing of the particles. The void ratio was calculated as the ratio of the volume of the voids to the volume of the particles, without considering the volume of the fibres. It increased linearly with the fibre content, especially in loose conditions. This implies that the fibres increased the permanent volumetric deformation exhibited by ballast during compaction and might be explained by the particles being disturbed by the inclusions in loose conditions but forcing them into the voids under significant compacting effort. For the tape-like fibres the disturbance to the packing of the particles was marginal if the normalised fibre width did not exceed 0.7, for the filament-like fibres if the normalised diameter was not greater than 0.1. Ballast propensity to be affected by compaction increased rapidly if the normalised width was greater than 1.5 or the normalised diameter greater than 0.2. Below these values it was only marginally affected by the reinforcement. The length of the inclusions had a relatively small effect on the void ratio.

Different techniques were implemented to capture the main characteristics of ballasted track behaviour. Linear variable displacement transducers were used to monitor the sleeper permanent and resilient vertical movements. Load cells were installed on the lateral sides of the rig to assess the longitudinal pressure in the ballast bed. Pressure sensitive paper was used to investigate the sleeper/ballast contact. Lateral plates, i.e. horizontal version of settlement plates, were installed in the shoulder to monitor the lateral spread via digital image analysis. Ballast particles were marked and placed beneath the sleeper to assess ballast damage.

6 TEST RESULTS 1 of 2 - CLIFFE HILL BALLAST

6.1 Introduction

This chapter describes the results of the first series of full size tests conducted in the Southampton Railway Testing Facility to understand the behaviour of fibre reinforced ballasted track. The fibres were obtained from polyethylene damp-proof course. The ballast was sourced from Cliffe Hill (CH) quarry. The testing methods and materials are described in the previous chapter.

The first part of this chapter presents the testing programme and its objectives. Then, test results are described in terms of sleeper settlement, sleeper resilient deflections, ballast longitudinal pressure and sleeper/ballast contact area. Finally, the main characteristics of the behaviour of ballasted track and the potential effect of fibre reinforcement on it are summarised.

A second series of tests was carried out using a different ballast. These are not directly comparable to those presented in this chapter, owing to the different performance of the ballast used, and are described in Chapter 7. The discussion and interpretation of all test results is in Chapter 8.

6.2 List of tests

The tests carried out are listed, in chronological order of execution, in Table 6-1. In each test, CH ballast and tape-like fibres were used (Section 5.3). In the first tests, CH.02^{c} and CH.03^{c}, no fibres were added to the crib, as crib fibres were not expected to affect sample response. This was confirmed by the comparison between test CH.03 and CH.03^{c}, which showed that the fibres placed in the crib had negligible effect on sample response. Therefore, CH.03^{c} and CH.03 are regarded as repeated tests.

Different combinations of fibre content and dimensions were used. The volumetric fibre ratio (V_{fr}) was varied between 0.6% and 1.2%, corresponding to relative fibre contents (RFC) of 0.5 and 1 respectively, as RFC was calculated using equation (5-6). These are representative of a moderate and a high amount of reinforcement. The length of the fibres (L_f) was varied between 75 mm and 300 mm and their width (W_f) between 25 mm and 100 mm, corresponding to a normalised fibre length (L_N) of 2.2 to 8.8 and a normalised fibre width (W_N) of 0.7 to 2.9 (Section 5.4.1). The fibre length was arbitrarily limited to L_f = 300 mm (L_N = 8.8), which is the depth of the ballast layer and, as observed by Ajayi et al. (2017), is big enough to mobilise tension in the reinforcement.

Unreinforced ballast was used in the first test (CH.01) and its repeat (CH.01^{r}), which represent the baseline. In test CH.02, a high content (RFC = 0.9) of wide and long fibres (W_N = 2.9 and L_N = 8.8) was used to maximise ballast shear strength (Section 4.2.2). However, this test showed poor ballast performance. In test CH.03 (and CH.03^{c}), a smaller fibre content of RFC = 0.5 was used to reduce the likelihood of fibre overlapping but ballast performance was still poor. Narrower fibres were used in tests CH.04 and CH.05, i.e. W_N = 1.4 and W_N = 0.7, to reduce the disruption of the packing of the particles (Section 4.3.2.7 and 5.4.3). These effectively improved ballast performance. Further tests were carried out to better understand, and improve, the behaviour of

reinforced ballast. A high fibre content was used in test CH.06, shorter fibres in tests CH.07 to CH.09. These latter tests were aimed at understanding the potential for small inclusions, like crumb rubber (Section 3.4.6), to improve ballast performance under cyclic loading, although they cannot take significant tensions and hence, increase the shear strength (Section 4.3.2.2).

Table 6-1. List of tests using Cliffe Hill ballast and tape-like fibres

No.	Label	L_f (mm)	W_f (mm)	V_{fr} (%)	L_N (-)	W_N (-)	RFC (-)
1	CH.01 - Unreinforced	-	-	0.00	-	-	-
2	CH.01[r] - Unreinforced	-	-	0.00	-	-	-
3	CH.02[c] - L_N=8.8 W_N=2.9 RFC=0.9	300	100	1.18	8.82	2.94	0.98
4	CH.03[c] - L_N=8.8 W_N=2.9 RFC=0.5	300	100	0.63	8.82	2.94	0.53
5	CH.03 - L_N=8.8 W_N=2.9 RFC=0.5	300	100	0.64	8.82	2.94	0.53
6	CH.04 - L_N=8.8 W_N=1.5 RFC=0.5	300	50	0.67	8.82	1.47	0.56
7	CH.05 - L_N=8.8 W_N=0.7 RFC=0.5	300	25	0.69	8.82	0.74	0.58
8	CH.06 - L_N=8.8 W_N=0.7 RFC=0.9	300	25	1.06	8.82	0.74	0.88
9	CH.07 - L_N=4.4 W_N=0.7 RFC=0.5	150	25	0.69	4.41	0.74	0.57
10	CH.08 - L_N=2.2 W_N=0.7 RFC=0.5	75	25	0.66	2.21	0.74	0.55
11	CH.09 - L_N=6.6 W_N=0.7 RFC=0.5	225	25	0.67	6.62	0.74	0.56

[c] no fibres in the crib ballast ; [r] repeat

6.3 Settlement

The sleeper settlement was defined as the average sleeper permanent deflection (Section 5.5.1) and re-zeroed after a small number of cycles, i.e. 1 or 10, to mitigate the effects of the variability of the initial conditions, e.g. bedding errors, for comparability (Section 5.6).

The effect of fibre content, width and length on the settlement response is shown in Figure 6-1, Figure 6-2 and Figure 6-3 respectively, which represent the evolution of the permanent deflections throughout the tests after the first load cycle (a parts) and the first 10 cycles (b parts), and the normalised settlement at 3 million cycles (c parts). The latter is the ratio of the settlement to the settlement for the baseline test.

In all tests the settlement increased approximately linearly with the logarithm of the number of cycles (Figure 6-1 to Figure 6-3, a and b). The results were not strongly affected by the number of cycles after which the settlement was re-zeroed, i.e. 1 or 10, which improves the confidence in their reliability. In general, the addition of narrow fibres reduced the settlement while wide ones increased it (Figure 6-1b), moderate fibre contents were more effective than high ones (Figure 6-3b) and the effect of the fibre length was small (Figure 6-2b). The fibres were not effective in the first ~ 500 cycles (Figure 6-1b, Figure 6-2b, Figure 6-3b). This can be explained by the inclusions requiring a certain settlement to become effective, i.e. 3 mm after the first cycle

(Figure 6-1a, Figure 6-2a, Figure 6-3a), and seems corroborated by the second series of tests, as explained in Section 8.4.

The effect of the fibre width, on the settlement is clearly shown in Figure 6-1c. The addition of a moderate amount (RFC = 0.6) of wide fibres increased the settlement. In contrast, narrow fibres reduced it by 20%, if only the first cycle is neglected, and by 23%, if the first 10 cycles are not considered. The settlement was only marginally affected by the width of the inclusions if $W_N \leq$ 1.5, suggesting the existence of a threshold width value, above which the fibres are less effective.

The effect of the fibre length was investigated only for the narrowest fibres tested (W_N = 0.7) and moderate fibre content ($RFC \cong 0.5$). The settlement vs number of cycles curves were only marginally affected by the length of the inclusions (Figure 6-2a, Figure 6-2b), with shorter fibres only ~4% less effective than long ones at reducing the permanent deformation (Figure 6-2c).

Like the fibre width, the content had a significant impact on the settlement. Compared with moderate fibre contents ($RFC \cong 0.5$), high ones ($RFC \cong 0.9$) were associated with a greater rate of permanent deformation from the very first load cycles (Figure 6-3a, Figure 6-3b). The effect of the fibre content on the long-term settlement for wide and narrow fibres (W_N = 2.9 and W_N = 0.7) is clear from Figure 6-3c. A moderate amount (RFC = 0.6) of narrow fibres (W_N = 0.7) reduced significantly the settlement while a higher content (RFC = 0.9) of the same fibre was less effective. Similarly, wide fibres (W_N = 2.9) increased the settlement by less than 10% if RFC = 0.5 and by about 30% if $RFC = 1$. Therefore, an optimum fibre content exists and, based on test results, might fall between RFC = 0.4 and RFC = 0.6.

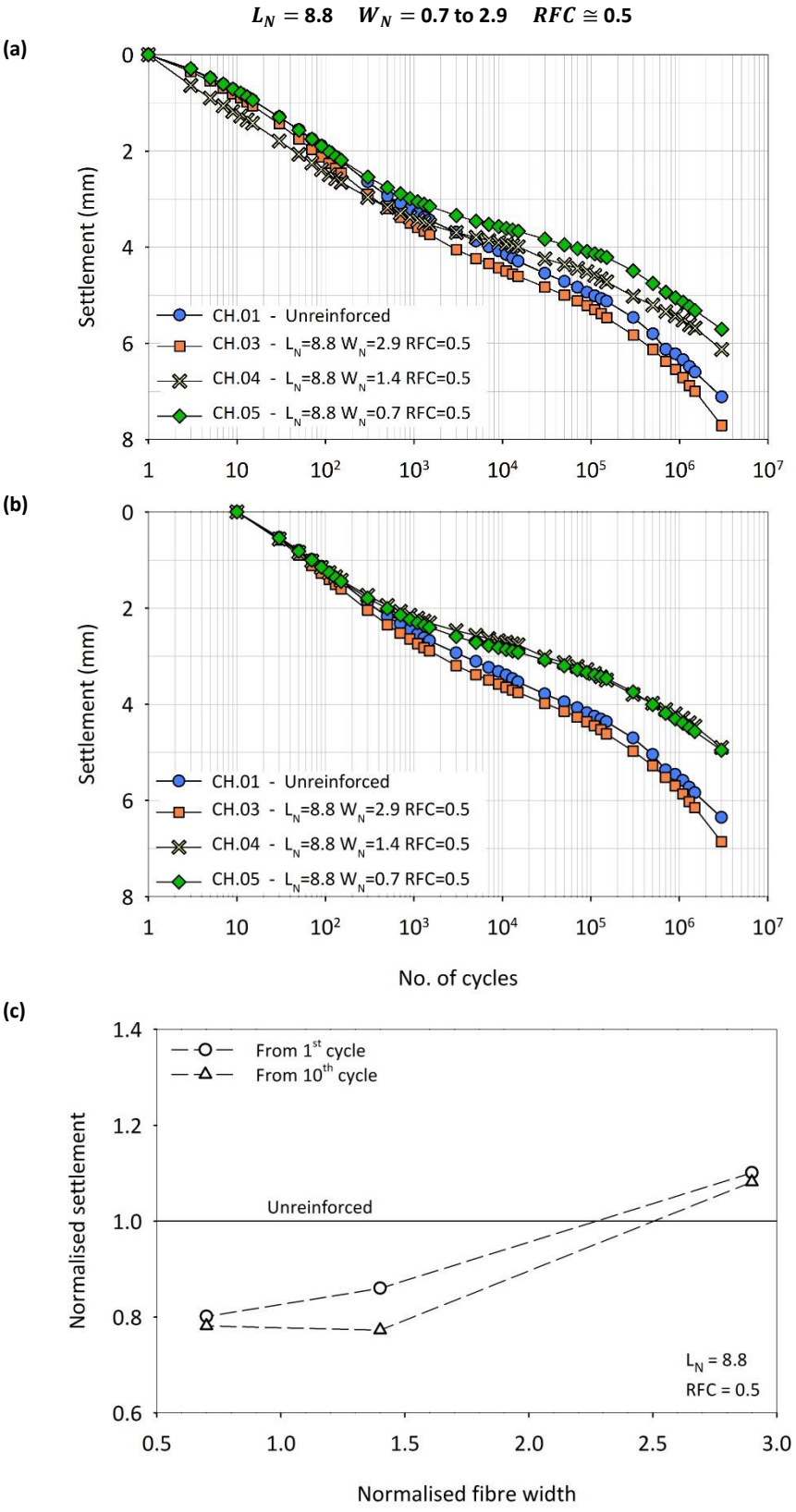

Figure 6-1. Effect of the width of tape-like fibres on CH ballast settlement response; settlement vs number of cycles: (a) zeroed after 1 cycle and (b) after 10 cycles; (c) normalised settlement at 3 million cycles vs normalised fibre width

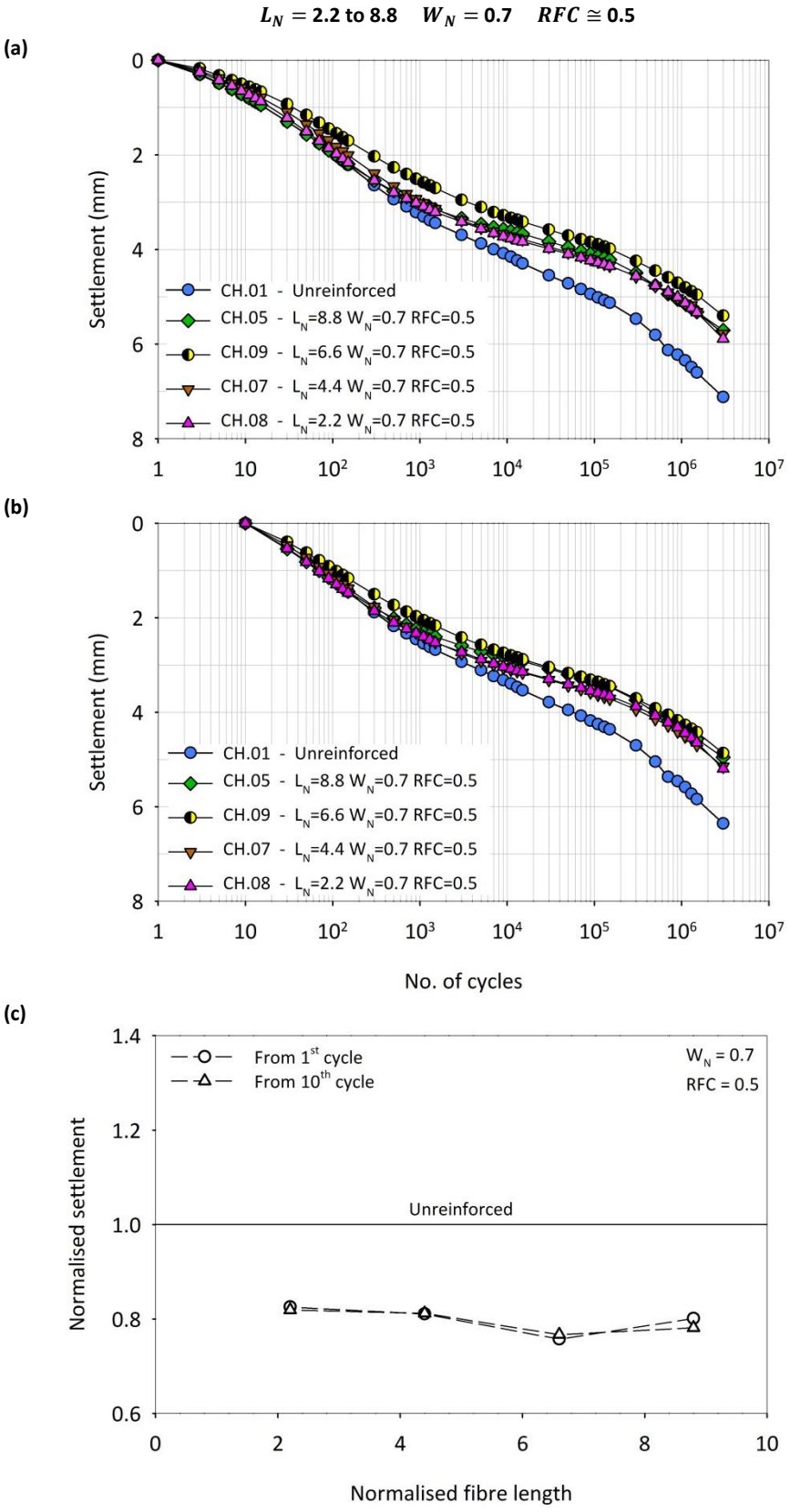

Figure 6-2. Effect of the length of tape-like fibres on CH ballast settlement response; settlement vs number of cycles: (a) zeroed after 1 cycle and (b) after 10 cycles; (c) normalised settlement at 3 million cycles vs normalised fibre length

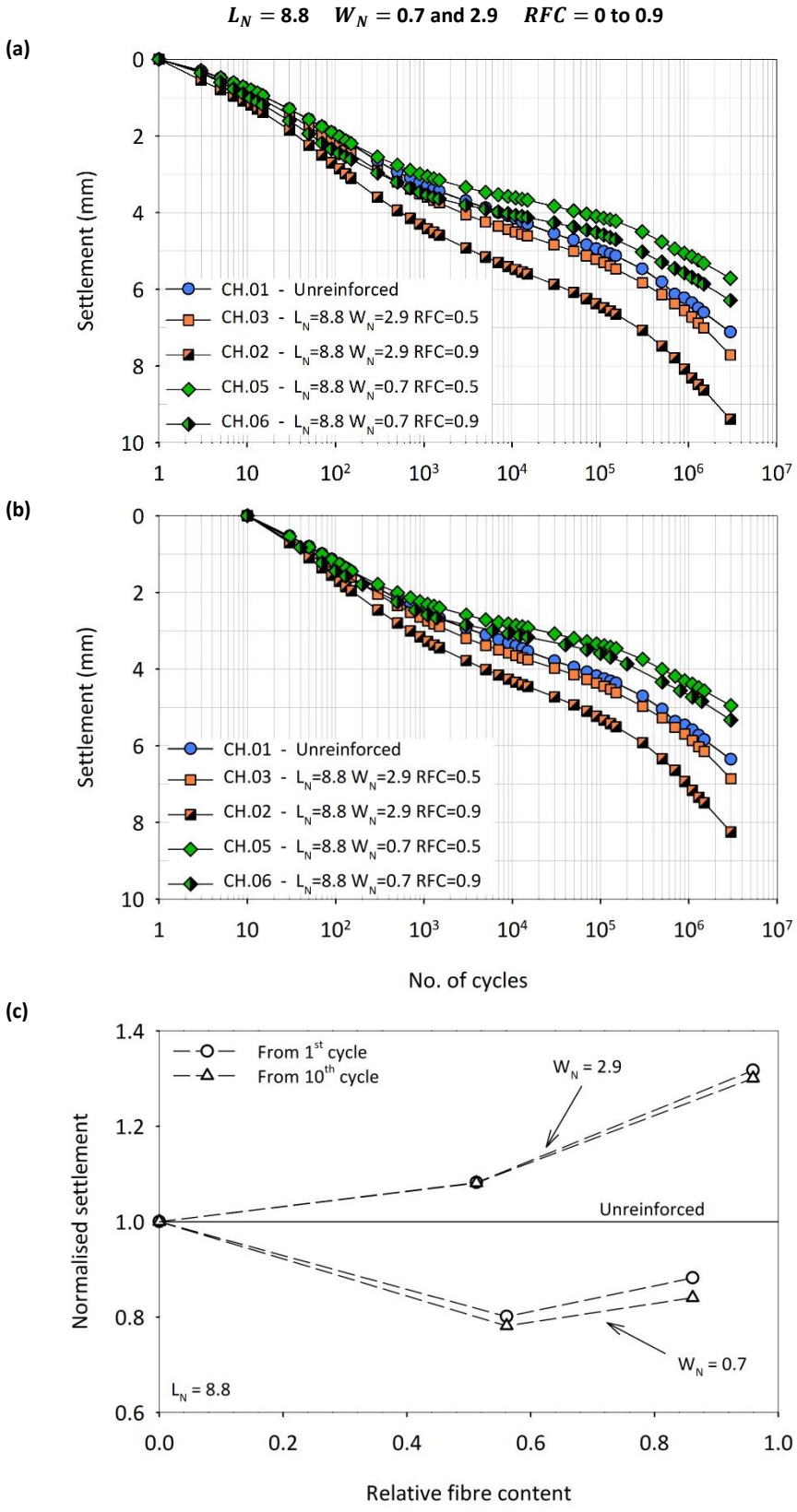

Figure 6-3. Effect of the content of tape-like fibres on CH ballast settlement response; settlement vs number of cycles: (a) zeroed after 1 cycle and (b) after 10 cycles; (c) normalised settlement at 3 million cycles vs relative fibre content

6.4 Resilient deflections

The resilient deflections were calculated as the difference between the maximum and minimum deflection recorded by each displacement sensor in each load cycle (Section 5.5.1). The present section describes both their magnitude and spatial distribution throughout the tests, aiming at understanding the sleeper/ballast interaction and the effect of fibre addition on it.

The development of the resilient movements with the cycles is shown in Figure 6-4. The average sleeper deflection, initially between 0.5 mm and 0.8 mm, reduced to 0.3-0.6 mm in the first ~300,000 cycles, beyond which it increased slightly (Figure 6-4a). This trend is explained by movements reducing at the middle and increasing at the sleeper ends. The former reduced monotonically with the cycles, from 0.4-0.9 mm to 0.2-0.4 mm (Figure 6-4b). The latter were between 0.4 mm and 0.7 mm in the first 30,000-100,000 cycles, beyond which they increased to 0.5-0.9 mm (Figure 6-4c).

To better visualise the sleeper deformed shape throughout the tests, the deflections were plotted against the sleeper length for some key cycles (Figure 6-5 to Figure 6-7). Results are shown in three different figures to emphasise the effect of the fibre width (Figure 6-5), length (Figure 6-6) and content (Figure 6-7). Usually, the sleeper showed sagging in the very first cycles, although the resilient deflections in the first cycles are affected by the initial bedding of the ballast. The sleeper deformed shape reversed within the first 10,000 cycles, owing mainly to the reduction of the middle deflections. In the longer term, especially after 100,000 cycles, sleeper hogging became particularly pronounced. As already observed, this is explained by the increase in movements of the sleeper ends and the reduction of those at the middle, with the former being typically 3 to 4 times bigger than the latter at 3 million cycles (Figure 6-4 b and c).

The effect of fibre addition on the sleeper resilient behaviour must be carefully evaluated, as the resilient deflections are very small, i.e. 0.2 mm to 0.8 mm, and the effect of the reinforcement is even smaller, i.e. less than 0.3 mm. Therefore, the effect of fibre addition on the resilient movements can be affected by small experimental errors. Hereafter, only the sleeper resilient behaviour at 3 million cycles is considered, as it is the least affected by sample initial conditions and is representative of track performance in the long term. The effect of the fibre width and length on the deflections is shown in Figure 6-8 and Figure 6-9 respectively, that of the fibre content in Figure 6-10 for wide fibres and Figure 6-11 for narrow ones. Each of these shows the increase (or reduction) of the resilient deflections and sleeper curvature with the addition of fibres. The curvature is expressed by the difference between the deflections at the middle and those at the ends of the sleeper. It must be pointed out that the baseline test and its repeat (CH.01 and CH.01^{r}) showed slightly different results, especially at the sleeper ends after 300,000 cycles (Figure 6-4c and Figure 6-5f). It is not clear which baseline is more accurate, as they both showed similar initial resilient shape (Figure 6-5a) and evolution of the deflections with the cycles (Figure 6-4). Therefore, the increase/reduction in resilient deflections, shown in Figure 6-8 to Figure 6-11, was calculated against the average between test CH.01 and CH.01^{r}.

The effect of the fibre width on the resilient deflections at 3 million cycles is shown in Figure 6-8. The addition of a moderate amount of long and narrow fibres ($RFC = 0.5$, $L_N = 8.8$, $W_N \leq 1.5$) increased slightly the movements at mid-sleeper but reduced those near the rail seats and, especially, at the sleeper ends. The use of wide fibres ($W_N = 2.9$) caused a greater increase in

movements at the middle and did not reduce those of the sleeper ends. On average, the narrow fibres reduced the resilient deflections while wide ones increased them (Figure 6-8b). The sleeper curvature reduced with the addition of a moderate amount of fibres and was not affected by the width of the inclusions (Figure 6-8b).

The influence of the fibre length for W_N = 0.7 and $RFC = 0.5$ is represented in Figure 6-9. Some data points, labelled as 'suspect', do not follow the trend suggested by the other ones and are not considered. These are associated with test MS.07, which also showed suspect sleeper/ballast contact area (Section 6.6). The fibre length did not affect significantly the resilient movements at mid-sleeper and near the rails (Figure 6-9a). The average sleeper deflection, which reduced with the addition of narrow fibres, was not affected by the length of the inclusions (Figure 6-9b). In contrast, the sleeper hogging was smaller for shorter fibres, as they further reduced the movements of the sleeper ends compared with long ones (Figure 6-9c). However, results do not show clear trends and should be carefully considered.

The effect of the fibre content for wide and narrow fibres of maximum length ($W_N = 2.9$ and 0.7, L_N = 8.8) is shown in Figure 6-10 and Figure 6-11. Compared with the baseline, the addition of a large amount of wide fibres ($RFC \cong 1$) increased the resilient deflections, especially at the sleeper ends, exacerbating the sleeper hogging (Figure 6-10). The use of a high content (RFC = 0.9) of narrow fibres had a relatively small effect on the resilient deflections. Compared with moderate fibre contents ($RFC \cong 0.5$), the addition of large amounts fibres, either narrow or wide, increased the resilient movements, especially at the sleeper ends and rails, and sleeper hogging (Figure 6-10, Figure 6-11). Therefore, high fibre contents seem to reduce the overall ballast stiffness and, most importantly, the support of the sleeper ends, increasing sleeper tendency to centre-bind.

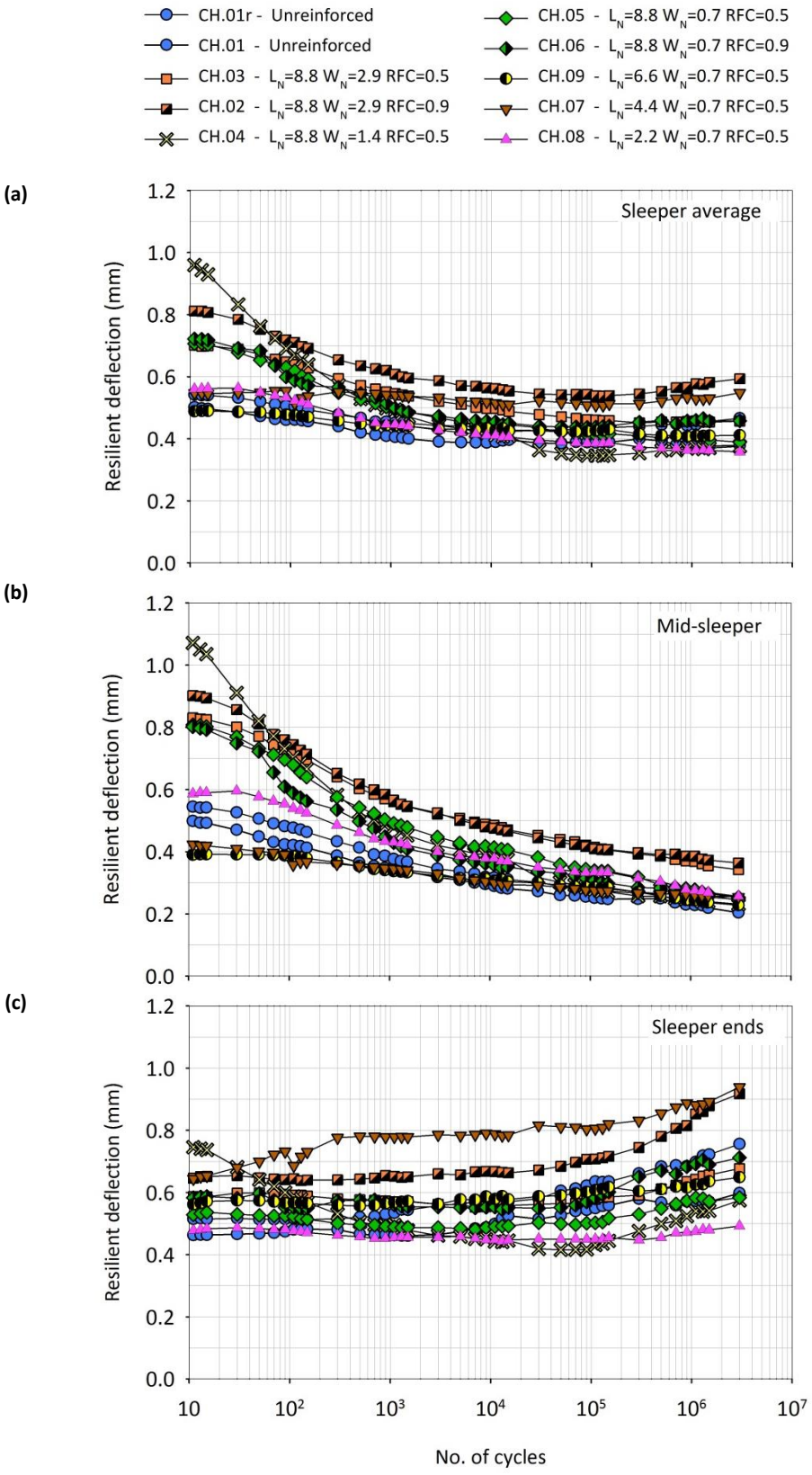

Figure 6-4. Resilient deflections vs number of cycles curves for tests using CH ballast; (a) sleeper average deflection; (b) deflections at mid-sleeper and (c) deflections of the sleeper ends

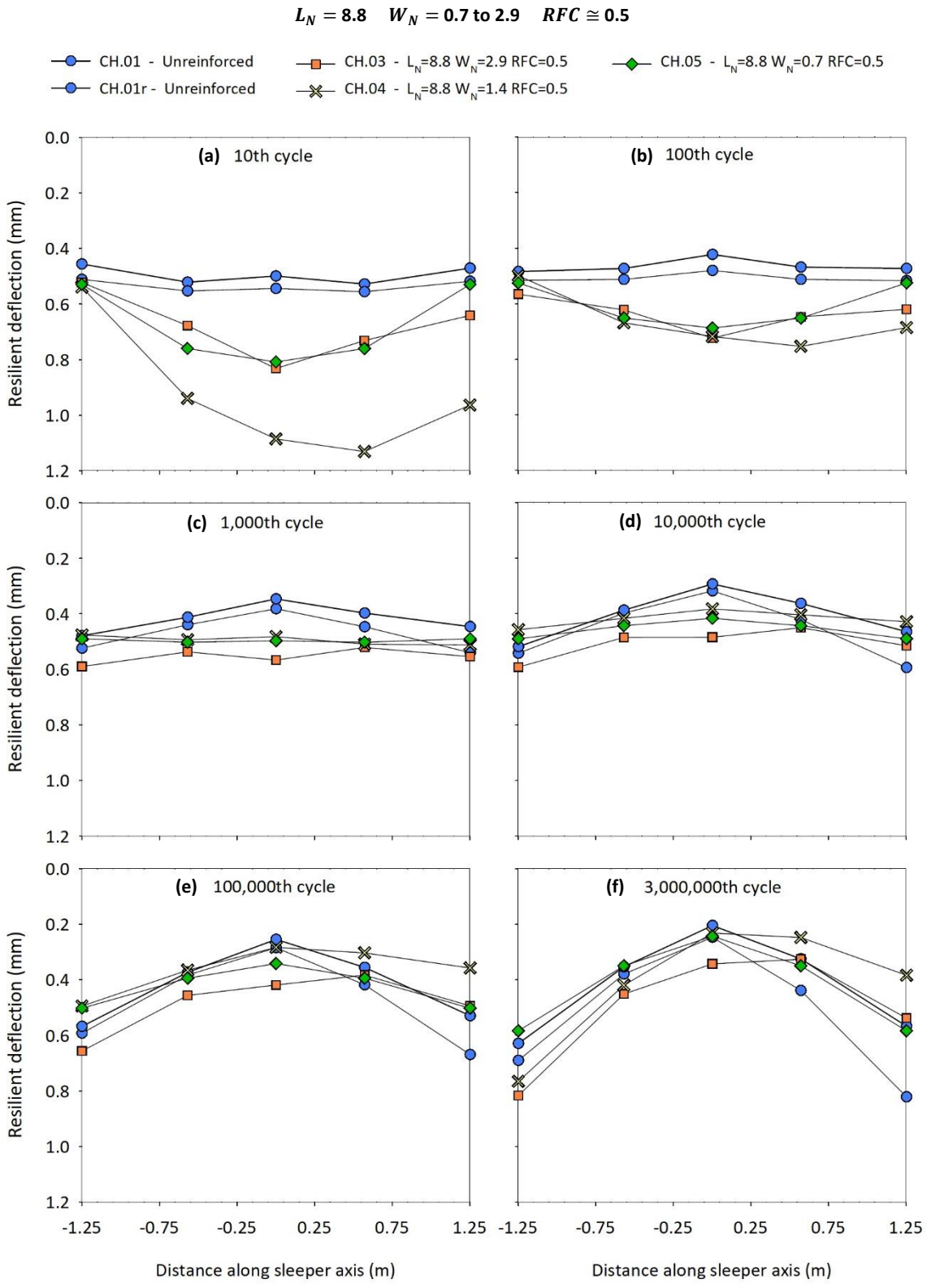

Figure 6-5. Sleeper deformed shape at key cycles; changing fibre width (tests using CH ballast)

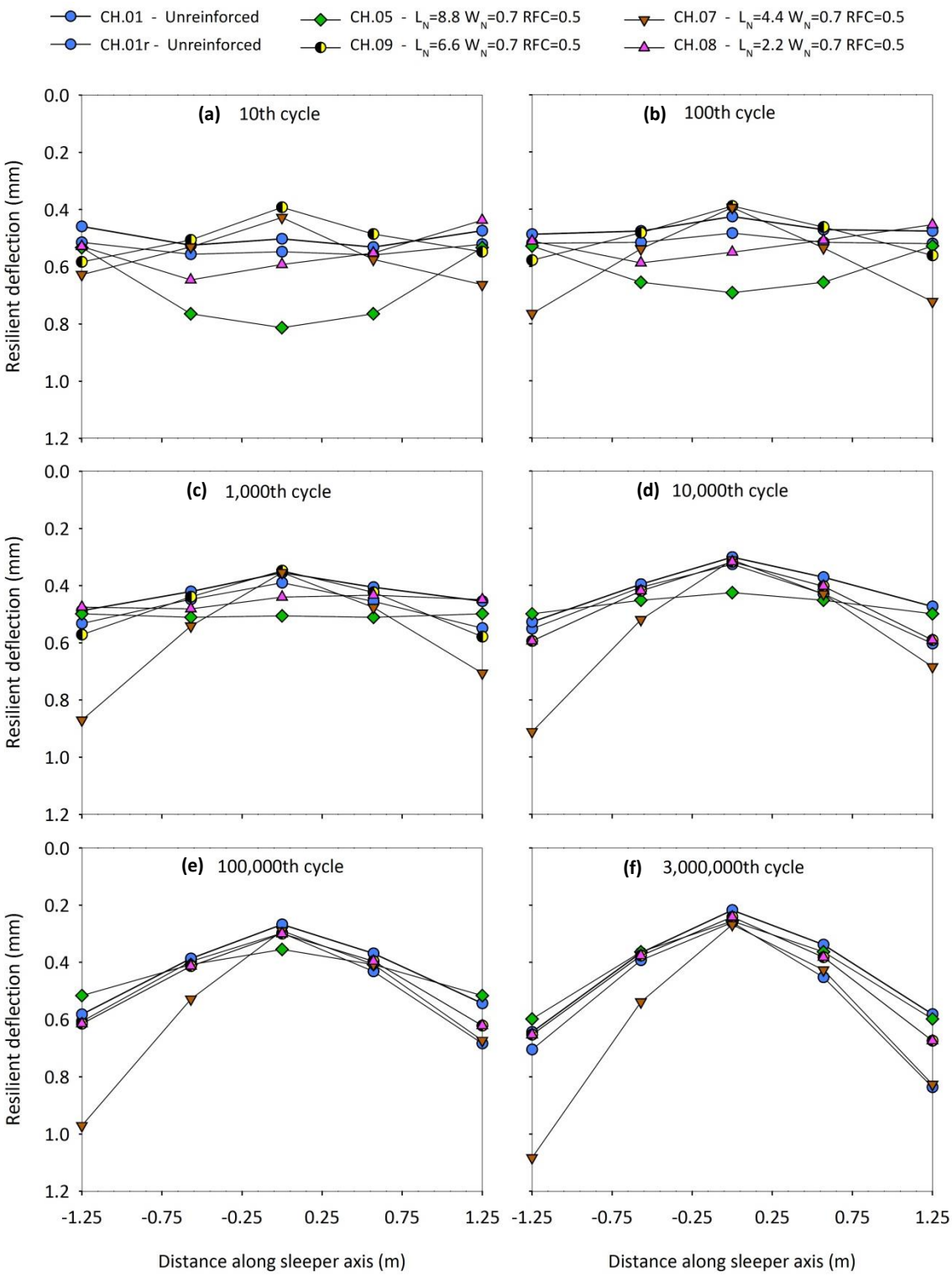

Figure 6-6. Sleeper deformed shape at key cycles; changing fibre length (tests using CH ballast)

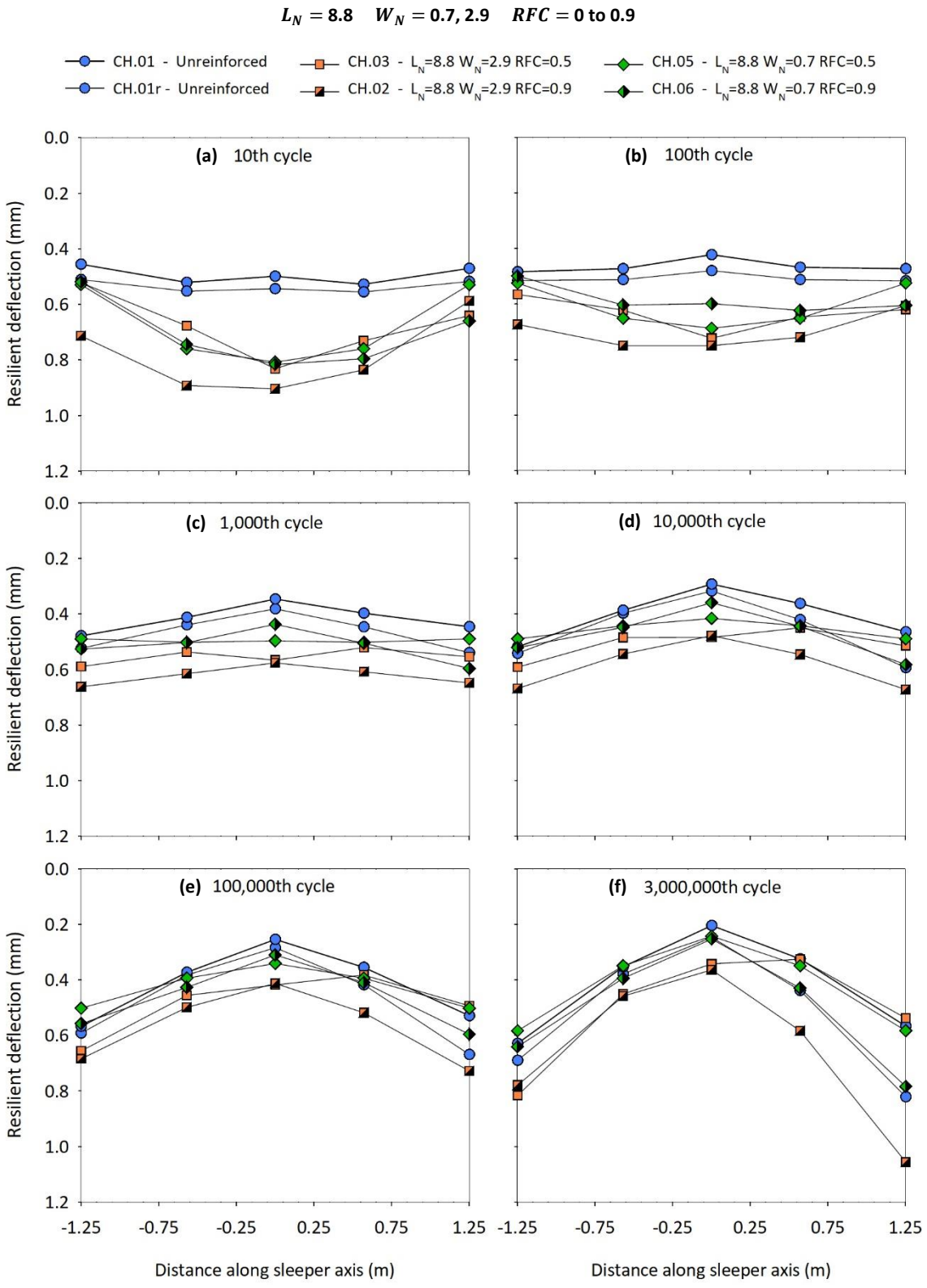

Figure 6-7. Sleeper deformed shape at key cycles; changing fibre content (tests using CH ballast)

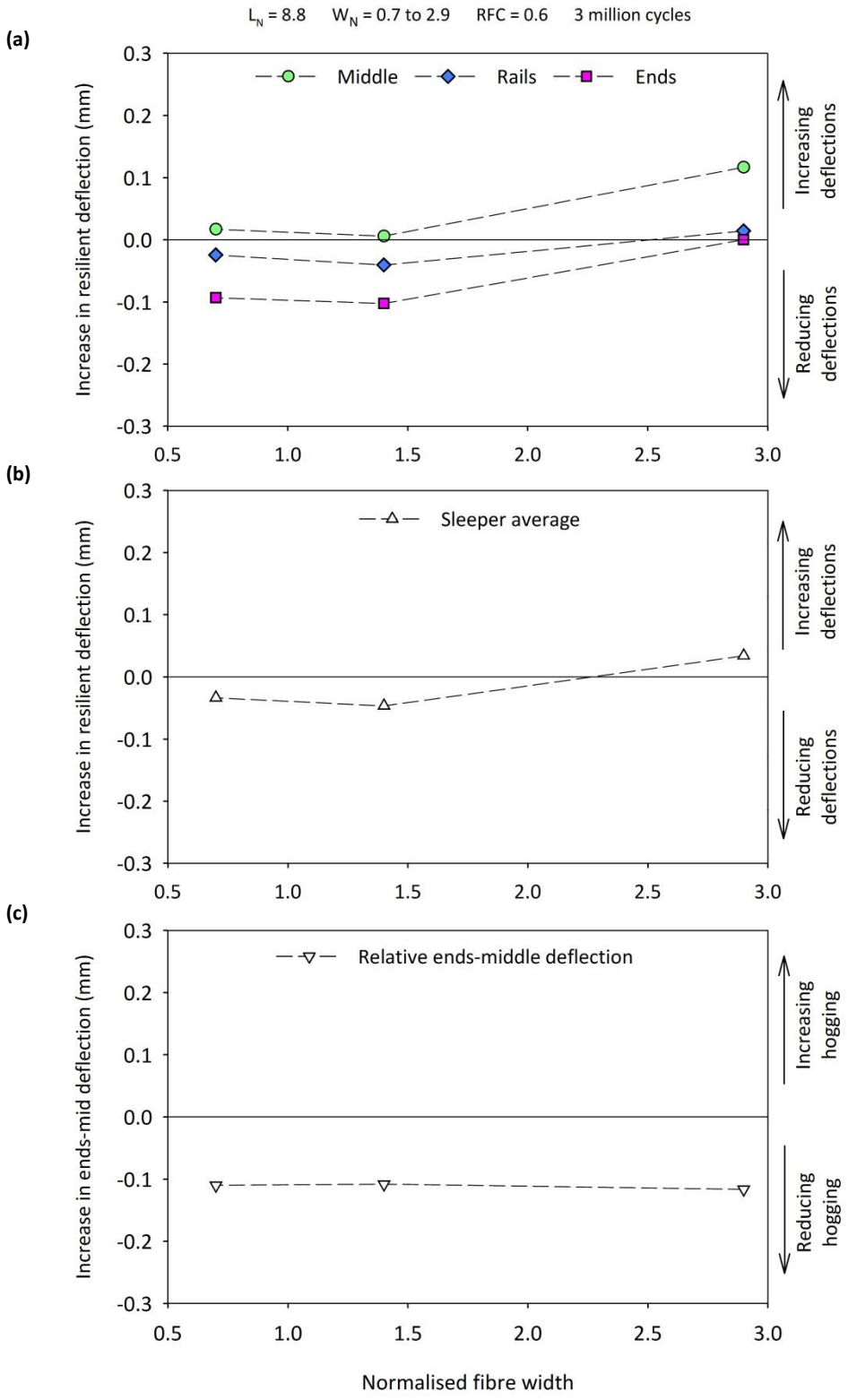

Figure 6-8. Effect of fibre width on sleeper resilient behaviour at 3 million cycles compared with the baseline; (a) middle, rails and ends; (b) sleeper average; (c) difference between ends and middle

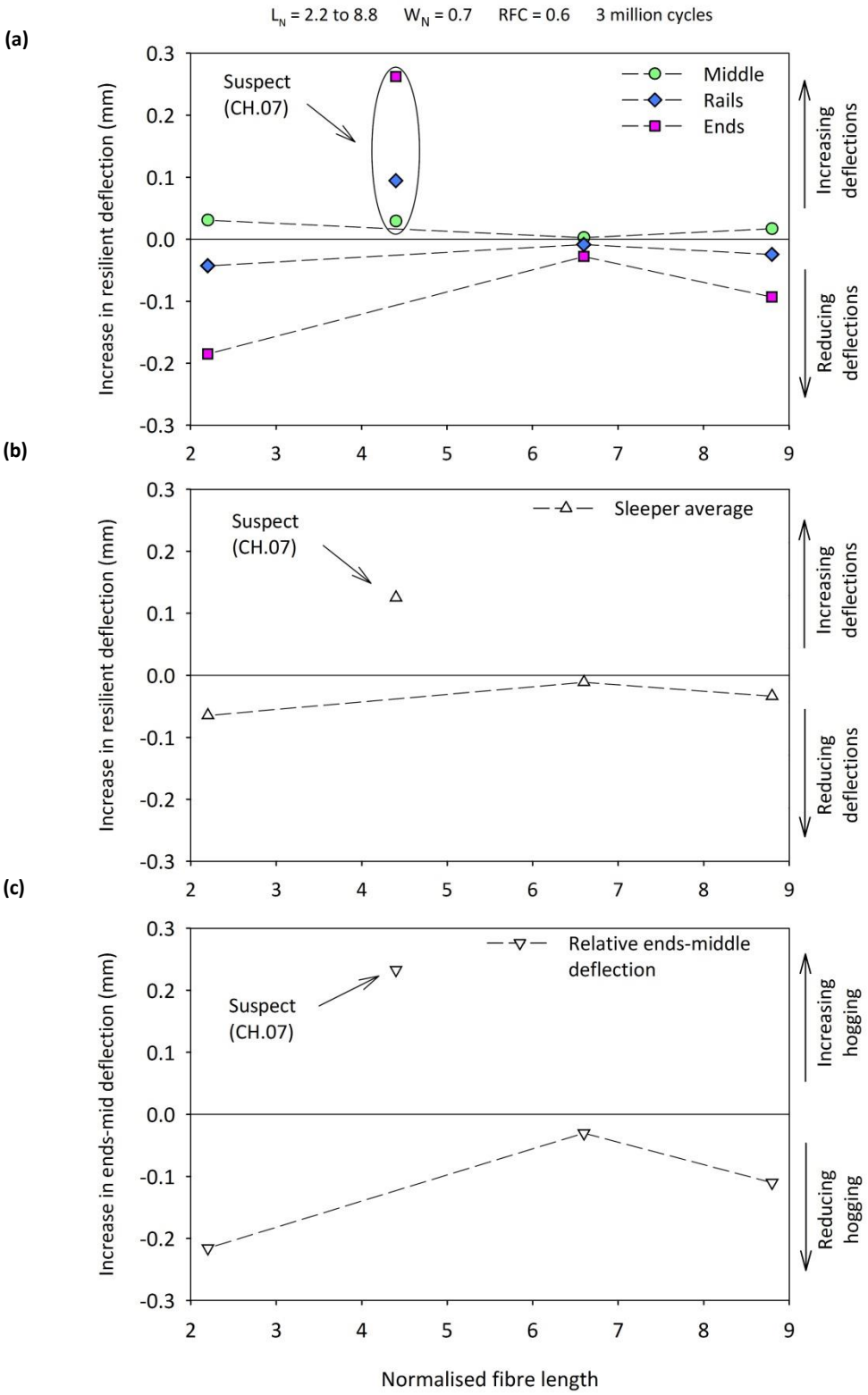

Figure 6-9. Effect of fibre length on sleeper resilient behaviour at 3 million cycles; increase in resilient deflection compared with the baseline; (a) middle, rails and ends; (b) sleeper average; (c) difference between ends and middle

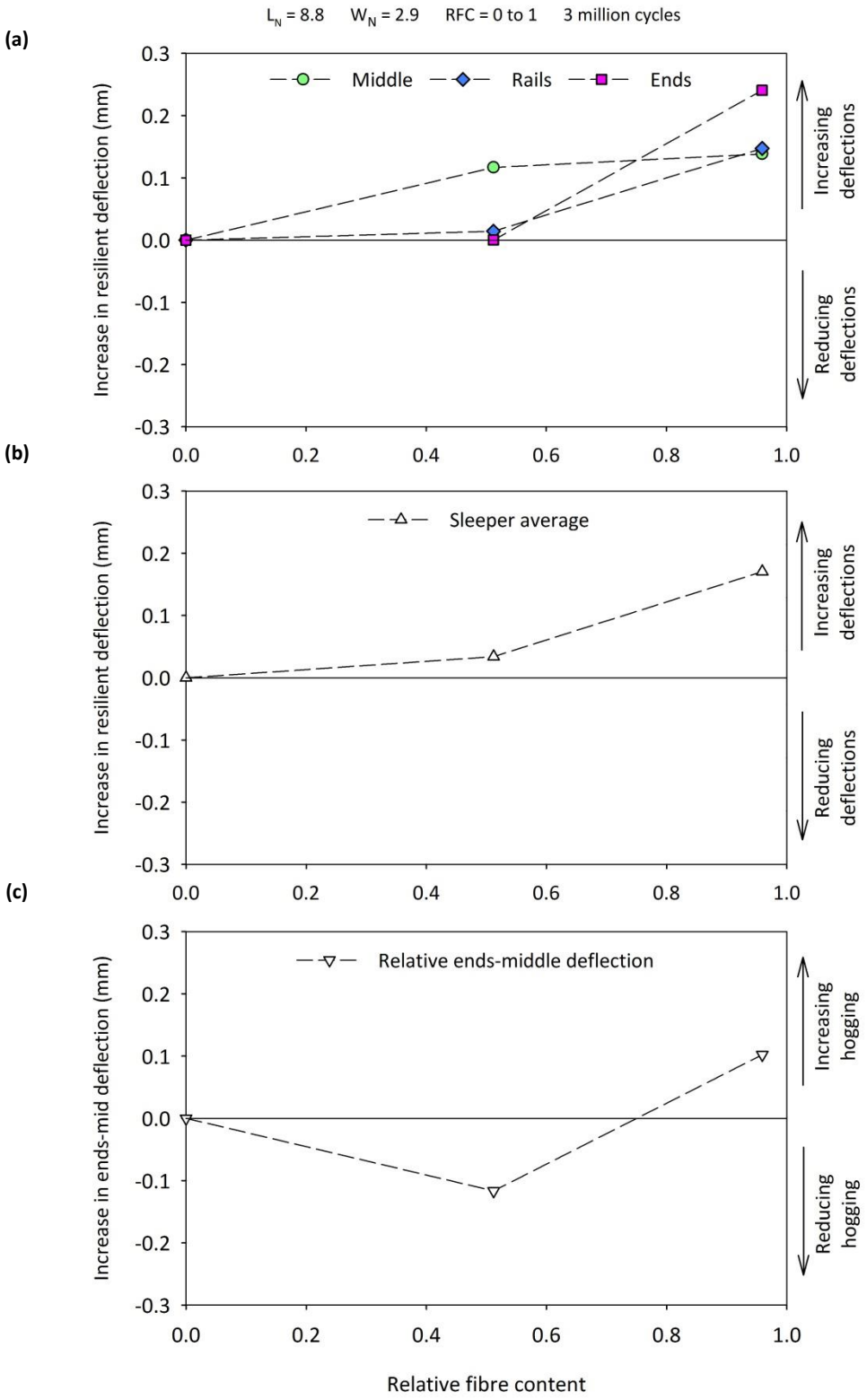

Figure 6-10. Effect of the content of wide fibres on sleeper resilient behaviour at 3 million cycles compared with the baseline; (a) middle, rails and ends; (b) sleeper average; (c) difference between ends and middle

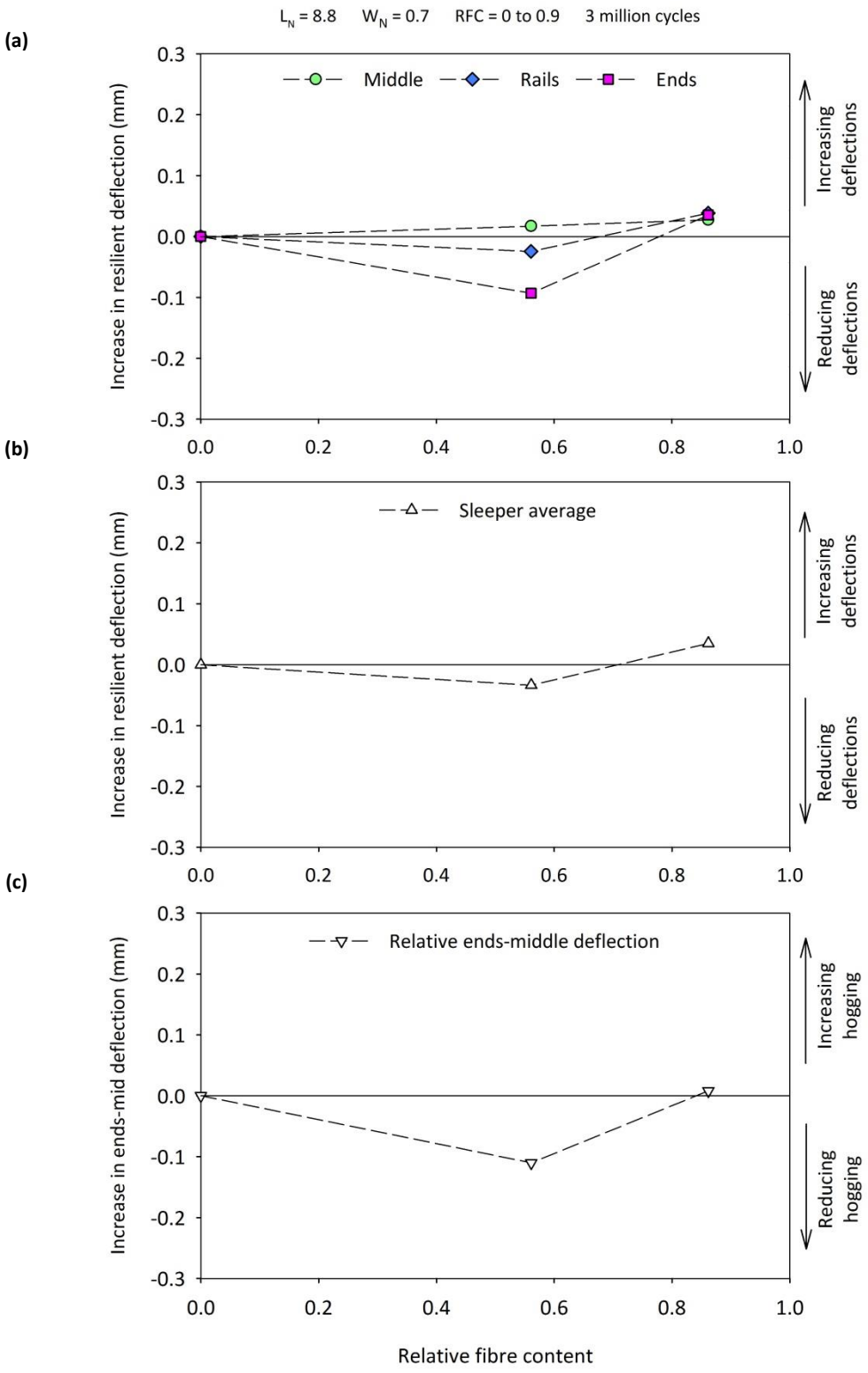

Figure 6-11. Effect of the content of narrow fibres on sleeper resilient behaviour at 3 million cycles compared with the baseline; (a) middle, rails and ends; (b) sleeper average; (c) difference between ends and middle

6.5 Ballast longitudinal pressure

The longitudinal pressure in the ballast was recorded by means of four pressure plates installed on one side of the testing rig (Section 5.5.2). Results are expressed in terms of minimum pressure in each cycle, which is representative of the longitudinal compressive stress accumulated in the ballast throughout the tests. Herein, the evolution and distribution of the pressure with the cycles, and the effect of fibre addition on it, are described.

The evolution of the average longitudinal pressure throughout the tests is shown in Figure 6-12a. In the first cycles it ranged from 5 kPa to 13 kPa, while at 3 million cycles was slightly higher, i.e. between 7 kPa and 13 kPa. Usually it increased in the first 10,000 to 100,000 cycles, after which it slowly decreased.

The longitudinal pressure under the middle of the sleeper and rails is shown in Figure 6-12b and Figure 6-12c respectively. At the beginning of the tests the pressure was typically bigger below the rails, i.e. 7-13 kPa, and smaller below the middle of the sleeper, i.e. 4-10 kPa. However, while the former decreased after the first 10,000-30,000 load cycles, the latter increased almost linearly with the logarithm of the number of cycles. At 3 million cycles the pressure was higher under the middle of the sleeper than below the rails, with the former ranging between 6 kPa and 17 kPa, and the latter between 6 kPa and 9 kPa. It can be noticed that, in general, fibres reduced the longitudinal pressure in the ballast. The effect of the reinforcement on the longitudinal pressure at 3 million cycles, which is the least affected by sample initial conditions and is representative of the long-term track performance, is shown in Figure 6-13 to Figure 6-16.

The effect of the content of wide and narrow fibres is represented in Figure 6-13 and Figure 6-14 respectively. Moderate fibre contents ($RFC \cong 0.5$) reduced significantly the pressure beneath the middle of the sleeper and lightly beneath the rails. In the middle, the effect of the fibres was strongly inhibited by the addition of higher fibre contents ($RFC \cong 0.9$). Below the rails, it was only marginally affected by the amount of reinforcement.

The fibre width had a relatively small effect on the longitudinal pressure, although wider fibres seem slightly more effective than narrow ones (Figure 6-15). However, results are scattered and must be considered carefully.

The effect of the fibre length is clearer, with the pressure reducing gradually and monotonically with the length of the inclusions (Figure 6-16). Such reduction was more pronounced below the middle of the sleeper. The lines fitting the data points suggest very short inclusions to have negligible effect on ballast longitudinal stresses.

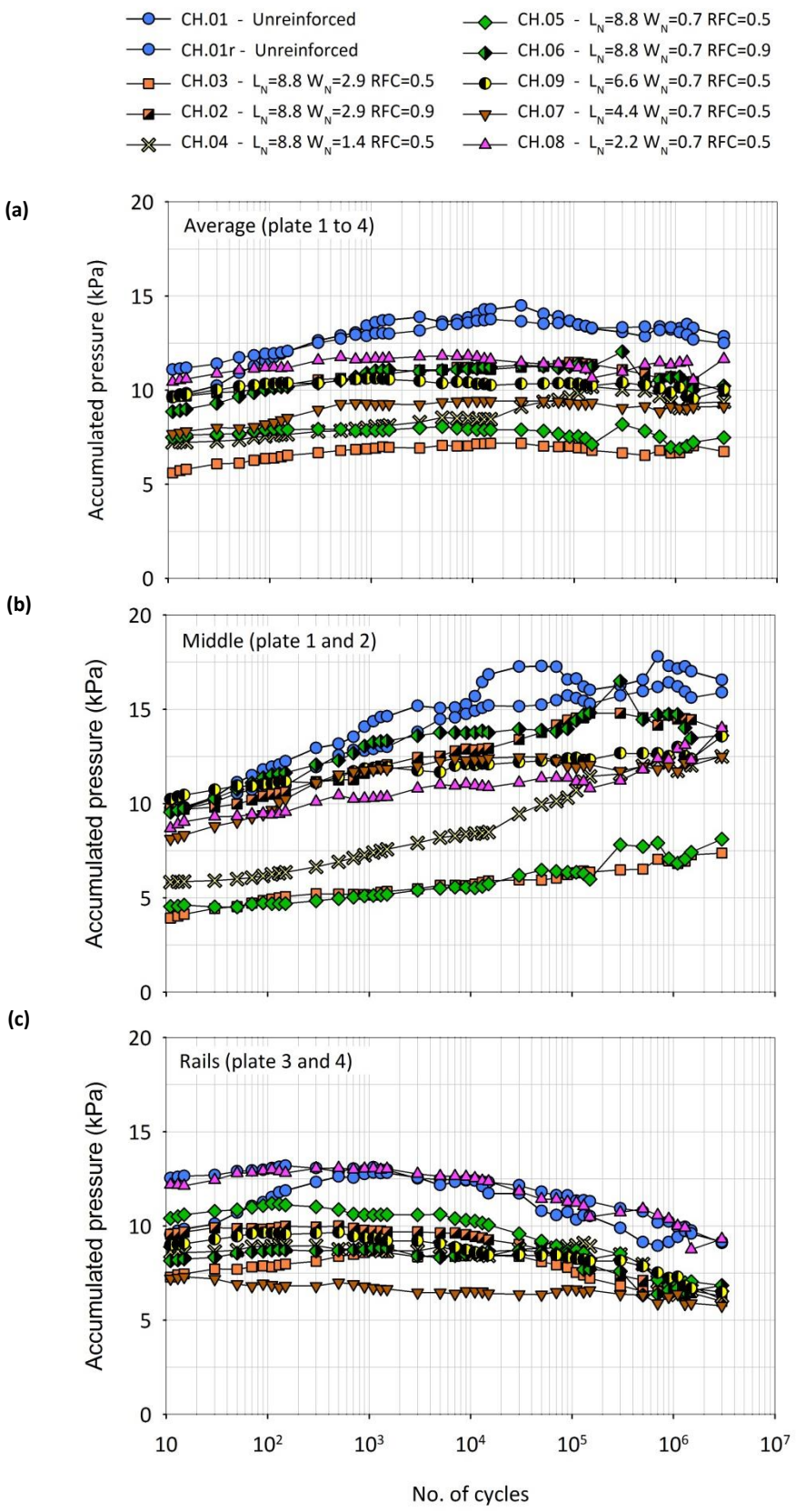

Figure 6-12. Longitudinal pressure accumulated in CH ballast vs number of load cycles; (a) average; (b) middle; (c) rails

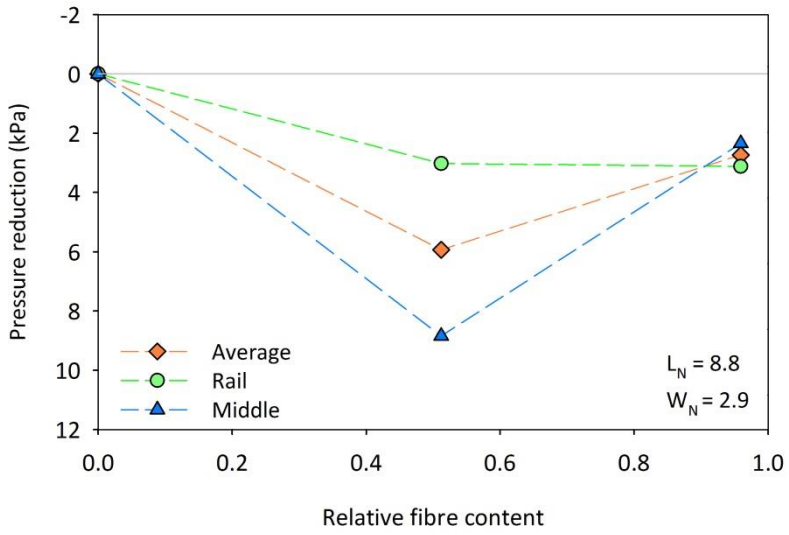

Figure 6-13. Effect of the content of wide tape-like fibres on the longitudinal pressure accumulated in CH ballast at 3 million cycles

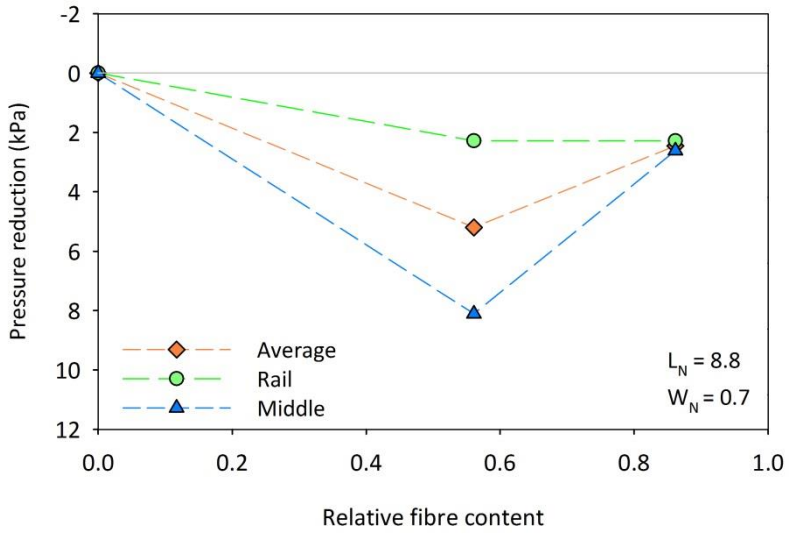

Figure 6-14. Effect the content of narrow tape-like fibres on the longitudinal pressure accumulated in CH ballast at 3 million cycles

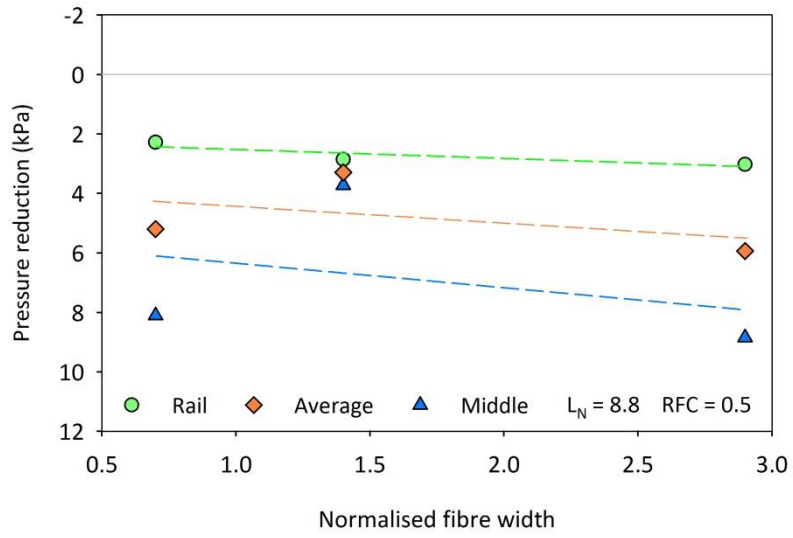

Figure 6-15. Effect of the width of tape-like fibres on CH ballast longitudinal pressure at 3 million cycles.

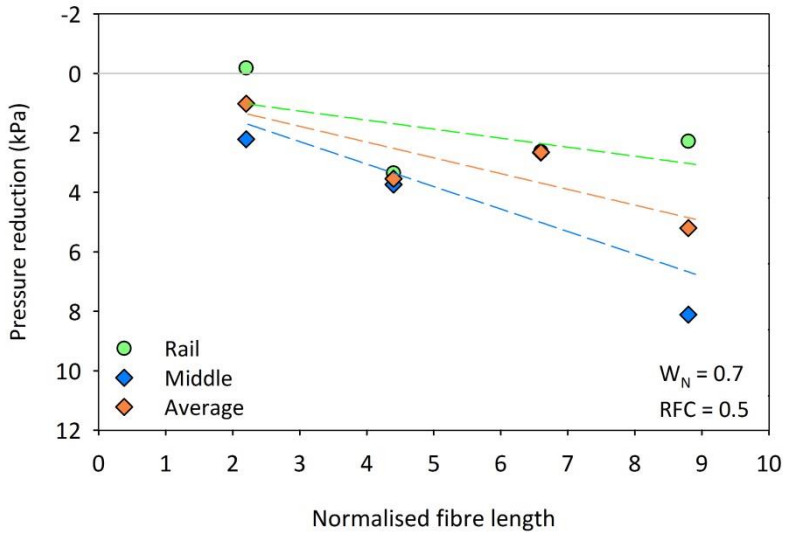

Figure 6-16. Effect of the length of tape-like fibres on CH ballast longitudinal pressure at 3 million cycles

6.6 Sleeper-ballast contact area

Pressure sensitive paper was attached to the sleeper base to assess the cumulative sleeper/ballast contact area below the rails and the middle of the sleeper (Section 5.5.4). In each location, both a low and a medium pressure paper were used, which are sensitive to pressures greater than 2.5 MPa and 10 MPa respectively. Photos of medium-pressure papers marked by the ballast particles pressing against the sleeper base are shown in Figure 6-17, for the tests with wide fibres, and Figure 6-18, for those with narrow ones.

Results are summarised in Table 6-2 in terms of contact area beneath the middle of the sleeper ($A_{c,m}$), average contact area beneath the rails ($A_{c,r}$), average contact area over the sleeper base ($A_{c,av}$), and ratio of the area at the middle to that at the rails (U_c). Pressure paper was used from test CH.02[c], hence no data are available for the baseline test, CH.01. The average contact area over the sleeper base ranged from 0.6% to 1.1% for the medium-pressure paper (i.e. pressure $\geq$ 10 MPa), and from 0.8% to 1.6% for the low-pressure one (i.e. pressure $\geq$ 2.5 MPa). At mid-sleeper the low-pressure papers showed a contact area of 0.25% to 1.2% and the medium ones of 0.2% to 0.7%. Below the rails it ranged from 0.9% to 1.7% for the low-pressure papers and 0.7% to 1.3% for the medium ones. The percentage of contact was always larger under the rails, with the ratio of the contact area at the middle to that at the rails between 0.1 and 0.8.

To highlight the influence of the fibres, results were plotted against the relative fibre content (Figure 6-21 and Figure 6-22), the normalised fibre width (Figure 6-20) and the normalised fibre length (Figure *6-19*).

As shown in Figure 6-19, the fibre length had a clear influence on the contact area, at least for moderate contents of narrow fibres ($RFC \cong 0.5$, W_N = 0.7). At mid-sleeper the contact area increased with the length of the inclusions while under the rails it reduced (Figure 6-19, a and b). As a result, longer fibres gave a more uniform contact (Figure 6-19d), although they did not affect its overall extent (Figure 6-19c). Like with the longitudinal pressure (Figure 6-16), the effect of the reinforcement was approximately linear with the length of the inclusions. As very short fibres had small effect on the longitudinal pressure, it was assumed that they also had negligible effect on the contact area. Hence, the contact area for the baseline test was estimated via linear extrapolation, as shown in Figure 6-19. Such assumption, however, is not based on strong physical evidence. Therefore, the estimated contact area for the baseline test must be considered very carefully. The data from test MS.07, which are labelled as “suspect”, were neglected, as they did not follow the trend suggested by the other data points. They might have been affected by local imperfections of the ballast bedding, e.g. the presence of higher spots, which might also have affected the resilient deflections (Section 6.4). However, they do not seem to have altered the ballast longitudinal pressure (Section 6.4) and, most importantly, the sleeper settlement (Section 6.3).

The effect of the fibre width on the contact area is highlighted in Figure 6-20. Wider fibres reduced the contact area in the middle and increased that below the rails (Figure 6-20, a and b). As the latter effect was more pronounced, they increased the extent and uniformity of the contact over the sleeper base (Figure 6-20, c and d).

The effect of the fibre content was assessed for both wide (W_N = 2.9) and narrow (W_N = 0.7) fibres (Figure 6-21, Figure 6-22). Compared with moderate fibre contents (RFC = 0.5), high ones (RFC = 0.9) increased both the area of contact at the middle of the sleeper and, to a smaller extent, at the rail seats (Figure 6-21, Figure 6-22, a and b). Hence, they were associated with greater and more uniform contact area (Figure 6-21, Figure 6-22, c and d). Assuming the estimated baseline reliable, a moderate amount of wide fibres would increase the contact area below the rails without affecting that at mid-sleeper (Figure 6-21, a and b). In contrast, narrow fibres would increase the contact area in the middle without affecting that below the rails (Figure 6-22, a and b). As a result, while wide fibres seem to increase the average contact area but not its uniformity (Figure 6-21, c and d), narrow ones might lead to a more uniform distribution of the contact without affecting its overall extent (Figure 6-22, c and d).

Table 6-2. Sleeper/CH ballast contact area measured using low and medium pressure paper

Test	Pressure > 2.5 MPa				Pressure > 10 MPa			
	$A_{c,r}$ (%)	$A_{c,m}$ (%)	$A_{c,av}$ (%)	U_c (-)	$A_{c,r}$ (%)	$A_{c,m}$ (%)	$A_{c,av}$ (%)	U_c (-)
CH.02 [c] - L_N=8.8 W_N=2.9 RFC=0.9	1.58	0.77	1.34	0.49	1.35	0.48	1.09	0.36
CH.03 [c] - L_N=8.8 W_N=2.9 RFC=0.5	1.87	0.25	1.38	0.13	1.20	0.17	0.89	0.14
CH.03 - L_N=8.8 W_N=2.9 RFC=0.5	1.65	0.40	1.28	0.24	1.14	0.28	0.88	0.24
CH.04 - L_N=8.8 W_N=1.5 RFC=0.5	1.27	0.66	1.09	0.52	1.16	0.39	0.93	0.34
CH.05 - L_N=8.8 W_N=0.7 RFC=0.5	0.94	0.49	0.80	0.52	0.75	0.44	0.65	0.58
CH.06 - L_N=8.8 W_N=0.7 RFC=0.9	1.58	1.18	1.46	0.75	1.20	0.64	1.03	0.53
CH.07 - L_N=4.4 W_N=0.7 RFC=0.5	1.67	0.71	1.38	0.42	1.27	0.57	1.06	0.45
CH.08 - L_N=2.2 W_N=0.7 RFC=0.5	0.99	0.31	0.78	0.31	0.83	0.27	0.66	0.33
CH.09 - L_N=6.6 W_N=0.7 RFC=0.5	0.98	0.39	0.80	0.40	0.85	0.37	0.71	0.44

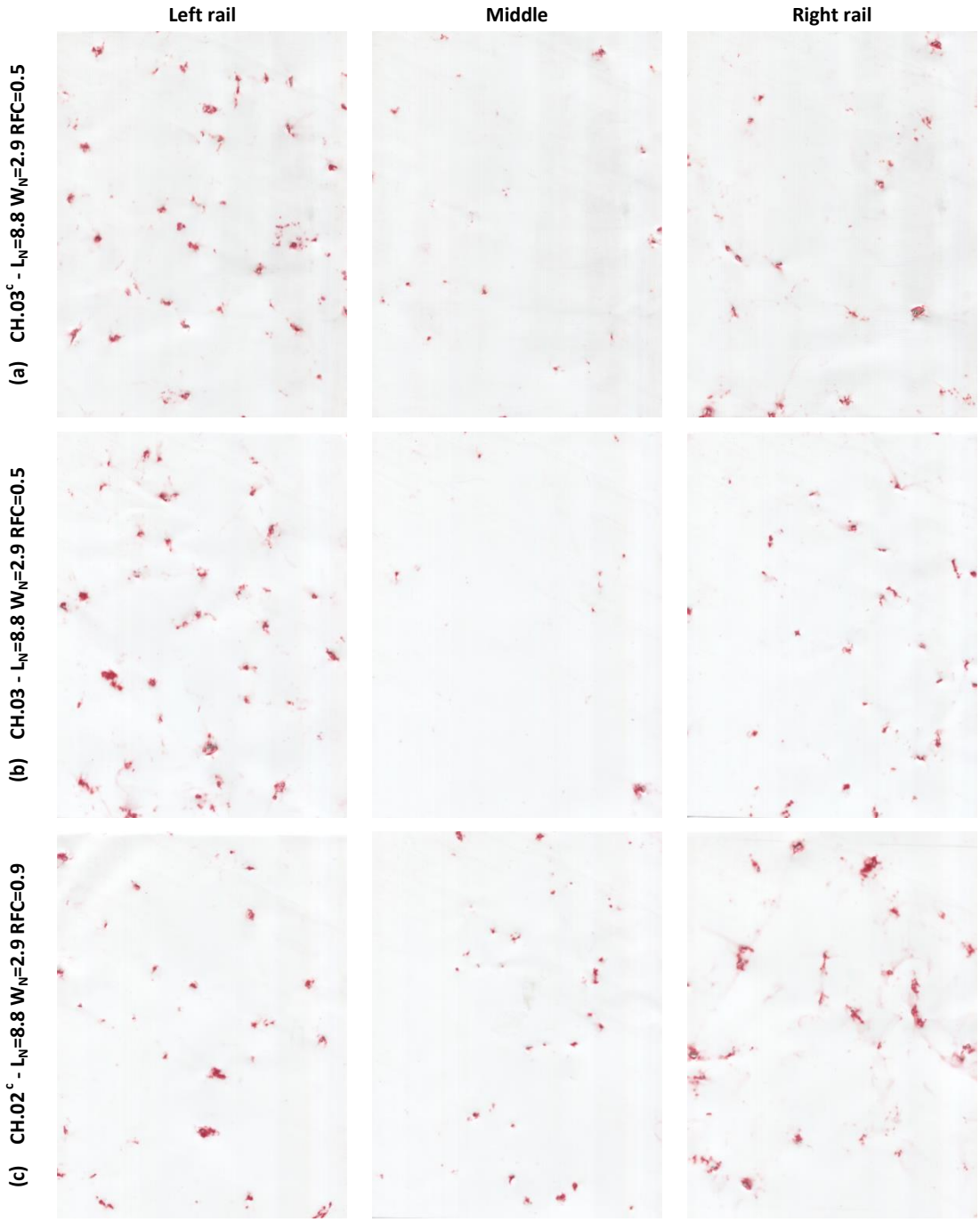

Figure 6-17. Medium pressure papers showing the sleeper/ballast contact for tests using CH ballast and long wide tape-like fibres: (a) and (b) moderate fibre content; (c) high fibre content

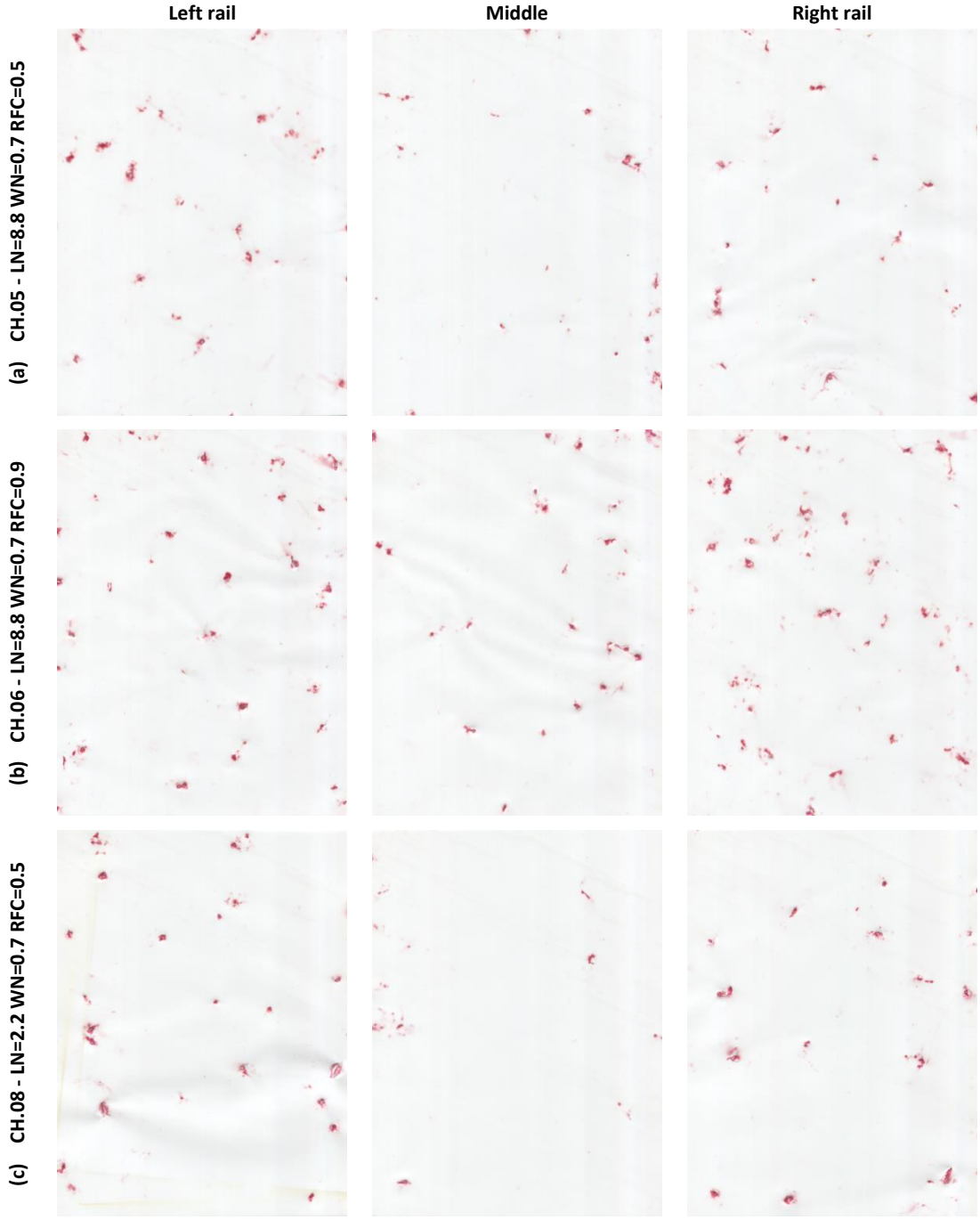

Figure 6-18. Medium pressure papers showing the sleeper/ballast contact for tests using CH ballast and narrow tape-like fibres: (a) moderate content of long fibres; (b) high content of long fibres; (c) moderate content of short fibres

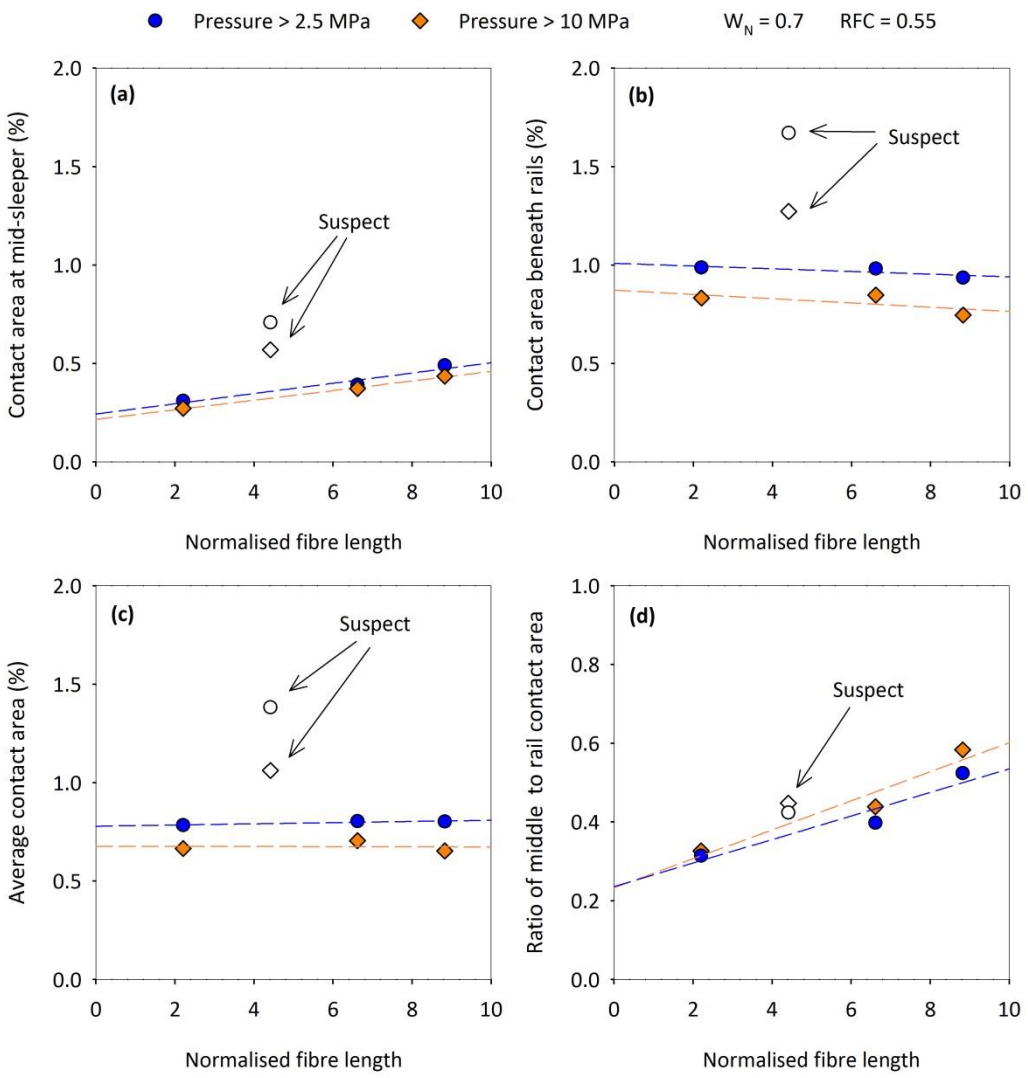

Figure 6-19. Effect of the length of tape-like fibres on the sleeper/CH ballast contact area

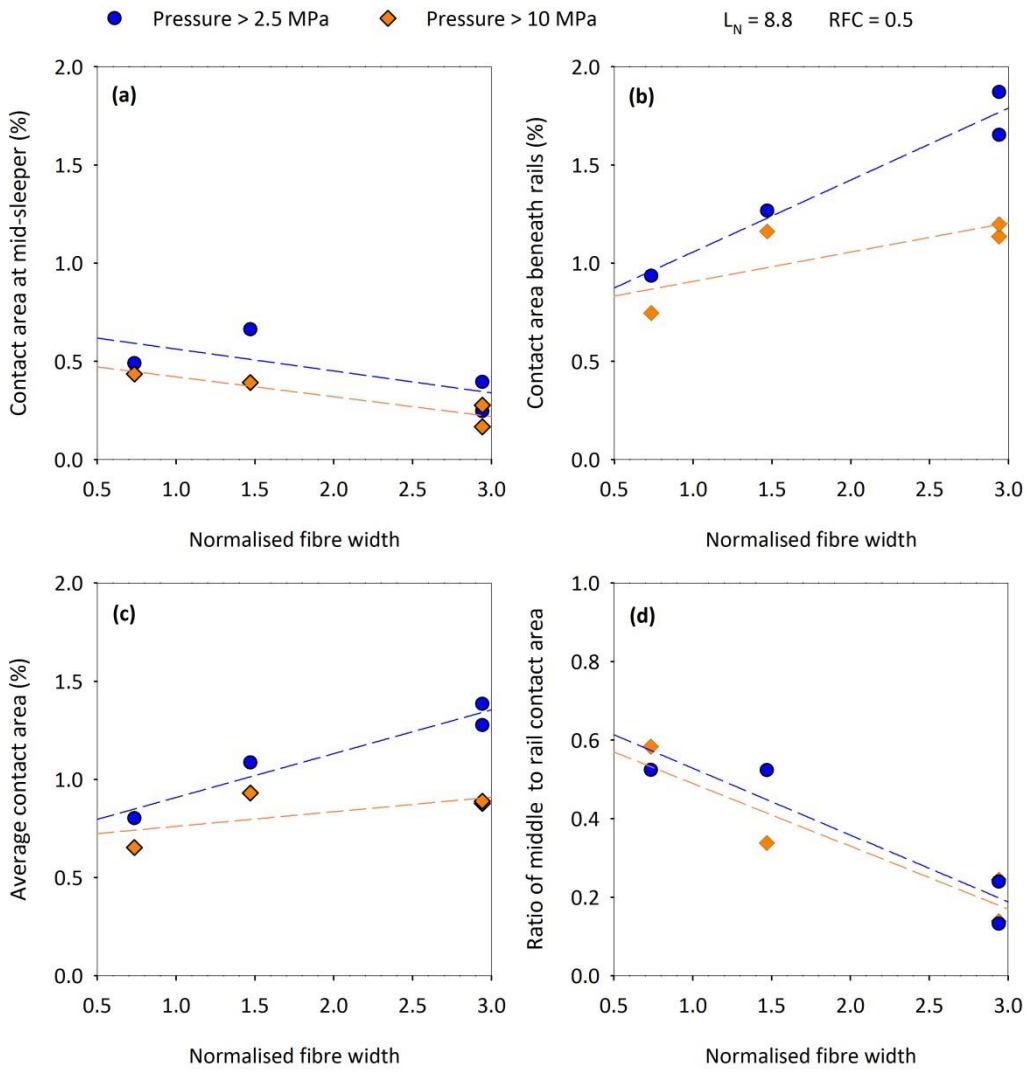

Figure 6-20. Effect of the width of tape-like fibres on the sleeper/CH ballast contact area

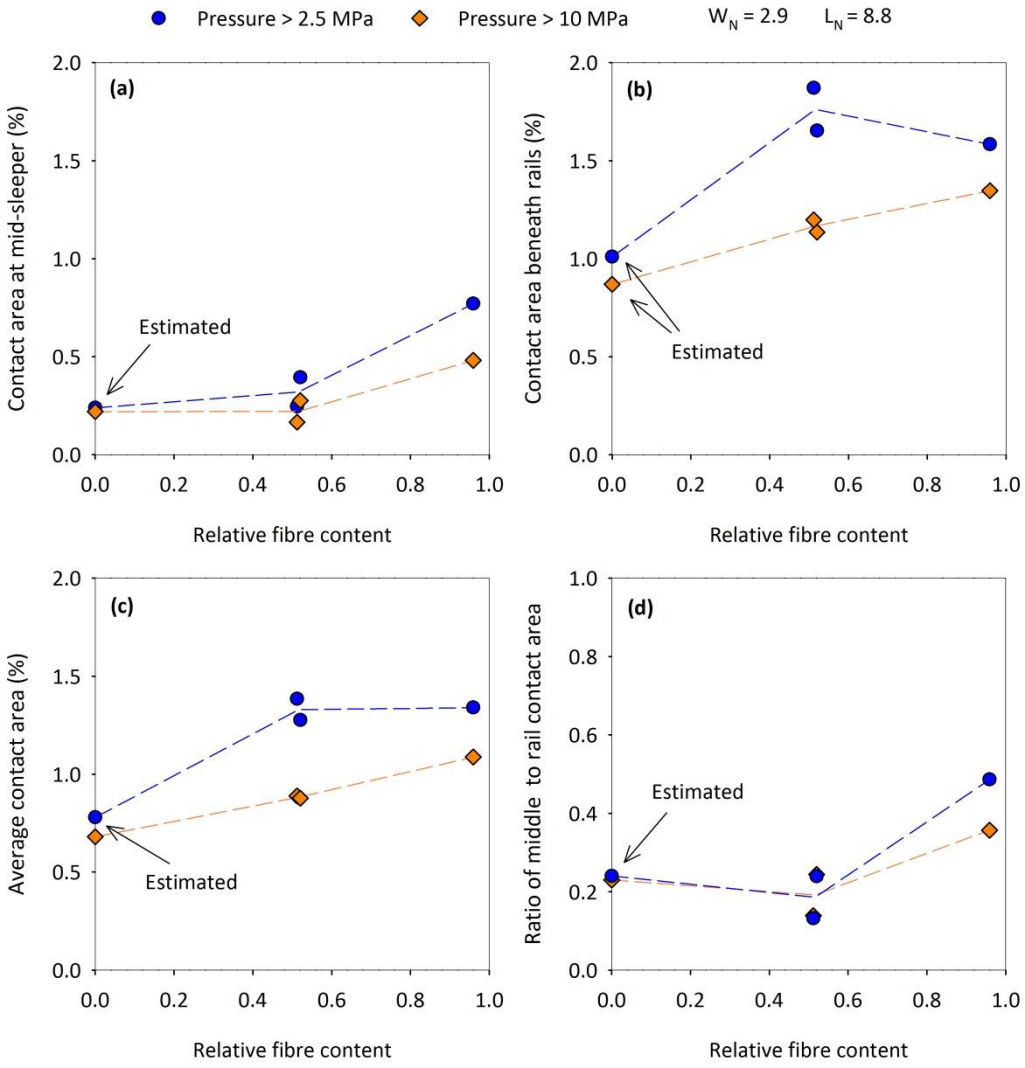

Figure 6-21. Effect of the content of wide tape-like fibres on the sleeper/CH ballast contact area

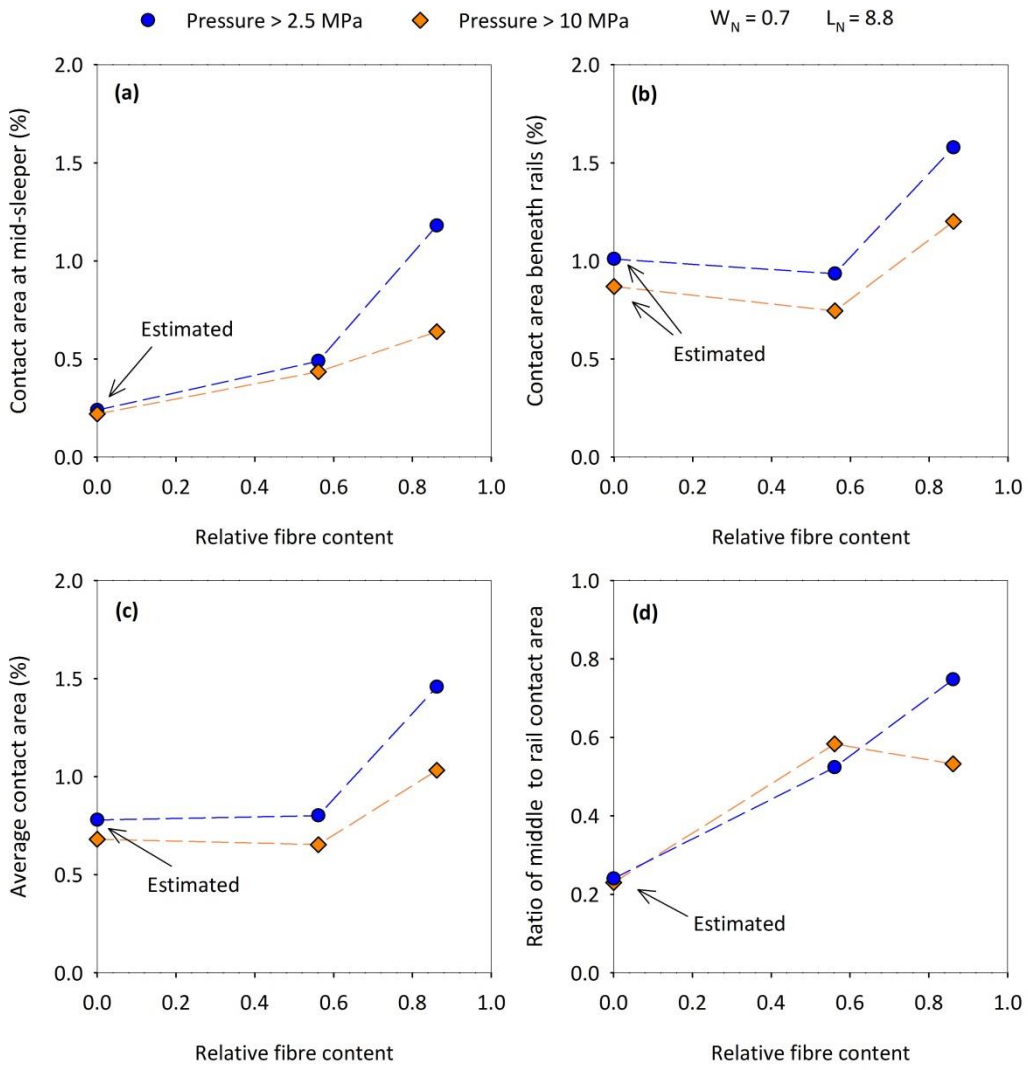

Figure 6-22. Effect of the content of narrow tape-like fibres on the sleeper/CH ballast contact area

6.7 Summary

A first series of full-size tests was carried out in the Southampton Railway Testing Facility to study the effect of the addition of thin tape-like fibres on CH ballast behaviour under cyclic loading. The fibre dimensions and content were varied throughout the tests and results are expressed in function of the normalised fibre length (L_N), normalised fibre width (W_N) and relative fibre content (RFC). The test outputs are the sleeper settlement and resilient deflections, the longitudinal pressure accumulated in the ballast and the contact area at the sleeper ballast interface. The latter was not assessed for the baseline test.

Three levels of fibre content were tested: none (baseline, RFC = 0), moderate (RFC = 0.5-0.6), and high (RFC = 0.9-1). The normalised fibre width was varied from 0.7 to 2.9, the length from 2.2 to 8.8. The latter was arbitrarily limited to 300 mm, which is the depth of the ballast bed.

The main characteristics of track behaviour can be summarised as follows:

- The settlement increased approximately linearly with the logarithm of the load cycles. Unreinforced ballast exhibited a total settlement of about 11 mm, of which 7.1 mm beyond the first cycle and 6.3 mm beyond the first 10 cycles. The addition of properly selected fibres reduced the settlement developed from the 10^{th} cycle to 4.9 mm.

- Except for the first cycles, the sleeper showed hogging, which became more pronounced throughout the tests, as the resilient movements reduced in the middle and increased at the sleeper ends. The resilient deflections of the middle of the sleeper were between 0.4 mm and 1.1 mm in the first cycles and between 0.2 mm and 0.4 mm at 3 million cycles. The range of movement of the sleeper ends was stable in the first 30,000-100,000 cycles, beyond which it usually increased slightly. In the first cycles it ranged from 0.5 mm to 0.7 mm, in the long term from 0.5 mm to 0.9 mm. Near the rails, the deflections were similar to those exhibited by the middle of the sleeper, although their reduction with the number of cycles was slightly less pronounced.

- The average longitudinal pressure in the ballast was relatively small, i.e. less than 18 kPa. In the first cycles, it was higher below the rails, i.e. 7-13 kPa, and lower under the middle of the sleeper, i.e. 4-10 kPa. The former was stable in the first 10,000-30,000 cycles, beyond which it reduced quite rapidly to the end of the tests. At 3 million cycles it ranged between 6 kPa and 9 kPa. In contrast, below the middle of the sleeper the pressure increased almost linearly with the logarithm of the load cycles. At the end of the tests it ranged from 6 kPa to 17 kPa. The addition of fibres reduced the longitudinal pressure, especially below the middle of the sleeper.

- The area of contact between the sleeper and the ballast was always less than 1.5%. In each test, it was smaller in the middle than beneath the rails, with the ratio of the former to the latter ranging between 0.2 and 0.8. The effect of the reinforcement on the contact area depends on the characteristics of the inclusions. The addition of moderate contents of narrow fibres was associated with a reduction of the contact area below the rails and an increase of that beneath the middle of the sleeper.

Tests showed that the addition of properly selected tape-like fibres can improve track performance, as it reduced the sleeper settlement and tendency to centre-bind. Moreover, it affected the longitudinal pressure in the ballast and the sleeper/ballast contact area. The effect of the reinforcement was strongly affected by the fibre dimensions and content:

- The fibre width had significant effect on ballast mechanical behaviour. Narrow fibres ($W_N \leq 1.5$) reduced the settlement developed after the very first cycles by over 20% while wide ones increased it. Sleeper hogging was inhibited using narrow inclusions, as they reduced the movements of the rails and sleeper ends while increased marginally those in the middle. Wide fibres reduced the hogging but increased significantly the middle deflections and the overall sleeper resilient movements. The fibre width does not seem to affect ballast longitudinal pressure. Larger fibres, compared with narrow ones, increased the sleeper/ballast contact area below the rails.

- High fibre contents, compared with moderate ones, increased the permanent and resilient deflections. Moreover, they exacerbated the sleeper hogging, as they increased

the resilient movements of the sleeper ends compared with those of the middle. The fibre content affected the longitudinal pressure in the ballast at 3 million cycles. Moderate contents reduced significantly the pressure under the middle of the sleeper and, to a much smaller extent, below the rails. High contents produced a far smaller reduction of the pressure below the middle. The sleeper/ballast contact was also affected by the fibre content, with high amounts of reinforcement increasing the contact area, especially under the rails.

- The fibre length had a relatively small effect on the sleeper movements. Very short inclusions were only 4% less effective than long ones at inhibiting the settlement; the resilient deflections were only marginally affected by the fibre length, although results are not clear. In contrast, the length affected the ballast longitudinal pressure and the sleeper/ballast contact area. The former reduced gradually with the length, with very short fibres having a negligible effect. The contact area under the middle of the sleeper increased with the length, while that below the rails reduced. Therefore, although the overall contact area was not affected the fibre length, longer inclusions increased its uniformity over the sleeper base. Interestingly, the effect of the fibres on the longitudinal pressure and on the sleeper/ballast contact increased roughly linearly with the length of the inclusions.

7 TEST RESULTS 2 of 2 – MOUNT SORREL BALLAST

7.1 Introduction

This chapter describes the second series of full-size tests carried out to assess the potential of a different type of fibre to improve ballast mechanical response to cyclic loading. These tests also provided a deeper understanding of the general behaviour of ballasted track, as the test set-up was enhanced: lateral plates were used to monitor ballast spreading and selected particles within the ballast bed to assess particle degradation.

Filament-like fibres and MS ballast were used in these tests. Tape-like fibres optimised from the first batch of tests, were also used for comparison.

The first part of this chapter presents the tests using MS ballast and different fibres. Then, test results are described in terms of sleeper settlement and resilient deflections, longitudinal stresses in the ballast, sleeper/ballast contact area, ballast spreading and particle degradation. Finally, the main characteristics of the behaviour of unreinforced and reinforced ballasted track are summarised.

7.2 List of tests

The tests described in this section and their main characteristics are summarised in chronological order of execution in Table 7-1.

In the first tests (MS.01, MS.01^r, MS.02) three lateral plates were installed in each shoulder (Figure 7-1a) to monitor lateral spreading. However, after test MS.02 showed that the addition of tape-like fibres had only a marginal effect on MS ballast mechanical response, no lateral plates were used in test MS.03 to check if they had affected test results. It was found that they had an effect, although small, on the behaviour of the samples, as will be clearer in Section 7.7. Therefore, they were modified to reduce their influence on shoulder ballast. In test MS.04 only one plate was installed in each shoulder (Figure 7-1b) and in test MS.05 they were placed further from the sleeper ends (Figure 7-1c). Nevertheless, they still affected sample behaviour. Therefore, from test MS.06, they were not used to avoid any disturbance to the ballast.

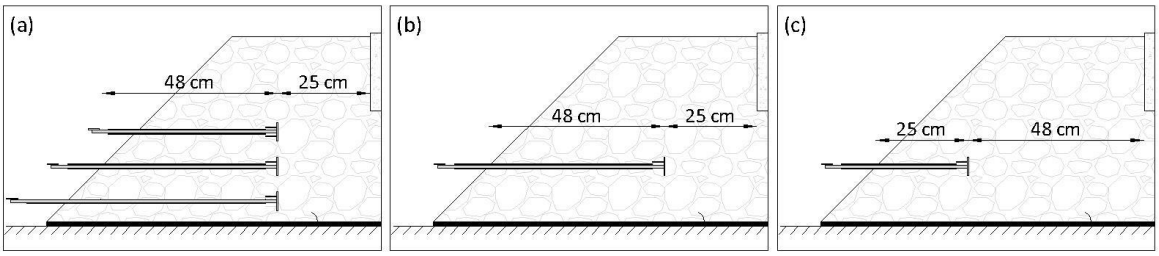

Figure 7-1. Arrangement of the settlement plates; (a) test MS.01, MS.01r and MS.02; (b) MS.04; (c) MS.05

The effect of the addition of filament-like fibres to ballast was investigated through four tests, MS.07 to MS.10. These were compared with tests MS.03 and MS.06, in which unreinforced ballast and ballast reinforced with tape-like fibres were used respectively. The tape-like fibres were

selected according to the results of the first part of the testing programme, i.e. W_N of 0.7 to 1.5 and RFC of 0.5 to 0.6. The filament-like fibres were varied in diameter and content. The diameters tested are 6 mm (d_N = 0.15) and 10 mm (d_N = 0.24), representative of thin and thick inclusions. Relatively small fibre contents were used, i.e. RFC of 0.3 and 0.6, to limit the overall volume of reinforcement. The effect of the fibre length was not investigated, as the tests using CH ballast showed it to be relatively small. In the last test (MS.10) fibres were placed only in the shoulders (Figure 7-2) to obtain a better understanding of the mechanics of fibre reinforced ballasted track.

Table 7-1. List of tests using Mount Sorrel ballast

No	Label	Fibre type	L_f (mm)	W_f or d_f (mm)	N_{fp} (%)	L_N (-)	W_N or d_N (-)	RFC (-)
12	MS.01 - Unreinforced[3p,1M]	None	-	-	0.0	-	-	0.00
13	MS.01[r] - Unreinforced[3p]	None	-	-	0.0	-	-	0.00
14	MS.02 - W_N=0.8 RFC=0.6[3p]	Tape	300	33	5.3	7.32	0.80	0.60
15	MS.03 - Unreinforced	None	-	-	0.0	-	-	0.00
16	MS.04 - Unreinforced[1p]	None	-	-	0.0	-	-	0.00
17	MS.05 - Unreinforced[1sp,2M]	None	-	-	0.0	-	-	0.00
18	MS.06 - W_N=0.8 RFC=0.8	Tape	300	33	5.3	7.32	0.80	0.59
19	MS.07 - d_N=0.15 RFC=0.3	Filament	300	6	6.0	7.32	0.15	0.33
20	MS.08 - d_N=0.24 RFC=0.3	Filament	300	10	6.0	7.32	0.24	0.33
21	MS.09 - d_N=0.15 RFC=0.6	Filament	300	6	10.8	7.32	0.15	0.60
22	MS.10 - d_N=0.15 RFC=0.6[S]	Filament	300	6	10.8	7.32	0.15	0.60

[1M] interrupted after 1 million cycles due to technical issues; [2M] interrupted after 2 million cycles; [3p] three lateral plates per shoulder (Figure 7-1a); [1p] one lateral plate per shoulder (Figure 7-1b); [1sp] one shallow lateral plate per shoulder (Figure 7-1c); [S] fibres only in the shoulders (Figure 7-2)

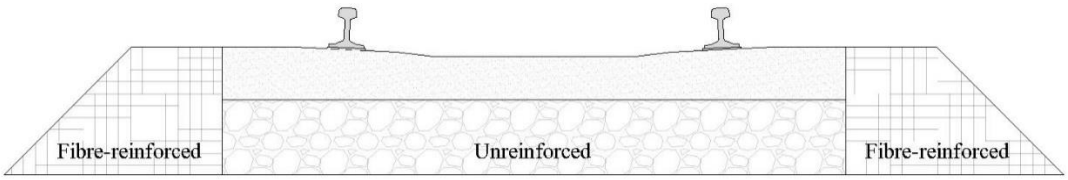

Figure 7-2. Distribution of the reinforcement in test MS.10

7.3 Settlement

The settlement is expressed in terms of average sleeper permanent deflection (Section 6.3) and was re-zeroed after a small number of cycles, e.g. 1 or 10, to minimise the effects of bedding variability (Section 5.6). However, for the tests using MS ballast, the results obtained by considering all cycles (Figure 7-3a) are consistent with those resulting from re-zeroing the settlement after the first cycles (Figure 7-3, b and c). This is particularly clear from Figure 7-4 and

Figure 7-5, which show the effect of fibre content and thickness on the normalised settlement at 3 million cycles when all cycles are considered and when the first cycles are neglected. This might be explained by a greater experience in test preparation, e.g. ballast levelling, which allowed for a smaller variability of initial sample condition. Nevertheless, it is preferable to re-zero the settlement after at least the first cycle to minimise experimental variation.

The evolution of settlement with cycles is shown in Figure 7-3. Like CH ballast, MS ballast settled approximately linearly with the logarithm of the number of cycles. However, while CH ballast accumulated a settlement of ~6.5 mm after the first cycle (Figure 6-1a), MS ballast settled by only ~4.5 mm (Figure 7-3b). The addition of tape-like fibres did not influence the settlement of MS ballast, while the filament-like fibres reduced it by up to ~1.5 mm if all cycles are considered (Figure 7-3a), and ~1 mm if the first cycle is neglected (Figure 7-3b). This seems explained by the fact that the tape-like fibres required an initial settlement to become effective, greater than that exhibited by MS ballast (Section 8.4). The extent of the improvement was affected by the characteristics of the fibres. Thick fibres (d_N = 0.24) were slightly counterproductive while thin ones (d_N = 0.14) reduced the permanent deformation. The addition of a small quantity of fibres (RFC = 0.3) was less effective than a moderate one (RFC = 0.6). Interestingly, placing the fibres only in the shoulders gave a significant settlement reduction (test MS.10).

The effect of fibre characteristics on the settlement is clearer from Figure 7-4 and Figure 7-5, where the normalised settlement at 3 million cycles is plotted against the normalised fibre diameter and relative fibre content.

The addition of a small quantity of fibres (RFC = 0.3) either reduced or slightly increased the settlement, depending on their diameter (Figure 7-4). Thin fibres (d_N = 0.15) reduced the settlement by 8%, if the first cycles are neglected, and 14% otherwise. Thick fibres (d_N = 0.24) were essentially ineffective. They reduced the total settlement by 2% and increased that accumulated after the first cycles by 3%.

The ability of the reinforcement to reduce ballast settlement increased approximately linearly with the fibre content, at least for d_N = 0.15 (Figure 7-5). The settlement accumulated after the first cycle reduced by only 8% for RFC = 0.3, and by 20% for RFC = 0.6. As already observed, the improvements are greater if all cycles are considered, with a settlement reduction of 14% and 26% for small and moderate fibre content respectively.

The addition of a moderate quantity of thin fibres (RFC = 0.6, d_N = 0.15) to the shoulders gave a smaller, but still significant, improvement. It reduced the settlement by ~15%, regardless of whether the first cycles are considered or not (Figure 7-5). This implies that, if the first few cycles are neglected, removing the fibres from the ballast beneath the sleeper would bring the settlement reduction from 20% to 15%. If all cycles are considered, it would reduce it from 26% to 15%. Therefore, the fibres beneath the sleeper might be more effective in the first loading cycles, with those in the shoulder giving a greater contribution in the longer term.

As already observed, the addition of narrow tape-like fibres did not affect the settlement response. However, a small reduction, i.e. 5%, of the sleeper permanent movement was observed after 300,000 cycles in test MS.02, in which the settlement was increased by the presence of

three lateral plates in each shoulder, as shown in Section 7.7, Figure 7-15b. This agrees with the results of the first series of tests, as discussed in Section 8.4.

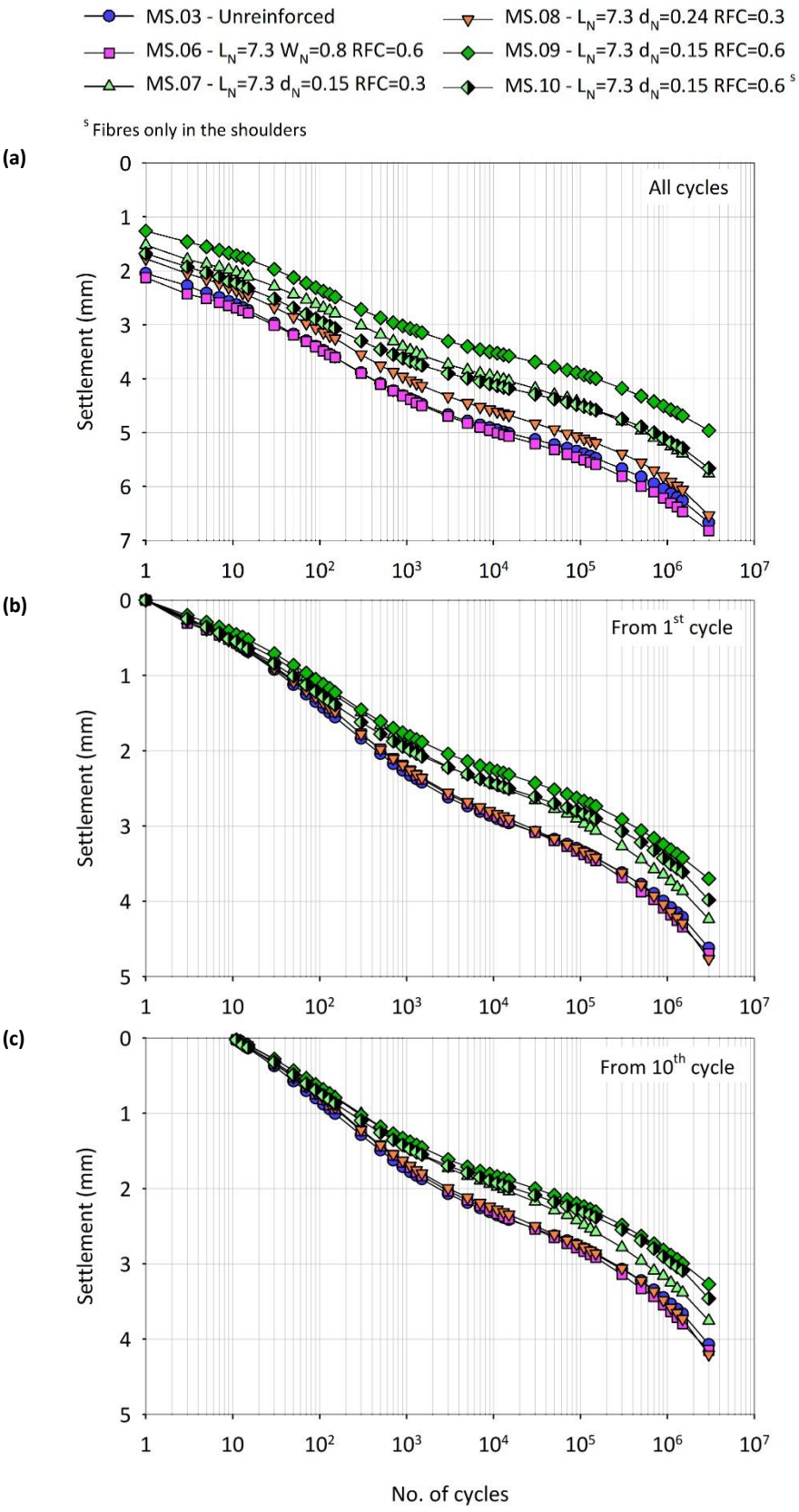

Figure 7-3. Settlement response of MS ballast reinforced with filament-like fibres; (a) all cycles; (b) settlement re-zeroed after 1 cycle and (c) after 10 cycles

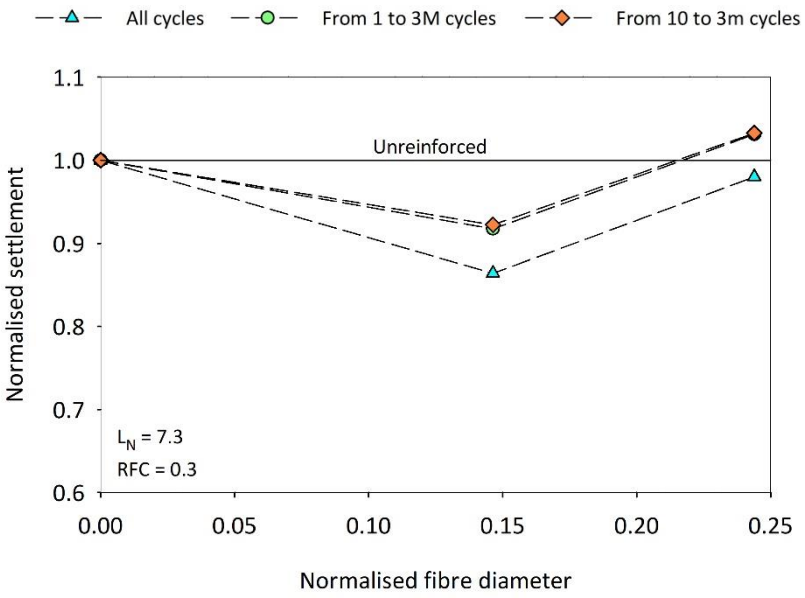

Figure 7-4. Effect of the diameter of filament-like fibres on MS ballast settlement at 3 million cycles

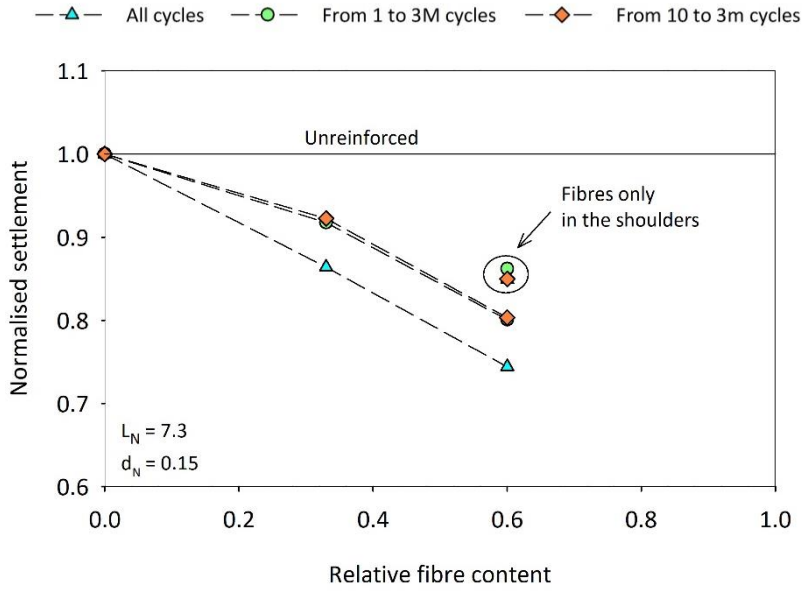

Figure 7-5. Effect of the content of filament-like fibres on MS ballast settlement at 3 million cycles

7.4 Resilient deflections

The distribution of the resilient sleeper deflections varied throughout each test, owing to sleeper tendency to centre-bind. Therefore, the understanding of sleeper interaction with ballast requires the analysis of the evolution of the sleeper deformed shape with the load cycles.

The resilient deflection by sleeper location vs number of cycles and for different tests is shown in Figure 7-6. Initially, the deflection of the middle of the sleeper was between 0.4 mm and 0.6 mm; beyond the first 1,000 cycles, it reduced to 0.3-0.4 mm (Figure 7-6a). Near the rail seats, the trend

was similar but less pronounced, with the resilient deflections reducing from ~0.6 mm to ~0.5 mm, especially after the first 1,000 cycles (Figure 7-6b). As expected from the tests using CH ballast, the movements of the sleeper ends were greater (Figure 7-6c). Initially they were between 0.6 mm and 0.9 mm, increased slightly during the first 100-300 cycles, reduced again for a few hundred cycles and beyond 200,000-700,000 cycles increased, reaching 0.7 mm to 0.9 mm at 3 million cycles. In general, fibre addition inhibited the movements of the sleeper ends and, except for test MS.06, those near the rail seats, while its effect on mid-sleeper deflections was small.

A better visualisation of the spatial distribution of the deflections is provided by Figure 7-7, which shows the sleeper resilient deformed shape at key cycles. From the very first cycles the sleeper showed hogging, which became more pronounced with the cycles, as the middle and rail deflections reduced slightly while those of the sleeper ends increased. At the end of the tests the movements of the sleeper ends were 2 to 3 times greater than those of the middle.

To highlight the effect of the properties of the fibres, the increase (or reduction) of the resilient deflections at 3 million cycles, which are the least affected by sample initial conditions and representative of long-term track performance, was plotted against the fibre content and dimensions (Figure 7-8, Figure 7-9).

The addition of thin filament-like fibres ($d_N = 0.15$) produced a slight increase in mid-sleeper deflections but reduced those near the rail seats and, especially, at the sleeper ends (Figure 7-8a). The reduction of the movements near the rails and sleeper ends was fairly linear with the fibre content, while the variation of the middle deflections was marginal. This was reflected in an almost linear reduction of the sleeper average deflection and hogging with the fibre content (Figure 7-8, b and c).

When the filament-like fibres were only added to shoulders, their effect on the middle deflections was barely noticeable but the reduction of the movements near the rails and sleeper ends became particularly pronounced (Figure 7-8a). As a result, the inhibition of sleeper average deflection and hogging was greater when fibres were added only to the shoulders (Figure 7-8, b and c).

Like the thin filament-like fibres, the narrow tape-like ones increased slightly the middle deflections but, in contrast, did not reduce the deflections near the rail seats and produced only a small reduction of the movements of the sleeper ends (Figure 7-8a). Thus, although filament-like and tape-like fibres had similar influence on the resilient deflections, the former had much stronger impact.

The influence of the fibre diameter was investigated for a small fibre content of $RFC = 0.3$. The increase/reduction of the resilient movements with the diameter of the filament-like fibres is shown in Figure 7-9, where infinitely thin fibres are assumed to have negligible effect. Thick fibres ($d_N = 0.24$) further reduced the resilient deflections compared with thin ones ($d_N = 0.14$), especially at the sleeper ends, where the deflections reduced almost linearly with the fibre diameter (Figure 7-9a). Hence the average sleeper movements and hogging reduced with the diameter of the fibres (Figure 7-9, b and c).

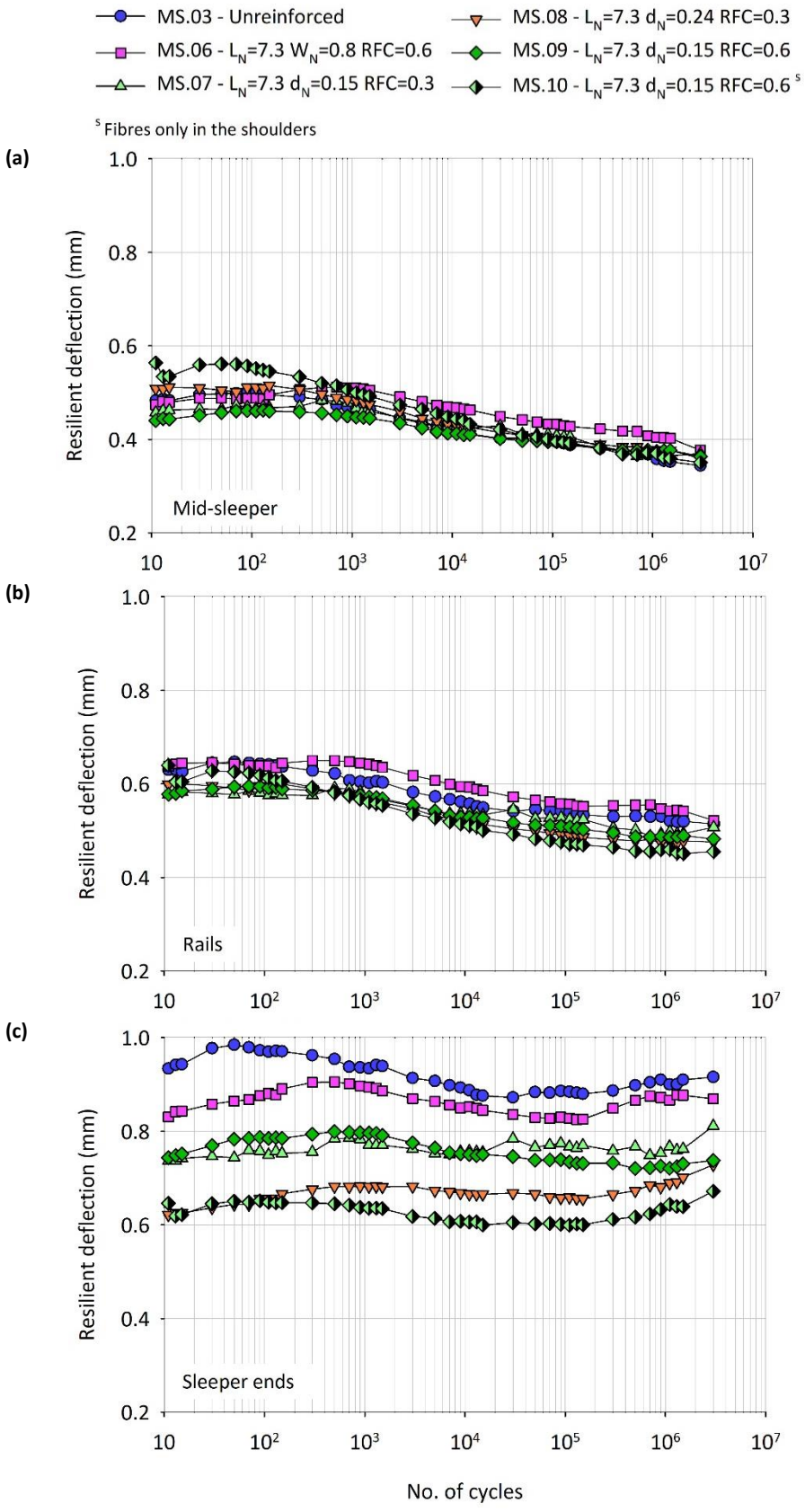

Figure 7-6. Resilient deflection vs number of cycles for tests using MS ballast; (a) average; (b) middle; (c) ends

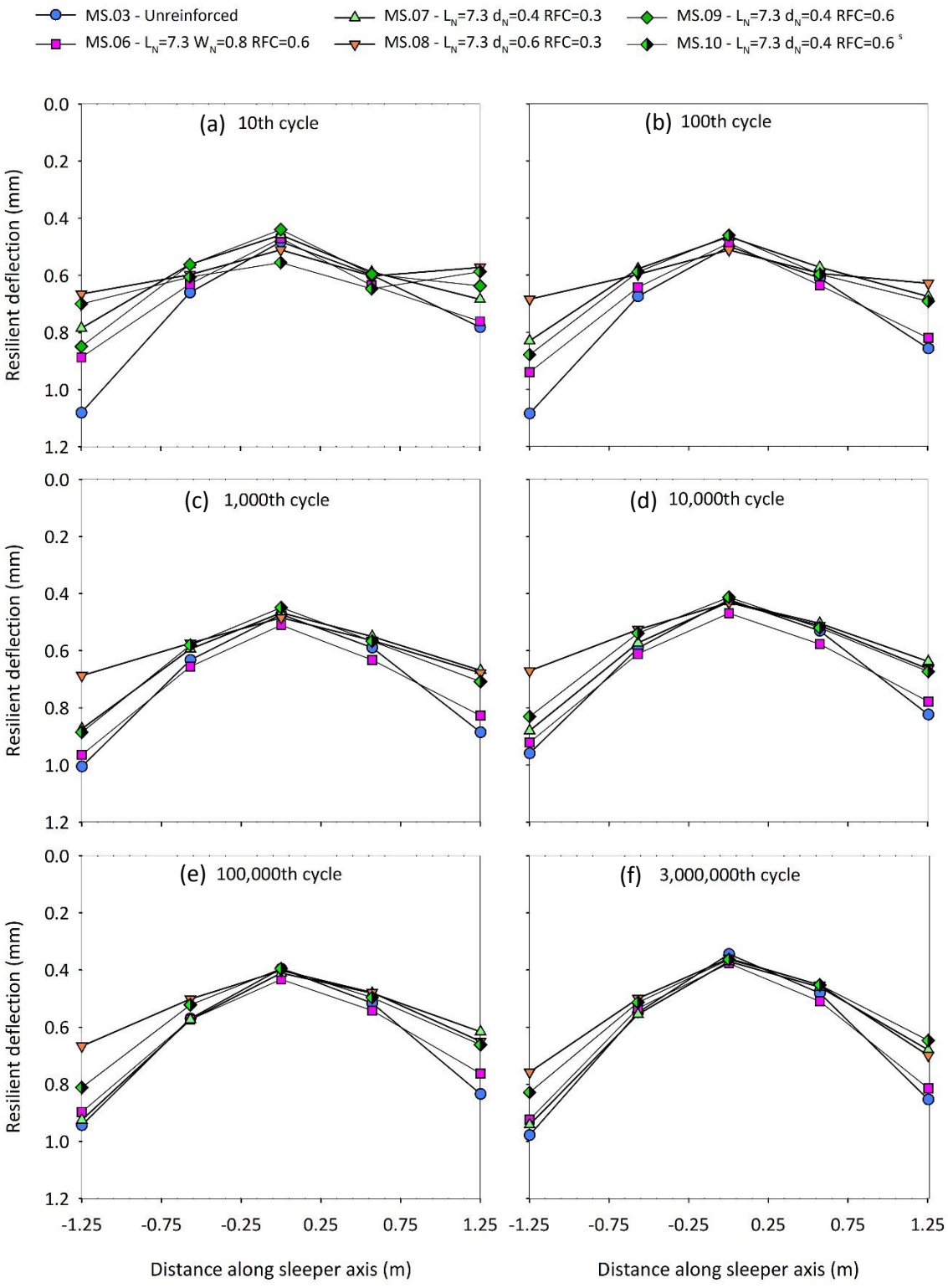

Figure 7-7. Sleeper resilient deformed shape at key cycles (tests using MS ballast)

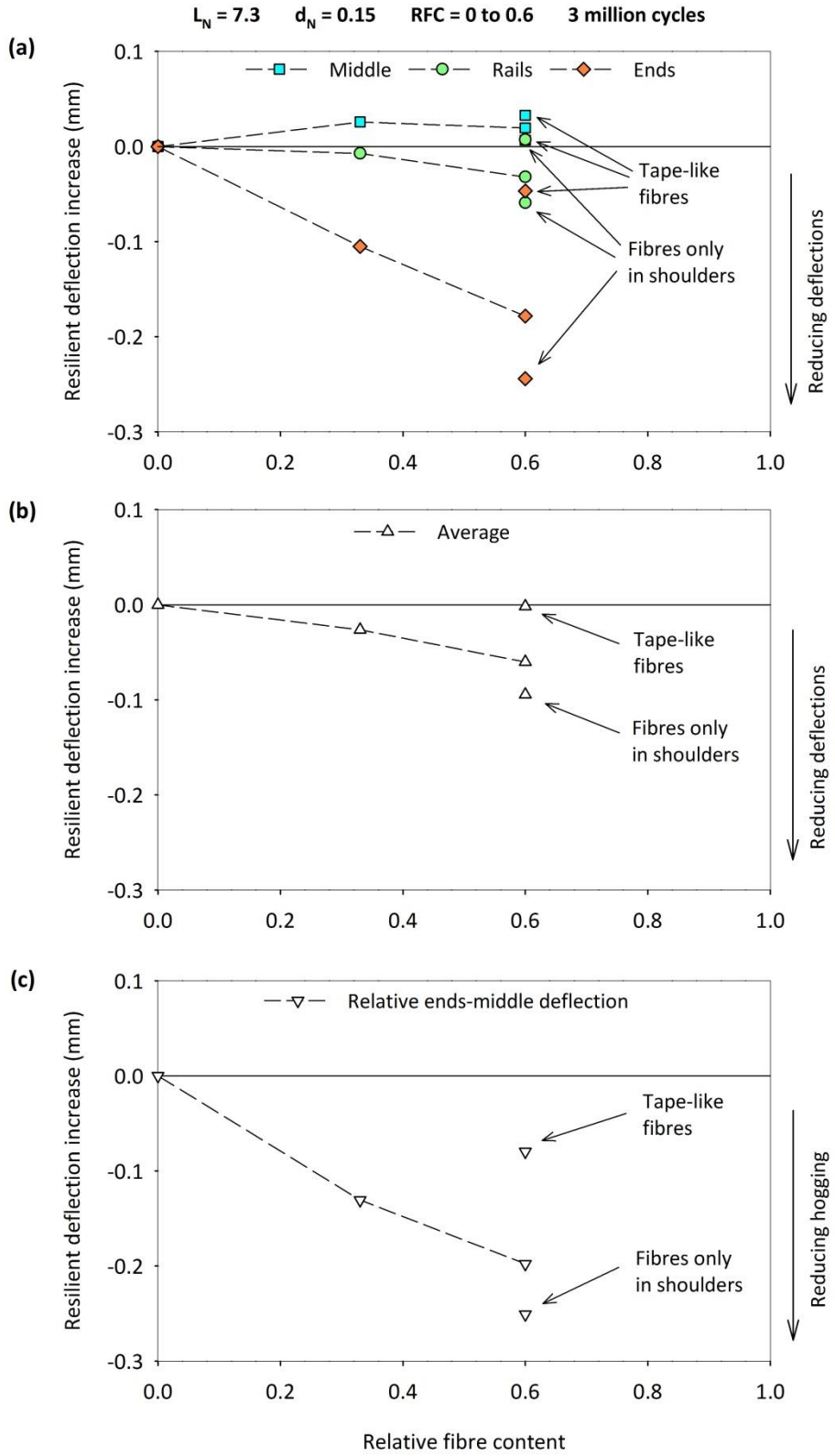

Figure 7-8. Effect of the content of filament-like and tape-like fibres on the resilient deflection at 3 million cycles; MS ballast; (a) middle, rails and middle deflections; (b) sleeper average deflection; (c) relative ends-middle deflection

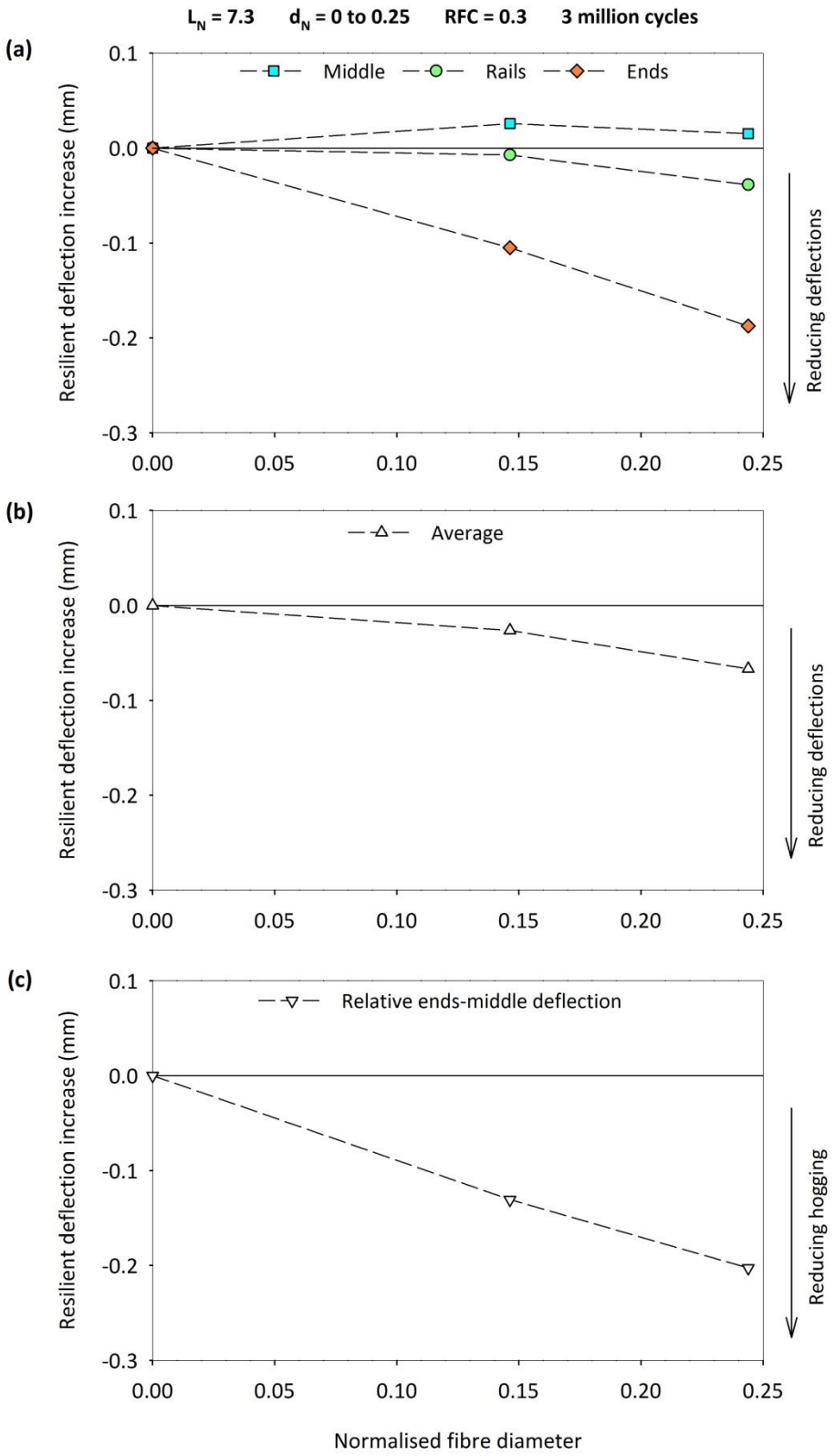

Figure 7-9. Effect of the diameter of filament-like fibres on the resilient deflection at 3 million cycles; MS ballast; (a) middle, rails and sleeper ends deflection; (b) average sleeper deflection; (c) relative ends-middle deflection

7.5 Ballast longitudinal pressure

The accumulated longitudinal pressure in the ballast was measured by means of 4 pressure plates installed on one side of the rig, as explained in Section 5.5.2. The evolution of the accumulated longitudinal pressure throughout the tests, i.e. the minimum pressure in each cycle, is described.

The evolution of the accumulated pressure with the number of load cycles for different locations and tests is shown in Figure 7-10. The average pressure ranged between 8 kPa and 12 kPa (Figure 7-10a). In all tests, it increased moderately in the first ∼2 thousand cycles, beyond which it typically reduced. Only the baseline test saw the pressure increasing slightly after 1 million cycles. Typically, under the middle of the sleeper it increased in the first 3,000 cycles, after which it remained almost constant (Figure 7-10b). Only tests MS.06 and MS.07 showed a different trend, with the pressure increasing slightly or remaining constant with the cycles. However, this might be explained by the variability of sample initial conditions which might have affected the initial pressure. In the first cycles, the middle pressure was between 7 kPa and 14 kPa. In the long term, it reached 10 kPa to 16 kPa. In contrast, the pressure beneath the rails remained substantially constant in the first ∼1,000, beyond which it typically reduced slightly (Figure 7-10c). Only test MS.10 saw a significant reduction of the pressure beneath the rails. This might be explained by the presence of fibres only in the shoulders, which might have altered locally the properties of the ballast bed and hence, the distribution of the stresses. In the first cycles, the pressure under the rails was between 7 kPa and 9 kPa, with only test MS.07 showing a higher pressure of 13 kPa. At 3 million cycles, it was slightly lower, i.e. between 6 kPa and 8 kPa. It can be noticed that usually fibres reduced the longitudinal pressure, especially under the middle of the sleeper.

The effect of fibre addition on the accumulated longitudinal pressure at the end of the tests, which is the least affected by sample initial conditions and representative of track long-term performance, is represented in Figure 7-11.

For thin filament-like fibres ($d_N = 0.14$), both the pressure beneath the middle of the sleeper and the rails reduced almost linearly with the fibre content (Figure 7-11a). The reduction was more pronounced in the middle, where the pressure at 3 million cycles was higher. Therefore, fibres inhibited the accumulation of longitudinal pressure in the ballast, which also became more uniform, as the difference between middle and rail pressure reduced (Figure 7-11b).

The presence of filament-like fibres only in the shoulders was associated with an even greater reduction of the pressure beneath the rails (Figure 7-11a) and hence, led to a particularly uniform distribution of the pressure at 3 million cycles (Figure 7-11b).

Compared with the filament-like fibres, the tape-like fibres had a smaller effect, as they only produced a slight reduction of the pressure under the middle of the sleeper (Figure 7-11a).

The influence of the diameter of the filament-like fibres is shown in Figure 7-11c, where infinitely thin fibres ($d_N \cong 0$) are assumed to have negligible effect on ballast behaviour, although they were not tested. Compared with thin fibres (d_N = 0.15), thick ones (d_N = 0.24) gave a greater reduction of the longitudinal pressure both under the middle of the sleeper and the rail seats. The effect of the fibre diameter was smaller than that of the fibre content. Moreover, while increasing the content gave a more uniform long-term distribution of the pressure, the use of thicker fibres affected the pressure beneath rails and middle of sleeper to similar extents.

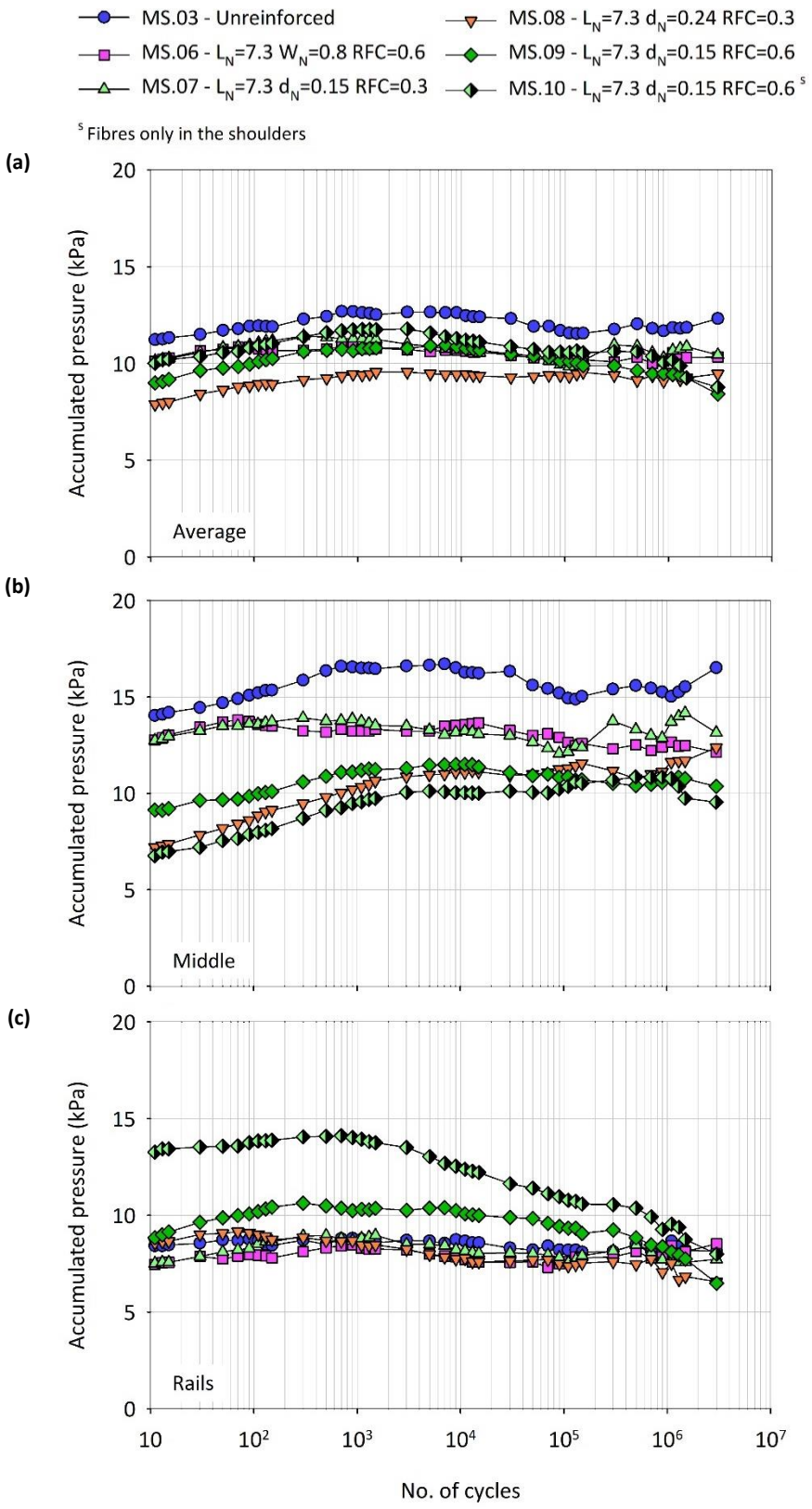

Figure 7-10. Longitudinal pressure accumulated in MS ballast vs number of cycles; (a) average, (b) middle, (c) rails

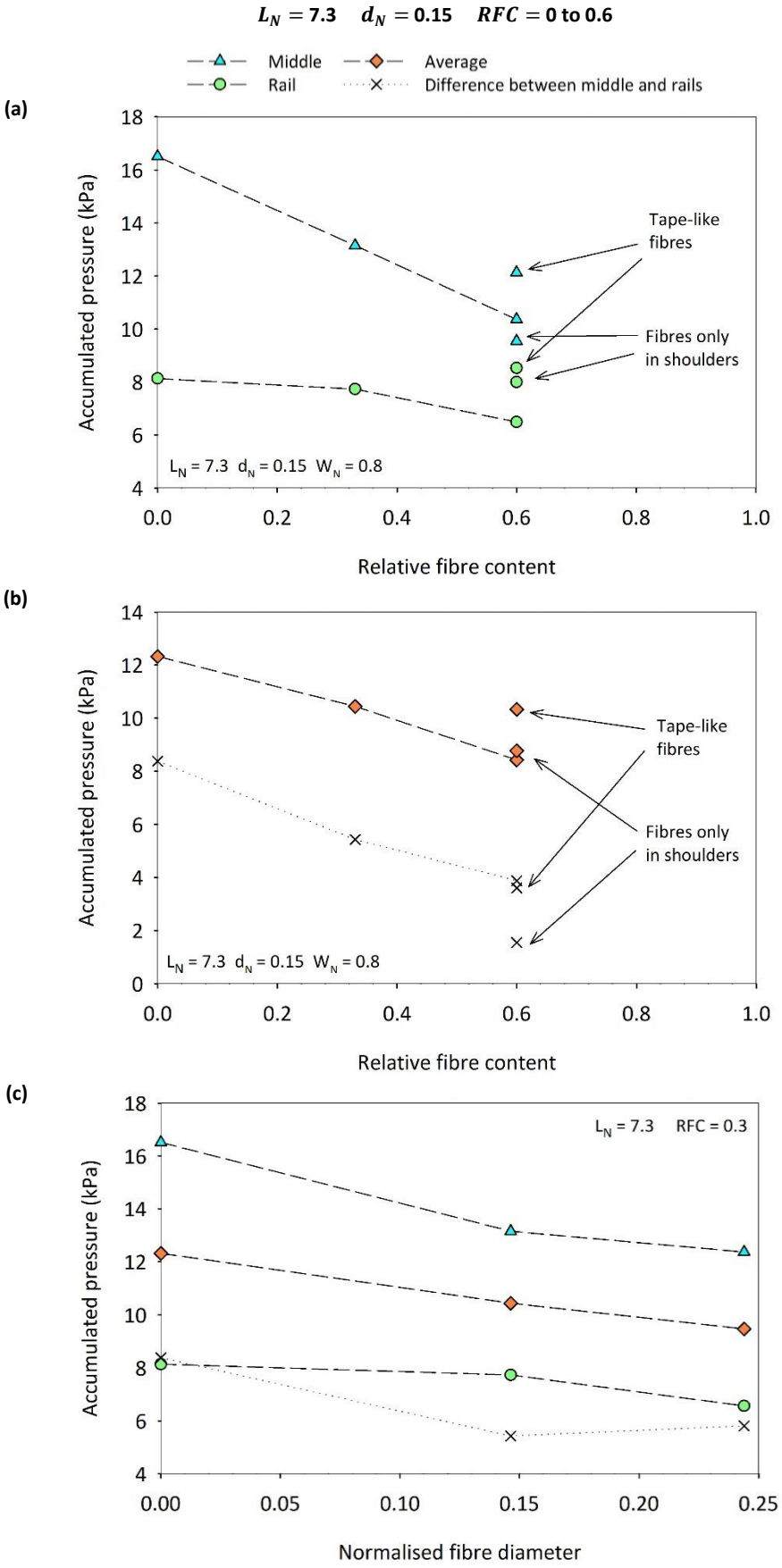

Figure 7-11. Effect of fibres on longitudinal pressure accumulated in MS ballast at 3 million cycles; (a) and (b) effect of fibre content; (c) effect of fibre diameter

7.6 Sleeper-ballast contact area

Low and medium pressure sensitive paper was used to assess the contact area at the interface between the sleeper and the ballast, as explained in Section 5.5.4. Some photos of medium pressure paper after three key tests are shown in Figure 7-12. Results are expressed in terms of contact area beneath the middle of the sleeper and rail seats ($A_{c,m}$ and $A_{c,r}$), average contact area over the sleeper base ($A_{c,av}$), and ratio of the area at the middle to that at the rail seats (U_c). The latter is representative of the uniformity of the contact.

Results are summarised in Table 7-2. As with the first series of tests, the contact area was always small, i.e. between 0.5% and 1%, and smaller under the middle of the sleeper than beneath the rail seats. For the low-pressure paper (i.e. pressure > 2.5 MPa) it ranged from 0.5% to 0.7% in the middle, from 1% to 1.4% at the rails and from 0.8% to 1.2% on average. For the medium-pressure paper (i.e. pressure > 10 MPa) it was smaller, i.e. 0.5% to 0.6% in the middle, 0.7% to 1.2% at the rails and 0.7% to 1.0% on average.

Table 7-2. Sleeper-MS ballast contact area measured using low and medium pressure paper

Test	Pressure > 2.5 MPa				Pressure > 10 MPa			
	$A_{c,m}$ (%)	$A_{c,r}$ (%)	$A_{c,av}$ (%)	U_c (-)	$A_{c,m}$ (%)	$A_{c,r}$ (%)	$A_{c,av}$ (%)	U_c (-)
MS.03 - Unreinforced	0.59	0.99	0.87	0.60	0.47	0.97	0.82	0.48
MS.06 - W_N=0.8 RFC=0.8	0.56	1.09	0.93	0.52	0.51	1.00	0.86	0.51
MS.07 - d_N=0.15 RFC=0.3	0.75	1.44	1.23	0.52	0.60	1.17	1.00	0.52
MS.08 - d_N=0.24 RFC=0.3	0.73	0.99	0.91	0.74	0.70	1.06	0.95	0.66
MS.09 - d_N=0.15 RFC=0.6	0.46	0.95	0.80	0.48	0.42	0.76	0.66	0.56
MS.10 - d_N=0.15 RFC=0.6[s]	0.51	0.93	0.81	0.55	0.42	0.81	0.69	0.52

The effect of the addition of thin filament-like fibres ($d_N = 0.14$) and narrow tape-like fibres ($W_N = 0.8$) is shown in Figure 7-13. The contact area below the middle of the sleeper was lightly affected by the addition of filament-like fibres (Figure 7-13a). Beneath the rails, it increased when a very small content was used, i.e. $RFC = 0.3$, while the addition of a larger quantity of reinforcement, i.e. $RFC = 0.6$, did not produce any substantial effects (Figure 7-13b). As a result, also the average contact area increased only when small fibre content was used (Figure 7-13c). However, the increase in contact area for $RFC = 0.3$ (test MS.07) is suspect, as the effect of fibre addition is expected to increase monotonically with the content. Such trend was observed for all other test outputs, i.e. settlement, resilient deflections, longitudinal pressure and particle degradation. Moreover, the addition of a very small quantity of thin fibres is unlikely to have a significant influence on the contact area. Hence the data points of Figure 7-13 associated with test MS.07 are labelled as "suspect". The effect of fibre addition on the uniformity of the contact area is also unclear, as the medium-pressure and low-pressure papers showed contrasting trends (Figure 7-13c). The addition of a moderate content ($RFC = 0.6$) of filament-like fibres to the shoulders and the use of tape-like fibres did not affect the extent and distribution of the

sleeper/ballast contact area (Figure 7-13). Therefore, if the suspect data are neglected, the influence of the addition of thin or narrow fibres on the sleeper/ballast contact is marginal.

The effect of the thickness of the filament-like fibres is shown in Figure 7-14. Compared with the baseline, a small amount of thick fibres ($d_N = 0.2$) increased slightly the contact area at the middle (Figure 7-14a), while it did not affect that beneath the rails (Figure 7-14b). This increased the uniformity of the contact (Figure 7-14d) but did not affect its average extent (Figure 7-14c).

In general, the second series of tests did not show any significant effect of fibre addition on the sleeper/ballast contact area.

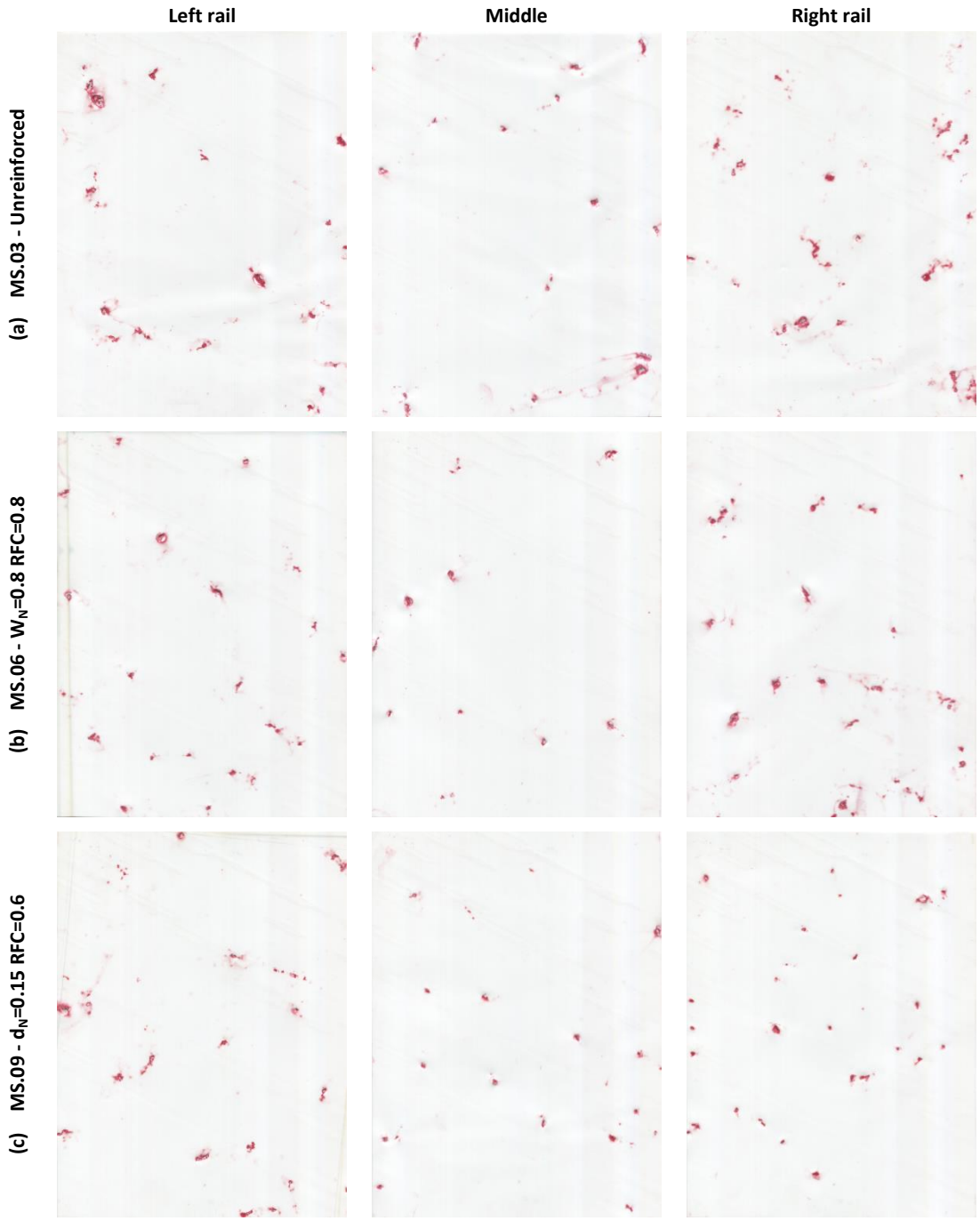

Figure 7-12. Medium pressure sensitive papers showing sleeper/ballast contact beneath middle of the sleeper and rails for three key tests: (a) unreinforced ballast; (b) tape-like fibres; (c) filament-like fibres

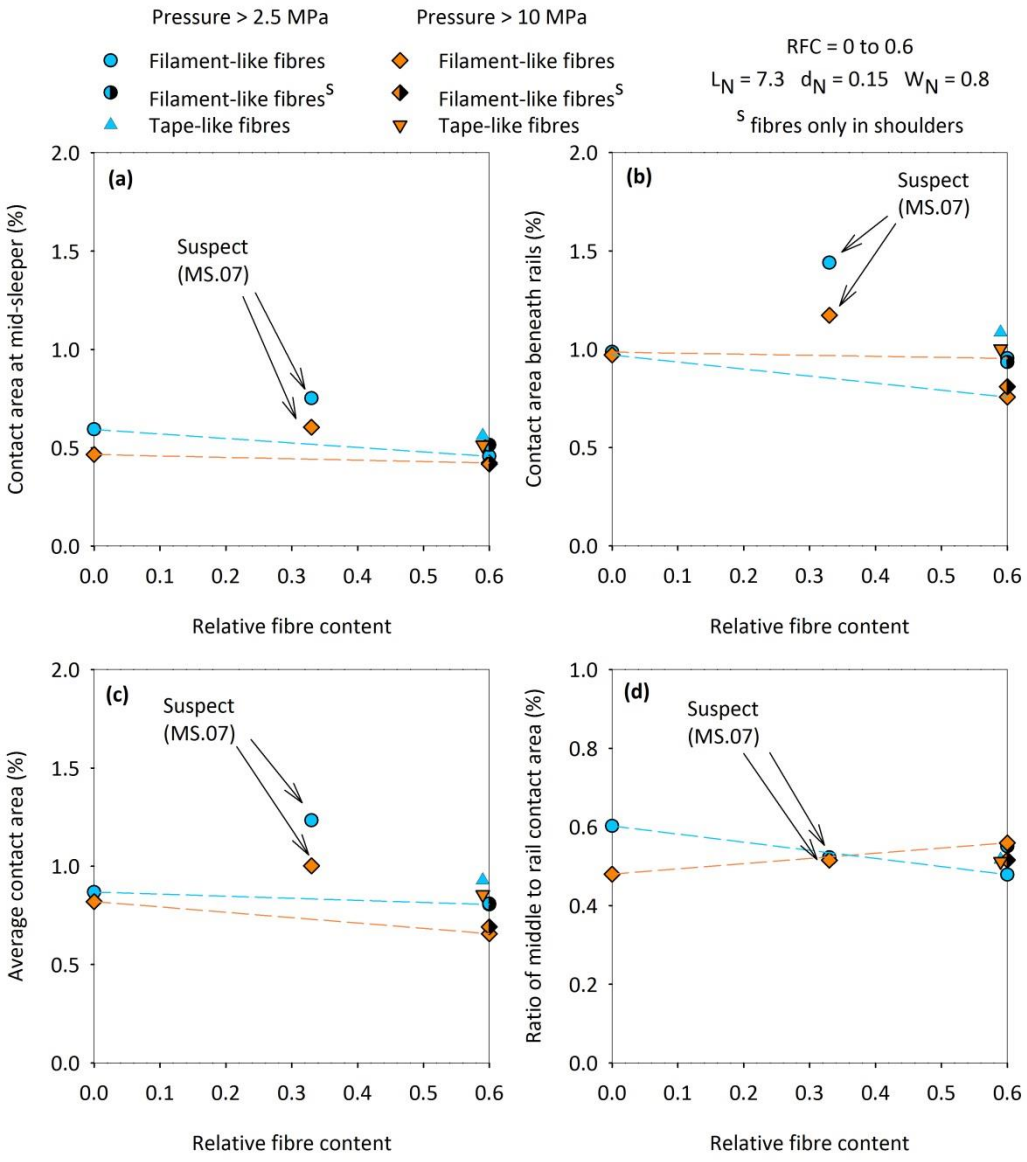

Figure 7-13. Effect of thin filament-like fibres and narrow tape-like fibres on sleeper/MS ballast contact area

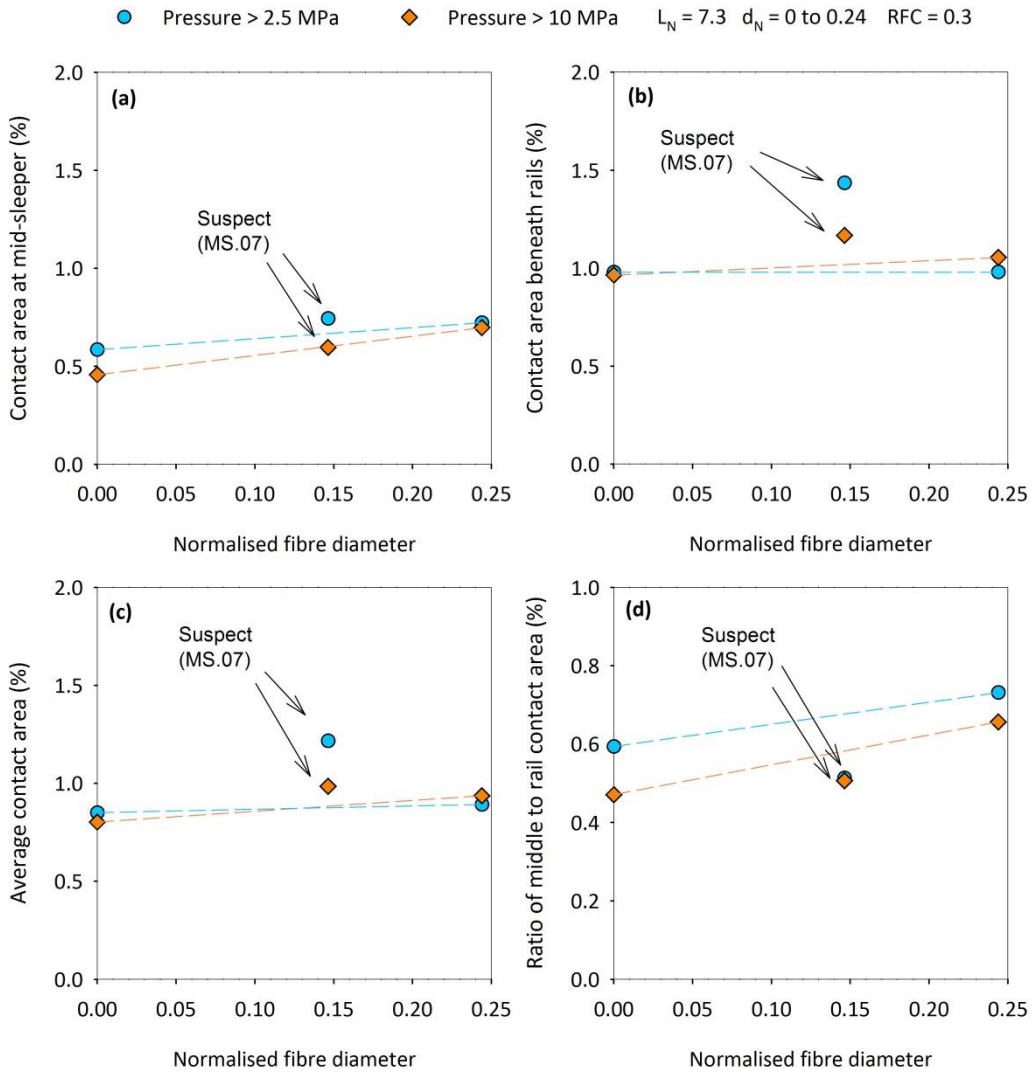

Figure 7-14. Effect of thick filament-like fibres on sleeper/MS ballast contact area

7.7 Ballast lateral spread

Lateral plates were used in some of the tests (MS.01, MS.01^r, MS.02, MS.04 and MS.05) to monitor ballast spreading (Section 5.5.3). In tests MS.01 (and its repeat, MS.01^r) and MS.02, three lateral plates were installed deep in the shoulders, as shown in Figure 7-1a. To verify that the plates had not affected sample behaviour, no plates were used in test MS.03. However, the comparison between test MS.01 (and its repeat) and MS.03 showed that the lateral plates had influenced sample response. They had increased slightly the settlement (Figure 7-15b), diminished the accumulated longitudinal pressures (Figure 7-16) and reduced the resilient movements (Figure 7-17). In the light of this, the lateral plates were modified to reduce their disturbance on shoulder ballast. In test MS.04 only one plate was installed in each shoulder (Figure 7-1b). This reduced the settlement compared with that measured in test MS.03 (Figure 7-15b), while it did not affect the ballast longitudinal pressure and sleeper resilient movements (Figure 7-16, Figure 7-17). In test MS.05 the plates were installed further from the

sleeper ends (Figure 7-1c) but this did not affect sample response compared with test MS.04. Therefore, from test MS.06, the use of lateral plates was abandoned to avoid any effects on ballast and fibres mechanical behaviour. Nevertheless, they provided interesting results, which contributed to the understanding of the general mechanical behaviour of ballasted track.

The evolution of the shoulder lateral movement and sleeper vertical settlement beyond the first load cycle is shown in Figure 7-15, a and b. As observed in Section 5.5.3, the vertical settlement was accompanied by ballast lateral spreading. Like the vertical permanent deformation, the lateral movements increased approximately linearly with the logarithm of the number of cycles. In general, the spreading at 3 million cycles was small, i.e. between 1.5 mm and 2.5 mm, but comparable to the settlement, which was between 4 mm and 5 mm.

The ratio of spreading to settlement increased linearly with the load cycles (Figure 7-15c). In the first cycles it ranged from 0.1 to 0.25 and reached values of 0.4 to 0.5 at 3 million cycles. A clearer comparison between vertical and lateral movements is shown in Figure 7-18, where the ballast spreading is plotted against the settlement. Except for test MS.01^{r}, all tests followed the same spreading vs settlement curve, although they showed different settlement response. The experimental data seem to follow a hyperbolic relationship, as they show an initial curvature which reduces rapidly tending to a line. In particular, they may be fitted by the following equation:

$$S = \frac{2.249\, S_h}{0.323 + S_h} + 1.423\, S_h \tag{7-1}$$

where S is the settlement and S_h is the spreading. In the first load cycles ($S_h \to 0$) the increase in lateral movement (δS) was less than 1/8 of the increase in settlement (δS_h). This proportion increased with the cycles, tending to a value of over 2/3. This might be explained by the settlement being mainly caused by particle densification in the first cycles but requiring the shoulder to move laterally in the longer term to allow for further particle rearrangement, as observed in Section 3.3.4.

Tests MS.01, MS.01^{r} and MS.02, in which three plates were installed in each shoulder, showed greater lateral movements at the top of the ballast layer, causing the shoulder slope to increase slightly, i.e. less than 0.5° (Figure 7-19, Figure 7-20). Like a geogrid, the rubber layer placed at the bottom of the rig might have retained the movements of the particles in contact with it, providing a certain degree of lateral confinement (Section 3.4.3).

Finally, it is worth pointing out that test MS.04 and MS.05, in which the plates were installed at different depth in the shoulder, showed almost identical settlement and spreading (Figure 7-15). This suggests that the shoulders shifted laterally like an almost rigid block, pushed aside as the particle rearranged under cyclic loading.

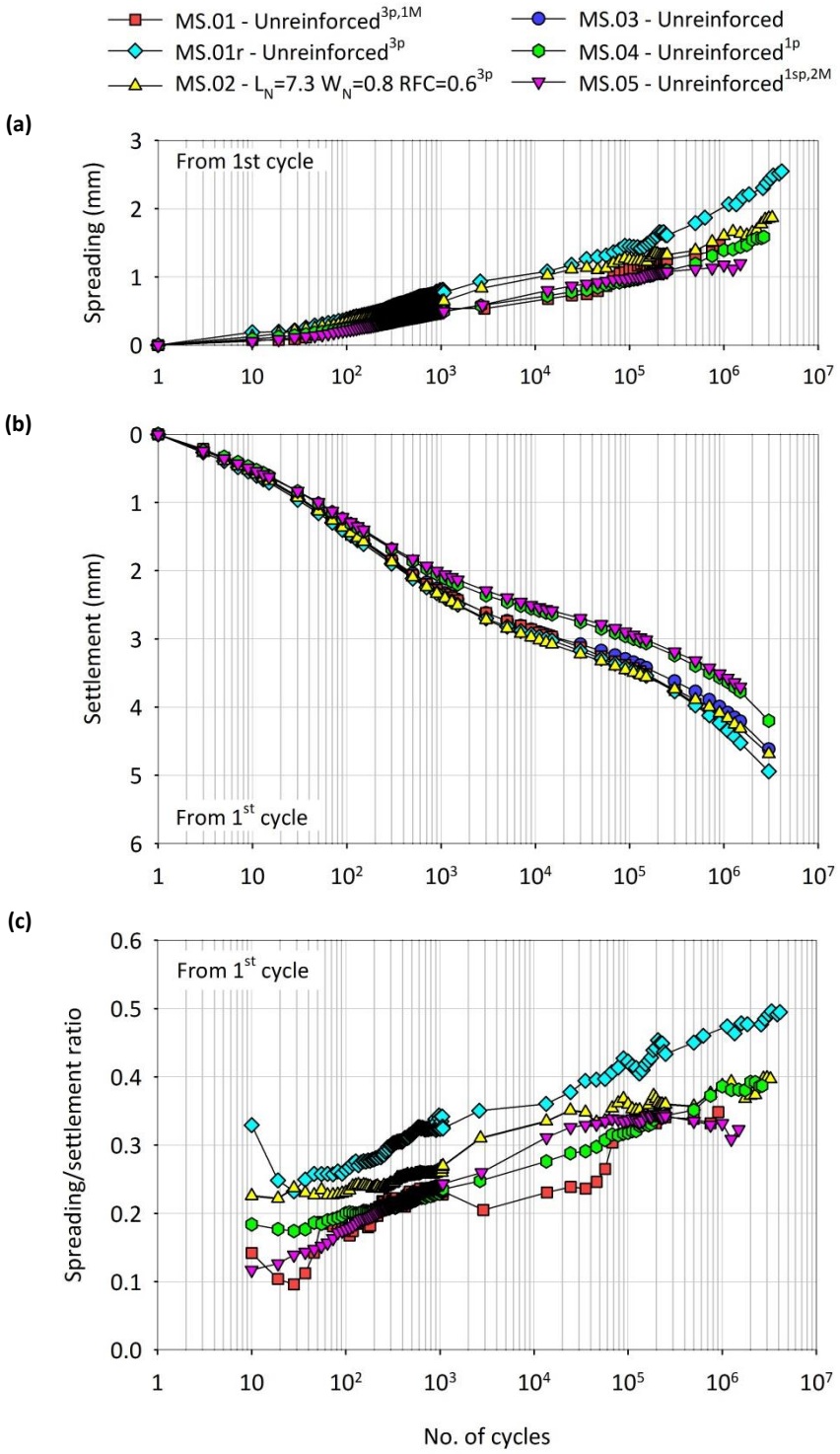

Figure 7-15. Evolution of (a) spreading, (b) settlement and (c) ratio of the spreading to the settlement with the number of cycles (tests using MS ballast)

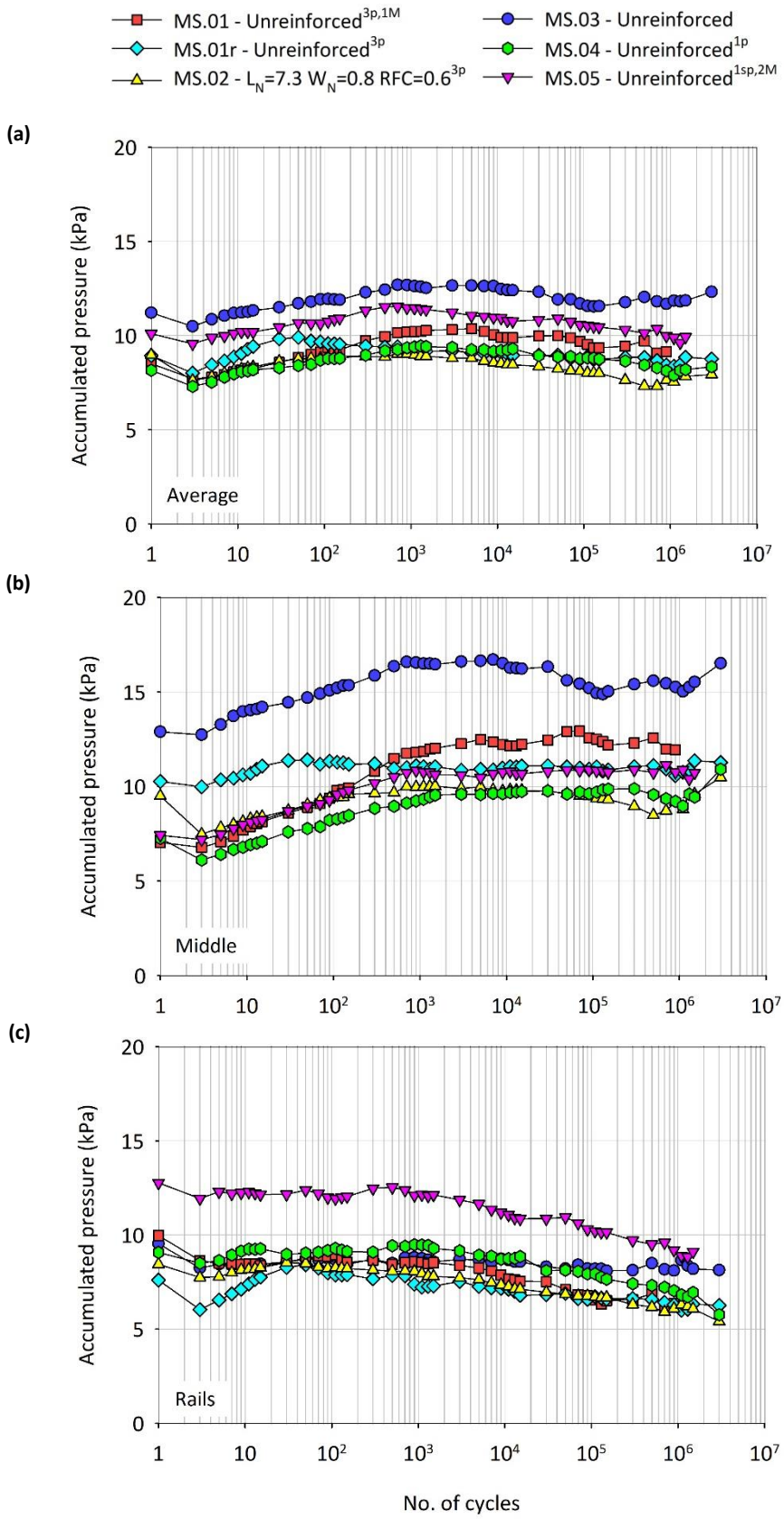

Figure 7-16. Effect of lateral plates on longitudinal accumulated pressure

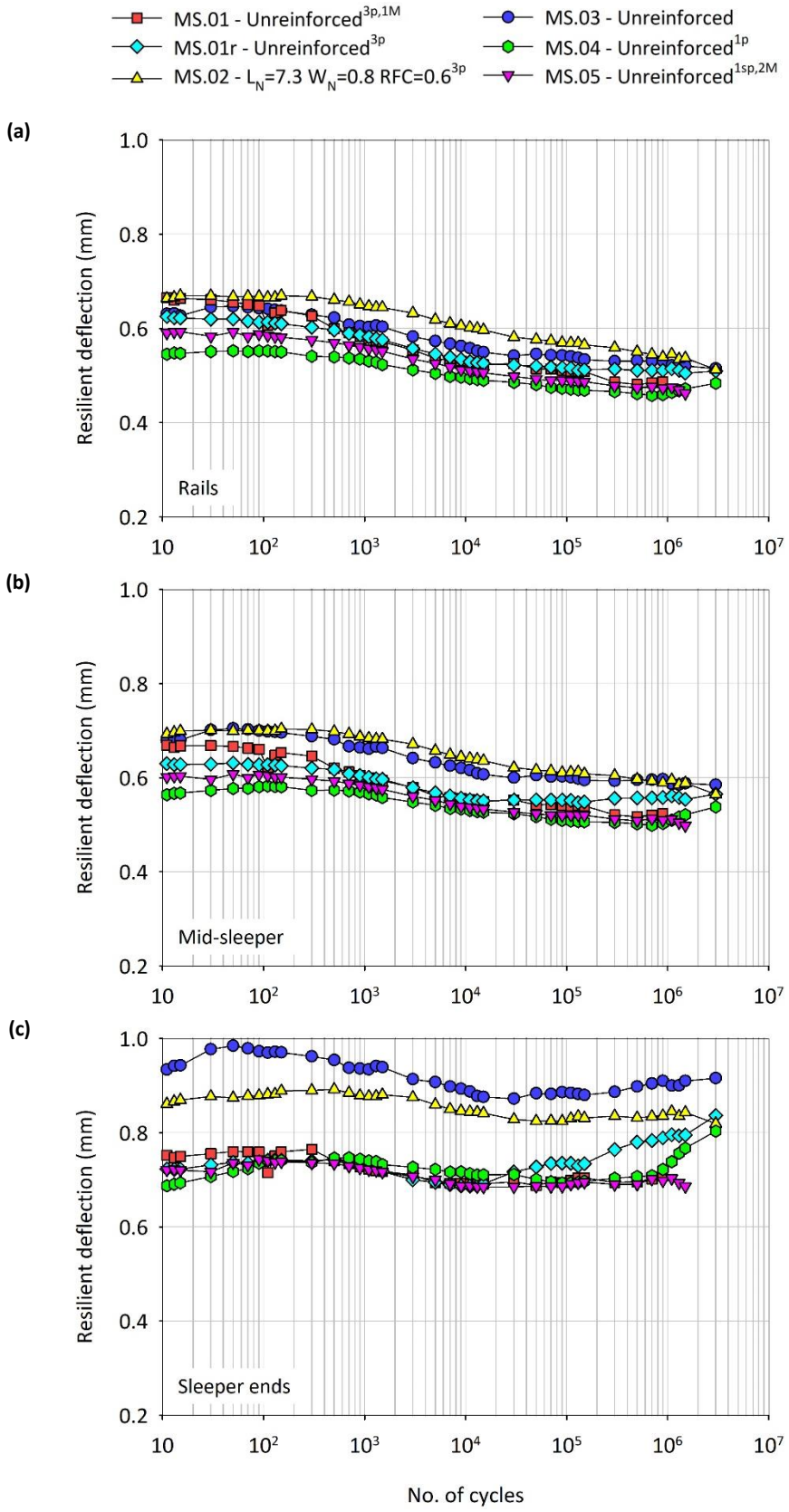

Figure 7-17. Effect of lateral plates on resilient deflections

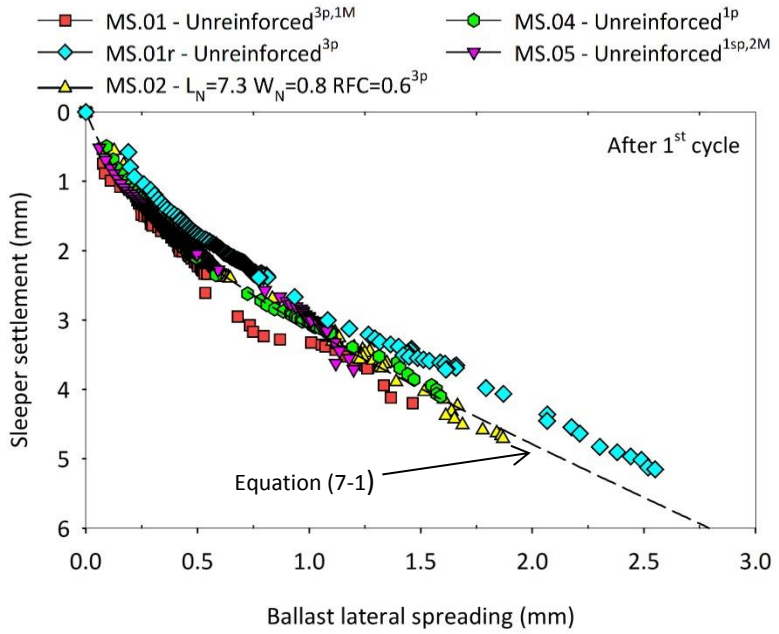

Figure 7-18. Settlement vs spreading relationship

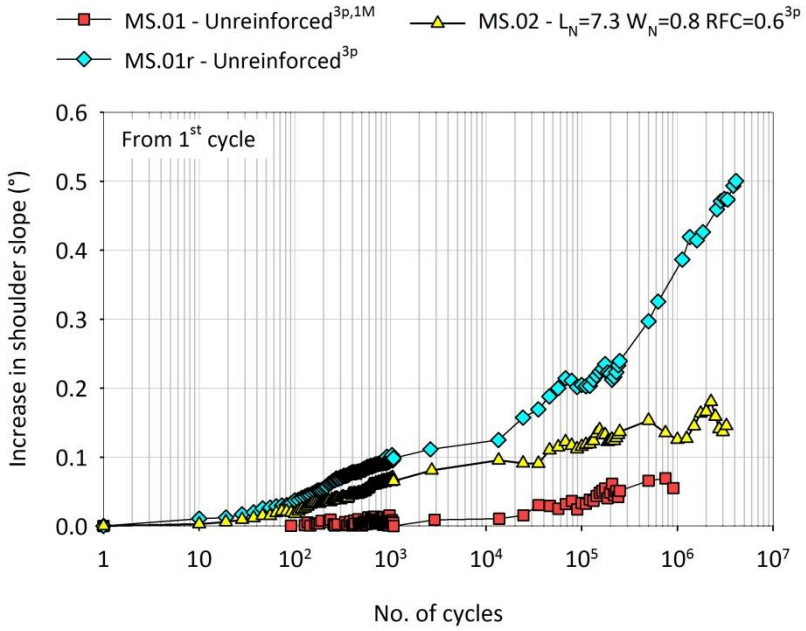

Figure 7-19. Increase in shoulder slope vs number of cycles

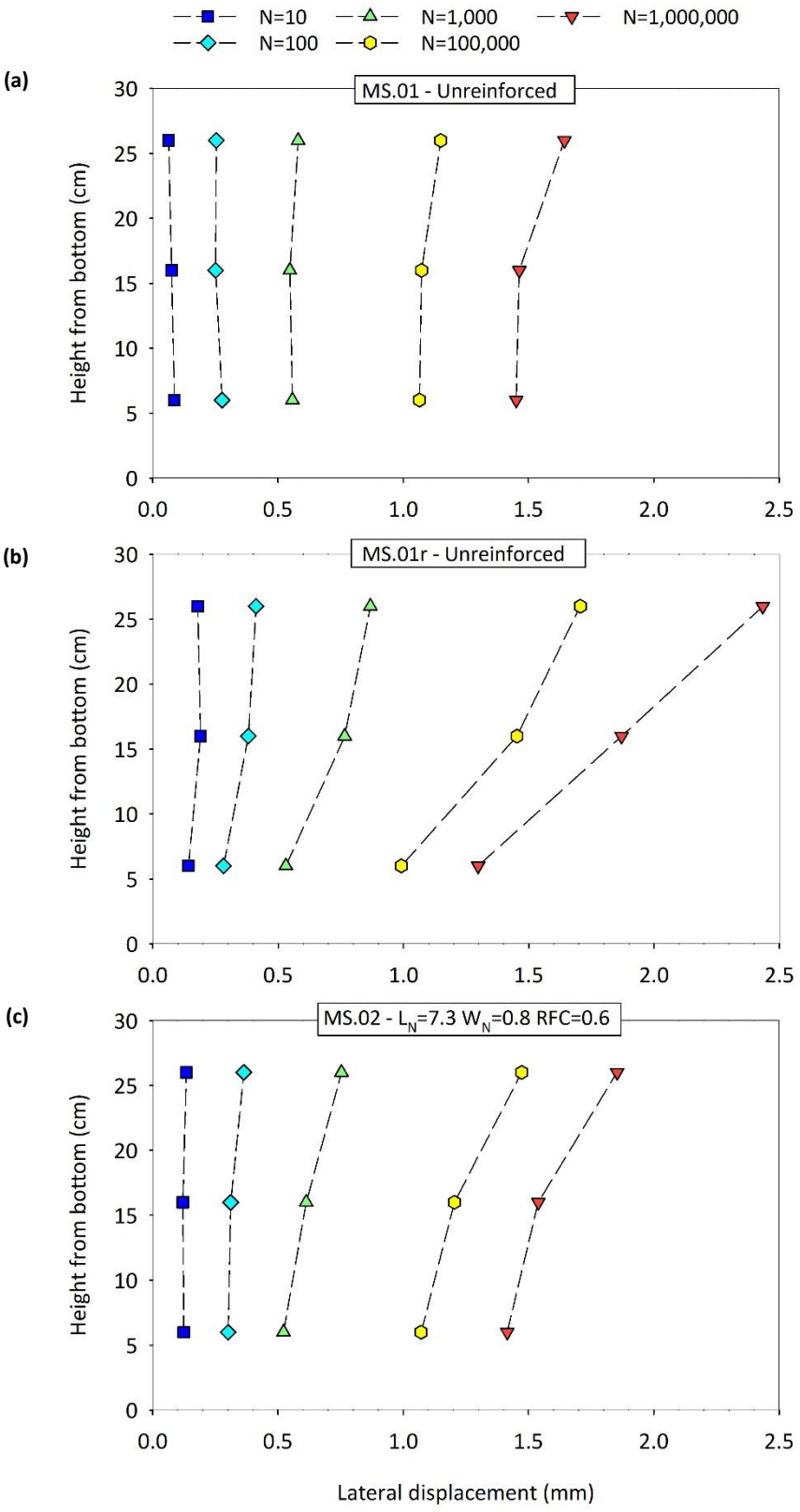

Figure 7-20. Lateral movements at different depths and key cycles

7.8 Particle degradation

Ballast particles were marked and placed in the top part of the ballast bed, beneath both rail seats and the middle of the sleeper, to assess their mechanical degradation during the tests (Section 5.5.5). This was expressed in terms of percentage mass loss (ΔM_p) and number of broken particles (N_{bp}). The former is representative of particle frictional wear and chipping, the latter of particle splitting and corner breakage.

Results are summarised in Table 7-3, which for each test reports the average mass loss and number of broken particles beneath each rail ("Rail"), the middle of the sleeper ("Mid."), and the whole sleeper footprint ("Av"). The mass loss could not be assessed for test MS.01^r. In this test, the particles were divided into a small number of batches, most of them containing broken particles. Therefore, the mass loss due to frictional wear could not be calculated. Hence, from test MS.02 the particles were split into a greater number of batches, i.e. 8, as explained in Section 5.5.5.

The average mass loss was always smaller than 0.1% and not more than 4 particles (out of ~350) fractured in each test. On average, both mass loss and number of broken particles were bigger beneath the middle of the sleeper (where ΔM_p = 0.08% and N_{bp} = 0.7) than beneath the rail seats (where ΔM_p = 0.07% and N_{bp} = 0.6). However, contrasting results were shown by single tests. The particles used to assess particle degradation were representative of the behaviour of the particles in the top-half of the ballast layer, except for those in direct contact with the sleeper base (Section 3.3.35.5.5). Therefore, test results can be used to estimate the total mass loss for the top half of the ballast bed. Assuming ballast stresses to follow a 2:1 trapezoid distribution (Figure 2-14), a percentage mass loss of 0.1% would correspond to a loss of about 145 g of material in the top half of the ballast bed, i.e. the mass of a 42 mm particle of MS ballast. Similarly, the breakage of 4 particles would correspond to the breakage of 14 particles. However, the particles in contact with the sleeper base and, in particular, with its edges are expected to suffer greater mechanical degradation as they are subjected to greater stresses.

Although the mass loss was marginal, the use of fibres seems to reduce it. As shown in Figure 7-21, all tests with fibres were characterised by smaller particle mass loss, compared with those in which the ballast was unreinforced. The only exceptions are tests MS.01 and MS.05, in which no fibres were used. However, this can be explained by the smaller duration of these tests.

The frictional wear seems dependent on the characteristics of the fibres. After 3 million load cycles, unreinforced ballast showed a particle mass loss of about 0.09%. For thin filament-like fibres (d_N = 0.15), the mass loss reduced with the fibre content, as ΔM_p = 0.08% for RFC = 0.3 and ΔM_p = 0.06% for RFC = 0.6 (Figure 7-23). Assuming the addition of a small amount infinitely thin fibres (RFC = 0.3, $d_N \rightarrow 0$) not to affect ballast behaviour, the mass loss reduced with the fibre thickness (Figure 7-24). The addition of a small quantity of thick fibres (RFC = 0.3, d_N = 0.24) was associated with an average mass loss of 0.06%, similar to that observed when a greater content of thin fibres (RFC = 0.6, d_N = 0.15) was used. The addition of a moderate amount of narrow tape-like fibres (RFC = 0.6, W_N = 0.8) gave a mass loss of ~0.7%, similar to that associated with a moderate amount of thin filament-like fibres. The addition of fibres only to the shoulders led to a small mass reduction. This was unexpected, as no fibres were placed under the sleeper, where the marked particles where placed. However, it can be attributed to experimental

variability or a change in the distribution of the stresses in the ballast due to the non-uniform support.

The influence of fibre addition on the particle breakage cannot be easily assessed because the number of broken particles in each test was not statistically significant. However, greater values of mass loss, hence frictional wear and chipping, seems associated with greater particle breakage, although no clear correlation can be derived (Figure 7-22). Therefore, fibres might reduce both particle abrasive wear and breakage. This was not relevant in the laboratory, where particle degradation was marginal, but it could be under more severe loading conditions (e.g. on poorly maintained tracks, high speed lines, transition zones etc.).

The percentage mass loss reduced with the particle size (Figure 7-25). Such reduction was similar in each test, as the lines fitting the experimental points in the mass loss vs particle size plane are almost parallel. The only exceptions are represented by test MS.02 and MS.03, in which the reduction in mass loss with the particle size was less pronounced. The reduction in percentage mass loss with the particle size can be explained by the fact that ΔM_p is calculated as the ratio of the mass loss to the initial mass of the particles. The former is proportional to the square of the particle size, as only the particle surface suffers frictional wear, while the latter is proportional to the volume of solids, hence the cube of the particle size. Therefore, the percentage mass loss, which is the ratio between the two of them, should theoretically increase with the inverse of the particle size. This is only partially confirmed by test results, which showed the percentage mass loss reducing with the particle size but do not show a hyperbolic relationship between the two of them.

Table 7-3. Particle degradation (tests using MS ballast)

Test	No. of cycles	Percentage mass loss			No. of broken particles		
		Rail	Mid.	Av.	Rail	Mid.	Tot.
MS.01 - Unreinforced^{3p,1M}	907173	0.053	0.091	0.064	0.0	0.0	0.0
MS.01^{r} - Unreinforced^{3p}	4097859	-	-	-	1.0	2.0	4.0
MS.02 - W_N=0.8 RFC=0.6^{3p}	3250001	0.040	0.085	0.054	0.0	1.0	1.0
MS.03 - Unreinforced	3174919	0.089	0.097	0.092	1.5	1.0	4.0
MS.04 - Unreinforced^{1p}	2663595	0.089	0.108	0.094	1.0	0.0	2.0
MS.05 - Unreinforced^{1sp,2M}	1500001	0.072	0.087	0.076	0.5	0.0	1.0
MS.06 - W_N=0.8 RFC=0.8	3180426	0.067	0.074	0.069	1.0	2.0	4.0
MS.07 - d_N=0.15 RFC=0.3	3133753	0.089	0.071	0.084	1.0	1.0	3.0
MS.08 - d_N=0.24 RFC=0.3	3154770	0.055	0.058	0.056	0.0	0.0	0.0
MS.09 - d_N=0.15 RFC=0.6	3123422	0.060	0.050	0.057	0.0	0.0	0.0
MS.10 - d_N=0.15 RFC=0.6^{s}	3172569	0.078	0.087	0.081	1.0	1.0	3.0
Average		**0.069**	**0.081**	**0.073**	**0.6**	**0.7**	**2.0**

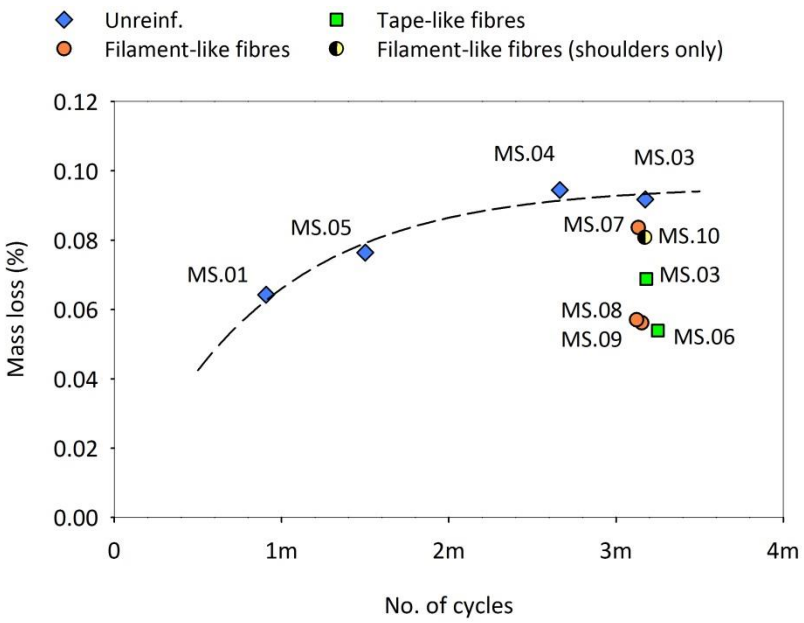

Figure 7-21. Mass loss vs total number of cycles (tests using MS ballast)

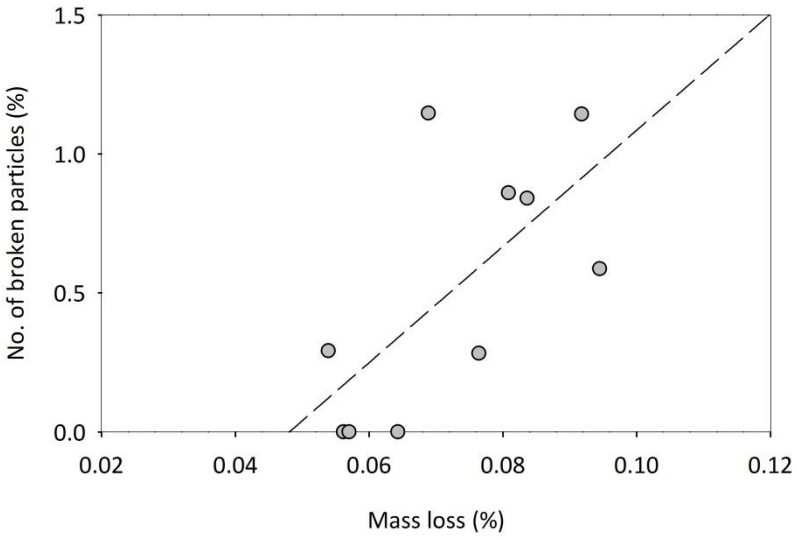

Figure 7-22. Number of broken particles vs mass loss

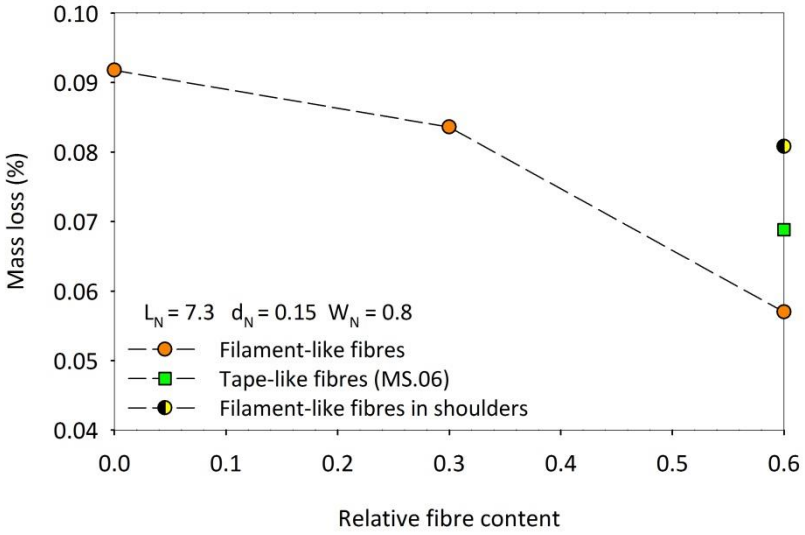

Figure 7-23. Effect of fibre content on average particle mass loss for tests using MS ballast

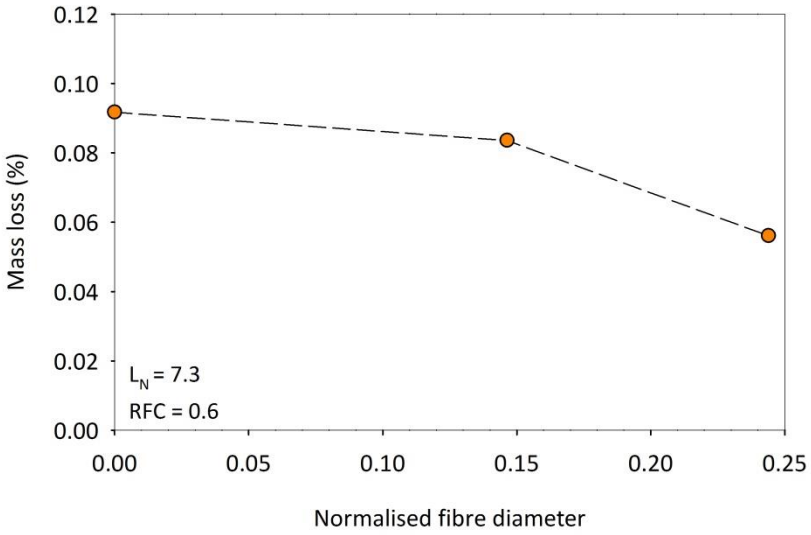

Figure 7-24. Effect of the diameter of filament-like fibres on average mass loss for tests using MS ballast

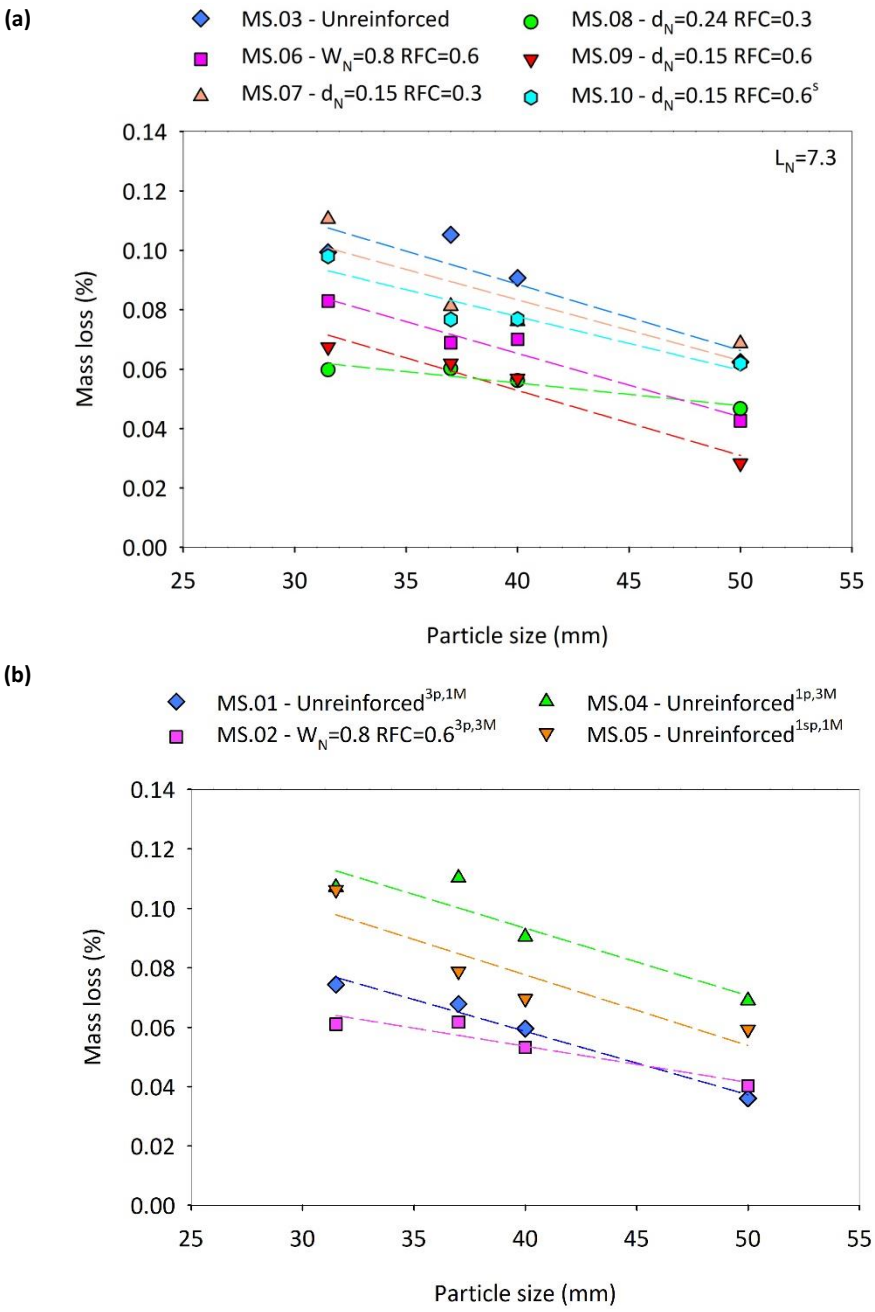

Figure 7-25. Particle mass loss vs size; MS ballast; tests without (a) and with (b) lateral plates; all results showed same trend and are represented in separate plots with the only purpose of reducing the number of data series in each of them

7.9 Summary

A second series of full-size tests was carried out to explore the effect of the addition of filament-like fibres to ballast compared with unreinforced ballast and ballast reinforced with tape-like fibres. Tests also provided a deeper understanding of ballasted track mechanical behaviour, as test set-up was enhanced to assess particle degradation and ballast spreading.

The ballast material was sourced from MS quarry and performed better than CH ballast, which was used in the previous tests. This might be related to either the characteristics of the material or its interaction with the layer of rubber placed beneath it (Section 8.2.1). A newer G44 concrete

sleeper was used, although the one used in the first series of tests was not damaged yet. The filament-like fibres were obtained from thin and thick polypropylene rope, with normalised diameter (d_N) of 0.14 and 0.24 respectively. Two different relative fibre contents were used, i.e. small (RFC = 0.3) and moderate (RFC = 0.6). The effect of the fibre length was not investigated, as it had already been studied in the first batch of tests. In one test, the filament-like fibres were only added to the shoulders, so that results could assist the understanding of the mechanical behaviour of fibre reinforced ballasted track. The tape-like fibres were used only in one test, for comparison. They were designed based on the results from the first part of the testing programme, i.e. normalised fibre width (W_N) of 0.8 and relative fibre content (RFC) of 0.6.

Test outputs common to all tests are the sleeper settlement and resilient deflections, ballast longitudinal pressure, sleeper/ballast contact area and particle degradation. The shoulder lateral movement (or ballast spreading) was monitored only in the first tests, in which no filament-like fibres were used, as the system used to assess it affected sample response.

The main characteristics of ballasted track behaviour can be summarised as follows:

- The settlement increased approximately linearly with the logarithm of the number of cycles. When the ballast was unreinforced or reinforced with tape-like fibres, the settlement accumulated after the first cycles was 4.5 mm. Well selected filament-like fibres reduced it to 3.5 mm.

- The sleeper showed hogging deformed shape, which became more pronounced with the cycles, owing to the middle and rail deflections reducing slightly and those of the sleeper ends increasing. At mid-sleeper and near the rails the resilient deflections were stable in the first $\sim$ 1,000 cycles, beyond which they reduced from 0.5 mm to 0.4 mm and from 0.6 mm to 0.5 mm respectively. At the sleeper ends they were initially between 0.6 mm and 0.9 mm and, after the first 100,000 to 700,000 cycles, increased slightly to 0.7-0.9 mm.

- On average the accumulated longitudinal pressure in the ballast was between 8 kPa and 12 kPa. Beneath the middle of the sleeper, it ranged between 7 kPa and 14 kPa and, especially after the first $\sim$ 3,000 cycles, it increased to 10-16 kPa. The pressure was lower under the rails. Initially it was $\sim$ 8 kPa and, after the first $\sim$ 1,000 cycles, reduced to $\sim$ 7 kPa. In general, the addition of fibres reduced the longitudinal pressure, especially below the middle of the sleeper.

- The sleeper/ballast contact area was very small, i.e. 0.8% to 1.2% on average, and larger at the rails, i.e. 1% to 1.4%, than at the middle, where it was between 1% and 1.4%. The contact area at mid-sleeper was 0.5 to 0.7 times that at the rails.

- The degradation of the ballast particles was marginal. The average mass loss in each test, which is representative of abrasive wear and chipping, was always smaller than 0.1% and only a few particles broke. The percentage mass loss reduced with the particle size. This might be explained by the fact that frictional wear develops on the surface of the particles. The addition of fibres led to smaller frictional wear and chipping and, as particle mass loss seemed proportional to the number of broken particles, can potentially reduce the breakage.

- Track shoulders, like an almost rigid block, shifted laterally as the sleeper settled. Test results suggested the existence of a unique relationship between settlement and lateral movements, which may be fit by a hyperbolic equation. In the first cycles the spreading was about 1/8 of the settlement, while in the long term the rates of the lateral and vertical movements were similar.

Tests showed that properly selected fibres can improve the performance of MS ballast. The addition of a moderate quantity of thin filament-like fibres reduced the sleeper settlement, its tendency to centre-bind and particle degradation. The effectiveness of the reinforcement was strongly dependent on the characteristics of the reinforcement:

- The addition of thin filament-like fibres reduced the settlement after the first cycle by 20% (26% if all cycles are considered) and inhibited the resilient deflections at the rails and sleeper ends, while those at the middle increased slightly. Fibres reduced the longitudinal pressure in the ballast, especially below the middle of the sleeper, leading to a more uniform stress distribution at 3 million cycles. The inclusions did not have a clear effect on the sleeper/ballast contact area. They reduced particle degradation. In general, the effect of the reinforcement increased strongly and approximately linearly with the content for $RFC \leq 0.6$.
- The thick filament-like fibres increased slightly the settlement developed after the first cycle. Compared with thin ones, they further reduced the resilient movements close to sleeper ends and rails, without affecting those at the middle; moreover, they led to even smaller ballast longitudinal pressure. The thick filament-like fibres increased the ballast/sleeper contact area below the middle of the sleeper. They also reduced particle degradation, although the relative fibre content was small.
- The narrow tape-like fibres did not affect the settlement, which reduced marginally only after 300 thousand cycles when the settlement was exacerbated by the installation of three lateral plates in each shoulder. Compared with the filament-like fibres, they were much less effective at reducing the resilient deflections near the rails and sleeper ends, and increased slightly those at the middle; moreover, they gave a smaller reduction of ballast longitudinal pressure beneath middle and rail. Like the filament-like fibres, they gave a more uniform distribution of the long-term ballast longitudinal pressure, did not affect the sleeper/ballast contact area, and reduced particle degradation. The ineffectiveness of the tape-like fibres, compared with the filament-like ones, seems related to them requiring a relatively big initial settlement to become active (Section 8.4)
- When the filament-like fibres were only added to the shoulders, both the total settlement and that developed after the first cycle reduced by 15%. Moreover, only a less particle degradation was observed. The addition of fibres to the shoulders was associated with a particularly pronounced reduction in resilient movements near the rails and sleeper ends, while it did not affect the deflections at mid-sleeper. Compared with uniformly distributed reinforcement, fibres also reduced ballast long-term longitudinal pressure below the middle of the sleeper, while that beneath the rails increased. Like uniform reinforcement, the addition of fibres to the shoulder had no significant effects on the sleeper/ballast contact area.

8 DISCUSSION

8.1 Introduction

Two series of full-size tests were carried out in the Southampton Railway Testing Facility to understand the mechanical behaviour of ballasted track reinforced with tape-like and filament-like fibres. Different ballasts were used, Cliffe Hill (CH) ballast in the first series of tests and Mount Sorrel (MS) ballast in the second. As they showed different performance under cyclic loading, the series of tests were described in separate chapters (Chapter 6 and Chapter 7). In this chapter, all results are considered together to obtain a general understanding of ballasted track mechanical behaviour and the effect of fibre addition on it.

This chapter consists of three main sections followed by conclusions. The first section analyses the results from the tests on unreinforced ballast to identify the main characteristics of its mechanical behaviour. The second section summarises the main effects of the addition of fibres on ballasted track response. These are further discussed and interpreted in the third section to clarify the mechanics of fibre-reinforcement.

8.2 The mechanical behaviour of ballasted track

8.2.1 Cliffe Hill vs Mount Sorrel ballast

The two series of full-size tests carried out as part of this research are not directly comparable, owing to the different behaviour exhibited by CH and MS ballast, especially in terms of resilient deflection and settlement.

The tests using MS ballast showed much greater sleeper resilient deflections (Figure 8-1a). This can be explained by its large particle size. To a first approximation, the number of ballast contacts on the rubber mat placed at the bottom of the rig is inversely proportional to the square of the particle size, which is 42 mm for MS ballast and 34 mm for CH ballast. Hence, the ratio of the force transmitted by an average particle of MS ballast to that transmitted by one of CH ballast would be $(42/34)^2 = 1.53$. As ballast deformability is negligible compared with that of the rubber, especially in the long term, then the average resilient deflection of MS ballast should be 1.53 times greater than that of CH ballast, at least if the deformation of the rubber increases linearly with the particle contact force. This seems consistent with the test results, as the average resilient deflections were 1.5 to 1.6 times bigger in the second series of tests (Figure 8-1b).

The settlement of MS ballast at 3 million cycles was almost 40% less than that of CH ballast (Figure 8-2a). It is possible that MS ballast offered a more stable support, owing to the greater particle size and, perhaps, roughness (Section 5.3.1). Moreover, as observed above, it exerted greater contact forces on the rubber mat placed at the bottom of the rig, causing deeper indentations in the rubber. These might have provided additional resistance to the lateral movement of the particles which, as explained in Section 8.2.5, can inhibit settlement.

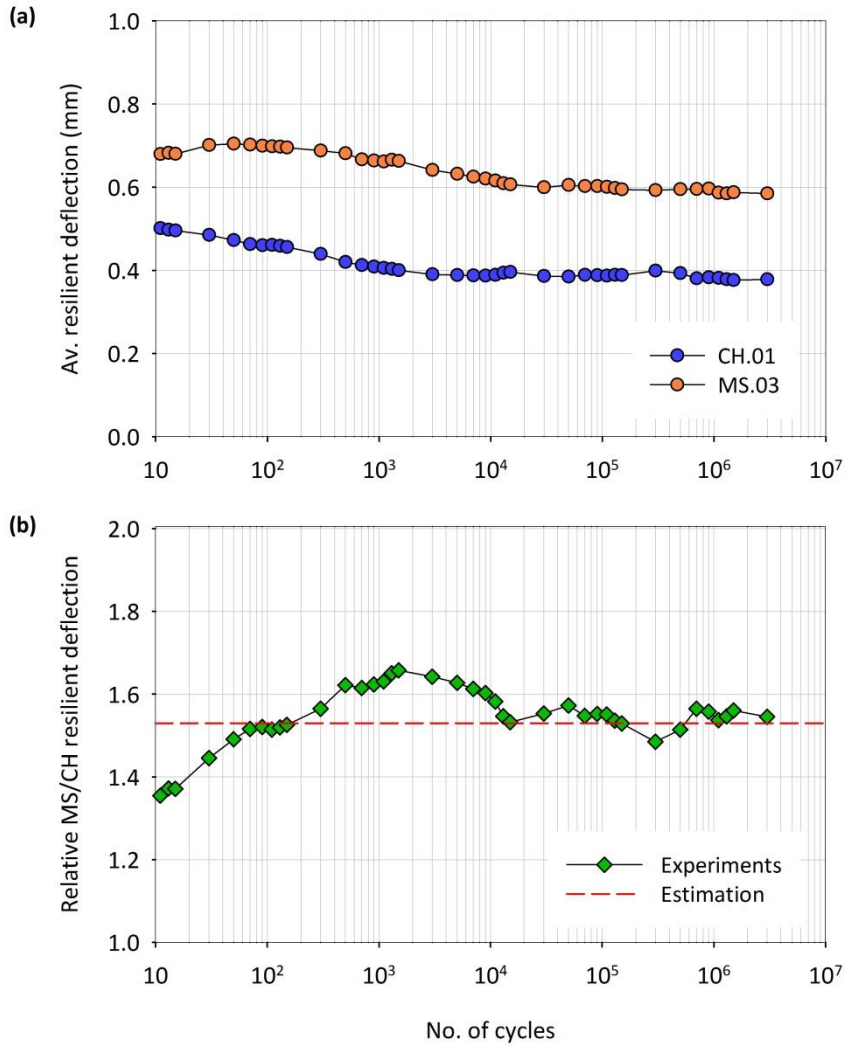

Figure 8-1. (a) Average resilient deflections of CH and MS ballast; (b) ratio of MS ballast to CH ballast deflection

8.2.2 Settlement response

Although CH and MS ballast showed different responses to cyclic loading, their settlement vs logarithm of number of load cycles curves have similar shapes. They are both approximately linear, with 30% to 35% of the total permanent deformation developing in the first cycle (Figure 8-2a), inflection points at ~200 and ~20,000 cycles (Figure 8-2b), and settlement rates reducing rapidly in the first few hundred cycles (Figure 8-2c).

As explained in Section 3.2.2, two phases of the settlement response can be identified, namely Phase 1 (ballast rapid densification or post-compaction) and Phase 2 (ballast long-term settlement at small rate).

Some researchers associate the duration of Phase 1 with the second inflection point of the settlement vs logarithm of the number of cycles, i.e. ~20,000 cycles (Section 3.2.2). However, the first inflection point might be more representative of ballast initial rapid densification, as in the first few hundred cycles the settlement rate reduced rapidly and was accompanied by relatively small lateral movements, as will be clearer in Section 8.2.5.

The development of further plastic deformation in the long term (Phase 2) can be explained by a slip-stick mechanism, as explained in Section 3.3.2. This can develop without particle breakage, which, in fact, was marginal in the laboratory tests (Section 8.2.4). In Phase 2, the settlement was accompanied by significant lateral spreading. As observed in Section 8.2.5, after the first few hundred cycles the rate of the lateral spreading was 0.5 to 0.7 times that of the settlement. This can be explained by the ballast approaching its minimum density in Phase 1, beyond which further particle reorientations tend to push the shoulders aside, causing them to shift laterally like an almost rigid body, as observed in Section 7.7. Therefore, long-term particle rearrangement seems strongly dependent on the freedom of the particles to move laterally, and interventions that stabilise track shoulders might be particularly effective at reducing the settlement. This seems consistent with the laboratory tests, as even light interventions to the shoulders, i.e. the installation of lateral plates (Figure 7-5) and the addition of fibres (Figure 7-15), reduced the settlement.

8.2.3 Sleeper centre-binding

All tests showed signs of sleeper centre-binding, i.e. the gradual loss of support at the sleeper ends (Section 2.3.2.2).

The resilient movement at the middle of the sleeper reduced with the number of cycles while those near the rails remained stable throughout the tests (Figure 8-3). This is explained by the well-confined ballast placed beneath the middle of the sleeper becoming denser and more resistant to permanent deformation while that closer to the shoulders, which is more lightly confined, remained looser and settled more. As a result, the support at the sleeper ends reduced and a greater proportion of the load was transferred to the ballast through the centre of the sleeper, as explained in Section 2.3.2.2.

The trend followed by the resilient movements is consistent with the evolution of ballast longitudinal pressure (Figure 8-4). Under the middle of the sleeper the pressure increased with the number cycles, while it remained stable beneath the rails. This can be explained as follows: in the first cycles the ballast placed beneath the rails and sleeper ends, which was lightly confined and under greater vertical pressure, exhibited greater permanent deformation; as a consequence, a greater proportion of the load was transferred to the centre ballast, which was further compacted and applied increasing pressure to the lateral walls. In contrast, the longitudinal stresses accumulated in the ballast placed under the rails and sleeper ends did not increase, as the vertical pressure exerting it reduced.

The loss of support at the sleeper ends can be expressed in terms of increase in relative sleeper ends-middle deflection compared with the first cycle. As shown in Figure 8-5, beyond a settlement of 4 mm to 5 mm the support at the sleeper ends reduced linearly with the settlement, with MS and CH ballast following a similar pattern. This suggests that track settlement can be estimated based on the evolution of the sleeper resilient deflections.

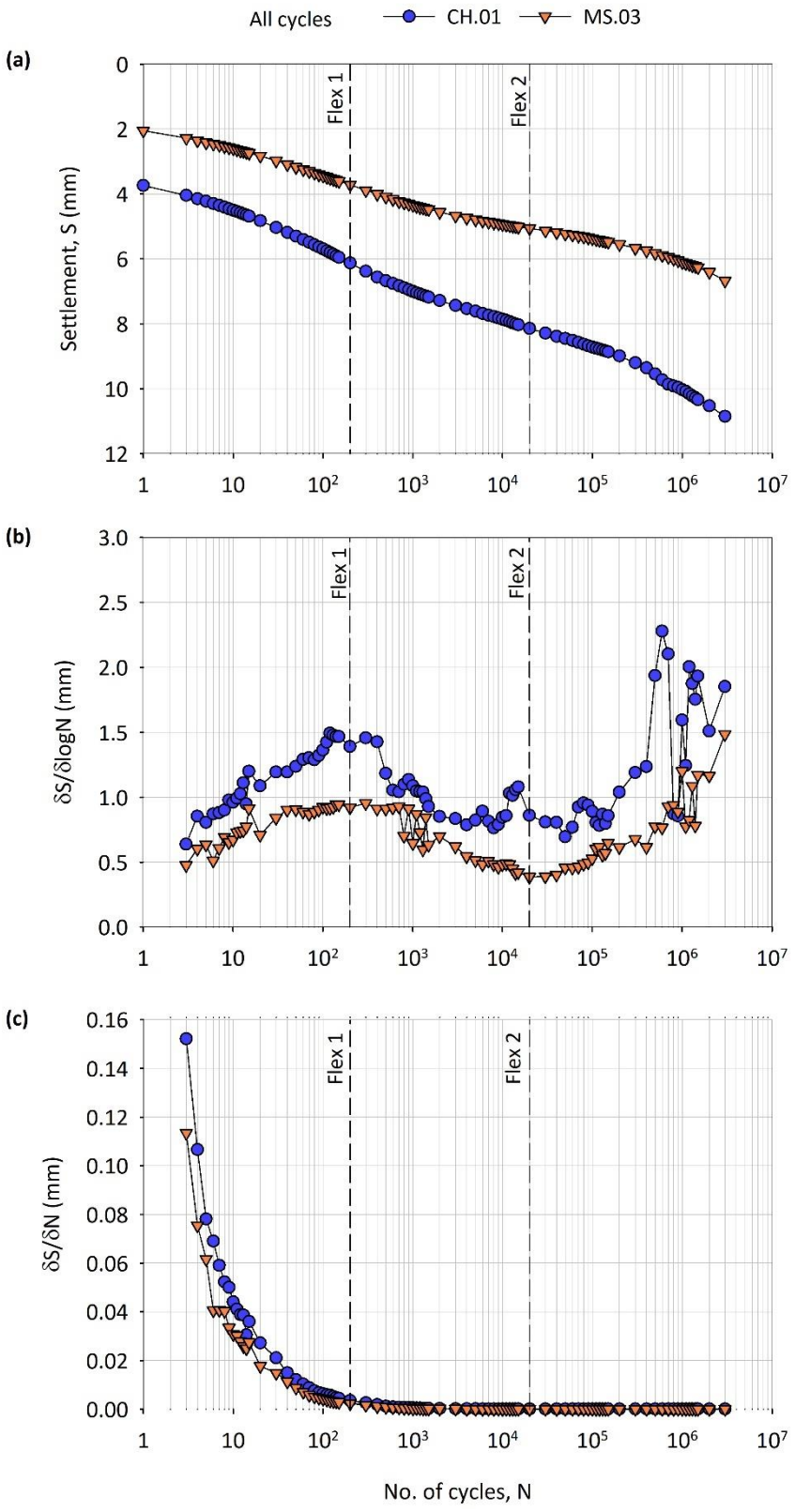

Figure 8-2. Settlement response of unreinforced CH and MS ballast with the number of cycles, N; (a) settlement, S; (b) first derivative of the settlement with respect to the logarithm of the number of cycles ($\delta S/\delta logN$); (c) settlement rate, $\delta S/\delta N$

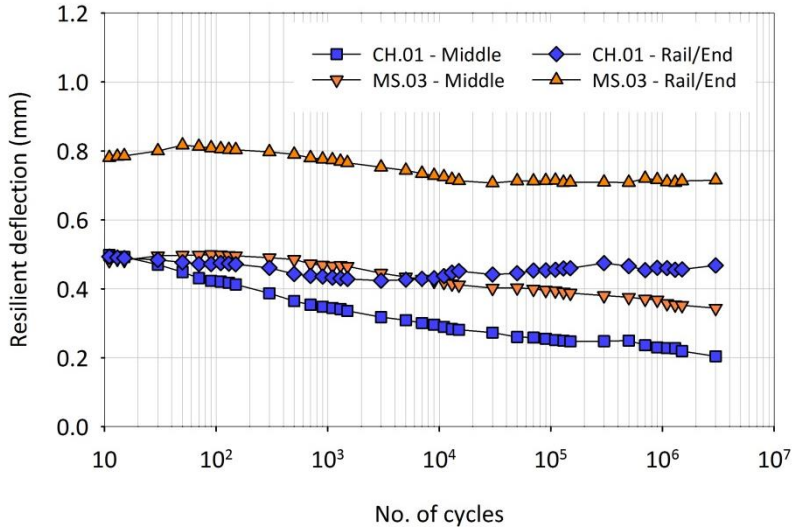

Figure 8-3. Evolution of sleeper resilient deflections at mid-sleeper and near the rails (unreinforced CH and MS ballast)

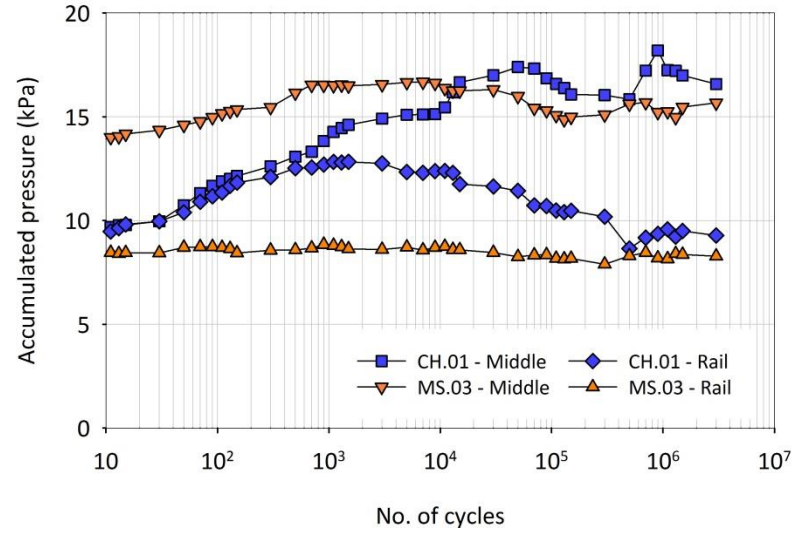

Figure 8-4. Evolution of the longitudinal pressure accumulated (unreinforced CH and MS ballast)

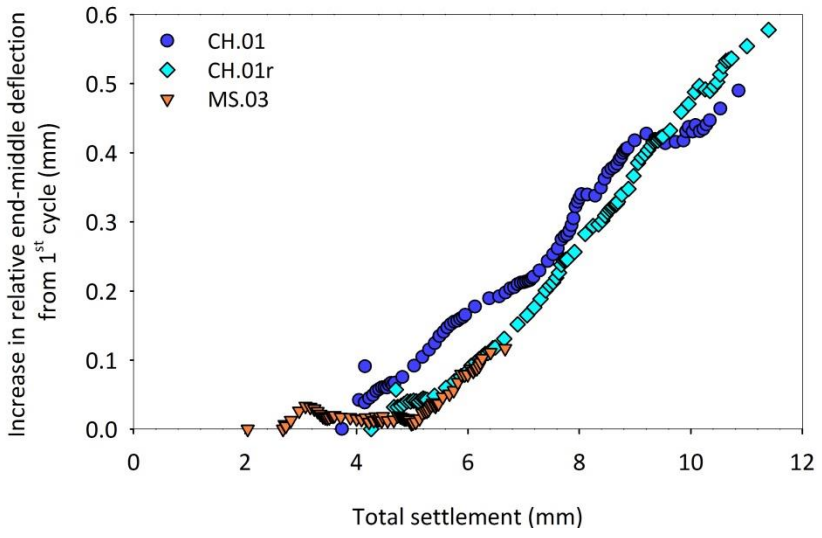

Figure 8-5. Sleeper tendency to centre bind; increase in sleeper hogging vs settlement (unreinforced CH and MS ballast)

8.2.4 Particle degradation

Particle degradation can increase the propensity of a material to settle by reducing the size, angularity and roughness of the particles, hence their ability to interlock (Section 3.3.3). In this research, particle degradation was expressed in terms of mass loss and number of broken particles, the former representative of frictional wear and chipping, the latter of corner breakage and splitting (Section 5.5.5).

The ballast used in the full-size tests was obtained from good quality rock, i.e. granite, and suffered only marginal particle degradation. Under the sleeper, in the top half of the ballast layer, the mass loss associated with frictional wear and chipping was less than 0.1% and fewer than 1.1% of the particles fractured. However, particle degradation was not assessed for the particles directly in contact with the sleeper base, which were subjected to higher stresses.

Surface abrasion at the interparticle contacts can potentially reduce the roughness locally, facilitating particle relative movement. However, the percentage mass loss was independent of the settlement, as explained in Section 8.3.5, suggesting that particle wear and chipping had no significant influence on ballast behaviour. As the number of broken particles was roughly proportional to the mass loss (Figure 7-22), particle breakage is also unlikely to have affected significantly ballast response. This is not surprising, as the effect of the breakage on the PSD was probably less significant than the difference between specimens.

Particle degradation results are consistent with those presented by others, which showed that ballast damage can be significant only at relatively high loading frequency (Section 3.3.3).

8.2.5 Ballast spreading

Ballast spreading was assessed by means of lateral plates installed in the shoulders (Section 5.5.3). These influenced the behaviour of the samples and, therefore, were used only in a limited number of tests, as explained in Section 7.7.

In each of these tests, lateral spreading accompanied settlement. In particular, it increased approximately linearly with the logarithm of the number of cycles but its rate reduced more slowly than that of the settlement (Figure 7-15). Results suggest the existence of a unique hyperbolic relationship between vertical and lateral movements, which is well expressed by Equation (7-1), where S and S_h are respectively the settlement and the spreading accumulated after the first cycle. This equation and its first derivative (dS/dS_h) are represented in Figure 8-6, parts a and b respectively. If the settlement is very small ($S \cong 0$), the lateral movements are marginal compared with the settlement, with $dS/dS_h \cong 9$. The rate of settlement reduces rapidly compared with the rate of spreading, with $dS/dS_h = 2.5$ after only ~2 mm settlement, which corresponds approximately to the transition between Phase 1 and Phase 2 (i.e. first inflection point of Figure 8-2a). In the long term, $dS/dS_h \to 1.4$. The relationship between settlement and spreading seems to justify the distinction between Phase 1 and Phase 2 of the settlement response, as explained in Section 8.2.1. However, further tests may be carried out to investigate the existence of the settlement-spreading relationship under a broader range of conditions (e.g. different ballasts, load magnitude/ frequency etc.).

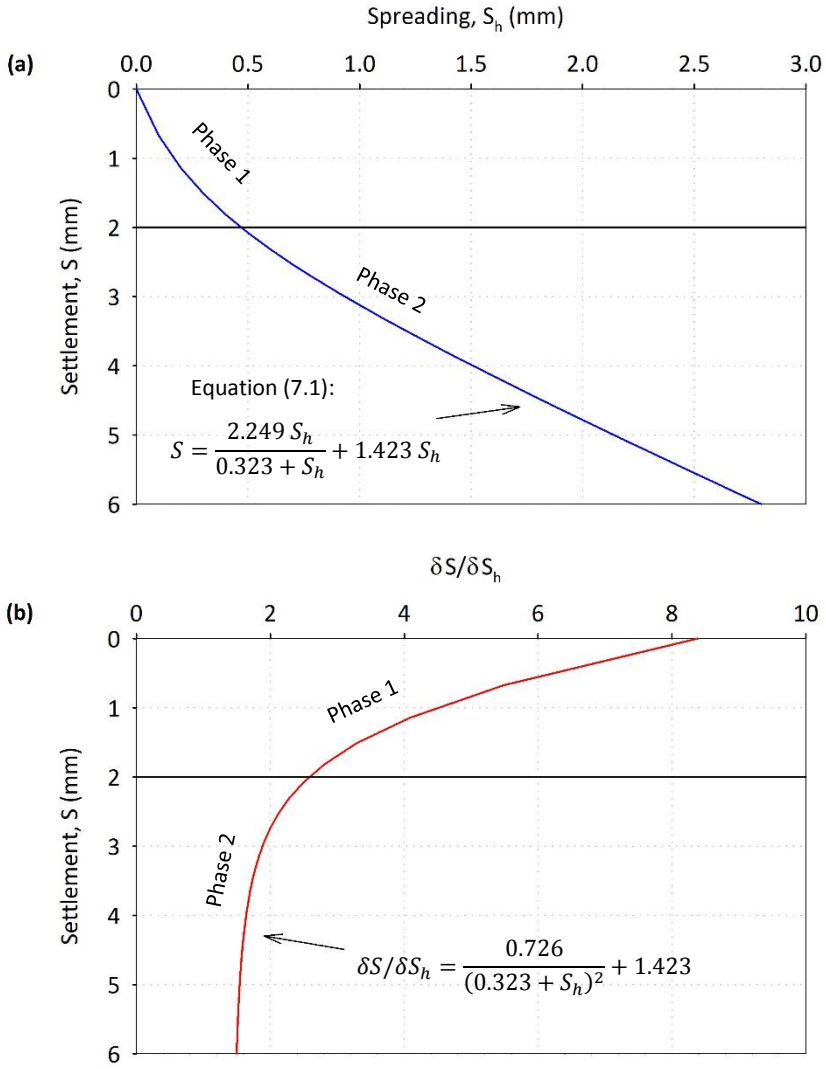

Figure 8-6. Settlement-spreading relationship according to Equation (7-1); transition between Phase 1 and Phase 2 approximately corresponding to the first inflection point of Figure 8-2

8.3 The effect of fibres on ballast mechanical behaviour

8.3.1 Settlement

Properly selected fibres reduced the settlement of ballasts of different characteristics and performance, such as CH and MS ballast. However, the effectiveness of the reinforcement was strongly affected by the properties of the fibres, i.e. their dimensions, content and type.

The first series of tests, in which CH ballast was used, showed that the addition of a moderate amount of narrow tape-like fibres ($RFC \cong 0.6$, $W_N \leq 1.5$) can reduce the settlement by ~20%, if the first load cycle is neglected. The addition of a moderate amount of thin filament-like fibres ($RFC = 0.6$, $d_N = 0.15$) to MS ballast also reduced settlement by ~20%. The tape-like fibres were ineffective at reinforcing MS ballast, but this can be explained by them requiring a certain amount of initial settlement to become active, as discussed in Section 8.4.

The geometry of the inclusions is key to the performance of the reinforcement. Wide tape-like and thick filament-like fibres ($W_N = 2.9, d_N = 0.24$) worsened track performance (Figure 6-1, Figure 7-4). In contrast, the effect of the length was secondary, as very short tape-like fibres ($L_N = 2.2$) were only 4% less effective than the longest ones (L_N = 8.8), as shown in Figure 6-2.

The influence of the fibre content on the settlement was also evident. The tape-like fibres performed best when their content was moderate ($RFC \cong 0.6$), with higher contents ($RFC \cong 0.9$) worsening ballast performance (Figure 6-3). In contrast, the settlement of MS ballast reduced almost linearly with the content of filament-like fibres for $RFC \leq 0.6$, suggesting that higher contents could further reduce it (Figure 7-5).

The addition of filament-like fibres to the shoulders, as shown in Figure 7-2, reduced the settlement by ~20% if the first cycle is neglected, and by ~15% if all cycles are considered (Figure 7-5). Therefore, although it is less effective than uniformly distributed reinforcement, it significantly improved track performance. This confirms that ballast permanent deformation is particularly sensitive to shoulder interventions, as observed in Section 8.2.2.

8.3.2 Resilient deflections

Although all tests showed signs of sleeper centre binding (Section 8.2.3), the magnitude and distribution of the sleeper deflections was affected by the addition of fibres.

Compared with the unreinforced tests, long-term sleeper hogging was inhibited by the addition of moderate contents of tape-like fibres, regardless of their length and width, but exacerbated by high contents (Figure 6-8c, Figure 6-9c, Figure 6-10c, Figure 6-11c). For the filament-like fibres, the hogging reduced approximately linearly with their content and diameter, although the former was limited to $RFC = 0.6$ (Figure 7-8, Figure 7-9, parts c). The reduction of sleeper hogging was particularly pronounced when the fibres were placed only in the shoulders, owing to a significant reduction of the movements of the sleeper ends (Figure 7-8a).

Usually, the inhibition of the sleeper hogging caused by fibre addition was accompanied by a reduction of the sleeper average deflection, as the movements at the sleeper ends and rails reduced and those at middle increased only marginally. Only wide tape-like fibres reduced the sleeper hogging while increasing its average deflection (Figure 6-8 b and c).

Results suggest a generic correlation between settlement and resilient deflections. For the tests using unreinforced or reinforced CH ballast, the resilient movements seem to increase with the settlement (Figure 8-7). For those using MS ballast, only the resilient deflections at the sleeper ends increased with settlement (Figure 8-8). However, this is not always true. For example: thick filament-like fibres reduced the resilient deflections of the sleeper ends but not the settlement; narrow tape-like fibres did not inhibit the settlement of MS ballast but reduced the resilient movements of the sleeper ends; and the addition of fibres to the shoulders gave a particularly pronounced reduction of the resilient movements of the ends, although it represented a less effective reinforcement than uniformly distributed reinforcement.

A stronger correlation is that between the total settlement and sleeper propensity to centre-bind (Figure 8-9), where the latter is expressed by the increase in relative ends-middle deflections

compared with the first cycle. The tests showing a greater increase in sleeper hogging with number of cycles, are those that exhibited greater settlement, as already observed in Section 8.2.3.

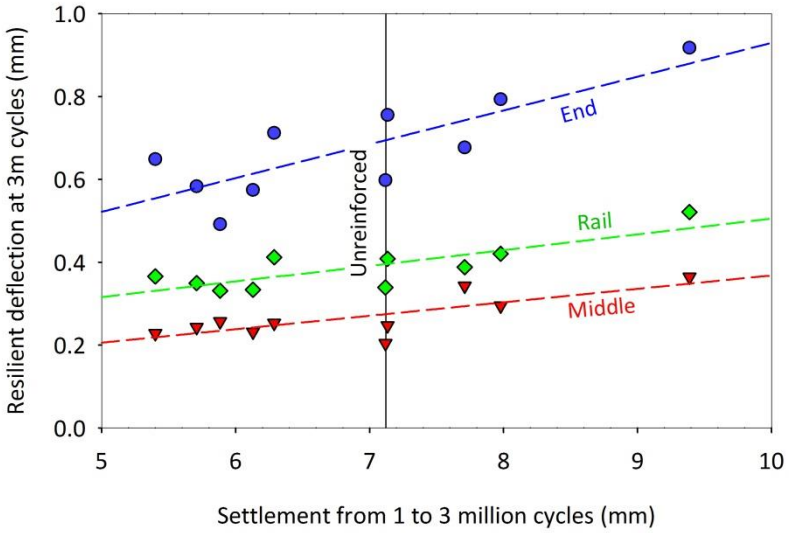

Figure 8-7. Long-term resilient deflections vs settlement for all tests using CH ballast

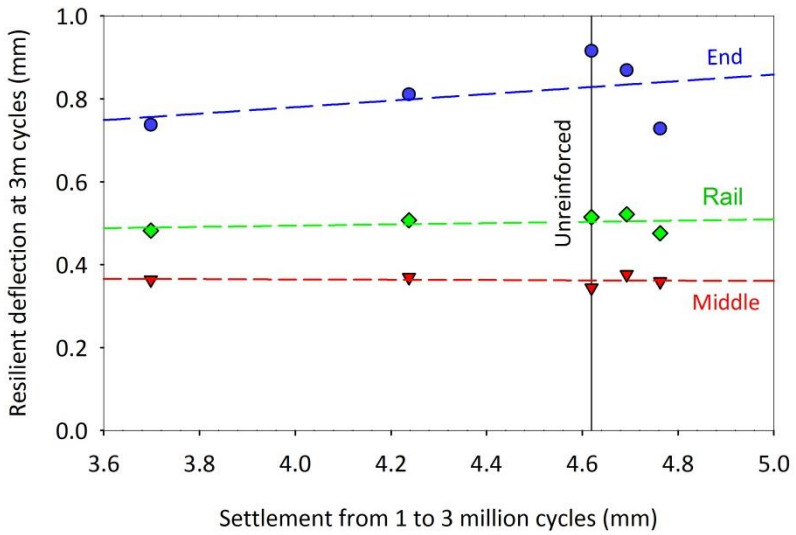

Figure 8-8.Long-term resilient deflections vs settlement for the tests using MS ballast, except those using lateral plates

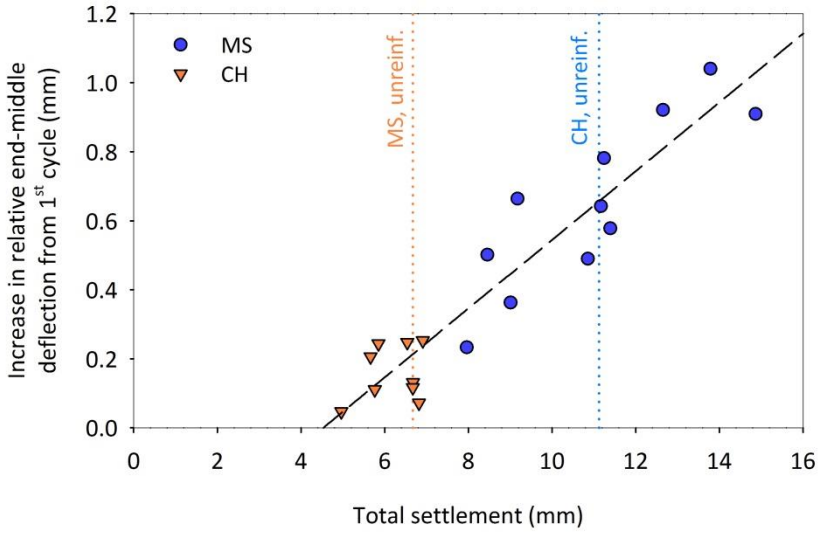

Figure 8-9. Ballast tendency to centre-bind vs settlement for the tests on CH and MS ballast (only the tests using lateral plates are not considered).

8.3.3 Longitudinal pressure

The longitudinal pressure in the ballast reduced with the addition of fibres, especially under the middle of the sleeper, depending on the characteristics of the reinforcement. The addition of tape-like fibres to CH and MS ballast reduced the longitudinal pressure by up to 5 kPa and 2 kPa respectively; and the addition of filament-like fibres to MS ballast by up to 4 kPa.

The effect of the fibres was influenced by their dimensions. The longitudinal pressure was not affected by the width of the tape-like fibres (Figure 6-15) but reduced gradually with their length, with very short fibres having negligible effect (Figure 6-16). The effect of the filament-like fibres increased linearly with their diameter and proportion (Figure 7-11).

The reduction in longitudinal pressure was significantly more pronounced under the middle of the sleeper than beneath the rails; only high contents of tape-like fibres gave a uniform, but much smaller, reduction (Figure 6-13, Figure 6-14). This seems consistent with the effect of the fibres on the resilient deflections, as they reduced the sleeper hogging unless high amounts of tape-like fibres were used (Section 8.3.2). Test results suggest that the longitudinal pressure under the middle of the sleeper tends to increase, compared with that under the rails, with the sleeper hogging. However, the relationship between pressure and resilient deflections is very scattered (Figure 8-10).

The reduction in longitudinal pressure with the addition of fibres seems explained by the ability of the fibres to mobilise tension with ballast deformation, as explained in more detail in Section 8.4.

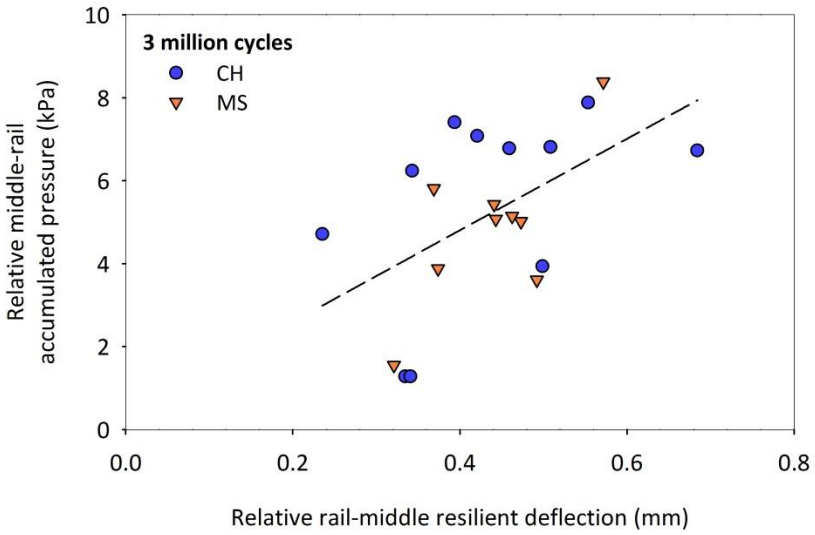

Figure 8-10. Relative rail-middle accumulated pressure vs relative ends-middle deflection (3 million cycles)

8.3.4 Sleeper-ballast contact area

The cumulative area of contact at the interface between the sleeper and the ballast was greater under the rails than the middle of the sleeper (Table 6-2, Table 7-2). This can be explained by the fact that greater particle rearrangement occurred under the rails, where the load was applied and ballast was not well confined compared with that under the middle of the sleeper.

The extent and distribution of the sleeper/ballast contact was affected by the addition of tape-like fibres. Longer and narrower fibres were associated with a smaller average contact area, as it reduced under the rails and increased slightly beneath the middle of the sleeper (Figure 6-19, Figure 6-20,). Only high fibre contents had a different effect, with the contact area increasing both in the middle and below the rails (Figure 6-21, Figure 6-22). As observed above, the cumulative area of contact is expected to increase with the rearrangement of the particles, hence ballast permanent deformation. This seems consistent with test results, as the contact area under the rails tended to increase with the settlement (Figure 8-11).

As observed in Section 7.6, the tests using MS ballast did not show any clear effect of the fibres on the sleeper/ballast contact, owing to the limited number of experiments and the small settlements. However, like those using CH ballast, they suggest that the cumulative contact area under the rails tends to increase with the settlement (Figure 8-12).

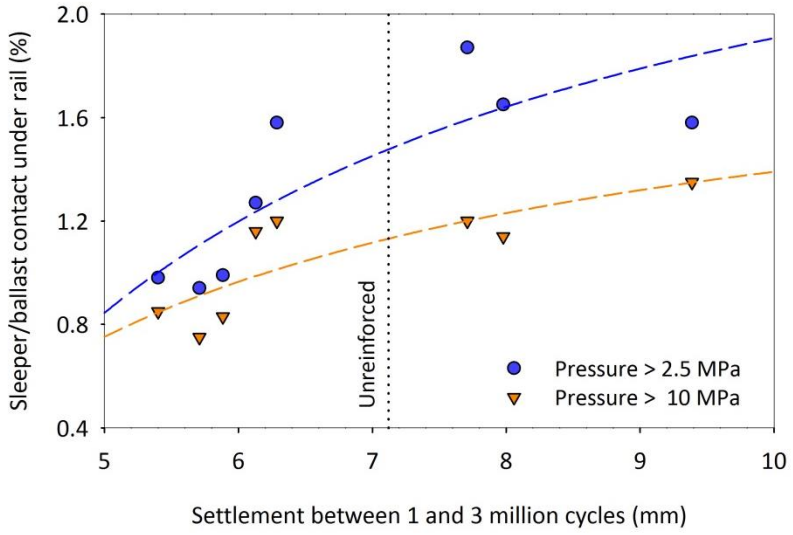

Figure 8-11. Contact area at rail vs settlement (CH ballast)

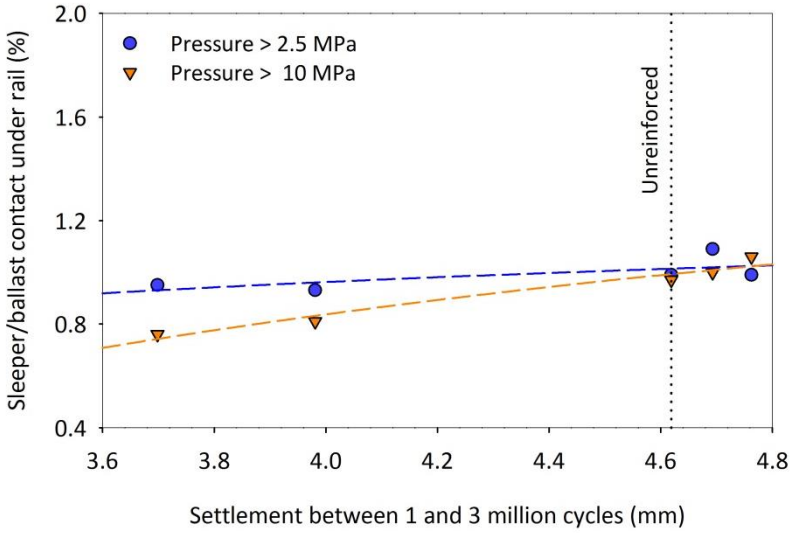

Figure 8-12. Contact area at rail vs settlement (MS ballast)

8.3.5 Particle degradation

Particle degradation was expressed in terms of mass loss and number of broken particles, with the former representative of abrasion and chipping, and the latter of corner breakage and splitting (Section 5.5.5). Only the effect of the fibres on the mass loss could be assessed, as the number of broken particles in each test was not statistically significant. Nevertheless, the former was roughly proportional to the breakage (Figure 7-22). Therefore, to a first approximation, particle degradation can be generally expressed in terms of mass loss.

As observed in Section 7.8, the mass loss was small but was further inhibited by the addition of fibres (Figure 7-21). It reduced with the addition of both tape-like and filament-like fibres and, in particular, with the amount and diameter of the latter (Figure 7-23, Figure 7-24). The addition of fibres to the shoulders reduced slightly the degradation of the particles placed beneath the

sleeper, where no reinforcement was present. This might be explained by a change in the distribution of the sleeper stresses, as observed in Section 8.3.3, or experimental variability.

Although the contribution of particle degradation to ballast response is difficult to quantify, it seems secondary. This is suggested by the absence of a relationship between settlement and particle degradation (Figure 8-13).

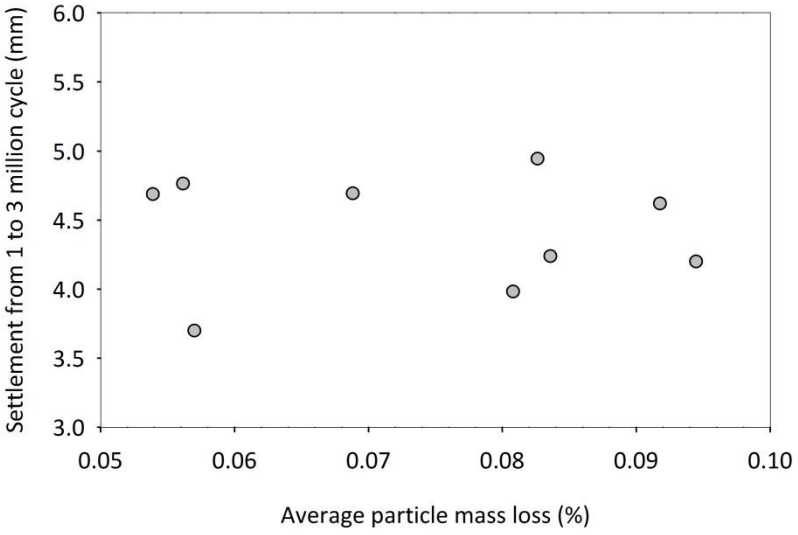

Figure 8-13. Absence of a relationship between settlement and particle degradation (tests using MS ballast)

8.4 On the mechanics of fibre reinforced ballast

As observed in the previous sections, random fibre reinforcement has the potential to improve the performance of ballasted track. It can reduce the settlement and, in turn, tendency of the sleeper to centre-bind, improve the support at the sleeper ends (hence track support stiffness), and reduce ballast damage.

Herein, all test results are analysed in the context of the literature (Chapter 4) to provide a likely explanation of the mechanics of fibre-reinforced ballast. However, as already mentioned, the full-size tests showed only the macro-scale behaviour and, therefore, the interpretations contained in this section will need to be corroborated by further experiments, designed specifically to capture the mechanics of the ballast and fibres at the particle scale.

Fibres are usually regarded as tensile reinforcements that mobilise tension with soil deformation, providing additional confining stress (Section 4.3.1). However, in all tests, ballast exhibited small vertical strain. At 3 million cycles the total settlement was always less than 12 mm for CH ballast and 7 mm for MS ballast. These values correspond to vertical strains of 4% and 2.2% respectively, assuming the strain to be constant with the depth of the ballast layer (i.e. 300 mm). Based on the results from monotonic triaxial tests on fibre reinforced granular materials, described in Section 4.2.2, for such small strain values fibres are expected to reduce, or increase slightly, the mobilised shear strength. Nevertheless, as observed in Section 8.3.3, the fibres reduced the longitudinal pressure accumulated in the ballast layer with the loading cycles, which might be explained by the fibres mobilising tension and providing additional confinement.

The ability of fibre reinforcement to take tension is usually considered proportional to their length, with very short fibres unable to contribute to the tensile strength (Section 4.3.2.2). Therefore, the effect of the additional confining stress was explored indirectly, by varying the length of the inclusions. This study showed that ballast longitudinal pressure reduced linearly with the length of the inclusions, with very short fibres ($L_N = 2.2$) having only a marginal effect (Section 8.3.3). This suggests that, although the specimens exhibited small deformation, the reinforcement mobilised tension and provided additional confinement. The confining effect did not increase with increasing width of the inclusions because, at constant relative fibre content, the total area and volume of reinforcement are independent of the fibre width (in other words, the fibres are fewer in number if they are wider). In contrast, the additional confining stress would be expected to be the greatest for the highest fibre content used. However, for the tape-like fibres, high amount of fibres reduced the confining effect, compared with moderate amounts. This might be explained by excessive fibre overlapping, as will be observed below. Ballast longitudinal pressure was also reduced by the addition of filament-like fibres, proportionally to the diameter and content of the inclusions. Thicker fibres, at constant relative fibre content (hence total length of reinforcement), might mobilise greater tension at a given deformation level because they are stiffer and, perhaps, more likely to engage particles. Higher amounts of filament-like fibres might provide greater additional confining stress due to the greater number of inclusions.

The reduction in ballast longitudinal pressure, which may be explained by the increase in confining stress, was not reflected in a significant improvement of ballast performance, as the longest fibres ($L_N = 8.8$) reduced the settlement by 20%, the shortest ones ($L_N = 2.2$) by 16% (Section 8.3.1). This might be explained by the fact that the additional confining stress was small (the longitudinal pressure reduced by less than 5 kPa) and implies that the permanent deformation of the ballast was mostly inhibited by a different mechanism. The fibres might stabilise the particles by impeding the micro-movements that they exhibit in each load cycle and hence, the slip-stick mechanism responsible for the accumulation of plastic deformation (Section 3.2.2). This would agree with Lees (2017), who observed that the analysis of the behaviour of geogrid reinforced granular soils should not only consider the additional tensile strength provided by the reinforcement, but also its ability to stabilise the grains, for example, by preventing their rotations. In consideration of this, the understanding of the mechanics of fibre reinforced ballast would require further laboratory and numerical experiments designed to capture the movements of the particles.

Other than inhibiting the permanent deformation, the fibres reduced long-term sleeper hogging (Section 8.3.2). Therefore, they must have modified the distribution of the sleeper stresses, reducing the proportion of load transferred to the centre of the sleeper. This is to be consistent with the reduction of the longitudinal pressure in the middle ballast compared with that under the rails (Section 8.3.1).

The change in distribution of the resilient deflections cannot be explained by a smaller permanent deformation of the ballast because the addition of wide or thick fibres reduced hogging and pressure under the middle of the sleeper but increased the settlement. Neither can it be explained by the greatest effectiveness of the fibres closer to the shoulders, where the confinement is smaller (Section 4.3.2.6), as sleeper hogging was reduced by short and long fibres to similar extents. Therefore, it is possible that the reinforcement reduced the stiffness of the

ballast under the middle of the sleeper compared with that closer to the shoulders. As observed by Sadeghi & Beigi (2014), the effect of the fibres on sand stiffness under cyclic loading depends on the on the confining stress (Figure 4-19).

The tests showed that fibres must be carefully selected to avoid negative effects on ballast performance. Wide tape-like fibres and thick filament-like ones (W_N = 1.5, d_N = 2.4) reduced sleeper hogging but increased settlement. This may be explained by the extensive disruption of the packing of the particles caused by wide or thick fibres, as ballast compactability increases dramatically for W_N > 1.5 and d_N > 2 (Section 5.4.3 - Figure 5-14, Figure 5-17). High contents of tape-like fibres ($RFC = 0.9$) increased both settlement and sleeper hogging. Possibly, excessive amounts of platy fibres introduced horizontal planes of weakness, as the inclusions tended to lay horizontally, enhancing the lateral spreading and hence the settlement, as explained in Section 8.2.2. In contrast, high contents of filament-like fibres might not jeopardise the reinforcing effect. This type of reinforcement forms a sort of discrete grid in the granular matrix which is not expected to introduce planes of weakness. In fact, the settlement reduced linearly with increasing content of filament-like fibres, at least for $RFC \leq 0.6$.

The tape-like fibres became effective only after an initial settlement of ~7 mm, including the first loading cycle. This explains their inability to inhibit the permanent deformation of MS ballast, which settled by only 6.7 mm in 3 million cycles. Perhaps, the greater thickness of the filament-like fibres (i.e. 6 mm), compared with the tape-like fibres (i.e. 0.5 mm), allowed for an almost immediate interaction between reinforcement and particles.

Fibre reinforced ballast saw less particle degradation (i.e. abrasive wear, chipping and breakage). This may be explained by the fibres cushioning the particles and hence, mitigating the high local stresses at the interparticle contacts. Particle degradation reduced with increasing diameter and content of filament-like fibres. Thicker fibres can potentially provide stronger stress mitigation. Higher amounts of fibres cushioned a greater proportion of the total particle surface. The effect of a moderate amount of narrow tape-like fibres ($W_N = 0.8$, $RFC = 0.6$) on particle wear was similar to that of a moderate amount of thin filament-like fibres ($d_N = 0.15$, $RFC = 0.6$).

8.5 Summary

The common features of the mechanical behaviour of ballasted track were identified through the analysis of the results of the tests using unreinforced CH and MS ballast:

- The tests using MS ballast showed greater resilient deflections and smaller settlement, compared with the tests using CH ballast. MS ballast consisted of bigger particles and, therefore, transferred the vertical load to the rubber mat placed at the bottom of the rig through a smaller number of contact points, increasing the local stresses and deformation in the rubber, hence the overall sleeper resilient deflection. This seems to be corroborated by simple calculations. The higher localised stresses caused deeper indentations in the rubber, which, possibly, restrained particle lateral movements, increasing track confinement and reducing the settlement. However, the smaller settlement of MS ballast might also be related to the greater size and, perhaps, roughness of its particles.

- The settlement increased approximately linearly with logarithm of the number of load cycles, with ~1/3 of the total permanent deformation developing in the first cycle, and inflection points at ~200 and ~20,000 cycles. The first inflection point seems to mark the transition between Phase 1 (rapid densification) and Phase 2 (long-term settlement). Initially, the settlement developed rapidly and was accompanied by marginal ballast spreading. In Phase 1, its rate reduced dramatically and became comparable to that of the spreading; in Phase 2, the settlement rate was very small and comparable to the spreading rate, suggesting that the permanent deformation of highly compacted ballast is strongly dependent on the freedom of the shoulders to move laterally.

- The evolution of the distribution of sleeper resilient deflections and ballast longitudinal pressures with number of load cycles suggests that each test exhibited sleeper centre-binding. The ballast closer to the shoulders, which is more lightly confined, exhibited greater permanent deformation, reducing the support at the sleeper ends. Hence a greater proportion of load was transferred through the centre of the sleeper to the middle ballast, which compacted, became stiffer and exerted greater pressure on the sides of the rig. In contrast, closer to the shoulders, the longitudinal pressure did not increase, because the stresses placed on the ballast reduced. After an initial settlement of 4-5 mm, sleeper hogging shape increased linearly with the permanent deformation of the ballast bed, as the sleeper tended to centre-bind.

- The degradation of the particles (i.e. surface abrasion, chipping, corner breakage and splitting) was marginal and did not appear to affect significantly ballast response in laboratory conditions.

- Ballast spreading was caused by the shoulders shifting laterally like almost rigid blocks. Vertical and lateral movements seem linked by a hyperbolic relationship, which should be investigated under a broader range of conditions (e.g. ballast type, loading magnitude/frequency, confinement etc.).

The addition of fibres affected the behaviour of ballasted track. Compared with the unreinforced tests, moderate contents of long narrow tape-like and thin filament-like fibres reduced settlement, sleeper hogging and longitudinal pressure in the ballast, especially in the middle. Very short fibres were slightly less effective at reducing the settlement and did not reduce the longitudinal pressure. Wide tape-like fibres and thick filament-like fibres increased settlement. Compared with moderate amounts of tape-like fibres, high contents led to greater settlement, sleeper hogging and ballast longitudinal pressure.

Test results have been analysed to provide a likely description of the mechanics of fibre-reinforced ballast:

- Longitudinal stress in the ballast reduced with the length of the inclusions, suggesting that fibres mobilised tension and provided additional confining stress. The latter seems to increase with content and thickness of filament-like fibres, hence their number and stiffness. Only high contents of tape-like fibres did not reduce significantly the longitudinal pressure. This might have been a result of excessive fibre overlapping, which

introduced horizontal planes of weakness, reducing ballast resistance to lateral movements.

- Long fibres reduced the settlement by 20%, short fibres by 16%, although the latter providing only marginal additional confining stress. Therefore, the additional confining stress, which was always less than 5 kPa, can only partly justify the improved ballast performance. However, as observed by Lees (2017), the performance of granular materials is also improved through the stabilisation of the particles. The presence of inclusions might have inhibited the micro-movements that the particles exhibited in each cycle, hence the slip-stick mechanism responsible for the accumulation of plastic deformation. Further laboratory and numerical experiments should be designed to capture fibre/particle interaction and allow for a clearer understanding of the micromechanics of fibre-reinforcement.

- Fibre-reinforcement is not always effective: wide tape-like and thick filament-like fibres might increase the settlement, as they significantly disrupt the packing of the particles and, if $W_N > 1.5$ and $d_N > 2$, increase ballast compactability (Section 5.4.3); high contents of tape-like fibres might reduce ballast resistance to lateral movements, as observed above; tape-like fibres, perhaps because they are very thin, were effective only after an initial ~7 mm settlement and, as a result, were unable to reinforce MS ballast.

- The analysis of test results suggested that the reinforcement modified the distribution of the support stiffness along the length of the sleeper, with the middle ballast becoming softer compared with that closer to the shoulders. As a result, fibres reduced sleeper hogging and proportion of load transferred to centre of the sleeper. This might be explained by the effect of the fibres on the stiffness varying with the confining pressure, as with fibre reinforced sand (Section 4.2.4). Only high contents of tape-like fibres increased sleeper hogging but this, as observed above, might be caused by an excessive fibre overlapping.

- In general, the tests exhibiting smaller settlement were characterised by a slower development of sleeper centre-binding and smaller sleeper/ballast contact area beneath the rail owing to the inhibition of particle rearrangement.

- The addition of fibres reduced particle degradation. This was attributed to a cushioning effect, which mitigated the stresses at the interparticle contacts and increased with increasing fibre thickness and content.

9 CONCLUSIONS

9.1 General conclusions

The aim of this research was to investigate the potential of a novel technique to improve the performance of ballasted track, which involves the addition of unbound randomly placed discrete fibres to ballast. This was achieved through two series of full-size laboratory tests conducted in the Southampton Railway Testing Facility, a reproduction of a full-size section of single line track including one sleeper and subjected to cyclic loading representative of train passage. Alongside the full-size tests, a large number of bulk density tests was carried out to assess the effect of the fibres on the natural packing of the particles.

The first series of tests used Cliffe Hill (CH) ballast and tape-like fibres, obtained from polyethylene damp proof course. The second one, used Mount Sorrel (MS) ballast, filament-like fibres, obtained from polypropylene rope, and, for comparison, tape-like fibres optimised from the first series of tests.

To account for the relative fibre-particle size, fibre length L_f, width W_f and diameter d_f were normalised to the average particle size D_{50}, i.e. $L_N = L_f/D_{50}$, $W_N = W_f/D_{50}$, $d_N = d_f/D_{50}$; the fibre content was expressed in terms of relative fibre content (RFC), i.e. the content normalised to the maximum content to avoid excessive fibre overlapping.

From the full-size tests using unreinforced ballast, the following characteristics of ballasted track behaviour can be identified:

- The settlement vs logarithm of number of cycles curves were approximately linear, with ~1/3 of the settlement developing in the first cycle, and inflection points at ~200 and ~20,000 cycles. Before the first inflection point, the settlement developed rapidly and ballast spreading was relatively small (Phase 1). In the longer-term, the settlement rate was particularly small and comparable to that of the spreading (Phase 2), suggesting that the settlement of highly compacted ballast is strongly dependent on the possibility of the shoulders to move laterally.

- All tests exhibited sleeper centre-binding. Sleeper hogging increased with the number of cycles, as the support of the sleeper ends reduced. Hence, a greater proportion of load was transferred to the ballast placed under the middle of the sleeper, which compacted, became stiffer and exerted greater pressure on the sides of the rig. After a small initial settlement, i.e. 4-5 mm, sleeper hogging increased linearly with the settlement which, therefore, can be potentially estimated based on the change in resilient movements.

- Particle degradation (i.e. surface abrasion, chipping, corner breakage and splitting) was marginal and did not affect ballast behaviour. However, real track might be subjected to more severe loading and exhibit greater particle damage.

- Settlement and lateral spreading seem linked by a unique hyperbolic relationship, showing an initial curvature and tending to a line. However, this should be further

investigated under a broader range of conditions (e.g. ballast type, load magnitude and frequency, confinement etc.).

- The cumulative sleeper/ballast contact area tended to increase with particle rearrangement, hence ballast permanent deformation.

The main effects of the addition of fibres on ballasted track behaviour can be summarised as follows:

- Moderate contents of narrow tape-like and thin filament-like fibres ($W_N \leq 1.5$, $d_N = 0.15$) reduced settlement, long-term sleeper hogging and, depending on their length, the longitudinal pressure in the ballast, especially under the middle of the sleeper. It is believed that the fibres stabilised the ballast particles by inhibiting the micro-movements they experienced in each load cycle and hence, the slip-stick mechanism responsible for the accumulation of permanent strain. Moreover, they provided some additional confinement. This, however, had little impact on ballast performance, as very short fibres ($L_N = 2.2$) were only slightly less effective than the longest ones tested ($L_N = 8.8$).

- Tape-like fibres reduced ballast permanent deformation only after an initial settlement of ~7 mm, while filament-like fibres, possibly because of their greater thickness, provided immediate stabilising effect.

- Fibres, except for high contents of tape-like inclusions, modified the distribution of the resilient deflections, reducing sleeper hogging, hence the proportion of load transferred to the ballast under the middle of the sleeper. This suggests that fibre-reinforcement changed the distribution of the support stiffness along the length of the sleeper, with middle ballast becoming softer compared with that closer to the shoulders.

- Wide tape-like fibres and thick filament-like fibres ($W_N = 2.9$, $d_N = 0.24$) reduced sleeper hogging and ballast longitudinal pressure but increased the settlement, as they significantly disrupted the packing of the particles. This agrees with the results of the bulk density tests, which showed that ballast compactability increases dramatically if $W_N >$ 1.5 or d_N > 0.2.

- High contents of tape-like fibres increased settlement and sleeper hogging, and reduced only marginally ballast longitudinal pressure. Possibly, they introduced horizontal planes of weakness, due to their tendency to lie horizontally combined with significant fibre overlapping, which might have reduced ballast resistance to lateral movements. In contrast, filament-like fibres formed a discrete grid that is not expected to jeopardise ballast lateral resistance and, in fact, their effectiveness increased linearly with their content, for $RFC \leq 0.6$.

- The addition of filament-like fibres only to the shoulders was surprisingly effective, compared with uniformly distributed reinforcement, especially in the long-term. Moreover, small interventions to the shoulders, such as the installation of lateral plates, affected the settlement. This highlights the critical role of track shoulders.

- Although particle degradation was marginal in laboratory conditions, it reduced with the content and thickness of the fibres, suggesting that the inclusions provided a cushioning effect that mitigated the high stress levels at interparticle contacts.

It can be concluded that fibres can improve the performance of ballasted track by reducing the settlement, increasing the long-term support of the sleeper ends (hence track stiffness) and reducing ballast damage. Fibres should be carefully selected so that they do not produce significant disruption of the packing of the particles or planes of weakness. Otherwise, they might even worsen track performance. Although the micromechanics of fibre-reinforcement could not be investigated in detail, as tests captured only the macro-scale behaviour of ballast, the analysis of test results suggested that fibres may: stabilise the particles by inhibiting their micro-movements in each cycle; provide small additional confinement which, however, may have little effect on the settlement; change the distribution of sleeper stresses by reducing the stiffness of the ballast under the middle of the sleeper compared with that closer to the shoulders.

9.2 Further research

This research provided input for further investigations:

- Micromechanics of unreinforced and fibre-reinforced ballast

  Specific laboratory and numerical experiments, able to capture ballast and fibres behaviour at the particle scale, should be designed to clarify the micromechanics of fibre-reinforcement.

- Practicality of fibre-reinforcement

  Field trials should be conducted to assess real-life performance of fibre-reinforced ballast (one such trial is already underway). These should be associated with life cycle assessment and life cycle cost analyses to assess the performance of fibre-reinforcement compared with other methods of track improvement.

- Laboratory vs real track behaviour

  Laboratory tests cannot faithfully reproduce track conditions or reliably predict track behaviour and, therefore, are mainly used for comparative purposes. Therefore, the results from laboratory tests and field monitoring should be carefully compared with further understand the extent to which the tests may be able to predict real track response, proposing, where possible, appropriate correlations to facilitate such predictions. Modifications of the testing methods could also be proposed, with the aim of obtaining a more realistic representation of track performance.

- Effect of shoulder interventions on track performance

  This research highlighted the critical role of ballast shoulders and, in particular, the potential for intervention on them to significantly improve track performance. In consideration of this, it is recommended to further investigate the effectiveness of novel methods to inhibit shoulder lateral movements.

REFERENCES

Abadi T. (2014). Effect of Sleeper and Ballast Interventions on Rail Track Performance. PhD thesis, University of Southampton.

Abadi T., Pen L. Le, Zervos A. & Powrie W. (2016a). A Review and Evaluation of Ballast Settlement Models using Results from the Southampton Railway Testing Facility (SRTF). In *Proceedings of the 3rd International Conference on Transportation Geotechnics*. Procedia Engineering, pp. 999–1006. Available at: http://dx.doi.org/10.1016/j.proeng.2016.06.089

Abadi T., Pen L. Le, Zervos A. & Powrie W. (2016b). Improving the performance of railway tracks through ballast interventions. *Proceedings of the Institution of Mechanical Engineers, Part F: Journal of Rail and Rapid Transit*, 0(0), pp.1–19. Available at: http://pif.sagepub.com/lookup/doi/10.1177/0954409716671545

Abadi T., Le Pen L., Zervos A. & Powrie W. (2015). Measuring the Area and Number of Ballast Particle Contacts at Sleeper-Ballast and Ballast-Subgrade Interfaces. *International Journal of Railway Technology*, 4(2), pp.45–72.

Aingaran S. (2014). Experimental investigation of static and cyclic behaviour of scaled railway ballast and the effect of stress reversal. PhD thesis, University of Southampton.

Ajayi O., Le Pen L., Zervos A. & Powrie W. (2017a). A behavioural framework for fibre-reinforced gravel. *Géotechnique*, 67(1), pp.56–68. Available at: http://www.icevirtuallibrary.com/doi/10.1680/jgeot.16.P.023

Ajayi O., Le Pen L., Zervos A. & Powrie W. (2014). Effects of Random Fibre Reinforcement on the Density of Granular Materials. In *International Symposium on Geomechanics from Micro and Macro*. Cambridge, UK, 01 - 03 Sep 2014: CRC Press; Balkema, pp. 1363–1367.

Ajayi O., Le Pen L., Zervos A. & Powrie W. (2017b). Scaling relationships for strip fibre-reinforced aggregates. *Canadian Geotechnical Journal*, 54(5), pp.710–719. Available at: https://doi.org/10.1139/cgj-2016-0346

Ajayi O.O. (2014). The Effect of Fibre Reinforcements on the Mechanical Behaviour of Railway Ballast. PhD thesis, University of Southampton.

AJP Automotive LTD (2018). Prescale. Available at: http://www.prescale.co.uk/prescale/prescale.html [Accessed June 10, 2018]

Al-Saoudi N.K.S. & Hassan K.H. (2014). Behaviour of Track Ballast Under Repeated Loading. *Geotechnical and Geological Engineering*, 32(1), pp.167–178. Available at: http://link.springer.com/10.1007/s10706-013-9701-z

Alonso-Marroquín F. & Herrmann H.J. (2004). Ratcheting of granular materials. *Physical review letters*, 92(5), p.54301.

Anderson W.F. & Fair P. (2008). Behavior of Railroad Ballast under Monotonic and Cyclic Loading. *Journal of Geotechnical and Geoenvironmental Engineering*, 134(3), pp.316–327. Available at: http://cedb.asce.org/cgi/WWWdisplay.cgi?163100

Aursudkij B., McDowell G.R. & Collop A.C. (2009). Cyclic loading of railway ballast under triaxial conditions and in a railway test facility. *Granular Matter*, 11(6), pp.391–401. Available at: http://link.springer.com/10.1007/s10035-009-0144-4

Bathurst R.J. & Raymond G.P. (1987). Geogrid reinforcement of ballasted track. *Transportation Research Record*, (1153), pp.8–14.

Boussinesq J. V. (1985). Application des potentials à l'etude de l'equilibre et du mouvement des solids elastiques. Paris: Gauthier-Villars.

Brown S.F., Kwan J. & Thom N.H. (2007). Identifying the key parameters that influence geogrid reinforcement of railway ballast. *Geotextiles and Geomembranes*, 25(6), pp.326–335.

BS 500:2000. Steel Sleepers. British Standards Institution.

BS EN 1097-6:2000. Tests for mechanical and physical properties of aggregates - Part 6: Determination of particle density and water absorption. British Standards Institution.

BS EN 13145:2001+A1:2011. Railway applications — Track — Wood sleepers and bearers. British Standards Institution.

BS EN 13230-1:2009. Railway Applications - Track - Concrete Sleepers and Bearers - Part 1: General Requirements. British Standards Institution.

BS EN 13230-2:2009. Railway Applications - Track - Concrete Sleepers and Bearers - Part 2: Prestressed monoblock sleepers. British Standards Institution.

BS EN 13230-3:2009. Railway Applications - Track - Concrete Sleepers and Bearers - Part 3: Twin-block reinforced sleepers. British Standards Institution.

BS EN 13230-4:2009. Railway Applications - Track - Concrete Sleepers and Bearers - Part 4: Prestressed bearers for switches and crossings. British Standards Institution.

BS EN 13230-5:2009. Railway Applications - Track - Concrete Sleepers and Bearers - Part 5: Special elements. British Standards Institution.

BS EN 13450:2002. Aggregates for railway ballast. British Standards Institution.

BS EN 13481:2012. Railway applications — Track — Performance requirements for fastening systems Part 1 : Definitions. British Standards Institution.

BS EN 13674:2011. Railway applications — Track — Rail. British Standards Institution.

BS EN 933-1:2012. Tests for geometrical properties of aggregates. Part 1 : Determination of particle size distribution — Sieving method. British Standards Institution.

BS EN ISO 14688-2:2004+A1:2013. Geotechnical investigation and testing - Identification and classification of soil - Part 2: Principles for a classification. British Standards Institution: British Standards Institution.

Cahill P., Nuallain N.A.N., Jackson N., Mathewson A., Karoumi R. & Pakrashi V. (2014). Energy Harvesting from Train-Induced Response in Bridges. *Journal of Bridge Engineering*, 19(9), pp.1–11. Available at: http://ascelibrary.org.ezlibproxy1.ntu.edu.sg/doi/10.1061/(ASCE)BE.1943-5592.0000608

Casagrande M.D.T. (2005). Behavior of fiber-reinforced soils under large shear strains. University of Rio Grande do Sul, Porto Alegre, Brazil.

Christie D., Nimbalkar S. & Indraratna B. (2009). The performance of rail track incorporating the effects of ballast breakage, confining pressure and geosynthetic reinforcement. In Tutumluer & Al-Qadi, eds. *Bearing Capacity of Roads, Railways and Airfields*. London: CRC Press, pp. 5–24. Available at: http://www.crcnetbase.com/doi/abs/10.1201/9780203865286.ch2

Claisse P. & Calla C. (2006). Discussion: Rail ballast specification: conclusions from a historical perspective. *Proceeding of the Institution of Civil Engineers - Transport*, 159(TR2), pp.69–74. Available at: http://www.icevirtuallibrary.com/doi/10.1680/tran.2007.160.3.147

Consoli N.C., Casagrande M.D.T., Thome A., Dalla Rosa F. & Fahey M. (2009). Effect of relative density on plate loading tests on fibre-reinforced sand. *Geotechnique*, 59(5), pp.471–476. Available at: https://doi.org/10.1680/geot.2007.00063

Dahlberg T. (2001). Some railroad settlement models - a critical review. *Journal of Rail and Rapid*

Transit, 215 Part F(4), pp.289–300. Available at: http://pif.sagepub.com/content/215/4/289

Dash S.K. & Shivadas A.S. (2012). Performance Improvement of Railway Ballast Using Geocells. *Indian Geotechnical Journal*, 42(3), pp.186–193.

Dersch M.S., Tutumluer E., Peeler C.T. & Bower D.K. (2010). Polyurethane Coating of Railroad Ballast Aggregate for Improved Performance. In *ASME/IEEE Joint Rail Conference*. Urbana, Illinois, USA, pp. 337–342.

Diambra A., Ibraim E., Russell A.R. & Muir Wood D. (2013). Fibre reinforced sands: from experiments to modelling and beyond. *Int. J. Numer. Anal. Meth. Geomech.*, 37, pp.2427–2455.

Diambra A., Russell A.R., Ibraim E. & Muir Wood D. (2007). Determination of fibre orientation distribution in reinforced sands. *Géotechnique*, 57(7), pp.623–628.

Draft BS ISO 12856 (2012). Plastic railway sleepers (railroad ties). British Standards Institution.

Esveld C. (2001). Moder Railway Track. MRT Productions.

García-Rojo R., Alonso-Marroquín F. & Herrmann H.J. (2005). Characterization of the material response in granular ratcheting. *Physical Review E*, 72(4), p.41302. Available at: https://link.aps.org/doi/10.1103/PhysRevE.72.041302

Gobel C.H., Weisemann U.C. & Kirschner R.A. (1994). Effectiveness of a Reinforcing Geogrid in a Railway Subbase Under Dynamic Loads. *Geotextiles and Geomembranes*, 13(2), pp.91–99.

Godley D. (2015). Ballast and Beyond - Keynote Address. *Presentation from PWI meeting of May 2015*.

Gray D.H. & Ohashi H. (1983). Mechanics of Fiber Reinforcement in Sand. *Journal of Geotechnical Engineering*, 109(3), pp.335–353. Available at: http://ascelibrary.org/doi/10.1061/%28ASCE%290733-9410%281983%29109%3A3%28335%29

Guérin N., Sab K. & Moucheront P. (1999). Identification expérimentale d'une loi de tassement du ballast. *Canadian Geotechnical Journal*, 36(3), pp.523–532. Available at: http://www.nrcresearchpress.com/doi/abs/10.1139/t99-004

Hardin B.O. (1985). Crushing of soil particles. *Journal of Geotechnical Engineering*, 111(10), pp.1177–1192. Available at: http://ascelibrary.org/doi/pdf/10.1061/(ASCE)0733-9410(1985)111%3A10(1177)

Heineck K.S., Coop M.R. & Consoli N.C. (2005). Effect of Microreinforcement of Soils from Very Small to Large Shear Strains. *Journal of Geotechnical and Geoenvironmental Engineering*, 131(8), pp.1024–1033.

Holtz W.G. & Gibbs H.J. (1956). Triaxial shear tests on pervious gravelly soils. *Journal of the Soil Mechanics and Foundation Division*, 82(1), pp.1–22.

Hossain Z., Indraratna B., Darve F. & Thakur P.K. (2007). DEM analysis of angular ballast breakage under cyclic loading. *Geomechanics and Geoengineering*, 2(3), pp.175–181. Available at: http://www.tandfonline.com/doi/abs/10.1080/17486020701474962

Hu J., Bian X. & Jiang J. (2016). Critical Velocity of High-speed Train Running on Soft Soil and Induced Dynamic Soil Response. In *The 3rd International Conference on Transportation Geotechnics*. Elsevier B.V., pp. 1034–1042. Available at: http://dx.doi.org/10.1016/j.proeng.2016.06.102

Hussaini S.K.K., Indraratna B. & Vinod J.S. (2015). Performance assessment of geogrid-reinforced railroad ballast during cyclic loading. *Transportation Geotechnics*, 2, pp.99–107.

Indraratna, B., Lackenby, J., and Christie D. (2005). Effect of Confining Pressure on the Degradation of Ballast under Cyclic Loading. *Geotechnique, Institution of Civil Engineers, UK*, 55(4), pp.325–328.

Indraratna B., Biabani M.M. & Nimbalkar S. (2015). Behavior of Geocell-Reinforced Subballast Subjected to Cyclic Loading in Plane-Strain Condition. *Journal of Geotechnical and Geoenvironmental Engineering*, 141(1).

Indraratna B. & Nimbalkar S. (2013). Stress-Strain Degradation Response of Railway Ballast Stabilized with Geosynthetics. *Journal of Geotechnical and Geoenvironmental Engineering*, 139(5), pp.684–700.

Indraratna B., Nimbalkar S., Christie D., Rujikiatkamjorn C. & Vinod J. (2010). Field assessment of the performance of a ballasted rail track with and without geosynthetics. *Journal of Geotechnical and Geoenvironmental Engineering*, 136(7), pp.907–917. Available at: http://ascelibrary.org/doi/abs/10.1061/(ASCE)GT.1943-5606.0000312

Indraratna B., Nimbalkar S. & Rujikiatkamjorn C. (2014). From theory to practice in track geomechanics – Australian perspective for synthetic inclusions. *Transportation Geotechnics*, 1(4), pp.171–187. Available at: http://dx.doi.org/10.1016/j.trgeo.2014.07.004

Indraratna B., Salim W. & Rujikiatkamjorn C. (2011). Advanced Rail Geotechnology - Ballasted Track. London, UK: Taylor & Francis Group.

Indraratna B., Thakur P.K. & Vinod J.S. (2010). Experimental and Numerical Study of Railway Ballast Behavior under Cyclic Loading. *International Journal of Geomechanics*, 10(4), pp.136–144. Available at: http://ascelibrary.org/doi/10.1061/%28ASCE%29GM.1943-5622.0000055

Johnson K.L. (1986). Plastic Flow, Residual Stresses and Shakedown in Rolling Contacts. In *Proc., 2nd Int. Conf. on Contact Mechanics and Wear of Rail/Wheel Systems.* Univ. of Rhode Island, Waterloo, Ont., Canada.

Kennedy J. (2011). A full-scale laboratory investigation into railway track substructure performance and ballast reinforcement. PhD thesis, Heriot-Watt University.

Kennedy J., Woodward P.K., Medero G. & Banimahd M. (2013). Reducing railway track settlement using three-dimensional polyurethane polymer reinforcement of the ballast. *Construction and Building Materials*, 44, pp.615–625.

Klarbring A., Barber J.R., Spagnoli A. & Terzano M. (2017). Shakedown of discrete systems involving plasticity and friction. *European Journal of Mechanics - A/Solids*, 64, pp.160–164. Available at: http://dx.doi.org/10.1016/j.euromechsol.2017.02.006

Lackenby J., Indraratna B., McDowell G. & Christie D. (2007). Effect of confining pressure on ballast degradation and deformation under cyclic triaxial loading. *Géotechnique*, 57(6), pp.527–536. Available at: https://doi.org/10.1680/geot.2007.57.6.527

Lakusic S., Ahac M. & Haladin I. (2010). An experimental study on the characteristics of polyurethane-mixed coarse aggregates by large-scale triaxial test. In *Proc. 10th Slovenian Road and Ttransportation Congress,*. Portorož, Slovenia, pp. 333–340. Available at: http://linkinghub.elsevier.com/retrieve/pii/S0950061817304853

Lee S.H., Lee S.J., Park J.G. & Choi Y.-T. (2017). An experimental study on the characteristics of polyurethane-mixed coarse aggregates by large-scale triaxial test. *Construction and Building Materials*, 145, pp.117–125. Available at: http://dx.doi.org/10.1016/j.conbuildmat.2017.03.107

Lees A. (2017). Simulation of geogrid stabilisation by finite element analysis. In *Proceedings of the 19th ICSMGE*. Seoul, pp. 1377–1380.

Lees G. & Kennedy C.K. (1975). Quality, shape and degradation of aggregates. *Q. Jl Engng Geol.*, 8, pp.193–209.

Leshchinsky B. & Ling H. (2013). Effects of Geocell Confinement on Strength and Deformation Behavior of Gravel. *Journal of Geotechnical and Geoenvironmental Engineering*, 139(2), pp.340–352.

Leshchinsky B. & Ling H. (2013). Numerical modeling of behavior of railway ballasted structure with geocell confinement. *Geotextiles and Geomembranes*, 36, pp.33–43.

Li D. & Selig E.T. (1998). Method for railroad track foundation design, I: Development. *Journal of Geotechnical and Geoenvironmental Engineering*, 124(4), pp.316–322.

Li X., Ekh M. & Nielsen J.C.O. (2016). Three-dimensional modelling of differential railway track settlement using a cycle domain constitutive model. *International Journal for Numerical and Analytical Methods in Geomechanics*, 40(12), pp.1758–1770. Available at: http://doi.wiley.com/10.1002/nag.2515

Lirer S., Flora A. & Consoli N.C. (2012). Experimental Evidences of the Effect of Fibres in Reinforcing a Sandy Gravel. *Geotechnical and Geological Engineering*, 30, pp.75–83.

Lirer S., Flora A. & Consoli N.C. (2011). On the Strength of Fibre-Reinforced Soils. *Soils and Foundations*, 51(4), pp.601–609.

Lobo-Guerrero S. & Vallejo L.E. (2006). Discrete Element Method Analysis of Railtrack Ballast Degradation during Cyclic Loading. *Granular Matter*, 8(3–4), pp.195–204. Available at: http://link.springer.com/10.1007/s10035-006-0006-2

Maherer M.H. & Gray D.H. (1990). Static Response of Sands Reinforced with Randomly Distributed Fibres. *J. Geotech. Eng.*, 116(11), pp.1661–1677. Available at: http://ascelibrary.org/doi/10.1061/%28ASCE%290733-9410%281983%29109%3A3%28335%29

Marsal R.J. (1967). Large-Scale Testing of Rockfill Materials. *Journal of the Soil Mechanics and Foundations Division*, 93(2), pp.27–43. Available at: http://cedb.asce.org/CEDBsearch/record.jsp?dockey=0014902

Mezher S.B., Connolly D.P., Woodward P.K., Laghrouche O., Pombo J. & Costa P.A. (2016). Railway critical velocity – Analytical prediction and analysis. *Transportation Geotechnics*, 6, pp.84–96. Available at: http://dx.doi.org/10.1016/j.trgeo.2015.09.002

Michalowski R.L. & Čermák J. (2002). Strength anisotropy of fiber-reinforced sand. *Computers and Geotechnics*, 29(4), pp.279–299.

Michalowski R.L. & Čermák J. (2003). Triaxial Compression of Sand Reinforced with Fibers. *Journal of Geotechnical and Geoenvironmental Engineering*, 129(2), pp.125–136.

Network Rail (2018a). A better railway for a better Britain - Strategic Business Plan 2019-2024. Available at: https://cdn.networkrail.co.uk/wp-content/uploads/2018/02/Strategic-business-plan-high-level-summary.pdf

Network Rail (2018b). About Us - An Introduction to Network Rail. Available at: https://cdn.networkrail.co.uk/wp-content/uploads/2018/04/Network-Rail-About-Us-full.pdf

Newmark N.M. (1935). Simplified computation of Vertical pressures in Elastic Foundations.

Le Pen L. (2008). Track behaviour: the importance of the sleeper to ballast interface. University of Southampton.

Le Pen L., Milne D., Thompson D. & Powrie W. (2016). Evaluating railway track support stiffness from trackside measurements in the absence of wheel load data. *Canadian Geotechnical*

Journal, 53(7), pp.1156–1166. Available at: http://www.nrcresearchpress.com/doi/10.1139/cgj-2015-0268

Le Pen L., Watson G., Hudson A. & Powrie W. (2017). Behaviour of under sleeper pads at switches and crossings – Field measurements. *Proceedings of the Institution of Mechanical Engineers, Part F: Journal of Rail and Rapid Transit*, 0(0), p.95440971770740. Available at: http://journals.sagepub.com/doi/10.1177/0954409717707400

Le Pen L., Watson G., Powrie W., Yeo G., Weston P. & Roberts C. (2014). The behaviour of railway level crossings: Insights through field monitoring. *Transportation Geotechnics*, 1(4), pp.201–213. Available at: http://dx.doi.org/10.1016/j.trgeo.2014.05.002

Powrie W., Yang L.A. & Clayton C.R.I. (2007). Stress changes in the ground below ballasted railway track during train passage. *Journal of Rail and Rapid Transit*, 221(2), pp.247–262.

prEN-13230-6:2014. Railway applications - Track - Concrete sleepers and bearers - Part 6: Design. British Standards Institution.

Presto Geosystems (2015). Geocells - The 3D Confinement System that Stabilizes Soils. Available at: http://www.prestogeo.com/geocells [Accessed November 10, 2015]

Priest J.A., Powrie W., Le Pen L., Mak P. & Burstow M.C. (2013). The effect of enhanced curving forces on the behaviour of canted ballasted track. *Proceedings of the Institution of Mechanical Engineers, Part F: Journal of Rail and Rapid Transit*, 227(3), pp.229–244. Available at: https://doi.org/10.1177/0954409712458623

Qian J.-G., Wang Y.-G., Yin Z.-Y. & Huang M.-S. (2016). Experimental identification of plastic shakedown behavior of saturated clay subjected to traffic loading with principal stress rotation. *Engineering Geology*, 214, pp.29–42. Available at: http://dx.doi.org/10.1016/j.enggeo.2016.09.012

Raymond G. & Ismail I. (2003). The effect of geogrid reinforcement on unbound aggregates. *Geotextiles and Geomembranes*, 21(6), pp.355–380.

Raymond G.P. (2002). Reinforced ballast behaviour subjected to repeated load. *Geotextiles and Geomembranes*, 20(1), pp.39–61.

Raymond G.P. (1985). Research on railroad ballast specification and evaluation. *Transportation Research Record*, 1006, pp.1–8.

Raymond G.P. & Diyaljee V.A. (1979). Railroad ballast sizing and grading. *Journal of the Geotechnical Engineering Division, ASCE*, 105(GT5), pp.676–681.

Ricceri G. & Soranzo M. (1985). Ricceri and Soranzo (1985).pdf. *R.I.G.*, (4), pp.177–188. Available at: http://www.associazionegeotecnica.it/sites/default/files/rig/RIG_1985_4_177.pdf

Sadeghi J. (2010). Field Investigation on Dynamics of Railway Track Pre-Stressed Concrete Sleepers. *Advances in Structural Engineering*, 13(1), pp.139–152. Available at: http://multi-science.metapress.com/openurl.asp?genre=article&id=doi:10.1260/1369-4332.13.1.139

Sadeghi J.M. (2008). Experimental evaluation of accuracy of current practices in analysis and design of railway track sleepers. *Canadian Journal of Civil Engineering*, 35(9), pp.881–893. Available at: http://www.nrcresearchpress.com/doi/abs/10.1139/L08-026

Sadeghi M.M. & Beigi F.H. (2014). Dynamic behavior of reinforced clayey sand under cyclic loading. *Geotextiles and Geomembranes*, 42(5), pp.564–572.

Sadek S., Najjar S.S. & Freiha F. (2010). Shear Strength of Fiber-Reinforced Sands. *Journal of Geotechnical and Geoenvironmental Engineering, ASCE*, 136(3), pp.490–499.

Santoni B.R.L., Tingle J.S. & Webster S.L. (2001). Engineering Properties of Sand-Fiber Mixtures for

Road Construction. *J. Geotech. Geoenviron. Eng.*, 127(3), pp.258–268.

Santos S. Dos, Consoli N.C. & Baudet B.A. (2010). The mechanics of fibre-reinforced sand. *Geotechnique*, 60(10), pp.791–799.

Selig E.T. & Waters J.M. (1994). Track geotechnology and substructure management. London, Telford: ASCE.

Shao W., Cetin B., Li Y., Li J. & Li L. (2014). Experimental Investigation of Mechanical Properties of Sands Reinforced with Discrete Randomly Distributed Fiber. *Geotechnical and Geological Engineering*, 32(4), pp.901–910.

Sharp R.W. & Booker J.R. (1984). Shakedown of Pavements Under Moving Surface Loads. *Journal of Transportation Engineering*, 110(1), pp.1–14. Available at: http://ascelibrary.org/doi/10.1061/%28ASCE%290733-947X%281984%29110%3A1%281%29

Sharpe P. & Caddick V.R. (2004). Accelerated testing of geosynthetics in trackbed Using Europe's largest full scale rail rig. In *Railway Engineering 2004*. London. Available at: http://www.geofabrics.com/docs/PAPER - Sharpe Railway Engineering 2004.pdf

Shenton M.J. (1978). Deformation of railway ballast under repeated loading conditions. In A. D. Kerr, ed. *Proceedings of Railroad Track Mechanics and Technology*. Princeton University, pp. 76-NaN-1-41.

Skempton A.W. & MacDonald D.H. (1956). The Allowable Settlements of Buildings. *Proc. I.C.E.*, 5, pp.727–768.

Sol-Sánchez M., Moreno-Navarro F. & Rubio-Gámez M.C. (2016). Analysis of ballast tamping and stone-blowing processes on railway track behaviour: the influence of using USPs. *Géotechnique*, 66(6), pp.481–489. Available at: http://www.icevirtuallibrary.com/doi/10.1680/jgeot.15.P.129

Sol-Sánchez M., Thom N.H., Moreno-Navarro F., Rubio-Gámez M.C. & Airey G.D. (2015). A study into the use of crumb rubber in railway ballast. *Construction and Building Materials*, 75, pp.19–24.

Steinbrenner W. (1934). Tafeln zur Setsungsberechnung. *Die Stresse*, 1, pp.121–124.

Steward H.E., Selig E.T. & Norman-Gregory G.M. (1985). Failure criteria and lateral stresses in track foundations. *Transportation Research Record*, pp.59–64.

Suiker A.S.J., Selig E.T. & Frenkel R. (2005). Static and Cyclic Triaxial Testing of Ballast and Subballast. *Journal of Geotechnical and Geoenvironmental Engineering*, 131(6), pp.771–782. Available at: http://ascelibrary.org/doi/10.1061/%28ASCE%291090-0241%282005%29131%3A6%28771%29

Sun Q.D., Indratratna B. & Nimbalkar S. (2014). Effect of cyclic loading frequency on the permanent deformation and degradation of railway ballast. *Geotechnique*, 64(9), pp.746–751. Available at: http://dx.doi.org/10.1680/geot.14.T.015

Talbot A.N. (1933). Stresses in Railroad, Track Report of the Special Committee to Report on Stresses in Railroad Track; Sixth Progress Report. *AREA Proceedings*, 45, pp.66–848.

Thakur P.K., Vinod J.S. & Indraratna B. (2013). Effect of confining pressure and frequency on the deformation of ballast. *Géotechnique*, 63(9), pp.786–790. Available at: http://www.icevirtuallibrary.com/doi/10.1680/geot.12.T.001

Thom N.H. & Brown S.F. (1988). The effect of grading and density on the mechanical properties of a crushed dolomitic limestone. *Australian Road Research Board (ARRB) Conference*, 14(7), pp.94–100.

Thom N.H. & Brown S.F. (1989). The mechanical properties of unbound aggregates from various sources. Unbound aggregates in roads. In *Proceedings of the 3rd international symposium*. University of Nottingham, pp. 130–142.

Venkatramaiah C. (2006). Geotechnical Engineering. New Delhi: New Age Publishers.

Webster S.L. & Alford S.J. (1978). Investigation of construction concepts for pavements across soft ground. *Tech Rep US Army Eng Waterw Exp Stn S-78-6*.

Woodward P.K., Kennedy J., Laghrouche O., Connolly D.P. & Medero G. (2014). Study of Railway Track Stiffness Modification by Polyurethane Reinforcement of the Ballast. *Transportation Geotechnics*, 1(4), pp.214–224.

Woodward P.K., Kennedy J., Medero G.M. & Banimahd M. (2011a). Application of in situ polyurethane geocomposite beams to improve the passive shoulder resistance of railway track. *Proceedings of the Institution of Mechanical Engineers, Part F: Journal of Rail and Rapid Transit*, 226, pp.294–304.

Woodward P.K., Kennedy J., Medero G.M. & Banimahd M. (2011b). Maintaining absolute clearances in ballasted railway tracks using in situ three-dimensional polyurethane GeoComposites. *Proceedings of the Institution of Mechanical Engineers, Part F: Journal of Rail and Rapid Transit*, 226(3), pp.257–271.

Woodward P.K., Thomson D. & Banimahd M. (2007). Geocomposite technology: reducing railway maintenance. In *Proceedings of the ICE - Transport 160*. pp. 109–115.